Glycosphingolipid dysregulation and lysosomal dysfunction in motor neuron disease

Carla Sofia da Silva Santos

A thesis submitted for the degree of
Doctor of Philosophy



Department of Pharmacology
Linacre College
University of Oxford

Hilary Term 2021

Acknowledgements

I would like to thank my supervisor, Professor Frances Platt for her immense support, encouragement and guidance over the course of this project. Thank you for being such a great role model as a successful woman in science, always happy to share your knowledge and enthusiasm.

I would also like to thank my co-supervisor Dr David Priestman for his support and enthusiasm over these years and for introducing me to the complex world of glycosphingolipids.

A big thank you also to all the present and past members of the Platt lab: Mylene, Allie, Dawn, Dave, Claire, Nick, Kerri, Maria, Jorge, Joseph, Doris, James, Ecem, Maysa, Hsin, Yuzhe, Raffaele and Lara. Thank you for all your support and help in and out of the lab and for all the great memories. You make our lab a happy place to work, where even the daunting task of doing a PhD becomes a great enjoyable experience.

I am also very grateful to the Motor Neurone Disease Association for funding my studentship and supporting my participation in the great ENCALS meetings and in an International Symposium on MND/ALS.

A special thank you to Professor Kevin Talbot for his availability and help with all the things MND related, and also to Dr David Gordon and Dr Jayden Clark in the Motor Neurone Disease Centre, in Oxford. Thank you to Dr Alexandre Henriques, Dr Michael Spedding and Professor Jean-Philippe Loeffler in Strasbourg, and Dr Melissa Bowerman in Oxford, for all your collaboration.

To all my friends who accompanied me through this journey, thank you for being there.

Um enorme obrigada aos meus pais e irmão pelo vosso apoio incondicional, mesmo a milhas de distância. As minhas conquistas são vossas. Obrigada!

Finally, I would like to thank my partner Rob for his enormous support, belief and cheerfulness throughout this time.

Abstract

Historically, the early-onset rare neurodegenerative lysosomal storage disorders (LSDs) have been studied as discrete metabolic diseases in their own right. However, some links with common late-onset neurodegenerative diseases, including motor neurone disease (MND), have recently emerged. Reports show lipid dysregulation, including increased levels of various glycosphingolipids (GSLs) and upregulation of enzymes responsible for GSL hydrolysis, in the spinal cord of MND patients and the $SOD1^{G93A}$ mouse model. Inhibition of glucosylceramide (GlcCer) synthesis, the precursor of the vast majority of GSLs, accelerated disease progression and decreased lifespan, whereas infusion with GM3 ganglioside significantly delayed disease progression and increased survival, in the same mouse model. Previous work in our laboratory showed that GlcCer and downstream metabolism is significantly altered in spinal cord and muscle of $SOD1^{G86R}$ mice, and inhibition of GlcCer catabolism preserved motor function and delayed disease onset. Together, these studies highlight the importance of GlcCer and other GSLs for maintenance and regeneration of motor units. However, the relationship between the basic biochemical mechanisms linking lipid dysregulation, lysosomal dysfunction and altered lysosomal enzymatic activity in MND remains poorly understood.

In this thesis, the basic biological processes that cause lipid changes and lysosomal dysfunction in MND were investigated. After optimising a protocol for quantification of GlcCer by normal-phase high-performance liquid chromatography (NP-HPLC), general changes in patterns of GSL expression in samples from $SOD1^{G86R}$, $SOD1^{G93A}$ and $TDP\text{-}43^{M337V}$ mouse models of MND in different stages of disease development were

characterised. In agreement with previous reports, in spinal cord and soleus muscle of SOD1^{G86R} mice, total GSL levels in gastrocnemius and tibialis anterior of SOD1^{G93A} mice were elevated at later stages of disease. However, the GSL content in these tissues from SOD1^{G93A} mice and in spinal cord and tibialis anterior of SOD1^{G86R} mice remained unchanged at the time of symptoms onset. In TDP-43^{M337V} mice, which show progressive motor function deficits much later than the SOD1 models, GSL levels in the spinal cord remained unchanged in asymptomatic and initial stages of disease, but some changes were found in the brain of these mice. Importantly, changes in the activity of the enzymes that regulate GSL catabolism were found both in the spinal cord and brain of TDP-43^{M337V} mice. These data suggest different changes in GSL catabolism occur in different stages of disease depending on the mutation or the aetiology of MND.

Finally, a pilot study exploring the effect of edaravone, a free radical scavenger used for the treatment of MND, in the TDP-43^{M337V} mouse model of MND and the *Hexb*$^{-/-}$ mouse model of the LSD Sandhoff disease showed no effect in the disease progression or the development of the main symptoms associated to MND or Sandhoff disease. Additional pharmacological studies are necessary to better investigate the potential common mechanisms between MND and LSDs.

Abbreviations

2AA	Anthanillic acid
4-MU	4-methylumbelliferone
ALS	Amyotrophic lateral sclerosis
BAC	Bacterial artificial chromosome
BMT	Bone marrow transplantation
Cer	Ceramide
CerS	Ceramide synthase
CERT	Ceramide-transfer protein
CLN2	Neuronal ceroid lipofuscinosis type 2
CNS	Central nervous system
CSF	Cerebrospinal fluid
CT	Crossing time
DOPC	Dipalmitoylphosphatidylcholine
EMA	European Medicines Agency
ER	Endoplasmic reticulum
ERT	Enzyme replacement therapy
FDA	The United States Food and Drug Administration
FT	Falling time
FTD	Frontotemporal dementia
FUS	Fused in sarcoma
GalCer	Galacstosylceramide
GARP	Golgi-associated retrograde protein
Gb3 or GL3	Globotriaosylceramide
GBA(1)	Lysosomal glucosylceramidase
GBA2	Non-lysosomal glucosylceramidase
GCase	β-glucocerebrosidase or glucosylceramidase
GCS	Glucosylceramide synthase
GlcCer	Glucosylceramide
GSL	Glycosphingolipid
GM2-AP	GM2 activator protein
GWAS	Genome-wide association studies
HEXA/B	α/β subunit of β-hexosaminidase
IP	Intraperitoneal
LacCer	Lactosylceramide
LC3	Microtubule-associated protein 1 light chain 3
LSD	Lysosomal storage disorder
MND	Motor neurone disease
MPS	Mucopolysaccharidosis
mTORC1	Mammalian target of rapamycin complex 1

NB-DGJ	*N*-Butyldeoxygalactonojirmycin
Neu	Neuraminidase
NMJ	Neuromuscular junction
NPC	Niemann-Pick disease type C
NP-HPLC or HPLC	Normal-phase high-performance liquid chromatography
Nrf2	Nuclear erythroid 2-related factor 2
NTg	Non-transgenic
Oxr1	Oxidation resistance 1
PSEN1	Presenilin 1
recEGC'ase I	Recombinant EndoGlycoCeramidase I
RAN	Repeat-associated non-ATG
ROS	Reactive oxygen species
SAP	Sphingolipid activator protein
SD	Standard deviation
SM	Sphingomyelin
SOD	Superoxide dismutase
SRT	Substrate reduction therapy
TA	Tibialis anterior
TFEB	Transcription factor EB
TGN	*Trans*-Golgi network
TDP-43	Transactivation response DNA binding protein of 43 kDa
WT	Wild-type

Table of contents

Acknowledgements ..... **i**
Abstract ..... **ii**
Abbreviations ..... **iv**
Table of contents ..... **vi**
1. Introduction **1**
1.1. Glycosphingolipids (GSLs) 1
1.1.1. Structure and biological functions of GSLs 1
1.1.2. Biosynthesis of GSLs 2
1.1.3. Catabolism of GSLs 5
1.2. Lysosomes 8
1.2.1. Lysosomal structure and function 8
1.2.2. Lysosomal storage disorders (LSDs) 8
1.2.3. Existing therapies for LSDs 12
1.2.4. LSDs and more common neurodegenerative diseases 14
1.3. Motor neurone disease (MND) 16
1.3.1. Definition and statistics of MND 16
1.3.2. Genetics of MND 17
1.3.3. Existing therapies for MND 21
1.3.4. The autophagic-lysosomal network in MND 22
1.3.5. Lipid and GSL metabolism in MND 23
1.4. Relevance and aims 26
2. Materials and methods **27**
2.1. Mouse models 27
2.1.1. Fabry disease (*Gla*$^{-/-}$) mouse model 27
2.1.2. SOD1^{G93A} ALS mouse model 28
2.1.3. SOD1^{G86R} ALS mouse model 28
2.1.4. TDP-43^{M337V} BAC mouse model 30
2.1.5. Sandhoff disease (*Hexb*$^{-/-}$) mouse model 31
2.2. Tissues homogenisation and protein quantification 32
2.3. Enzyme assays 32

2.4. Quantification of glycosphingolipids (NP-HPLC) 33
2.5. Preparation of liposomes 35
2.6. Lysosomal enzyme assays 35
2.7. Drug administration 37
2.8. Mouse behavioural analysis 37
2.8.1. Rotarod 37
2.8.2. Manual rearing 38
2.8.3. Gait analysis 38
2.8.4. Horizontal bar crossing 38
2.9. Statistical analysis 39
3. Measuring glucosylceramide (GlcCer): protocol optimisation 40
3.1. Introduction 40
3.1.1. GlcCer 40
3.1.2. GlcCer and MND 42
3.1.3. GlcCer quantification 44
3.1.4. Aims 45
3.2. Results 45
3.3. Discussion 63
4. GSL metabolism in the SOD1^{G86R} and the SOD1^{G93A} mouse models 66
4.1. Introduction 66
4.1.1. SOD1 mutations in MND 66
4.1.2. GSLs in MND and SOD1 mouse models: a review 68
4.1.3. Aims 72
4.2. Results 72
4.3. Discussion 85
5. GSL metabolism in the TDP-43^{M337V} BAC mouse model 90
5.1. Introduction 90
5.1.1. TDP-43 pathology in MND 90
5.1.2. GSL metabolism and TDP-43 pathology 93
5.1.3. Aims 94
5.2. Results 94
5.2.1. GSL metabolism in the TDP-43$^{M337V/M337V}$ mouse 94
5.2.2. GSL metabolism in the 12 months TDP-43$^{M337V/-}$ mouse 114
5.3. Discussion 121
6. A pilot study of the effects of edaravone on the TDP-43$^{M337V/M337V}$ and *Hexb*$^{-/-}$ mouse models 128

6.1. Introduction 128
6.1.1. Edaravone and MND 128
6.1.2. Edaravone and GM2 gangliosidoses 130
6.1.3. Aims 132
6.2. Results 133
6.2.1. Edaravone and the TDP-43$^{M337V/M337V}$ mouse model 133
6.2.2. Edaravone and the *Hexb*$^{-/-}$ mouse model 139
6.3. Discussion 144
7. Conclusion and future directions 149
Bibliography 158
Supplementary information 182

1. Introduction

1.1. Glycosphingolipids (GSLs)

1.1.1. Structure and biological functions of GSLs

Glycosphingolipids (GSLs) are amphipathic molecules composed of one or more sugars (glycans) linked to a ceramide moiety via a β-glycosidic bond. The simplest GSLs are glucosylceramide (GlcCer) and galactosylceramide (GalCer), with glucose or galactose as their oligosaccharide unit, respectively (**Figure 1.1**). GlcCer and GalCer are called monoglycosylceramides or simply cerebrosides. There are a large variety of oligosaccharides and ceramides which can be combined in different ways, creating a widely varied and complex range of GSL structures, which can be subdivided into acidic and neutral GSLs[1,2]. GSLs derived from GlcCer with sialic acid(s) (e.g. *N*-Acetylneuraminic acid) in the oligosaccharide head group are charged GSLs named gangliosides, which are the major GSLs in the nervous system (e.g. GM1a, GD1a, GD1b and GT1b, **Figure 1.1**)[3–5].

GSLs are distributed heterogeneously in the outer leaflet of the plasma membrane, interacting directly with the lipid bilayer or with specific receptors within it and forming clusters or aggregates known as lipid rafts or GSL microdomains, important for cell recognition and cell signalling processes[6,7]. Even though the functions of each GSL are still mostly not fully understood, GSLs are known to modulate several cellular processes, including intracellular transport, endocytosis, cell migration, cell adhesion, growth regulation, cell proliferation, differentiation, apoptosis, senescence, immune response and various neurological functions[8,9]. Importantly, abnormalities in GSL metabolism have

been associated with various diseases in humans, including the lysosomal storage disorders (LSDs, **Chapter 1.2.2**), more common neurodegenerative diseases and cancer, making GSLs targets for treating these diseases[1,2].

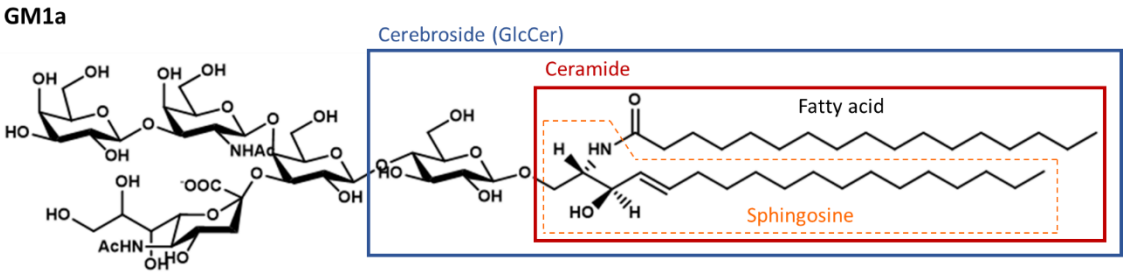


Figure 1.1. The structure of glycosphingolipids (e.g. GM1a).
Ceramide is composed of sphingosine and a fatty acid. The addition of a glucose or a galactose to the hydroxyl group of sphingosine originates a cerebroside, GlcCer or GalCer, respectively (in this case GlcCer). Further addition of oligosaccharides make up more complex GSLs, in this case the ganglioside GM1a. Modified from[10].

GSL levels are tightly regulated, due to the expression and subcellular localisation of the enzymes involved in their biosynthesis and trafficking within the different compartments of the ER and Golgi apparatus and their catabolism in lysosomes. Their expression is highly consistent and specific for each microenvironment, cell type, and development stage or species[2,7,11–13].

1.1.2. Biosynthesis of GSLs

The biosynthesis of GSLs starts in the endoplasmic reticulum (ER), with the condensation of the sphingoid bases sphingosine (resulting from lysosomal degradation of sphingolipids, the salvage pathway) or sphinganine (from *de novo* synthesis) with acyl-CoA to form ceramide or dihydroceramide, respectively[1,14–17]. Sphingosine and sphinganine are the most common sphingoid bases in mammals, with 18 carbon atoms,

but others also occur in smaller amounts, varying between 12 to 26 carbon atoms[18]. Ceramide and dihydroceramide synthesis are catalysed by different ceramide synthases (CerS) depending on the specific length of the acyl chain of acyl-CoA, which can vary significantly[1,19,20]. The majority of dihydroceramide is then converted into ceramide, and ceramide can then be galactosylated to form galactosylceramide (GalCer) in the ER lumen, used in the biosynthesis of sphingomyelin (SM) after being transported to the *trans*-Golgi network (TGN) by the ceramide-transfer protein CERT, or glucosylated by glucosylceramide synthase (GCS) to produce glucosylceramide (GlcCer) on the cytosolic leaflet of early *cis*-Golgi complex membranes (**Figure 1.1** and **Figure 1.2**)[2,21–24].

GalCer and GlcCer are the precursors of all GSLs synthesised in the Golgi apparatus. GalCer is transported to the Golgi to generate the gala series of GSLs, e.g. GalCer sialylation results in the GM4 ganglioside, while GalCer sulfation forms sulfogalactolipids (sulfo-GalCer)[1,2,5]. GlcCer can either be translocated into the luminal leaflet of the Golgi by vesicular transport or taken from the *cis*-Golgi and delivered to the TGN membranes by the transfer protein FAPP2[25–28]. When in the luminal leaflet of the *trans*-Golgi, GlcCer is galactosylated to generate lactosylceramide (LacCer), the percursor for the biosynthesis of various complex GSLs: GA2 (GalNAcβ1-4Galβ1-4Glcβ1-1Cer) by *N*-acetylgalactosamine transferase (GalNAcT) to originate the asialo series of GSLs; GM3 (NeuAcα2-3Galβ1-4Glcβ1-1Cer) which is a substrate for the ganglio series; Gb3 (Galα1-4Galβ1-4Glcβ1-1Cer or globotriaosylceramide) as the first of the globo series; iGb3 (Galα1-3Galβ1-4Glcβ1-1Cer) as the first of the isoglobo series; and Lc3 (GlcNAcβ1-3Galβ1-4Glcβ1-1Cer), by *N*-acetylglucosamine transferase (GluNAcT), for the neolacto series of GSLs (**Figure 1.2**)[1,2,5]. Further synthesis of the various complex GSLs

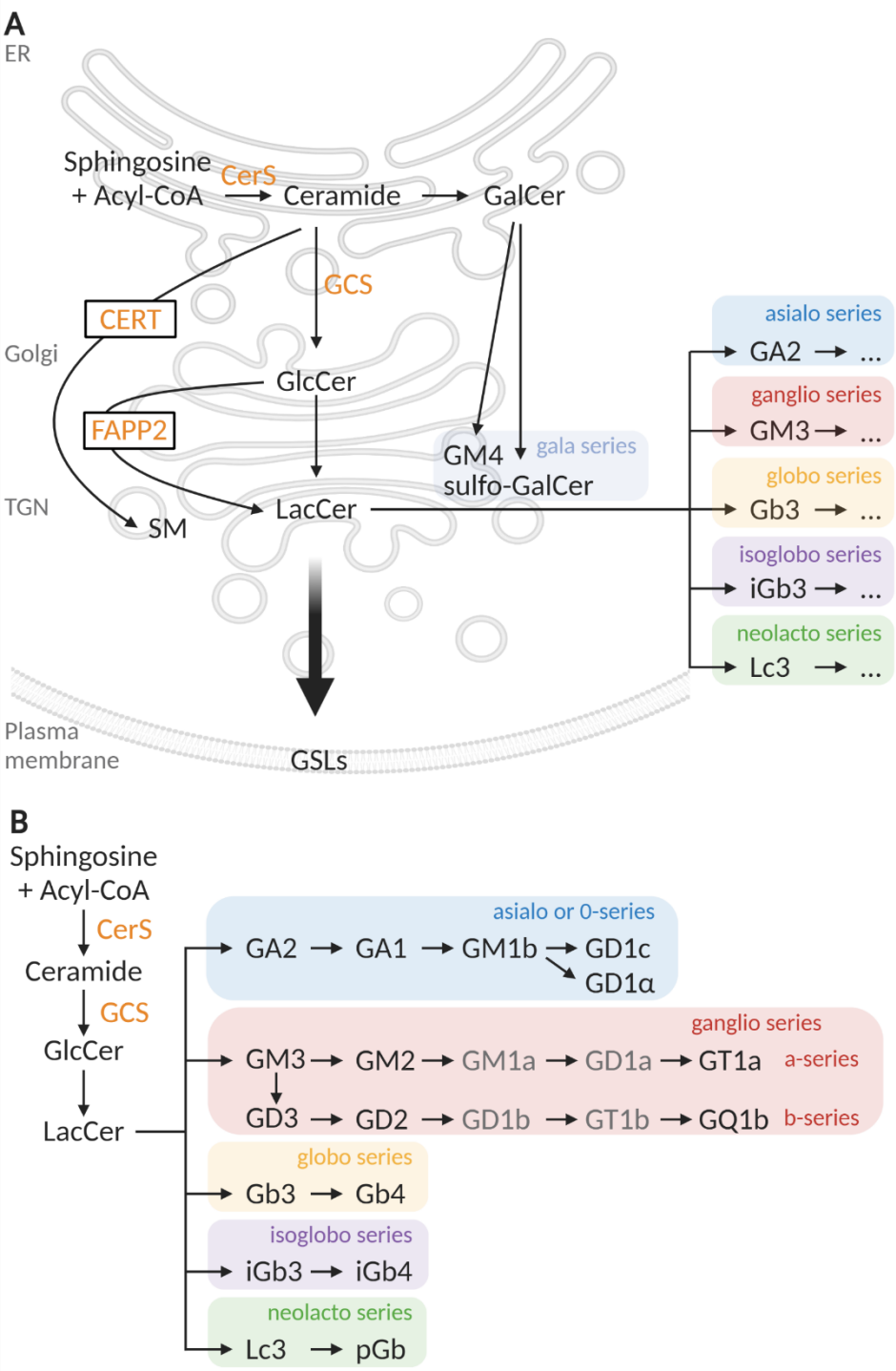


Figure 1.2. Schematic representation of the GSL synthetic pathways.
A. Ceramide is synthesised in the ER to generate GalCer or, in the Golgi apparatus, GlcCer. GalCer is the substrate to the GSLs from the gala series, including GM4 or sulfo-GalCer, and SM. GlcCer is transported to the TGN by vesicular transport or via FAPP2 to then be galactosylated into LacCer. **B.** LacCer is the substrate for the biosynthesis of more complex GSLs from the asialo or 0-series (in blue), the ganglio or a- and b-series (which include the most common GSLs in mammals, in red), the globo series (in yellow), the isoglobo series (in purple) or the neolacto series (shown in green), as detailed. Major gangliosides in the central nervous system (CNS) (GM1a, GD1a, GD1b and GT1b) are shown in grey. Created with BioRender.com.

occurs with the action of glucosyltransferases still in the Golgi apparatus[13]. These series are also frequently categorised as 0-, a-, b- or c-series depending on the presence of no or one to three sialic acid residues linked to the 3-position of the inner galactose moiety, respectively. The most common GSLs in mammals are from the a and b series (**Figure 1.2**)[1,5].

Finally, GSLs and SM are transported in membrane bound transport carriers to the plasma membrane, or through the endo-lysosome system to be degraded[29].

Diseases associated with GSL biosynthesis are rare[5]. When GSL biosynthesis is eliminated in mice by disrupting GCS, embryonic development and differentiation beyond gastrulation does not occur[30]. However, mutant cells deficient in GCS and mice with disrupted enzymes downstream of GlcCer synthesis are viable, suggesting GSL biosynthesis is essential for normal development but the loss of some complex GSLs can be tolerated[31–33]. Indeed, in humans, GM3 synthase and GM2/GD2 synthase deficiency are the only two disorders described to date caused by deficient ganglioside biosynthesis due to mutations in the *ST3GAL5* and *B4GALNT1* genes, respectively[34–37].

1.1.3. Catabolism of GSLs

Complex GSLs are mainly catabolised in late endosomes/lysosomes (**Chapter 1.2**). There are different ways for GSLs to get to lysosomes. Larger structures containing GSLs can be phagocytosed (e.g. senescent cells are phagocytosed by macrophages); GSLs can also be delivered to lysosomes by receptor-mediated endocytosis (together with low-density lipoproteins, or LDL); or they can be endocytosed from the plasma membrane. GSL rich microdomains are internalised and fuse with early endosomes,

where GSLs are sorted by the formation of multivesicular bodies and finally delivered to lysosomal membranes[38–41]. Within late endosomes and lysosomes, GSLs are catabolised in an acidic environment by hydrolases and accessory proteins at the surface of internal membrane vesicles or endocytosed lipoproteins[41–44]. Sphingolipid activator proteins (SAPs), saposins A, B, C, D or the GM2 activator protein (GM2-AP) are necessary to facilitate the interaction of glycosidases with their specific substrate or GSL[1,40,45,46].

Several exoglycosidases are responsible for sequentially releasing the carbohydrate residues from the non-reducing end of GSLs. In the final step, GlcCer is degraded into glucose and ceramide in lysosomes by β-glucocerebrosidase (GCase or GBA1) and in the presence of the accessory protein saposin C[46]. Ceramide is further hydrolysed by acid ceramidase back into free fatty acids and sphingosine, which can be taken back from lysosomes to the ER for GSL biosynthesis, the salvage pathway, or can be used for the synthesis of sphingosine-1-phosphate[1,47]. Degradation pathways for some sphingolipids and the enzymes and SAPs responsible for each reaction are shown in **Figure 1.3**. Importantly, reduced or loss of function of a hydrolase or a SAP results in the accumulation of the substrate/target lipid(s), leading to a family of lysosomal storage diseases (LSDs) named sphingolipidoses (**Chapter 1.2.2**)[5,48].

However, not all endocytosed GSLs get fully catabolised in lysosomes and GSL catabolism/remodelling is not restricted to endo-lysosomal compartments. GlcCer can be redirected back to the ER or Golgi apparatus for the synthesis of complex GSLs[49]. Remodelling of GSLs can also occur directly at the plasma membrane[50]. Additionally, catabolism of some GSLs occurs in the cytoplasm, as exemplified by the hydrolysis of GlcCer by β-glucocerebrosidase 2 (GBA2), an enzyme with optimal activity at neutral pH (as opposed to GBA1 which has optimal activity around pH 4.0-4.5)[1,51–53].

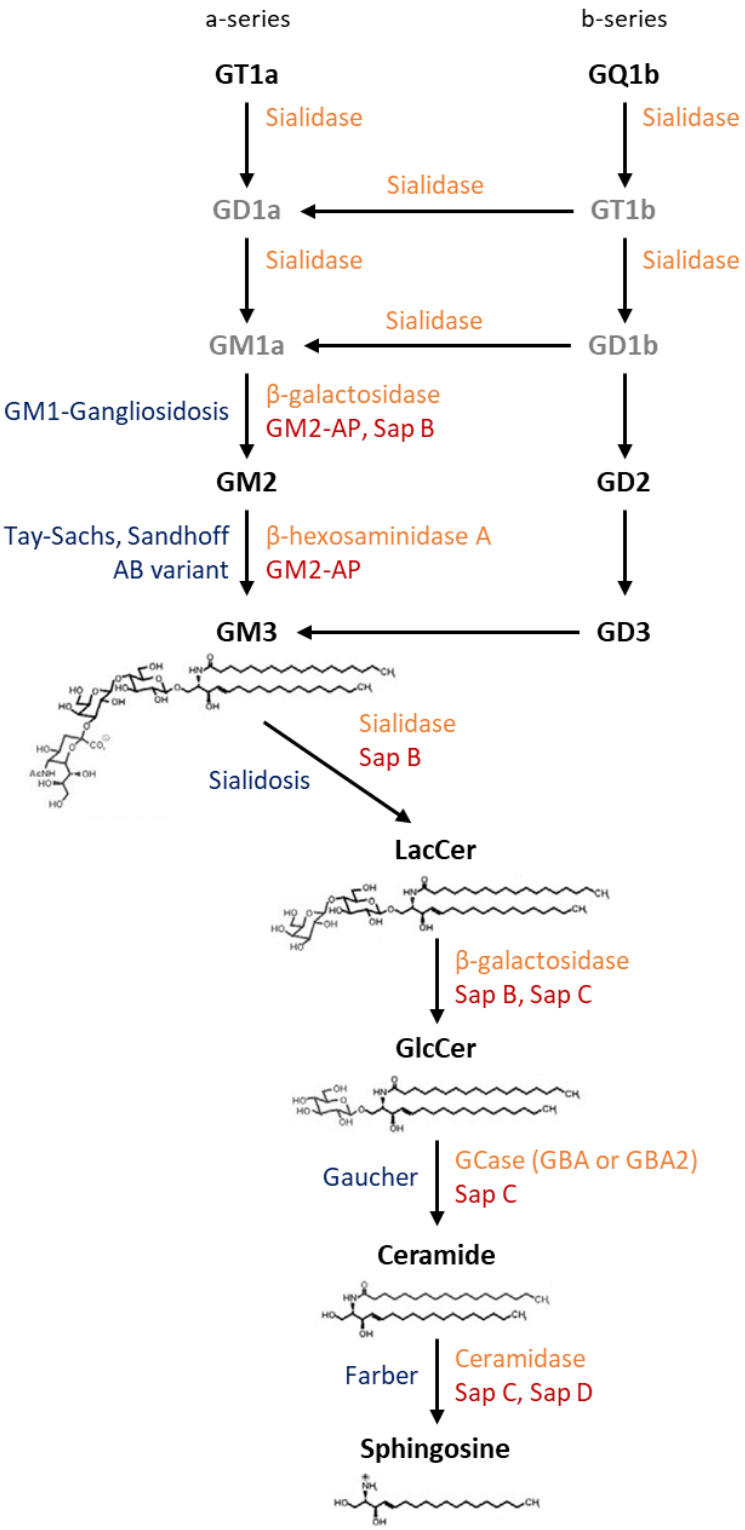


Figure 1.3. Schematic representation of the degradation of the main sphingolipids in the mammalian system, including the enzymes and SAPs responsible for each reaction and associated sphingolipidoses.

The names of the catabolic enzymes are indicated in orange and the SAPs required for their activity are in red. LSDs resultant from loss of function of the corresponding hydrolase or auxiliary proteins are indicated in blue. Major gangliosides in the CNS (GM1a, GD1a, GD1b and GT1b) are shown in grey. Adapted from[40,54].

1.2. Lysosomes

1.2.1. Lysosomal structure and function

Lysosomes are membrane-bound acidic organelles that contain hydrolases responsible for degrading and recycling macromolecules. Lysosomes are responsible for the catabolism of nucleic acids, proteins, carbohydrates and lipids derived from multiple routes within the endosomal, autophagic and phagocytic pathways. However, since they were first described in the 1950's by Christian de Duve, lysosomes were found to be more than static cellular "recycling centres"[55–57]. They were found to be highly dynamic organelles and important metabolic sensors, changing in number, size and shape, composition and consequently function and capable of moving within the cytoplasm depending on the cellular and intracellular environment and needs. Mammalian cells typically contain between 50 and 1,000 lysosomes. Lysosomes are essential for nutrient sensing, ion and amino acid homeostasis and calcium signalling[58–60]. They interact and form contact sites with other organelles, participating in plasma membrane repair, cell adhesion and migration processes, and immunity. Any changes in their function has catastrophic consequences for cells, organs and individuals, of which LSDs are the prime example, but also common neurodegenerative diseases, metabolic disorders and cancer[56,57].

1.2.2. Lysosomal storage disorders (LSDs)

Lysosomal storage disorders (LSDs) are rare metabolic, often neurodegenerative diseases, typically inherited in an autosomal recessive manner (although three are

X-linked)[5]. There are more than 70 different LSDs documented to date and they are caused by mutations in genes encoding proteins critical for the function of the lysosomal system, which can be lysosomal enzymes, integral membrane proteins, transporters, enzyme modifiers or activators[48]. Most LSDs result from inactive or poorly active lysosomal enzymes, which promote the progressive accumulation of macromolecules within the lysosome and cause lysosomal malfunction, with consequent cellular dysfunction, increased inflammatory response and cell death[5,48]. The glycosphingolipidoses constitute a subgroup of these diseases and are caused by the lysosomal storage of GSLs[5,44].

LSDs comprise a heterogeneous group of multimorbidity diseases which commonly manifest as paediatric neurodegenerative diseases, frequently along with visceromegaly, but other symptoms can be presented depending on the macromolecules stored[61]. These diseases are usually clinically classified depending on the type of disorder and the age of onset of symptoms in congenital or infantile (which are usually the most severe cases), late-infantile, juvenile and adult. However, diagnosis is dependent on both the evaluation of the clinical symptoms and enzymatic or genetic analysis to confirm lysosomal storage or the presence of a genetic mutation[61]. Especially in late onset cases, there are many confounding diseases, with similar clinical symptoms, which causes a delay in diagnosis, but newly developed diagnostic methods (e.g. whole-exome sequencing) have the potential to speed up this process[48].

Some LSDs mentioned throughout this thesis are summarised below.

1.2.2.1. Fabry disease

Fabry disease is one of the most common LSDs, with an estimated prevalence of up to 2.5 cases per 100,000 births[48]. It is X-linked and results from mutations in the *GLA* gene that encodes α-galactosidase A and leads to the progressive storage of Gb3. Gb3 accumulates in lysosomes of a variety of cell types resulting in various presenting symptoms like acroparesthesias, gastrointestinal symptoms, angiokeratoma in a bathing suit distribution (angiokeratoma corporis diffusum), small fiber neuropathy, cornea verticillata, anhidrosis and albuminuria in juvenile cases mostly affecting males; or progressive renal failure, hypertrophic cardiomyopathy and cerebrovascular disease in adult cases (mainly affecting females, but also some non-classical Fabry male patients)[48,62].

1.2.2.2. Gaucher disease

The second most common LSD is Gaucher disease, affecting up to 2 in every 100,000 individuals worldwide[48], but with higher prevalence among the Ashkenazi Jewish population affecting 1 in 800 to 1,000 people[63]. This disease is caused by mutations in the *GBA1* gene resulting in reduced GCase activity and progressive accumulation of GlcCer and glucosylsphingosine in macrophages, known as Gaucher cells[64]. Gaucher disease is subcategorised into type 1, if it affects peripheral tissues and not the central nervous system (CNS), with juvenile to adult onset patients showing symptoms including hepatosplenomegaly, haematological defects, inflammation and bone disease; type 2, is acute neuronopathic, typically manifesting in early infancy; and type 3, which can affect peripheral tissues and involve neuropathology, affecting mainly juvenile patients[5,63].

There is also a perinatal lethal form of Gaucher disease. A variant form of Gaucher disease is caused by deficiency of saposin C, which also causes the storage of GlcCer in macrophages and in the CNS[65–67]. Importantly, population genetics have shown that patients with Gaucher disease type 1 or carriers of *GBA* mutations have higher probabilities of developing Parkinson's disease or Lewy body disorders[68–71].

1.2.2.3. Sandhoff disease

Sandhoff disease is a GM2 gangliosidosis along with Tay-Sachs disease and GM2 activator deficiency and affects 1:422,000 births[72,73]. Sandhoff disease is caused by mutations in *HEXB* which result in malfunctioning β-hexosaminidase (β subunit) and consequent storage of the GM2 ganglioside[5,74,75]. Patients suffer from progressive neurodegeneration due to the accumulation of GM2 in the CNS, increased inflammation and premature death[73,76]. This disease can develop at any time between infancy and adulthood, but like other LSDs, the earlier the onset the more rapid the rate of progression[48,75].

1.2.2.4. Niemann-Pick disease type C

Niemann-Pick disease type C (NPC) is caused by mutations in the *NPC1* or *NPC2* genes which result in storage of all GSLs, cholesterol, SM and sphingosine, with an incidence of 1 in 120,000 worldwide[77]. However, contrary to the aforementioned LSDs and contrary to Niemann-Pick disease types A (infantile) and B (juvenile), caused by mutations in sphingomyelin phosphodiesterase with consequent accumulation of SM, *NPC1* and *NPC2* do not encode lysosomal enzymes. NPC1 is a membrane protein of the

lysosomal membrane and NPC2 is a soluble cholesterol binding protein[77]. Together, NPC1 and NPC2 are responsible for lysosome-ER contact site formation, lysosomal fusion and trafficking and mutations in these proteins cause progressive neurodegeneration, with patients presenting with symptoms including ataxia, vertical supranuclear gaze palsy, dystonia, liver disease, splenomegaly, interstitial lung disease, difficulty swallowing, intellectual decline and seizures[48]. Dementia is a common symptom of NPC, which is visible in the post-mortem brain of patients that show similar pathological hallmarks associated with late onset Alzheimer's disease[78]. NPC can manifest at any age[48,77].

1.2.3. Existing therapies for LSDs

Over the past few years, various treatments have been approved for patients with some LSDs (**Table 1.1**), and many others are going through clinical trials or in preclinical development. With diagnostic delay and the lack of new-born screening, the need for therapies remains urgent, but because LSDs are generally monogenic diseases, a good knowledge of the molecules and pathways affected in these disorders offers various therapeutic targets[79,80]. In patients where the cause of disease is loss of function of a lysosomal enzyme, the use of enzyme replacement therapy (ERT) by the infusion of recombinant enzymes or bone marrow transplantation (BMT) from healthy individuals has been shown to be efficient at replacing the missing enzymes. ERT does not cross the blood brain barrier so was particularly successful in the treatment of type 1 non-neuropathic Gaucher disease, with administration of recombinant GCase and early treatment can prevent the development of symptoms. Imiglucerase, velaglucerase alfa and taliglucerase alfa are the approved enzymes by the European Medicines Agency and

the United States Food and Drug Administration (EMA and FDA) for the treatment of type 1 and type 3 Gaucher disease[81–86].

Disease	Defective enzyme	Type of therapy	Therapeutic agent
Fabry disease	α-galactosidase A	ERT	• Agalsidase beta • Agalsidase alfa
		Chaperone therapy	• Migalastat
Gaucher disease (type 1)	GCase	ERT	• Imiglucerase • Velaglucerase alfa • Taliglucerase alfa
		SRT	• Miglustat • Eliglustat
NPC	NPC1 and NPC2	SRT	• Miglustat
CLN2 disease	Tripeptidyl-peptidase 1	ERT	• Cerliponase alfa
Pompe disease	α-glucosidase	ERT	• Alglucosidase alfa
MPS I (Hurler-Scheie and Scheie syndromes)	α-iduronidase	ERT	• Laronidase
MPS II (Hunter syndrome)	Iduronidase-2-sulfatase	ERT	• Idursulfase • Idursulfase beta
MPS IV (Morquio syndrome A)	*N*-acetylgalactosamine-6-sulfate sulfatase	ERT	• Elosulfase
MPS VI (Maroteaux-Lamy syndrome)	*N*-acetylgalactosamine-4-sulfatase (arylsulfatase B)	ERT	• Galsulfase
MPS VII (Sly syndrome)	β-glucoronidase	ERT	• Vestronidase alfa
Wolman disease	Lysosomal acid lipase deficiency	ERT	• Sebelipase alfa

Table 1.1. Approved therapies for LSDs by the EMA or the FDA.
MPS: mucopolysaccharidosis. Adapted from[48,87].

Some success has also been achieved with ERT in Fabry disease and other LSDs with little CNS involvement[88–90]. Neuronal ceroid lipofuscinosis type 2 (CLN2) was the first neuropathic LSD with an approved therapy that targets directly the brain[91,92]. However, many other therapies have also shown some success such as substrate reduction therapy (SRT, e.g. miglustat and eliglustat), chaperone therapy (e.g. ambroxol and migalastat),

stem cell and gene therapies, and even anti-inflammatory and antioxidant therapies[48,79,93–98]. Just this year, arimoclomol, an amplifier of heat-shock proteins, is under evaluation by the FDA as the first treatment for NPC (clinical trials NCT04316637 and NCT02612129) and was also granted fast track designation for the treatment of amyotrophic lateral sclerosis (ALS) (clinical trials NCT03836716 and NCT03491462). Arimoclomol is not yet approved for any disease but a decision on NPC is pending in 2021.

Successful treatments for LSDs might help in the search for better therapeutics for more common diseases with similar etiology[48,79,99].

1.2.4. LSDs and more common neurodegenerative diseases

Defects in the endo-lysosomal system and the pathological storage of macromolecules in the lysosome do not occur solely in LSDs. Lysosomal dysfunction has also been found in various common neurodegenerative diseases such as Parkinson's disease, Alzheimer's disease, ALS, frontotemporal dementia (FTD), Huntington's disease and others, and also in ageing[100–103]. Some neurodegenerative diseases show mutations in genes necessary for lysosomal function, others display impairment of the autophagic-lysosomal pathway, which causes protein aggregation. In other cases the protein aggregation is the cause for dysfunction of the autophagosome-lysosome, contributing to protein aggregation and cytotoxicity. Understanding the common pathogenic mechanisms shared between rare and common neurodegenerative diseases is fundamental for a better understanding of neurodegeneration *per se* and for the development of better treatments[57,99,104].

One of the most striking genetic links found between LSDs and a common neurodegenerative disease was the discovery of heterozygous mutations in *GBA1* (responsible for Gaucher disease if homozygous) as a strong risk factor for Parkinson's disease and Lewy bodies dementia[69,105–107]. Also in Parkinson's disease, disfunction of the autophagic-lysosomal pathway was found to promote the accumulation and aggregation of α-synuclein in Lewy bodies and neuronal processes, a neuropathological hallmark of the disease[108,109]. Alpha-synuclein aggregates are cytotoxic and cause the rupture of lysosomes due to impaired function of the transcription factor EB (TFEB, a major transcriptional regulator of the autophagic-lysosomal pathway), which consequently is thought to cause a cathepsin B dependent increase in reactive oxygen species (ROS), mitochondrial dysfunction and increased inflammation[110–112].

Mutations in the presenilin 1 gene (*PSEN1*) are the most common cause of familial Alzheimer's disease and are now known to impair lysosomal acidification and reduce lysosomal Ca^{2+} stores[113–115]. PSEN1 is a subunit of γ-secretase, which regulates the intramembrane cleavage of amyloid precursor protein (APP) and production of amyloid-β peptides. Extracellular plaque deposits of amyloid-β peptides are one the hallmark pathologies required for the diagnosis of Alzheimer's disease[116–118]. Accumulation of lysosome-like organelles with low levels of proteases were found in swollen neuronal axons surrounding extracellular amyloid-β at amyloid plaques, suggesting amyloid-β deposits are impeding endo-lysosomal maturation[119]. At the same time, impaired endo-lysosomal transport was shown to promote changes in the production of amyloid-β peptides[120].

The role of GSL storage, lysosomal dysfunction and associated pathways in ALS will be discussed in the following chapter.

1.3. Motor neurone disease (MND)

1.3.1. Definition and statistics of MND

Motor neurone disease (MND) is an umbrella term for a group of prematurely fatal progressive neurodegenerative conditions with poorly understood aetiology. ALS is the most common clinical manifestation of MND, first described by Charles Bell in 1824, the reason why both terms are largely considered synonymous[121,122]. MND is generally characterized by degeneration of upper and lower motor neurons, with progressive paralysis and death from respiratory failure within 3 to 5 years of symptoms onset[122,123]. MND affects people of any age but it is more common in people between 50 to 70 years old, and it is more frequent in men than women, with an incidence of 2.1 to 3.8 per 100,000 person-years in Europe[124–126]. For the majority of patients the cause of MND is unknown, but 5 to 10 % of the patients have a family history of MND and several genes have been identified as promoters of motor neuron degeneration (e.g. *C9orf72*, *SOD1*, *TARDBP*, *FUS*, etc.)[127]. Ageing has been shown to be an important risk factor for MND, though this has not been confirmed in individuals over 85 years old[127]. Lifestyle and environmental factors also seem to contribute for MND and associations between higher risk of MND and smoking, higher levels of physical activity, trauma including head injury or the involvement of chemicals (e.g. heavy metals, pesticides or cyanotoxins) have been explored, but the evidence is not definitive[128–132].

A MND diagnosis is mainly based on clinical history and examination of the patient and laboratory and imaging tests that are usually done to exclude other potential causes of the presented symptoms (disease confounders or mimics e.g. radiculopathies), and nerve conduction studies and tissue biopsies help supporting the diagnosis and minimise

false positive diagnosis. Genetic testing is usually only done in patients with a family history of MND or FTD, or those with a particularly early onset (younger than 50 years old)[133].

Patients can show a variety of symptoms, the most common being muscle spasticity, muscle weakness and muscle atrophy, respiratory insufficiency, dysphasia, or in some cases cognitive (60 %) and behavioural (30 %) impairment[133,134]. About 13 % of the patients also present a behavioural variant of FTD[135]. Studies on FTD revealed MND and FTD share common pathogenic pathways and associated genetic mutations and there are case reports of patients with both ALS and FTD symptoms. However, FTD is a group of disorders characterised by the degeneration of neurons in the frontal and temporal cerebral cortex and basal ganglia (as opposed to motor neurons in MND), which results in cognitive and language deficits and changes in personality and behaviour[136,137]. MND can be subcategorised according to the involvement of upper vs. lower motor neurones, or the presence of frontotemporal dysfunction, though a better system to breakdown and approach this disease has been under discussion to allow for the finding of more reliable biomarkers and better treatments[138].

1.3.2. Genetics of MND

Genetic research of MND has been useful for the understanding of the underlying mechanisms of disease pathology and identifying potential biomarkers and therapeutic targets[139]. Most of the genes found so far have revealed the main known MND pathogenic pathways: autophagy, proteostasis, axonal transport, cytoskeleton,

mitochondrial dysfunction, excitotoxicity, neuroinflammation, RNA metabolism and DNA repair[137,138].

As previously mentioned, about 5 to 10 % of patients with MND have a family history of MND, FTD or both, and familial MND has a genetic component. However, genetic mutations can also be found in sporadic cases (https://alsod.ac.uk/). Familial and sporadic MND are mostly clinically indistinguishable, which suggests they share common pathological mechanisms[123,125].

1.3.2.1. Mutations in *C9orf72*

The most common genetic cause of ALS are hundreds to thousands of GGGGCC hexanucleotide repeat expansions in the first intron (non-coding portion) of the *C9orf72* gene, which normally only reach a maximum of 30 units[140,141]. These repeats have been detected in approximately 40 % of the cases of familial ALS and FTD and about 7 % of the cases of sporadic ALS[142]. The cellular functions of C9orf72 still remain largely unknown, but mutations in the *C9orf72* gene have been suggested to cause pathology by promoting haploinsufficiency (if the expanded repeats affect the expression levels of C9orf72), RNA-mediated toxicity (due to the accumulation and aggregation of RNA transcripts, RNA foci, both in the nucleus and the cytoplasm) and dipeptide repeat protein toxicity, related to repeat-associated non-ATG (RAN) translation of the expanded C9orf72 gene[143,144]. Mutations in *SOD1*, *FUS* and *TARDBP* are the remaining most common genetic variants identified so far[133].

1.3.2.2. Mutations in *SOD1*

The first mutations found in patients with MND were in the Cu/Zn superoxide dismutase gene *SOD1*[145,146]. These mutations are thought to account for about 20 % of the familial cases and some sporadic cases[147,148]. The function of SOD1 as a free radical scavenger has been widely studied[149]. *SOD1* mutations in MND are usually autosomal dominant and cause the SOD1 protein to misfold and aggregate, becoming toxic to cells. It was also recently found that wild-type SOD1 can also aggregate in the CSF of patients without *SOD1* mutations, suggesting this is a pathological process of MND independent of mutations[150]. Importantly, the $SOD1^{G93A}$ mouse was the first mouse model of ALS and is the most widely investigated[151,152]. It expresses a mutant form of human SOD1 and develops progressive motor neuron degeneration similar to what happens in patients, without affecting SOD1 activity[151,152].

1.3.2.3. Mutations in *FUS*

Mutations in the fused in sarcoma, or *FUS*, gene are found in a small number of MND patients, accounting for about 4 % of familial and 1 % of sporadic cases[153,154]. Over 50 *FUS* mutations have been reported in MND and most of them are missense, but a few are in-frame deletions or insertions[153,155–157]. FUS is a RNA binding protein with various functional domains including a RNA-recognition motif and a highly-conserved C-terminal nuclear localization signal, where the majority of *FUS* mutations were discovered[153,158]. The biological function of FUS is still not fully understood, but it is involved in transcription control, RNA processing (regulation of pre-mRNA) and DNA repair under normal conditions[159–162]. In MND, FUS has been found to form immunoreactive inclusions

in the cytoplasm (it is usually located in the nucleus), or, in oxidative stress conditions, recruited into stress granules where it can sequester wild-type FUS and disrupt RNA processing[158,163,164].

1.3.2.4. Mutations in *TARDBP* and TDP-43 pathology

The transactivation response DNA binding protein (or TDP-43) is a 43 kDa ubiquitously expressed protein encoded by the *TARDBP* gene, with various domains including two highly conserved RNA recognition motifs and a glycine-rich C-terminal domain[154,165]. TDP-43 stays mainly in the nucleus of cells and is responsible for several physiological roles through the regulation of various genes by DNA/RNA binding, splicing and protein-protein interactions[166–171]. Mutations in the *TARDBP* gene have been found in a very small percentage of both MND and FTD patients, most of which are dominant missense mutations and located in the C-terminal region, responsible for RNA-protein and protein-protein interactions and for the tendency of TDP-43 to aggregate[168,172,173]. However, 98 % of all sporadic and familial cases of MND, and the majority of the behavioural variant of (Tau-negative) FTD cases, present cytoplasmic neuronal and glial inclusions (insoluble ubiquitinated aggregates) of TDP-43, making TDP-43 proteinopathy a pathological hallmark of the disease[135,174,175]. The specific molecular mechanisms through which *TARDBP* mutations cause pathology are still under debate, but studies suggest it might be caused by a TDP-43 loss of function with impaired RNA-binding capacity and splicing dysfunction, it might be due to a toxic gain of function with the mislocalisation and aggregation of the protein in the cytoplasm, or a combination of both[176,177].

1.3.2.5. Other mutations

Several other new genes have been associated with MND in the past few years using genome-wide association studies (GWAS), whole genome studies or exome sequencing[139,178]. With the approval of a few gene therapy products for genetic disorders and base editing techniques advancing, the interest and relevance of the genetic components of MND has been increasing[178,179]. From the study of the mutations associated with MND, new and better models for MND have been discovered[180].

1.3.3. Existing therapies for MND

There is currently no cure for MND and many drugs have been studied for its treatment, but only two drugs have been approved for the treatment of MND: riluzole and edaravone[181]. Riluzole (or Rilutek®) was the first FDA-approved drug (1995) and is currently the only EMA approved drug for the treatment of ALS[182,183]. The mechanism of action of riluzole is still undetermined, but it is thought to act as an inhibitor of glutamatergic neurotransmission by blocking voltage-gated sodium channels on pre-synaptic neurons, modulating mitochondrial function and potentiating calcium-dependent potassium currents[184]. It has also been suggested that riluzole might have an antioxidant effect[185]. Importantly, treatment with riluzole is associated with increased survival of 2-3 months if administered in an advanced stage of disease[186].

On the other hand, edaravone (Radicut® or Radicava®) is a free radical scavenger and inhibitor of lipid peroxidation which was primarily used in Japan to help with recovery following an acute ischemic stroke[187–189]. Oxidative stress is a known feature of motor neuron degeneration in MND[190–192], therefore edaravone was tested and approved

for the treatment of MND in Japan in 2015, and subsequently approved in other countries including the United States (FDA approved) in 2017, but not yet by the EMA[193–195]. Edaravone has failed to extend survival but it can slow disease progression in some patients with early onset and rapidly progressing disease[123,196].

The failure to find better treatments is in part due to the clinical and pathogenic heterogeneity of MND, lack of good animal models of the disease and poor design of clinical trials[123,180,197]. MND symptoms are currently managed with physical therapy, nutritional support and artificial ventilation in the later stages[197].

1.3.4. The autophagic-lysosomal network in MND

Abnormal formation of protein inclusions in motor neurons is a hallmark of both familial and sporadic MND[198]. One of the major pathways through which cells degrade misfolded proteins and dysfunctional cytoplasmic organelles in cells is autophagy. Substrates due for degradation are surrounded by a double-membrane compartment named autophagosome which fuses with late-endosomes/lysosomes, where the substrates are finally degraded by hydrolases[199,200]. Alterations in the autophagic-lysosomal pathway have been described in several neurodegenerative diseases including MND[102,200]. However, the role of autophagy in motor neuron degeneration is complex and contradictory data can be found in the literature[199,201].

Levels of the microtubule-associated protein 1 light chain 3 (LC3) were shown to be increased in the spinal cord of $SOD1^{G93A}$ mice, suggesting autophagosome formation is increased, possibly via enhancement of the mammalian target of rapamycin complex 1 (mTORC1) signalling[202]. Sequestosome 1 and LC3 were also found to be reduced due to

an hyperactivation of the autophagic-lysosomal pathway, at least in part via mTORC1, in motor neurons from G85R SOD1YFP mice[203]. Additionally, TFEB and beclin1 expression were found to be increased in motor neurons of the SOD1^{G93A} mouse[204] and BEC1 levels (autophagy regulator) were upregulated in the SOD1^{G86R} mouse model[205]. Together these studies suggest the autophagic-lysosomal pathway is overactive in MND and down-regulation of autophagy could delay disease progression[206]. On the other hand, other studies in motor neurons of asymptomatic and pre-symptomatic SOD1^{G93A} mice have shown that mutant SOD1 aggregates interfere with dynein mediated endosomal trafficking (axonal retrograde transport), resulting in lysosomal deficits, reduced autophagic clearance, consequent increased stress and axonal degeneration as disease progresses[207–209]. Therefore, a lower flux through the autophagic-lysosomal pathway can also promote motor neuron degeneration.

Changes associated with autophagy have also been found in other models of MND[102,200]. However, further studies are necessary to better understand the complex alterations described in the literature and better explore the regulation of autophagic-lysosomal pathway as a therapy for MND.

1.3.5. Lipid and GSL metabolism in MND

There is still a lot to understand about lipid (including GSL) dysregulation and lysosomal dysfunction in MND. Over the past five years, several studies have emphasised its relevance and complexity[210–213]. A wide variety of pathological mechanisms cause and are caused by lipid dysregulation in MND, including increased lipid accumulation, increased oxidative stress and lipid peroxidation, which cause mitochondrial dysfunction

and contribute for neuroinflammation, altered membrane composition in neurons and consequent defects in the cytoskeleton and reduced neurotransmitter release (**Figure 1.4**)[212,213].

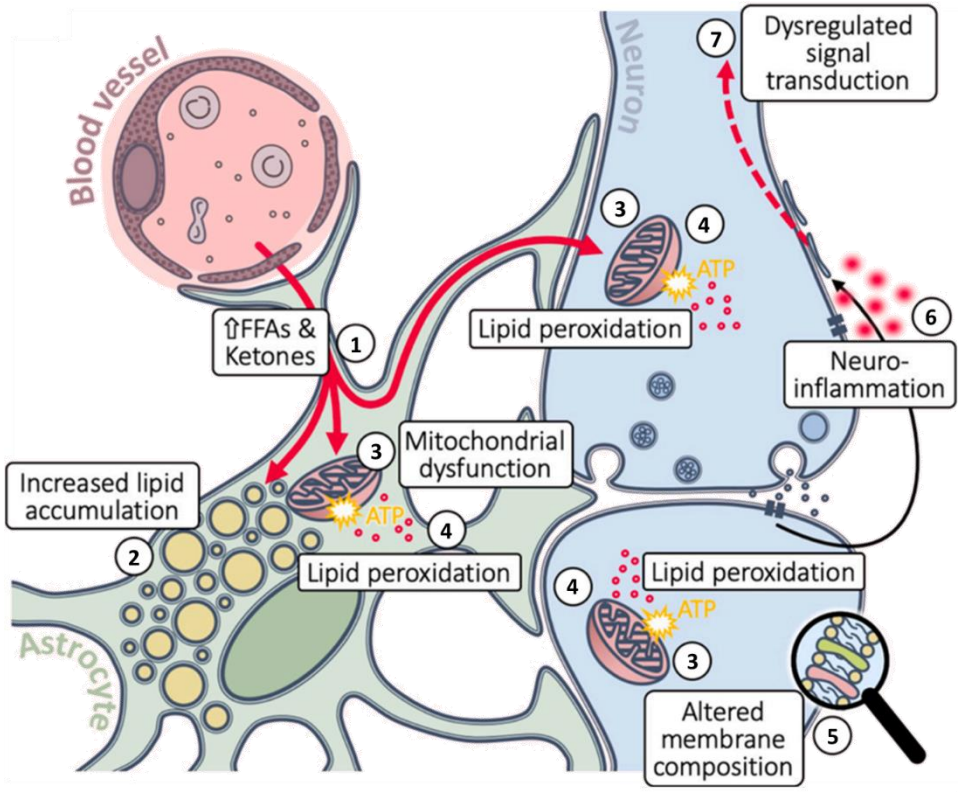


Figure 1.4. Lipid dysregulation and MND in the CNS.
Several pathological mechanisms promote and are caused by lipid dysregulation in MND. In the CNS, dysregulated lipid metabolism can be found in: **(1)** significantly elevated levels of free fatty acid (FFA), **(2)** increased accumulation of lipid droplets in astrocytes, **(3)** mitochondrial dysfunction in different cell types, which contributes to **(4)** increased oxidative stress and consequent lipid peroxidation; **(5)** altered neuronal lipid membrane composition and increased concentration of sphingolipids, **(6)** activation of neuroinflammatory processes and **(7)** dysregulation of signal transduction mechanisms. Adapted from[213].

Several studies have explored the specific role of GSL metabolism in MND[214–219]. ALS patients and the mouse model of MND SOD1^{G93A} show increased and altered GSL levels and activity of the enzymes that regulate their metabolism in the spinal cord. Pharmacological inhibition of GSL biosynthesis in the SOD1^{G93A} mouse accelerated

disease progression, while administration of GM3 slowed it down, which strongly suggests changes in GSL metabolism contribute to neurodegeneration[214].

Inhibition of GlcCer degradation in another model of MND, the SOD1^{G86R} mouse, also delayed disease onset and improved motor function[216]. Additionally, inhibition of GlcCer degradation also accelerated recovery after peripheral nerve injury in wild type mice[216]. Also, inhibition of GBA2 (a non-lysosomal enzyme that degrades GlcCer) was shown to improve motor function and extend survival in SOD1^{G86R} mice[218]. Globally these studies suggest GSLs might have a protective or compensatory role in MND pathogenesis and GlcCer is required for maintenance and regeneration of motor units. Furthermore, a recent study showed how altered sphingolipid metabolism contributes to neurodegeneration and proposes that reducing the excess of sphingolipid levels (by inhibiting SM synthesis with myriocin) improves wellness scores, grip strength, neuropathology and survival in wobbler mice (with a mutation in *Vps54*, a gene that encodes a component of the Golgi-associated retrograde protein (GARP) complex), but GLS biosynthesis was not specifically inhibited in this study[219].

All these studies stress the importance of a better understanding the role of GlcCer and GSLs in MND, for different mutations and for sporadic cases, in different stages of disease. They also present evidence that modulation of GSL metabolism is a potential therapeutic target for MND.

1.4. Relevance and aims

There are lipid abnormalities and clinical manifestations shared in common in LSDs and several diseases of the motor system, including MND and Parkinson's disease[211]. Several studies have shown altered GSL metabolism in post-mortem tissue from ALS patients and from symptomatic SOD1 mouse models of MND[214–216,218,220]. However, the relationship between the basic biochemical mechanisms linking GSL dysregulation, lysosomal dysfunction and altered lysosomal and non-lysosomal enzyme activity in MND remains poorly understood, particularly the role of GSL metabolism in the initial stages of pathology. Additionally, due to the heterogeneity of MND, it is vital to understand the role of different MND genes in GSL metabolism.

The aims of this thesis are therefore to:

- optimise the protocol for GlcCer quantification by high-performance liquid chromatography (HPLC) (**Chapter 3**);
- characterise GlcCer and downstream GSL metabolism in tissues from SOD1 mouse models (the $SOD1^{G93A}$ and the $SOD1^{G86R}$) and the TDP-43^{M337V} mouse model of MND, at different stages of disease development, by HPLC and enzymatic assays (**Chapters 4 and 5**);
- evaluate in a pilot study the effect of edaravone, used for the treatment of MND, in the TDP-43^{M337V} mouse model of MND and the *Hexb*$^{-/-}$ mouse model of the LSD Sandhoff disease, in order to investigate the potential common mechanisms between these two groups of diseases and to better understand MND pathology (**Chapter 6**).

2. Materials and methods

2.1. Mouse models

All experimental procedures were conducted in accordance with the UK Home Office Animal Scientific Procedures Act, 1986. All animals were housed in ventilated cages and maintained by heterozygous mating, in a 12:12 h light/dark cycle, with an ambient temperature of 20-23°C, with regular rodent chow (5053 irradiated PicoLab® Rodent Diet 20, from PMI LabDiet®, USA) and water available *ad libitum*.

2.1.1. Fabry disease (*Gla*$^{-/-}$) mouse model

Fabry disease (*Gla*$^{-/-}$) mice were kindly provided by Ashok B Kulkarni (National Institutes of Health, USA)[221]. Fabry mice are α-Galactosidase A-deficient mice, bred on a 129S4/SvJae X C57BL/6 background and originally generated by replacing exon 3 and intron 3 of the galactosidase alpha (*Gla*) gene with a neomycin resistance cassette, abolishing gene expression. Hemizygous male mice have abnormal kidney and liver morphology, with accumulation of globotriaosylceramide, mild cardiomyopathy and abnormal cardiovascular physiology[221]. Animals were sacrificed with a lethal dose of pentobarbital (200 mg/kg), intracardially perfused with PBS at 4°C and brains were collected and fast frozen by Claire Smith (Genotyping Research Technician in the Platt group, Department of Pharmacology, University of Oxford). Brains from 52.1 weeks old

male Fabry mice were used for optimization of the protocol for quantification of glucosylceramide (**Chapter 3**).

2.1.2. SOD1^{G93A} ALS mouse model

Experiments on the SOD1^{G93A} mouse model were performed by Dr Melissa Bowerman (Department of Physiology, Anatomy & Genetics, University of Oxford). This mouse model of ALS is maintained on a C57BL/6 background and expresses a G93A mutant form of human SOD1, with a single amino acid substitution of glycine to alanine at codon 93, regulated by its endogenous *SOD1* promoter. SOD1^{G93A} mice have a reduced survival (4-5 months), becoming paralysed in one or more limbs due to loss of motor neurons from the spinal cord[151]. No gender differences were observed on the median survival of these mice[222]. In the experiments performed, mice were considered asymptomatic at 30 days of age, pre-symptomatic at 84 days (just before the appearance of the first symptoms) and symptomatic at 140 days (**Figure 2.1**). Gastrocnemius and tibialis anterior (TA) muscles from 30, 84 and 140 days old female SOD1^{G93A} mice and age-matched wild-type (WT) littermates were collected for GSL measurements and lysosomal hydrolase activity assays (**Chapter 4**).

2.1.3. SOD1^{G86R} ALS mouse model

SOD1^{G86R} mouse experiments were performed by Dr Alexandre Henriques (Inserm, U1118, Mécanismes Centraux et Périphériques de la Neurodégénérescence, Université de Strasbourg, France), following current European Union regulations (Directive 2010/63/EU) and after approval by the ethics committee of the University of Strasbourg

(license No. AL/01/20/09/12, AL/02/21/09/12 and AL/ 15/44/12/12). Genotyping of SOD1^{G86R} mice was also performed by Dr Alexandre Henriques according to Ripps and colleagues[223]. The SOD1^{G86R} mouse is another mouse model used to study ALS. They are bred on an FVB/N background and express the missense mutant mouse *Sod1* under the control of the endogenous promoter[223]. The missense mutation is a point mutation in exon 4 resulting in a glycine-86 to arginine substitution, which corresponds to amino acid position 86 in the human SOD1 protein[223]. At 3-4 months of age progressive loss of motor function begins, with limb spastic paralysis and muscle wasting, leading to death at around 4 months of age[223,224]. More specifically, until approximately 75 days of age SOD1^{G86R} mice are referred to as pre-symptomatic because they show no signs of motor impairment. Early symptoms start at ~90 days of age (onset). Mice are considered symptomatic at ~100 days of age, when they show apparent signs of paresis in at least one limb (**Figure 2.1**)[215,225]. Age-matched wildtype FVB/N littermates were used as controls. Mice were sacrificed by decapitation after deep anaesthesia with sodium pentobarbital (120 mg/kg) and intracardially perfused with PBS at 4°C. Lumbar spinal cord and muscles of these mice were dissected, frozen in liquid nitrogen and stored at -80°C. Glycosphingolipid levels were measured in spinal cord and soleus muscles of 90 days old SOD1^{G86R} mice (**Chapter 4**).

Both SOD1^{G86R} and SOD1^{G93A} mouse models express a mutant form of SOD1 which promotes motor neuron degeneration, which results in paralysis in one or more limbs and reduced survival similar to what happens in humans with MND[151,152,223]. However, the SOD1^{G93A} mouse model expresses a mutant form of human SOD1 with a high transgene copy number (producing a great excess of SOD1 protein), which negatively correlates with survival time[151,226]. On the other hand, the SOD1^{G86R} mouse expresses a

mutant form of mouse SOD1 with a smaller number of transgene copies, allowing for the study of the toxic gain of function of mutant SOD1 without the possible interference by extreme overexpression of the mutant protein[223]. Nevertheless, SOD1^{G86R} mice reach symptoms onset and morbid state earlier than SOD1^{G93A} mice (**Figure 2.1**).

2.1.4. TDP-43^{M337V} BAC mouse model

The TDP-43^{M337V} BAC mouse was provided by Prof. Kevin Talbot (Nuffield Department of Clinical Neurosciences, University of Oxford, JAX stock #029266)[227]. The TDP-43^{M337V} is a methionine to valine missense mutation associated with increased low molecular weight aggregates and neuronal dysfunction[227,228]. The TDP-43^{M337V} BAC allele has a *loxP*-flanked, full-length human *TARDBP* genomic locus with the M337V mutation in exon 6 and a C-terminal fluorescent Ypet tag inserted into the Rosa26 (Gt(ROSA26)Sor) locus. In the presence of Cre recombinase the TDP-43^{M337V} BAC sequences are deleted[227–229]. TDP-43^{M337V} BAC mice are considered asymptomatic at 3 months of age, while showing elevated levels of human TDP-43 in cortex and spinal cord. From approximately 6 months of age, they develop progressive weight loss, motor function deficits due to neuromuscular junction abnormalities, with homozygous (TDP-43$^{M337V/M337V}$) mice performing significantly worse than hemizygous (TDP-43$^{M337V/-}$) littermates and the mice die prematurely (**Figure 2.1**)[227]. Animals were housed in pathogen free conditions, but were positive for *Helicobacter* species, including *Helicobacter hepaticus* and *Helicobacter rodentium*, on the health screening. Three, six and nine months-old TDP-43$^{M337V/M337V}$ and 12 months-old TDP-43$^{M337V/-}$ BAC mice were sacrificed with an intraperitoneal (IP) injection of pentobarbital (200 mg/kg), intracardially perfused with PBS at 4°C and tissues

were rapidly dissected and fast frozen in dry ice. Age-matched C57BL/6J littermates were used as non-transgenic controls (NTg, **Chapter 5**). A separate cohort of 6 month old female TDP-43$^{M337V/M337V}$ BAC mice was used to test the effect of edaravone (**Chapter 2.7**). After 5 weeks of treatment and behavioural analysis (**Chapter 2.8**), mice were sacrificed, and liver and brain tissues were collected as before for biochemical analysis (**Chapter 6**).

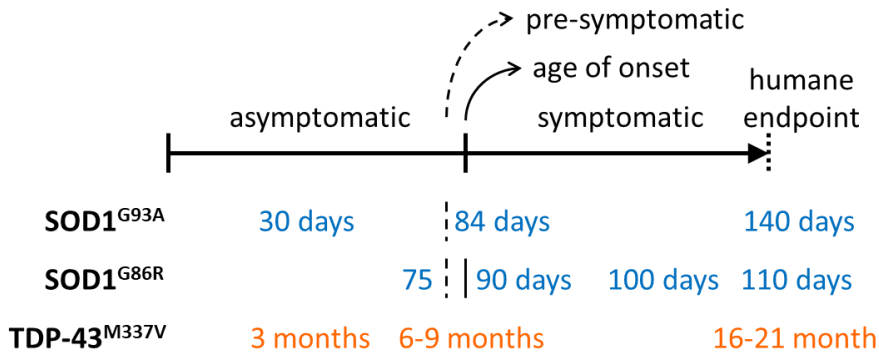


Figure 2.1. Timeline for development of symptoms in the SOD1^{G93A}, SOD1^{G86R} and TDP-43^{M337V} BAC mouse models of ALS.
SOD1^{G93A} mice show no symptoms at 30 days of age, develop symptoms a few days after they are 84 days old and quickly become symptomatic and morbid, at 140 days old. Similarly, the SOD1^{G86R} mice are pre-symptomatic when they are about 75 days old, the first symptoms start at 90 days, they are symptomatic at 100 days and morbid at 110 days old. TDP-43^{M337V} BAC mice are asymptomatic when they are 3 months-old, the onset of symptoms happens between 6 and 9 months, depending on the degree of mutation (heterozygous or homozygous), surviving until they are 16-21 months-old.

2.1.5. Sandhoff disease (*Hexb*$^{-/-}$) mouse model

Sandhoff (*Hexb*$^{-/-}$) mice were provided by Dr Richard L Proia (National Institutes of Health, USA). Sandhoff mice were generated by insertion of a neomycin resistance vector disrupting exon 13 of the hexosaminidase B (*Hexb*) gene and, consequently, no detectable functional protein[230]. Homozygous Sandhoff mice display gangliosidoside storage, with accumulation of GM2 and GA2, developing motor defects from 12 weeks of

age until they reach a humane endpoint at approximately 15 weeks of age[230]. The humane endpoint is applied when the mice became unable to right themselves when laid on their side for 30 s. Sandhoff female mice were used to test the effect of edaravone (**Chapter 2.7**). After treatment and behavioural testing (**Chapter 2.8**), animals were culled when they reached the humane endpoint or at 16 weeks of age. Mice were intracardially perfused with PBS at 4°C, and liver and brain tissue collected and fast frozen in dry ice for biochemical analysis (**Chapter 6**).

2.2. Tissues homogenisation and protein quantification

Brain and spinal cord were homogenised in water (20 mg/mL wet tissue) using an Ultra-Turrax T25 probe homogenizer (IKA, Germany). Muscle was digested using a Precellys® 24 tissue homogeniser (Bertin Instruments, France). Protein was quantified using a commercial bicinchoninic acid (BCA) protein assay kit (Sigma, Cat. No. BCA1)[231]. Briefly, tissue homogenates and protein standards were diluted in MilliQ-H_2O and added to a 96-well plate. A solution of BCA and copper II sulphate was then added. The reaction was left at 37°C for 30 min. Absorbance was measured using a FLUOstar OPTIMA plate reader (BMG Labtech, Ortenberg, Germany) at 562 nm.

2.3. Enzyme assays

Cerezyme® (imiglucerase for injection 400 Units, Genzyme Corporation, Cambridge, MA, USA) and VPRIV® (velaglucerase alfa for injection, Shire Pharmaceuticals Limited, Takeda) were kindly donated by Gaucher disease patients (residual volume of enzyme

remaining in the vials post-IV infusion mailed at room temperature). Specific activity of each batch received was measured with 4-methylumbelliferone (4-MU) assay, where an ester of 4-MU (4-MU β-D-glucoside) is cleaved by an enzyme (recombinant GCase imiglucerase or velaglucerase alfa) to release the fluorescent molecule 4-MU that emits light at 460 nm when excited by 360 nm light. Briefly, the enzyme was incubated with 4.5 mM 4-MU β-D-glucoside in 100 mM citrate and 200 mM sodium phosphate buffer pH 5.2, with 0.25 % TritonX-100 as substrate, at 37°C for 30 min. The reaction was stopped by addition of 0.5 M sodium carbonate pH 10.7 at 4°C. The released 4-MU fluorescence was measured in a FLUOstar OPTIMA plate reader (BMG Labtech, Ortenberg, Germany) at 360 nm excitation and 460 nm emission and a standard curve of free 4-MU was used to calculate enzyme activity.

2.4. Quantification of glycosphingolipids (NP-HPLC)

Svennerholm extraction of glucosylceramide and downstream glycosphingolipids was performed as previously described[215,216,232]. Lipids were extracted from tissue homogenates with chloroform/methanol (C:M) 1:2 (v/v) overnight at 4°C. For purification, the mixture was centrifuged (1,600 G for 10 min at room temperature), PBS and chloroform were added to the supernatant and the mixture was centrifuged once more (1,600 G for 10 min at room temperature). The lower phase was dried under a stream of nitrogen in a dry block heater at 42°C, re-suspended in C:M 1:3 (v/v) and combined with the upper phase. Total GSLs were loaded onto solid-phase C18 SPE columns 100 mg/1 mL (Telos, Kinesis, UK), pre-equilibrated with methanol and Milli-Q water. Samples were washed with Milli-Q water and eluted with C:M 98:2, C:M 1:3 (v/v)

and methanol. After elution, GSL fractions were split in half, dried down under a stream of nitrogen at 42°C and treated with either imiglucerase, to release glucose from GlcCer (this reaction is discussed and optimised in **Chapter 3**), or the recombinant EndoGlycoCeramidase I (recEGC'ase I, a ceramide glycanase extracted from *E. coli* and kindly donated by Orphazyme, Copenhagen, Denmark) to obtain oligosaccharides from other GSLs.

Released oligosaccharides (glucose and more complex glycans) were fluorescently labelled with anthanillic acid (2AA). To remove excess free label, samples were diluted in acetonitrile:Milli-Q water (97:3 v/v) and separated in Discovery DPA-6S SPE columns 50 mg/1 mL (Supelco, PA, USA), pre-equilibrated with acetonitrile, Milli-Q water and acetonitrile. Columns were washed with acetonitrile:Milli-Q water 95:5 (v/v) and eluted with Milli-Q water.

Purified 2AA-labeled glucose and 2AA-labeled oligosaccharides were separated and quantified by normal-phase high-performance liquid chromatography (NP-HPLC), with a Waters Alliance 2695 separations module and an in-line Waters 2475 multi λ-fluorescence detector, set at 360 nm excitation and 425 nm emission. The solid phase on the NP-HPLC system was a 4.6 x 250 nm TSK gel-Amide 80 column kept at 30°C (Anachem, Luton, UK). The mobile phases were acetonitrile (solvent A), Milli-Q water (solvent B) and 100 mM ammonium acetate hydroxide pH 3.85 (solvent C). Samples run for 60 min, with a chromatographic flow rate of 0.8 mL/min. Starting conditions were of 71.6 % solvent A, 8.4 % solvent B and 20 % solvent C. Over the first 40 min, solvent B gradually increased to 57 %, and then, from 41 to 60 min, 71.6 % solvent A was used. With each NP-HPLC data set, a standard of 2AA-labelled glucose homopolymer ladder (Ludger, UK) was also run to further calculate the glucose units of each individual peak,

corresponding to the different identified GLS species. Finally, results were normalised to wet weight or protein content.

2.5. Preparation of liposomes

Liposomes were prepared as previously described[233–235]. Briefly, 5 mol% cholesterol and 95 mol% dipalmitoylphosphatidylcholine (DOPC) were mixed in C:M 2:1 (v/v). The solvent from the resulting solution was evaporated under a stream of nitrogen in a dry block heater at 42°C. The lipid mixture was hydrated in 20 mM citrate buffer, pH 4.5, containing 150 mM NaCl to a final lipid concentration of 4 µmol/mL. The mixture was vortexed, sonicated at 120 W for 20 s in a Vibra-Cell™ ultrasonic liquid processor CV33 (Sonics and Materials, Inc, CT, USA) on ice and subjected to eight freeze-thaw cycles, using liquid nitrogen and a dry block heater (at 42°C).

2.6. Lysosomal enzyme assays

Lysosomal enzyme activities were measured using artificial substrates containing the fluorophore 4-MU[236], similar to what was described in section 2.3. Tissue homogenates in PBS with 0.1 % Triton X-100 and an artificial 4-MU substrate were incubated at 37°C for 30 min (60 min for β-galactosidase, 2 h for neuraminidases). Specifically, the substrate used to measure α-galactosidase activity was 5 mM 4-MU α-D-galactoside in 100 mM sodium citrate buffer pH 4.0, with 0.1 % Triton X-100. For β-galactosidase activity, 1 mM 4-MU β-D-galactopyranoside in 200 mM sodium acetate buffer pH 4.3, with 100 mM NaCl, 0.1 % Triton X-100 was used. To distinguish between

the lysosomal GBA β-glucosidase and non-lysosomal GBA2 activities, samples were incubated in the presence or absence of 1 mM *N*-Butyldeoxygalactonojirmycin (NB-DGJ, lucerastat) for 30 min on ice prior to the assay, as previously described[236,237]. Briefly, NB-DGJ does not affect GBA activity and exclusively inhibits GBA2 (IC_{50} = 1-6 μM), so GBA activity was defined as the NB-DGJ non-sensitive activity (activity in the presence of NB-DGJ) at pH 5.2 (GBA is a lysosomal enzyme with pH optimum 3.5-5.5) and GBA2 activity was defined as the NB-DGJ sensitive activity ((total activity) – (activity in the presence of NB-DGJ)) at pH 5.5 (GBA2 is a non-lysosomal enzyme with pH optimum 5.5-6.0)[236,237]. Therefore, for GBA β-glucosidase activity the substrate used was 4.5 mM 4-MU β-D-glucoside in 100 mM citrate and 200 mM sodium phosphate buffer pH 5.2, with 0.25 % TritonX-100, 0.25 % sodium taurocholate, 1.25 mM EDTA and 4 mM 2-mercaptoethanol. For GBA2 β-glucosidase activity, 4.5 mM 4-MU β-D-glucoside in 100 mM citrate and 200 mM sodium phosphate buffer pH 5.5, with 0.1 % Triton X-100 was used as a substrate. For β-hexosaminidase activity, the substrate used was 3 mM 4-MU *N*-acetyl-β-D-glucosaminide dihydrate in 100 mM citrate and 200 mM sodium phosphate buffer pH 4.5, with 0.1 % Triton X-100. For neuraminidases (Neu1, Neu3 and Neu 4) activity, 0.8 mM 4-MU *N*-acetylneuraminic acid in 0.1 M acetate buffer pH 4.6, with 0.1 % Triton X-100 was used as a substrate. Reactions were stopped by addition of 0.5 M sodium carbonate pH 10.7 at 4°C. The released 4-MU fluorescence was measured in a FLUOstar OPTIMA plate reader (BMG Labtech, Ortenberg, Germany) at 360 nm excitation and 460 nm emission. A standard curve of free 4-MU was used to calculate the enzyme activity and results were normalised to protein on each sample[236].

2.7. Drug administration

Edaravone (Edastar) 1.5 mg/mL 20 mL was obtained from Lupin Ltd, India (BDR Pharmaceuticals International Pvt. Ltd). Female Sandhoff (*Hexb*$^{-/-}$) mice were treated intraperitoneally (i.p.) with 15 mg/kg per day of edaravone (or equivalent volume of PBS for controls), from Monday to Friday, from 3 weeks of age (weaning) to 16 weeks or humane endpoint. TDP-43$^{M337V/M337V}$ BAC female mice were also treated with 15 mg/kg per day of edaravone or PBS, Monday to Friday, from 6 months of age (early symptomatic), for 5 weeks. Mice weight was recorded from the beginning of the treatment onwards (**Chapter 6**).

2.8. Mouse behavioural analysis

2.8.1. Rotarod

A 47650 Mouse RotaRod NG apparatus (Ugo Basile®) was used for rotarod experiments, weekly, from 6 weeks of age for Sandhoff mice and from 6 months of age for TDP-43$^{M337V/M337V}$ BAC mice[227]. In each trial, the mouse was held by the tail and placed on the still rod, facing the direction of rotation. The rotarod was then activated with increasing speed from 5 to 50 rpm, gradually, over a 300 s period. Animals were trained for 10 s on the rotating rod before the experimental trial. When each mouse fell off the rod into the trip-box, the rotarod software recorded the time to fall (latency), the speed of the rotarod at the time of the fall, the number of revolutions and the travelled distance.

2.8.2. Manual rearing

Mice were placed in an open field box for 2 minutes for habituation and 5 minutes of testing[238]. A side rear was recorded when mice reared on hind legs using the side of the cage as support. A centre rear was recorded when mice reared on hind legs un-aided. Rearings where the mouse fell over were discounted[238]. This was performed in TDP-43$^{M337V/M337V}$ BAC mice, following 5 weeks of edaravone treatment.

2.8.3. Gait analysis

Motor coordination and gait were measured in TDP-43$^{M337V/M337V}$ BAC mice using the footprint pattern test following 5 weeks of edaravone treatment[239]. Each mouse was placed individually, with its hind paws painted red and front paws painted blue, at the end of an approximately 60 cm long open-roofed tunnel, lined with white paper and facing a dark enclosure at the opposite end. The distance between each stride, hind-base width between the hind paws, front-base width between the front paws and forepaw/hindpaw overlap were measured from multiple footprints per mouse and mean values calculated per group.

2.8.4. Horizontal bar crossing

Briefly, a metal bar (0.12 x 26 cm) was suspended horizontally between two wooden supports 30 cm high over a cushioned surface[240]. The animal was held by the tail and allowed to grasp the centre of the bar with forepaws only, the tail was released, and the clock started. Latency to cross or fall from the bar was scored, with 120 s maximum,

to termination of each trial. A score was given to each animal between -120 and 120. If crossing time (CT) was greater than 0, then score = 120 - CT. If falling time (FT) was greater than 0, the score = FT - 120[240]. This test was performed on Sandhoff mice once a week from 6 weeks of age, the typical age of appearance of the first disease symptoms, onwards.

2.9. Statistical analysis

Data were plotted in Excel (Microsoft Office 365 ProPlus, USA). All statistical analysis was performed using GraphPad Prism v6.07 (GraphPad Software Inc., California, USA). Error bars represent ±SD. Differences with *p*-values of <0.05 were considered significant. Statistical tests and post-hoc analysis are detailed in the results section of each chapter.

3. Measuring glucosylceramide (GlcCer): protocol optimisation

3.1. Introduction

3.1.1. GlcCer

Glucosylceramide or GlcCer is the simplest GSL, composed of one glucose residue linked to a single ceramide moiety. GlcCer is synthesised on the external leaflet of the early Golgi apparatus by the activity of the enzyme glucosylceramide synthase (GCS), which transfers a glucose unit to the acceptor ceramide[241]. GlcCer is the precursor of lactosylceramide (LacCer) and almost all GSLs, with the exceptions of galactosylceramide (GalCer) generated by GalCer synthase and its derivatives such as digalactosyl ceramide and sulfatides[64]. Together with other GSLs, GlcCer is found at the plasma membrane and is mainly internalised by endocytosis and degraded in the lysosome by β-glucocerebrosidase (GCase)[242,243]. Importantly, the accessory protein saposin C and a specific lipid micro-environment are essential for GCase activity and GlcCer hydrolysis in cells, as saposin C is thought to promote changes in the lipid bilayer facilitating the interaction of the enzyme GCase with its substrate GlcCer and strongly potentiate its hydrolysis[233,244–246].

The metabolism of GlcCer and other GSLs is tightly regulated and essential for lipid homeostasis. When GSL synthesis is abolished in mice, embryonic development and differentiation of some tissues does not occur, which suggests GSLs are essential for embryogenesis and organogenesis[30]. Also, in the absence of GlcCer and all GlcCer-derived

GSLs specifically in neural cells, mice develop severe neural defects after birth, dying approximately 3 weeks after birth[247]. However, the study of mutant cells deficient in GCS revealed that GlcCer based GSLs are not essential for cells viability and growth[32,33]. This was further confirmed by the absence of toxicity when GSL levels were significantly reduced (50-70 %) in young mice after treatment with *N*-butyldeoxynojirimycin[248].

There are, however, mutations which lead to GlcCer dysregulation and disease. Gaucher disease is a rare inherited disease, the second most common of the lysosomal storage diseases (LSDs), affecting 1 in every 40,000 to 100,000 births worldwide and 1 in 800 to 1,000 in the Ashkenazi Jewish population[63]. Gaucher disease is caused by mutations in the *GBA1* gene which result in the impairment of GCase activity, and the systemic accumulation of GlcCer in macrophages that transform into Gaucher cells[64]. Gaucher disease is subdivided into three forms: type 1 affects peripheral tissues, with no involvement of the CNS (hepatosplenomegaly, haematological defects and bone disease are the characteristic features of this disease); type 2 is acute neuronopathic, manifesting in early infancy; and type 3 can be neuronopathic or affect peripheral tissues[5,63]. Deficiency of saposin C in humans also causes a variant form of Gaucher disease characterized by accumulation of GlcCer in the macrophages and CNS[65–67]. Also, importantly, *GBA1* haploinsufficiency and subsequent reduction of GCase activity is one of the most common genetic risk factors for Parkinson's disease[68–71]. GBA activity was shown to be reduced, with consequent GSLs accumulation, in the post-mortem midbrain tissue of human sporadic cases[236]. Furthermore, GlcCer levels were shown to be elevated in the brain of healthy aged mice, possibly constituting a predisposition for Parkinson's and other neurodegenerative aging-associated diseases[249]. Additionally, a case report described a patient diagnosed with type 3 Gaucher disease and, a few years later, with

MND, suggesting a potential link between the two diseases and, importantly, between accumulation of GlcCer and motor neuron degeneration[250].

3.1.2. GlcCer and MND

The involvement of GSL metabolism in motor neuron disease pathogenesis has recently been investigated[211,251]. GCS expression was found to be elevated in muscle of ALS patients when compared to control subjects, suggesting an increase in GlcCer synthesis[215]. In line with those findings, GlcCer accumulation and increased GBA activity were found in the spinal cord of ALS patients[214]. Furthermore, a lipidomics study found elevated levels of sphingomyelin (SM) and GlcCer in the cerebrospinal-fluid (CSF) of ALS patients[220].

GSL metabolism has also been examined in various MND mouse models. Accordingly, high levels of GlcCer were measured in the spinal cord of $SOD1^{G93A}$ mice and it was observed that inhibition of GlcCer (and other GSLs) synthesis accelerated disease progression (while GM3 intracerebroventricular infusion slowed disease progression)[214]. However, in spinal cord of $SOD1^{G86R}$ mice, GlcCer levels were shown to decrease with age similarly to their corresponding wild-type (WT) controls[215]. Indeed, GBA2 (non-lysosomal GCase) activity was increased in the spinal cord of these mice, but not GBA1 (lysosomal GCase)[218]. However, GlcCer and GCS expression were significantly higher in skeletal muscle of the $SOD1^{G86R}$ mice[215]. Additionally, inhibition of GCase activity in early symptomatic $SOD1^{G86R}$ mice improved the integrity of motor units, promoted neuroprotection and delayed disease progression (**Table 3.1**Error! Reference source not found.)[216].

 **ALS patients**	**CSF**	↑ GlcCer and SM[220]
	Spinal cord	↑ GlcCer & GBA activity[214]
	Muscle	↑ GCS expression[215]
 **SOD1^{G86R} mice**	**Spinal cord**	↑ GBA2[218]
	Muscle	↑ GlcCer & GCS expression[215] GCase inhibition ↑ motor units integrity ↑ neuroprotection and ↓ disease progression (early symptomatic)[216]
 **SOD1^{G93A} mice**	**Spinal cord**	↑ GlcCer[214] GCS inhibition ↑ disease progression GM3 intracerebroventricular infusion ↓ disease progression[214]
 **WT mice**	**Spinal cord**	Peripheral nerve injury ↑ GCS activity, GlcCer levels Peripheral nerve injury & GCS inhibition ↓ GlcCer levels & motor function regeneration[215]
⇨ GlcCer seems to modulate disease progression and changes in GBA activity appear to work as a compensatory mechanism, slowing it down.		

Table 3.1. GlcCer in motor neuron disease: a summary of what is known so far.

Finally, using a different approach, surgical peripheral nerve injury of WT mice promoted a significant increase in GCS activity and GlcCer levels, but inhibition of GCS following muscle denervation decreased GlcCer levels by 33 % and delayed motor function regeneration (**Table 3.1**)[215].

Together, these data suggest that GlcCer modulates disease progression in MND and changes in GBA activity might reveal a compensatory mechanism to slow it down[211,252]. In order to further study the role of GlcCer in MND and to quantify GlcCer in other tissues from other MND mouse models, a robust GlcCer quantification assay had to be developed and is the focus of this chapter.

3.1.3. GlcCer quantification

For GSL quantification by NP-HPLC, lipids must be first isolated and purified, then the linkage between the oligosaccharide and ceramide moiety needs to be cleaved in order to release the carbohydrate head group and subsequently fluorescently label the oligosaccharides for further separation and quantification. Recombinant endoglycoceramidase II (rEGCase II) is the enzyme used for GSL quantification by NP-HPLC. rEGCase II cleaves the linkage between oligosaccharides and ceramides of acidic and neutral GSLs, but it is inefficient at degrading monohexosyl GSLs, including GlcCer[253]. Therefore, in order to develop a HPLC assay to measure GlcCer, GCase is the enzyme necessary to efficiently release glucose from ceramide.

Imiglucerase and velaglucerase alfa are two EMA/FDA approved recombinant forms of GCase used as enzyme replacement therapy (ERT) in type 1 and type 3 Gaucher disease patients (**Figure 3.1**)[84–86].

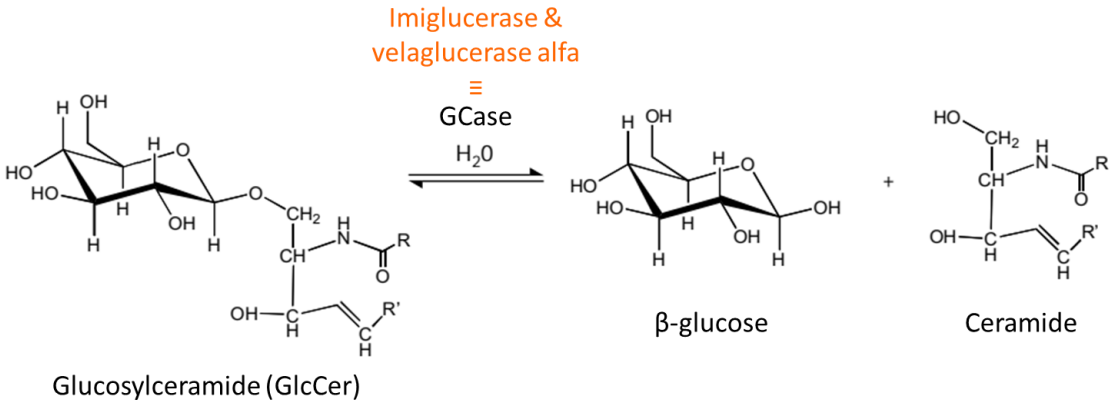


Figure 3.1. Schematic representation of GlcCer hydrolysis by GCase and its recombinant forms imiglucerase and velaglucerase alfa, to release glucose and ceramide[254].

To study the specific role of GlcCer in MND, a protocol for GlcCer quantification was therefore developed using GCase. The same protocol for GSL isolation and purification,

and later labelling of the glucose units was used (described in **Chapter 2**). However, the specific conditions for efficient and complete enzymatic digestion by imiglucerase and/or velaglucerase alfa had to be determined and optimised.

3.1.4. Aims

In this chapter, an established protocol for GSL isolation and quantification by NP-HPLC was used as a starting point to determine the best enzyme and specific conditions for the efficient and complete enzymatic digestion of GlcCer by imiglucerase and/or velaglucerase alfa, to achieve accurate quantification of GlcCer.

3.2. Results

For optimisation of the *in vitro* hydrolysis of GlcCer, GSLs were extracted from whole brain tissue of Fabry disease male mice. Fabry disease is an X-linked LSD caused by α-galactosidase A deficiency and progressive accumulation of globotriaosylceramide (Gb3) but with normal levels of GlcCer, which is why α-galactosidase A knock-out (Fabry disease) mice were used here[62,221]. Brain tissue was used because it typically has high and consistent levels of GlcCer, easily detectable by HPLC and because this protocol was meant to be used primarily in brain and spinal cord tissues.

The extraction method used was the same used to isolate and purify complex GSLs (**Chapter 2**). Firstly, GSLs from 2.5 mg of wet whole brain tissue were incubated at 37°C with 5 µL of imiglucerase (Cerezyme®, Genzyme Corporation, Cambridge, MA, USA) or velaglucerase alfa (VPRIV®, Shire Pharmaceuticals Limited, Takeda) and 20 µL of a variety of different buffers (summarised in **Table 3.2**), for 72 h (**Figure 3.2** and **Table S.1**). Both

imiglucerase and velaglucerase alfa were reconstituted in sterile water for injection and kindly donated by Gaucher disease patients in the UK (residual volume of enzyme remaining in the vials post-IV infusion and mailed at room temperature), ranging from one month to one year post-clinical use. Therefore, two batches were tested of each enzyme: 1 month and 1 year post-clinical use (**Figure 3.2**, **Table 3.2** and **Table S.1**). Different buffers were tested in order to find what is/are the best detergent/s to disturb the lipid bilayer of the micelles formed after GSL extraction, and facilitate the access of the recombinant enzymes to hydrolyse GlcCer into glucose and ceramide (**Table 3.2**). Finally, the labelling of the resulting glucose units for GlcCer quantification was also done as described for the quantification of complex GSLs (**Chapter 2**) and GlcCer quantification was normalised to milligrams of wet tissue.

Imiglucerase showed similar activity when comparing vials from 1 month and 1 year (black vs. stripped bars, **Figure 3.2** and **Table S.1**), consistent with long-term stability of the enzyme. However, this was not the case with velaglucerase alfa (green vs. squared bars, **Figure 3.2**). On the other hand, velaglucerase alfa digested more GlcCer than imiglucerase under the same conditions (black vs. green and squared bars, **Figure 3.2** and **Table S.1**). Also, buffers 2 and 3 with Triton X-100 promoted a more complete digestion of GlcCer with both enzymes (buffer 1 vs. buffer 2 and 3, **Figure 3.2** and **Table 3.2**) and there was no additional effect when sodium taurodeoxycholate was added to the mixture (buffer 2 vs. buffer 3, **Figure 3.2** and **Table 3.2**).

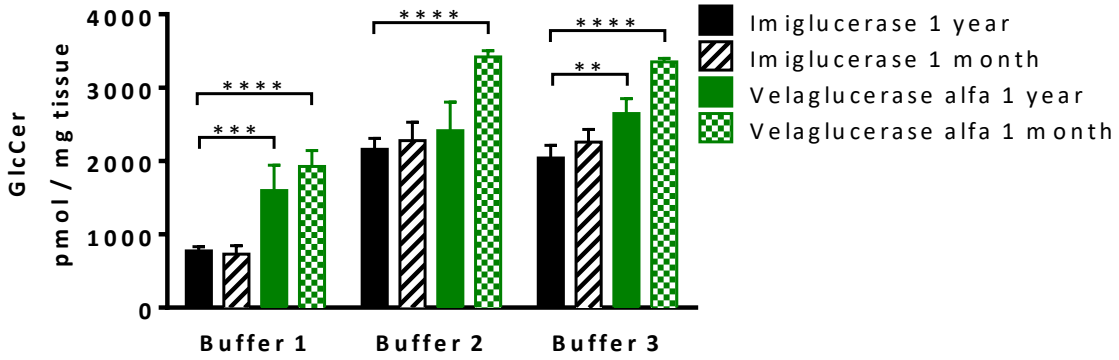


Figure 3.2. Velaglucerase alfa digested more GlcCer than imiglucerase under the same conditions, but only the enzymatic activity of imiglucerase was stable for at least a year after reconstitution.
Quantification of GlcCer from 72 h incubation at 37°C of extracted GSLs from 2.5 mg of brain tissue of Fabry male mice with 5 µL of 1 year (clear) or 1 month old (patterned) **imiglucerase** (black and stipes) or **velaglucerase alfa** (green and squares), and 20 µL of buffer. **Buffer 1**: 50 mM sodium acetate, 0.1 % sodium taurodeoxycholate, pH 5.0. **Buffer 2**: 50 mM sodium acetate, 0.6 % Triton X-100, pH 5.0. **Buffer 3**: 50 mM sodium acetate, 0.6 % Triton X-100, 0.1 % sodium taurodeoxycholate, pH 5.0. Data are presented as the mean ±SD. Data were analysed using 2-way ANOVA, Dunnett's multiple comparisons test. $^{**}p < 0.01$, $^{***}p < 0.001$, $^{****}p < 0.0001$ vs. old imiglucerase (black bars) (**Table S.1**), n = 3.

Imiglucerase	1 year after reconstitution
	1 month after reconstitution
Velaglucerase alfa	1 year after reconstitution
	1 month after reconstitution
Buffer 1	50 mM sodium acetate and 0.1 % sodium taurodeoxycholate, pH 5.0
Buffer 2	50 mM sodium acetate and 0.6 % Triton X-100, pH 5.0
Buffer 3	50 mM sodium acetate, 0.1 % sodium taurodeoxycholate and 0.6 % Triton X-100, pH 5.0

Table 3.2. Summary of enzymes and buffers tested in the first step for GlcCer protocol optimization (Figure 3.2).

Two more buffers were then tested and compared with sodium acetate buffer containing sodium taurodeoxycholate or Triton X-100: a sodium acetate buffer containing 0.1 % sodium taurocholate; and a buffer containing 100 mM citrate, 200 mM phosphate and 0.1 % Triton X-100, pH 5.5 (used to measure GBA and GBA2 β-glucosidase activity, respectively, by 4-MU assay[236,249]) (**Figure 3.3**, **Table 3.3** and **Table S.2**). Simultaneously,

quantification of GlcCer from 1.25 mg and 2.5 mg of wet brain tissue were compared to see if the amount of tissue was a limiting factor in GlcCer quantification (black vs. white bars, **Figure 3.3**).

Sodium taurocholate 0.1 % promoted a better digestion with imiglucerase than sodium taurodeoxycholate 0.1 % (buffer 3 vs. buffer 1, **Figure 3.3** and **Table S.3**), but not 0.6 % Triton X-100 (buffer 2, **Figure 3.3** and **Table S.4**). However, buffer 4 with only 0.1 % Triton X-100 showed little digestion of GlcCer (buffer 4, **Figure 3.3** and **Table S.4**). According to these results, both buffers with 0.6 % Triton X-100 (buffer 2, **Figure 3.3** and **Table S.4**) and with 0.1 % sodium taurocholate (buffer 3, **Figure 3.3** and **Table S.4**) gave the best results for GlcCer digestion of brain tissue. Buffer 2, with 50 mM sodium acetate, 0.6 % Triton X-100, pH 5.0, was the one chosen for further optimisation of this enzymatic reaction. Additionally, quantification of GlcCer from 1.25 mg and 2.5 mg of wet brain tissue was only significantly different when using buffer 3, with 0.1 % sodium taurocholate (black vs. white bars, **Figure 3.3**), so 2.5 mg of wet brain tissue continued to be used.

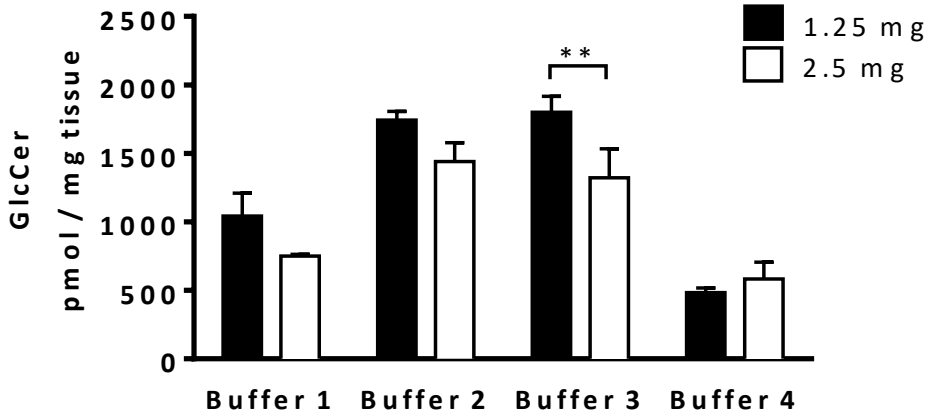


Figure 3.3. Buffer 2, with 50 mM sodium acetate and 0.6 % Triton X-100, pH 5.0, promoted a better digestion of GlcCer by imiglucerase from both 1.25 mg and 2.5 mg of brain tissue than all the other buffers tested.
Quantification of GlcCer from 72 h incubation at 37°C of extracted GSLs from 1.25 mg (black) or 2.5 mg (white) of brain tissue of Fabry male mice, with 5 µL of imiglucerase and 20 µL of buffer. **Buffer 1**: 50 mM sodium acetate, 0.1 % sodium taurodeoxycholate, pH 5.0. **Buffer 2**: 50 mM sodium acetate, 0.6 % Triton X-100, pH 5.0. **Buffer 3**: 50 mM sodium acetate, 0.1 % sodium taurocholate, pH 5.0. **Buffer 4**: 100 mM citrate, 200 mM phosphate, 0.1 % Triton X-100, pH 5.5. Data are presented as the mean ±SD. Data were analysed using 2-way ANOVA, Tukey's multiple comparisons test and adjusted *p* values are presented in **Table S.2**. ** $p < 0.01$, n = 3.

Brain tissue (wet weight)	1.25 mg 2.5 mg
Buffer 1	50 mM sodium acetate and 0.1 % sodium taurodeoxycholate, pH 5.0
Buffer 2	50 mM sodium acetate and 0.6 % Triton X-100, pH 5.0
Buffer 3	50 mM sodium acetate and 0.1 % sodium taurocholate, pH 5.0
Buffer 4	100 mM citrate, 200 mM phosphate and 0.1 % Triton X-100, pH 5.5

Table 3.3. Summary of tissue quantities and buffers tested in the second step for GlcCer protocol optimization (Figure 3.3).

Different concentrations of imiglucerase and velaglucerase alfa were then investigated by changing the volume of buffer (**Figure 3.4**, **Table 3.4** and **Table S.3**) or of enzyme (**Figure 3.5** and **Table 3.5**).

GlcCer digestion decreased with increased dilution of the enzyme, when comparing 20 to 10 or 5 % of enzyme concentrations (corresponding to 5 µL enzyme in 20, 45 or 95 µL of buffer), for both imiglucerase and velaglucerase alfa, which can be explained by a reduced probability of contact between substrate and enzyme. Also, GlcCer values

obtained using imiglucerase (black bars, **Figure 3.4**) or velaglucerase alfa (green bars, **Figure 3.4**) had the opposite pattern to that observed in **Figure 3.2** (black vs. green bars respectively), with imiglucerase being significantly better at digesting GlcCer than velaglucerase alfa. This may be because the two enzymes may require different buffers, as the buffer used here was one that was optimal for imiglucerase (see **Figure 3.3** and **Table 3.3**).

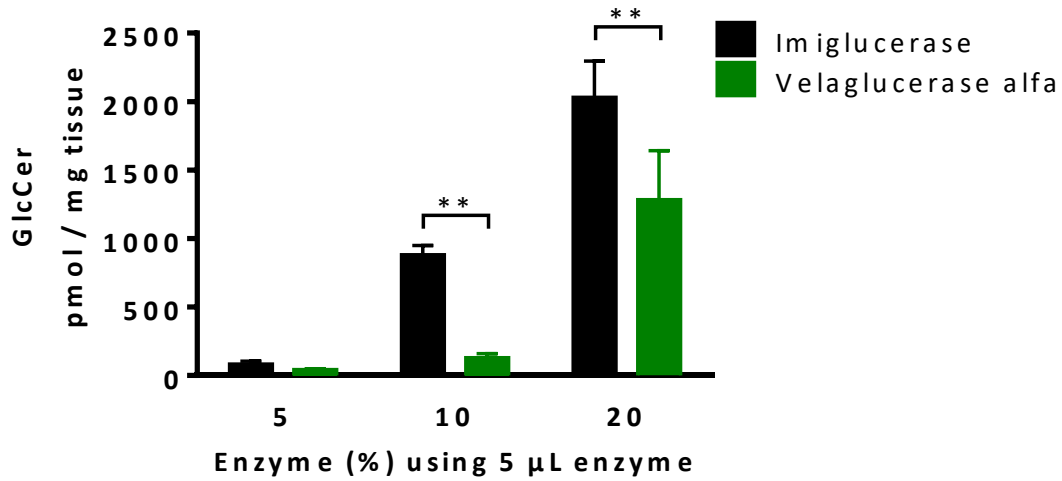


Figure 3.4. GlcCer digestion decreased with the dilution of the enzyme from 20 % to 10 % or 5 % for both imiglucerase and velaglucerase alfa.
Quantification of GlcCer from 72 h incubation at 37°C of extracted GSLs from 2.5 mg of brain tissue of Fabry male mice with 5 %, 10 % and 20 % of imiglucerase (black) or velaglucerase alfa (green) concentration in 50 mM sodium acetate buffer with 0.6 % Triton X-100, pH 5.0. Data are presented as the mean ±SD. Data were analysed using 2-way ANOVA, Tukey's multiple comparisons test and adjusted *p* values are presented in **Table S.3**. ** $p < 0.01$, n = 3.

5 % enzyme	5 µL imiglucerase or velaglucerase alfa plus **95 µL buffer** (50 mM sodium acetate and 0.6 % Triton X-100, pH 5.0)
10 % enzyme	5 µL imiglucerase or velaglucerase alfa plus **45 µL buffer** (50 mM sodium acetate and 0.6 % Triton X-100, pH 5.0)
20 % enzyme	5 µL imiglucerase or velaglucerase alfa plus **20 µL buffer** (50 mM sodium acetate and 0.6 % Triton X-100, pH 5.0)

Table 3.4. Percentages of imiglucerase and velaglucerase alfa concentration used in the third step for GlcCer protocol optimization (Figure 3.4).

Then, in order to test different concentrations of imiglucerase and velaglucerase alfa by changing the volume of enzyme, extracted GSLs from 2.5 mg of brain tissue were incubated at 37°C with 4, 10, 20, 40, 60 and 100 % of enzyme concentration (corresponding to 1, 2.5, 5, 10, 15 or 25 µL of enzyme) in 50 mM sodium acetate buffer with 0.6 % Triton X-100, pH 5.0 (**Figure 3.5** and **Table 3.5**).

Imiglucerase showed increasing values of GlcCer, until it reached a plateau of maximal GlcCer digested per sample in these conditions, at 40 % of enzyme concentration (10 µL enzyme and 15 µL of buffer). However, for increasing concentrations of velaglucerase alfa, GlcCer levels increased in an atypical manner for an enzymatic reaction and were much higher than the ones obtained with imiglucerase (specially for 60 % and 100 % enzyme concentrations), suggesting this enzyme follows very different kinetics or that the intravenous solution contains glucose as one of the excipients, despite not being mentioned on the product characteristics description leaflet (for 4 % enzyme $p = 0.9968$, 10 % $p = 0.1488$, 20 % $p = 0.0559$, and for 40 %, 60 % and 100 % $p < 0.0001$, **Figure 3.5**).

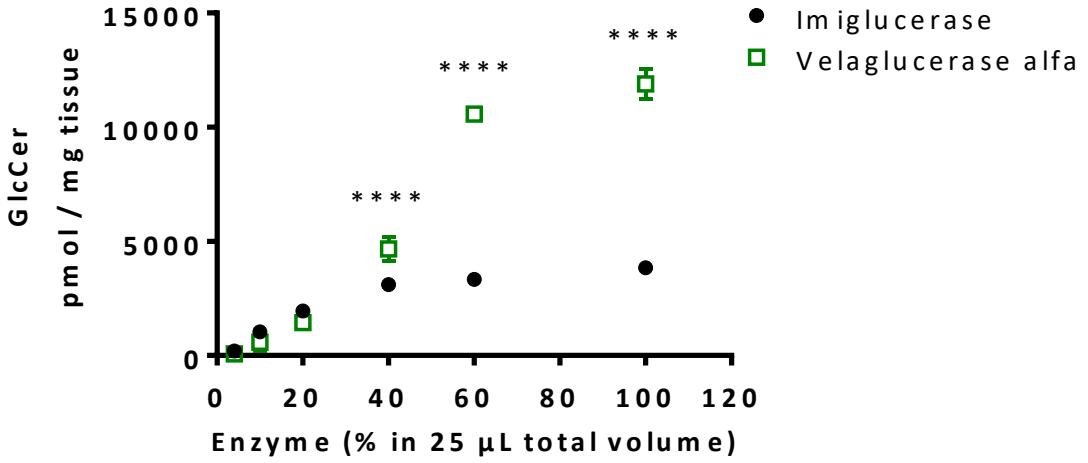


Figure 3.5. GlcCer digestion increased with the concentration of imiglucerase until it reached a plateau at 40 % (10 µL enzyme plus 15 µL buffer), but it kept increasing in an atypical manner with the concentration of velaglucerase alfa.
Quantification of GlcCer from 72 h incubation at 37°C of extracted GSLs from 2.5 mg of brain tissue of Fabry male mice with 4 %, 10 %, 20 %, 40 %, 60 % or 100 % of imiglucerase (black) or velaglucerase alfa (green) concentration in 50 mM sodium acetate buffer with 0.6 % Triton X-100, pH 5.0. Data are presented as the mean ±SD. Data were analysed using 2-way ANOVA, Sidak's multiple comparisons test. ****p < 0.0001 imiglucerase vs. velaglucerase alfa, n = 3-6.

4 % enzyme	**1 µL** imiglucerase or velaglucerase alfa plus 24 µL buffer (50 mM sodium acetate and 0.6 % Triton X-100, pH 5.0)
10 % enzyme	**2.5 µL** imiglucerase or velaglucerase alfa plus 22.5 µL buffer (50 mM sodium acetate and 0.6 % Triton X-100, pH 5.0)
20 % enzyme	**5 µL** imiglucerase or velaglucerase alfa plus 20 µL buffer (50 mM sodium acetate and 0.6 % Triton X-100, pH 5.0)
40 % enzyme	**10 µL** imiglucerase or velaglucerase alfa plus 15 µL buffer (50 mM sodium acetate and 0.6 % Triton X-100, pH 5.0)
60 % enzyme	**15 µL** imiglucerase or velaglucerase alfa plus 10 µL buffer (50 mM sodium acetate and 0.6 % Triton X-100, pH 5.0)
100 % enzyme	**25 µL** imiglucerase or velaglucerase alfa neat

Table 3.5. Quantities of imiglucerase and velaglucerase alfa and buffer used in the fourth step for GlcCer protocol optimization (Figure 3.5).

Subsequently, control samples were run in the absence of tissue extract, with 10 µL of each enzyme neat, with no (T_0) or 72 h of incubation at 37°C, with only 10 µL buffer and with 10 µL of enzyme plus 10 µL of buffer (**Figure 3.6** and **Table 3.6**).

All the samples containing velaglucerase alfa showed high levels of GlcCer, despite no GSL extract being present (black vs. green bars, enzyme neat T_0 p < 0.0001, enzyme

neat 72 h incubation p = 0.0007, buffer only p = 1.0 and enzyme plus buffer p = 0.0020, **Figure 3.6**). This false positive reading indicates that velaglucerase alfa solution contains glucose and cannot be used in this assay. Therefore, imiglucerase is the appropriate enzyme to use for this assay.

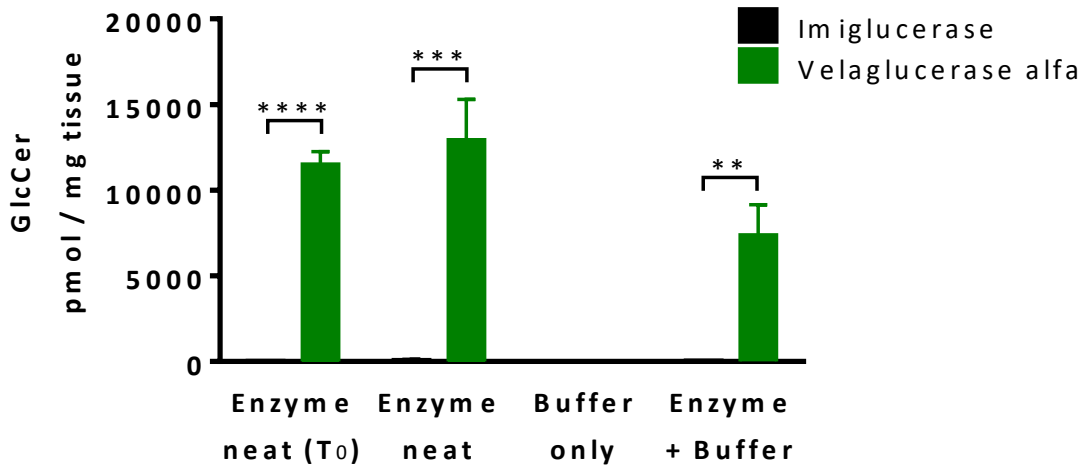


Figure 3.6. All samples containing velaglucerase alfa showed high levels of GlcCer despite no GSL extract being present.
Quantification of GlcCer from the 72 h or no (T_0) incubation at 37°C of 10 µL of imiglucerase (black), velaglucerase alfa (green) or buffer (50 mM sodium acetate, 0.6 % Triton X-100, pH 5.0) or 10 µL of enzyme and 10 µL of buffer. Data are presented as the mean ±SD. Data were analysed using multiple t-tests, with the Holm-Sidak multiple comparisons method. **p < 0.01, ***p < 0.001, ****p < 0.0001, n = 3.

Enzyme neat (T_0)	10 µL imiglucerase or velaglucerase alfa with **no incubation** at 37°C, no buffer or tissue extract
Enzyme neat	10 µL imiglucerase or velaglucerase alfa with **72 h incubation** at 37°C, no buffer or tissue extract
Buffer only	10 µL buffer (50 mM sodium acetate and 0.6 % Triton X-100, pH 5.0), with no incubation at 37°C, no buffer or tissue extract
Enzyme + Buffer	10 µL imiglucerase or velaglucerase alfa and 10 µL buffer (50 mM sodium acetate and 0.6 % Triton X-100, pH 5.0), with no incubation at 37°C or tissue extract

Table 3.6. Different tested conditions in the fifth step for GlcCer protocol optimization (Figure 3.6).

The effect of different concentrations of imiglucerase (10, 20, 40, 60 and 100 %, equivalent to 2.5, 5, 10, 15 and 25 µL of imiglucerase, in a total volume of 25 µL) to digest

GlcCer from various amounts of wet tissue (0.1, 0.25, 0.5, 0.625, 1.25, 2.5 mg) were then tested (**Figure 3.7**, **Table 3.7** and **Table S.4**).

The highest levels of GlcCer per mg of wet tissue were measured for 1.25 mg and 2.5 mg of brain tissue, reaching its maximum when GLSs were incubated for 72 h at 37°C with 60 % imiglucerase (15 µL imiglucerase and 10 µL of buffer, black circles and black squares, **Figure 3.7**). On the other hand, the digestion from 0.625, 0.5, 0.25 and 0.1 mg (grey diamonds and purple circles, squares and diamonds, **Figure 3.7**) showed lower values of GlcCer per mg wet tissue overall, which suggests that using less than 1 mg wet tissue does not allow for a robust quantification of GlcCer. With no significant difference in the amount of GlcCer measured per mg of brain tissue, the digestion of GSLs from 1.25 mg or 2.5 mg of tissue using 15 µL of imiglucerase and 5 µL of buffer (60 %) were the most effective (black circles and black squares, **Figure 3.7** and **Table S.4**). The amount of 1.25 mg of brain tissue and 15 µL of imiglucerase and 5 µL of buffer for the GlcCer digestion were used to continue the protocol optimisation.

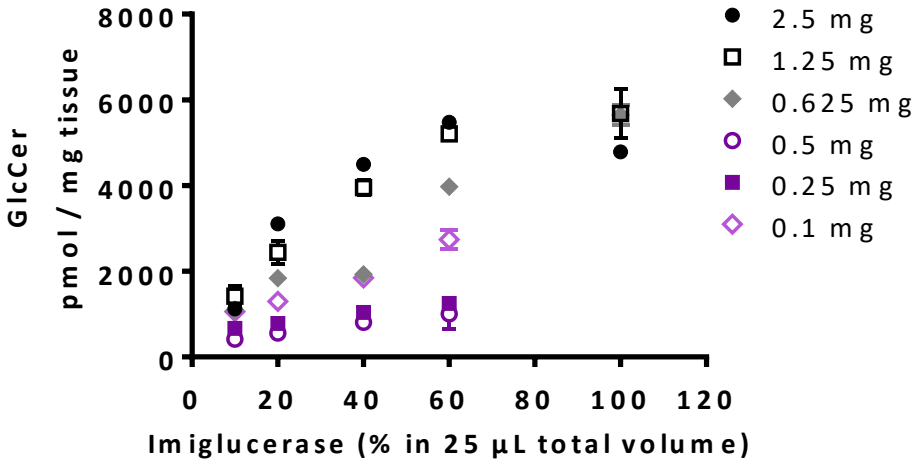


Figure 3.7. GlcCer digestion was most effective when using GSLs extracted from 1.25 mg or 2.5 mg of tissue, and 15 µL imiglucerase and 5 µL buffer (60 %).
Quantification of GlcCer from 72 h incubation at 37°C of extracted GSLs from 2.5 mg (black circles), 1.25 mg (black squares), 0.625 mg (grey diamonds), 0.5 mg (purple circles), 0.25 mg (purple squares) and 0.1 mg (purple diamonds) of brain tissue of Fabry male mice with 10 %, 20 %, 40 %, 60 % and 100 % (or 2.5 µL, 5 µL, 10 µL, 15 µL and 25 µL) of imiglucerase and 50 mM sodium acetate abuffer with 0.6 % Triton X-100, pH 5.0 (adjusted volume for a total of 25 µL). Data are presented as the mean ±SD. Data were analysed using 2-way ANOVA, Tukey's multiple comparisons test (except for 25 µL imiglucerase) and adjusted *p* values are presented in **Table S.4**. n = 3.

Brain tissue (wet weight)	2.5 mg	0.5 mg
	1.25 mg	0.25 mg
	0.65 mg	0.1 mg
10 % imiglucerase	**2.5 µL** imiglucerase plus **22.5 µL** buffer (50 mM sodium acetate and 0.6 % Triton X-100, pH 5.0)	
20 % imiglucerase	**5 µL** imiglucerase plus **20 µL** buffer (50 mM sodium acetate and 0.6 % Triton X-100, pH 5.0)	
40 % imiglucerase	**10 µL** imiglucerase plus **15 µL** buffer (50 mM sodium acetate and 0.6 % Triton X-100, pH 5.0)	
60 % imiglucerase	**15 µL** imiglucerase plus **10 µL** buffer (50 mM sodium acetate and 0.6 % Triton X-100, pH 5.0)	
100 % imiglucerase	**25 µL** imiglucerase neat	

Table 3.7. Different quantities of wet tissue and of imiglucerase tested in the sixth step for GlcCer protocol optimization (Figure 3.7).

Three individual experiments to test different enzymatic incubation times at 37°C were then performed (**Figure 3.8** and **Table 3.8**). For each experiment, all samples were incubated simultaneously with 15 µL of imiglucerase and 5 µL of buffer at 37°C and put

into the freezer at different times for future labelling and HPLC analysis. For the first experiment, incubation periods of 4, 8, 16 h and 1-3 days were tested (run 1, black circles, **Figure 3.8**). After 3 days of incubation, the levels of GlcCer were still increasing, showing that it was not completely digested yet. The same was observed on the second experiment, when 0, 30 min, 1, 2, 4, 8, 16 h and 1-3 days of incubation period were tested (run 2, black squares, **Figure 3.8**). However, when the same experiment was repeated and 0, 30 min, 1, 2, 4, 8, 16 h and 1-10 days incubation periods were tested (run 3, purple diamonds, **Figure 3.8**), the levels of GlcCer seemed to get to a maximum, a plateau, after 2-3 days of incubation.

Taking into account the differences seen between the three experiments, three days (72 h) of incubation at 37°C continued to be used for further optimisation of the protocol.

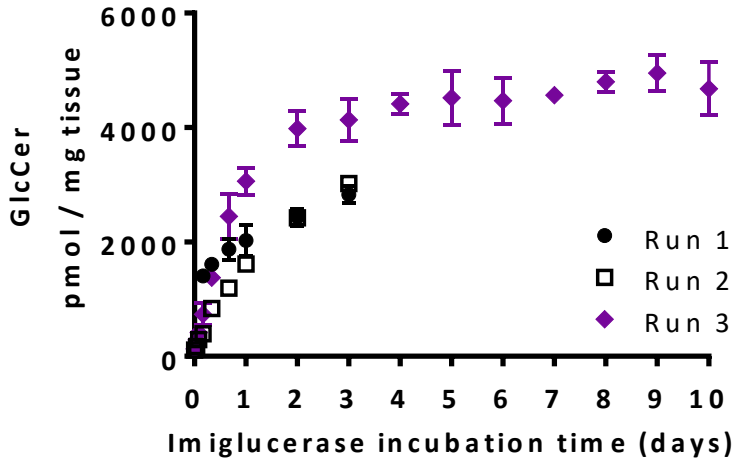


Figure 3.8. The complete enzymatic digestion of GlcCer seemed to take 2-3 days in run 3, but the different results obtained for different runs indicate these are not yet the optimal conditions for the enzymatic reaction to occur.
Quantification of GlcCer from the incubation at 37°C of extracted GSLs from 1.25 mg of brain tissue of Fabry male mice with 15 µL of imiglucerase and 10 µL of buffer (50 mM sodium acetate, 0.6 % Triton X-100, pH 5.0) for 0, 30 min, 1 h, 2 h, 4 h, 8 h, 16 h and 1-10 days. Three runs or experiments are shown individually in black circles, black squares or purple diamonds. Data are presented as the mean ±SD. n = 3.

Incubation period of GSLs (extracted from 1.25 mg of brain tissue) with imiglucerase at 37°C	No incubation	16 h	6 days
	30 min	1 day	7 days
	1 h	2 days	8 days
	2 h	3 days	9 days
	4 h	4 days	10 days
	8 h	5 days	

Table 3.8. Incubation times tested in 3 individual experiments for the seventh step of GlcCer protocol optimization (Figure 3.8).

In the lysosome, *in vivo*, GCase requires the presence of saposin C for optimal activity[233,246]. Thus, the effect of saposin C (1.25 μg per sample) on the enzymatic reaction was evaluated for 0, 30 min, 1, 2, 4, 8, 16 h and 1-4 days of incubation at 37°C (**Figure 3.9**). Blank samples with 15 μL of imiglucerase and 10 μL of buffer and no tissue were also incubated for 0 h, 16 h and 4 days (grey diamonds, **Figure 3.9** and **Table 3.9**)

The presence of saposin C increased significantly the efficacy of the enzymatic reaction, especially for 3 and 4 days of incubation, when compared to the corresponding control conditions, without saposin C (black squares vs. circles, for 0 min p = 0.3820, 30 min p = 0.2278, 1 h p = 0.8626, 2 h p = 0.2564, 4 h p = 0.0130, 8 h p = 0.0046, 16 h p = 0.0152, 1 day p = 0.0269, 2 days p = 0.0272, 3 days p = 0.0009, 4 days p = 0.0001, **Figure 3.9**). However, the velocity of the reaction did not seem to have changed and maximum levels of GlcCer digestion were not achieved (it did not reach a plateau, **Figure 3.9**).

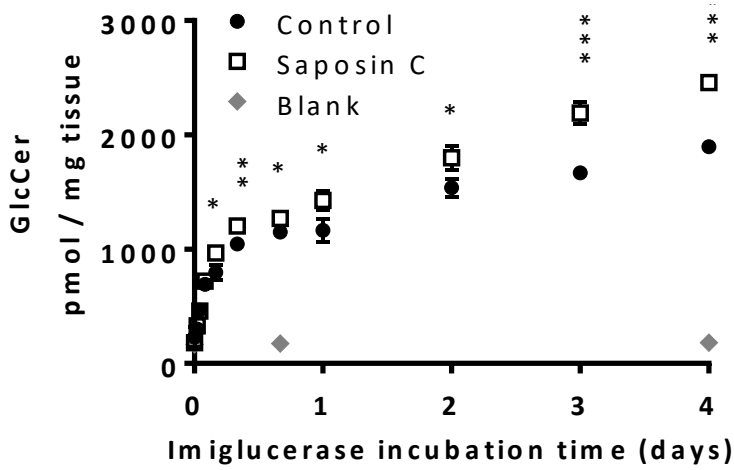


Figure 3.9. Saposin C significantly increased the efficacy of the enzymatic digestion of GlcCer, but it did not contribute for a faster or complete enzymatic reaction.
Quantification of GlcCer from the incubation at 37°C of extracted GSLs from 1.25 mg of brain tissue of Fabry male mice with 15 µL of imiglucerase, 2.36 µL saposin C (1.25 µg, black squares) and adjusted volume of buffer (50 mM sodium acetate, 0.6 % Triton X-100, pH 5.0) for a total of 25 µL, for 0, 30 min, 1 h, 2 h, 4 h, 8 h, 16 h and 1-4 days. Blank samples had 15 µL of imiglucerase and 10 µL of buffer but no tissue and were incubated for 0 h, 16 h and 4 days (gray diamonds). Data are presented as the mean ±SD. Data were analysed using multiple t-tests and corrected for multiple comparisons using the Holm-Sidak method. *$p < 0.05$, **$p < 0.01$, ***$p < 0.001$ vs. corresponding controls (black circles), n = 3.

Control	15 µL imiglucerase plus 10 µL buffer (50 mM sodium acetate and 0.6 % Triton X-100, pH 5.0)	
Saposin C	15 µL imiglucerase, 2.36 µL saposin C (1.25 µg) plus 7.64 µL buffer (50 mM sodium acetate and 0.6 % Triton X-100, pH 5.0)	
Blank	15 µL imiglucerase plus 10 µL buffer (50 mM sodium acetate and 0.6 % Triton X-100, pH 5.0), no tissue extract	
Incubation period of GSLs (extracted from 1.25 mg of brain tissue) with imiglucerase at 37°C	No incubation	16 h
	30 min	1 day
	1 h	2 days
	2 h	3 days
	4 h	4 days
	8 h	

Table 3.9. Different conditions used to test the effect of saposin C in the eighth step for GlcCer protocol optimization (Figure 3.9).

When the ratio of imiglucerase and buffer (50 mM sodium acetate, 0.6 % Triton X-100, pH 5.0) used was changed from 5 µL of enzyme and 20 µL buffer to 15 µL of enzyme and 10 µL buffer (after the results shown on **Figure 3.7**), the pH of the solution

was also changed from about pH 5 to pH 6. Physiologically, GlcCer can be degraded in the cytosol by GBA2 (pH optimum 5.5-6.0), but it is primarily degraded in the lysosome by GBA1 (pH optimum 3.5-5.5). For that reason, the same buffer composition was tested again but at pH 4.5, for a final pH of 5.2 (**Figure 3.10** and **Table 3.10**).

In vivo, hydrolysis of GlcCer by GCase occurs in the lysosome within a lipidic environment. Hence, we also tested the effect of the addition of saposin C and both saposin C and liposomes (8 nmol, prepared with cholesterol and di-oleoyl phosphatidyl choline[233]) to the enzymatic reaction (patterned and white bars, **Figure 3.10**). A set of samples with saposin C and saposin C and liposomes with no tissue were run as controls (but not included in the analysis).

When incubating GSLs extracted from brain tissue with 15 µL of imiglucerase and 10 µL of buffer at 37°C for 16 h (the 72 h period was shortened for practical reasons), the change for a more acidic pH of 5.2 resulted in significantly higher levels of GlcCer than at pH 6.0 for control conditions (black bars, p = 0.0162, **Figure 3.10**), in the presence of saposin C (patterned bars, p = 0.0002, **Figure 3.10**) and both saposin C and liposomes (white bars, p = 0.0056, **Figure 3.10**). At pH 6.0, saposin C alone did not improve the enzymatic reaction efficiency (p = 0.5810), but the combination of saposin C and liposomes improved it significantly (p = 0.0285, **Figure 3.10**). Nevertheless, at pH 5.2 (optimal for *in vitro* GlcCer degradation, see **Figure 3.12**), the presence of saposin C improved significantly the enzymatic reaction efficiency at 16 h of incubation (p = 0.0067), with the addition of liposomes showing no further benefit (p = 0.0098, **Figure 3.10**).

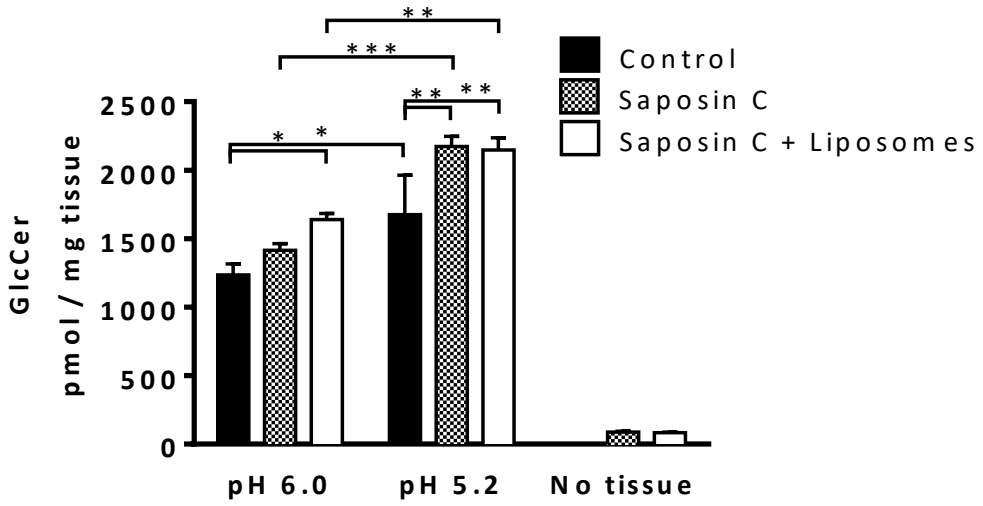


Figure 3.10. After 16 h, the enzymatic digestion of GlcCer by imiglucerase was more efficient in the presence of saposin C at pH 5.2 than at pH 6.0, and the addition of liposomes to the reaction did not show any further benefit.
Quantification of GlcCer from 16 h incubation at 37°C of extracted GSLs from 1.25 mg of brain tissue of Fabry male mice with 15 µL of imiglucerase (control, black bars), 2.36 µL saposin C (1.25 µg, patterned and white bars), 2 µL liposomes (8 nmol, white bars) and adjusted volume of buffer (50 mM sodium acetate, 0.6 % Triton X-100, pH 5.0 or 4.5) for a total of 25 µL. Samples with saposin C and saposin C + liposomes with no tissue were run as controls (but not included in the analysis). Data were analysed using 2-way ANOVA, Tukey's multiple comparisons test. *$p < 0.05$, **$p < 0.01$, ***$p < 0.001$, n = 3.

Control	15 µL imiglucerase plus 10 µL buffer (50 mM sodium acetate and 0.6 % Triton X-100, pH 5.0 or 4.5)
Saposin C	15 µL imiglucerase, 2.36 µL **saposin C** (1.25 µg) plus 7.64 µL buffer (50 mM sodium acetate and 0.6 % Triton X-100, pH 5.0 or 4.5)
Saposin C + Liposomes	15 µL imiglucerase, 2.36 µL **saposin C** (1.25 µg), 2 µL **liposomes** (8 nmol) plus 5.64 µL buffer (50 mM sodium acetate and 0.6 % Triton X-100, pH 5.0 or 4.5)
Reaction pH 6.0	Buffer (50 mM sodium acetate and 0.6 % Triton X-100) at **pH 5.0**
Reaction pH 5.2	Buffer (50 mM sodium acetate and 0.6 % Triton X-100) at **pH 4.5**
No tissue	Buffer (50 mM sodium acetate and 0.6 % Triton X-100) at pH 5.0, but with **no tissue extract**

Table 3.10. Different conditions used to test the effect of saposin C and liposomes in the nineth step for GlcCer protocol optimization (Figure 3.10).

Additionally, GlcCer from 1.25 mg of brain tissue was quantified for an enzymatic reaction with 15 µL of imiglucerase and 10 µL of buffer (50 mM sodium acetate, 0.6 % Triton X-100, pH 4.5 or 5.0) in order to evaluate the effect of a final pH of 5.2 vs. pH 6.0

for different incubation periods (0, 30 min, 1, 2, 4, 8, 16 h and 1-4 days) at 37°C (**Figure 3.11** and **Table 3.11**).

For both pH 5.2 and pH 6.0, GlcCer hydrolysis seemed to happen until it reached a maximum plateau after 1 day of incubation for pH 5.2 and 2 days for pH 6.0, but the digestion at pH 6.0 was never complete (for 0 min $p = 0.2071$, 30 min $p = 0.0015$, 1 h $p < 0.0001$, 2 h $p = 0.0007$, 4 h $p = 0.0013$, 8 h $p = 0.0154$, 16 h $p < 0.0001$, 1 day $p = 0.0136$, 2 days $p = 0.0227$, 3 days $p = 0.0239$, 4 days $p = 0.0149$, **Figure 3.11**). As observed in **Figure 3.10**, the samples incubated for 16 h at pH 5.2 show significantly higher values and, therefore, a more efficient hydrolysis of GlcCer, than for pH 6.0. This significant difference was measured just after 30 min incubation and sustained for the 4 experimental days of incubation (**Figure 3.11**).

Because the plateau was reached after 1 day of incubation for pH 5.2, earlier than for pH 6.0 (2 days), like previously seen on **Figure 3.8** (2-3 days), and the presence of saposin C, where a plateau was never reached (**Figure 3.9**) but consistent to the 16 h incubation (**Figure 3.10**), a compromise was made and an incubation period of 2 days (48 h) was chosen, without the addition of saposin C to the samples, as the best conditions for an efficient and complete GlcCer hydrolysis.

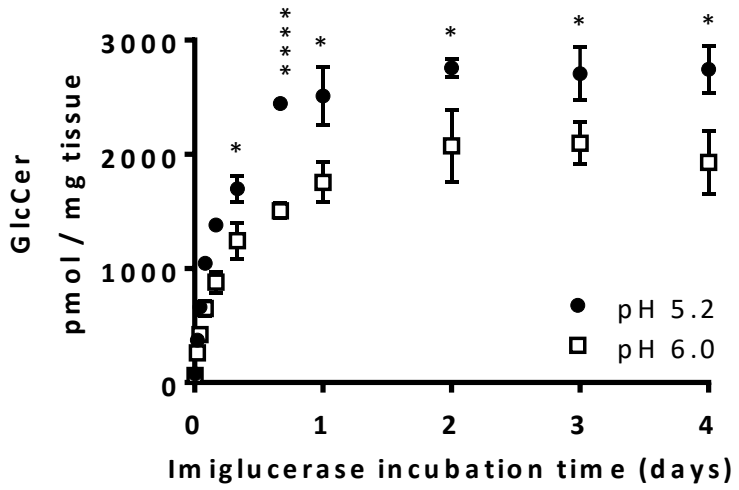


Figure 3.11. The enzymatic digestion of GlcCer was more efficient at pH 5.2 and reached its maximum (plateau) after 1-2 days of incubation time.
Quantification of GlcCer from the incubation at 37°C of extracted GSLs from 1.25 mg of brain tissue of Fabry male mice with 15 µL of imiglucerase and 10 µL of buffer (50 mM sodium acetate, 0.6 % Triton X-100, pH 4.5 or 5.0) for a final pH of 5.2 (circles) or pH 6.0 (squares), for 0, 30 min, 1 h, 2 h, 4 h, 8 h, 16 h and 1-4 days. Data are presented as the mean ±SD. Data were analysed using multiple t-tests and corrected for multiple comparisons using the Holm-Sidak method. *p < 0.05, ****p < 0.0001 (0-4 h significant values are omitted for simplification), n = 3.

Reaction pH 5.2	Buffer (50 mM sodium acetate and 0.6 % Triton X-100) at **pH 4.5**	
Reaction pH 6.0	Buffer (50 mM sodium acetate and 0.6 % Triton X-100) at **pH 5.0**	
Incubation period of GSLs (extracted from 1.25 mg of brain tissue) with imiglucerase at 37°C	No incubation	16 h
	30 min	1 day
	1 h	2 days
	2 h	3 days
	4 h	4 days
	8 h	

Table 3.11. Different pH values and incubation times tested in the tenth step for GlcCer protocol optimization (Figure 3.11).

Finally, to confirm the best pH for GlcCer degradation really is pH 5.2, samples were incubated for 24 h (the 48 h period was shortened once again for practical reasons) with buffers prepared to obtain the final pH of 4.5, 5.0, 5.2, 5.5 and 6.0 (**Figure 3.12** and **Table 3.12**).

When looking at the range of acidic pH values tested, pH 5.0 or pH 5.2 were indeed the pH values that promoted a more efficient degradation of GlcCer (**Figure 3.12**).

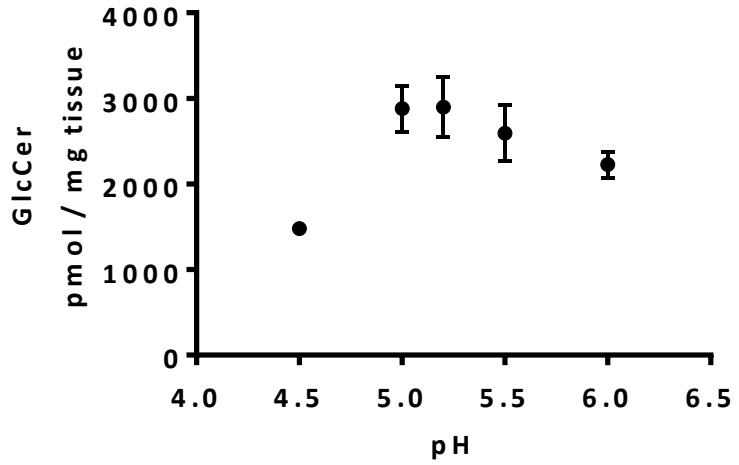


Figure 3.12. The enzymatic digestion of GlcCer by imiglucerase is optimal when the reaction occurs at pH 5.0-5.2.
Quantification of GlcCer from 24 h incubation incubation at 37°C of extracted GSLs from 1.25 mg of brain tissue of Fabry male mice with 15 µL of imiglucerase and 10 µL of buffer (50 mM sodium acetate, 0.6 % Triton X-100) for a final pH of 4.5, 5.0, 5.2, 5.5 or 6.0. Data are presented as the mean ±SD. n = 3-6.

Reaction pH 4.5	Buffer (50 mM sodium acetate and 0.6 % Triton X-100) at **pH 3.8**
Reaction pH 5.0	Buffer (50 mM sodium acetate and 0.6 % Triton X-100) at **pH 4.3**
Reaction pH 5.2	Buffer (50 mM sodium acetate and 0.6 % Triton X-100) at **pH 4.5**
Reaction pH 5.5	Buffer (50 mM sodium acetate and 0.6 % Triton X-100) at **pH 4.7**
Reaction pH 6.0	Buffer (50 mM sodium acetate and 0.6 % Triton X-100) at **pH 5.0**

Table 3.12. Different incubation pH values tested in the final step for GlcCer protocol optimization (Figure 3.12).

Therefore, the GlcCer enzymatic digestion by imiglucerase seemed to be more efficient and effective when extracted GSLs from 1.25 mg of wet tissue are incubated at 37°C, for 48 h, with 15 µL of enzyme and 10 µL of buffer containing 50 mM sodium acetate, 0.6 % Triton X-100, pH 4.5.

3.3. Discussion

As for general GSL quantification, GlcCer quantification starts with Svennerholm extraction of GSLs[232]. Then, in order to label the molecules of interest and subsequently

quantify both GSLs and GlcCer by NP-HPLC, an efficient enzymatic digestion is necessary. The recombinant enzyme rEGCase II has been widely used for GSLs quantification[253,255,256]. This enzyme cleaves the linkage between oligosaccharides and ceramides of acidic and neutral GSLs, but it does not act on galactosylceramide and is inefficient at hydrolysing glucosylceramides[253]. Therefore, in order to quantify GlcCer in the tissues of interest, we tested imiglucerase and velaglucerase alfa, the two β-glucocerebrosidases approved for enzyme replacement therapy in type 1 Gaucher disease patients world-wide[84–86]. These recombinant enzymes hydrolyse GlcCer to yield glucose and ceramide (**Figure 3.1**)[254]. The enzymatic digestion of the extracted GlcCer is the step optimised in this chapter.

The velaglucerase alfa solution was found to contain glucose (**Figure 3.6**). Velagluserase alfa list of excipients includes sucrose, sodium citrate dihydrate (E331), citric acid monohydrate (E330) and polysorbate 20. Glucose is not mentioned but sucrose is a disaccharide composed of glucose and fructose. Therefore, the glucose detected in the velaglucerase alfa solution possibly comes from sucrose degradation, making this enzyme not appropriate for the assay, as it would mask the quantification of glucose resulting from the GlcCer hydrolysis.

Different incubation buffers, with different detergents, were tested (**Figure 3.2** and **Figure 3.3**), but it was the buffer containing 50 mM sodium acetate and 0.6 % Triton X-100 that promoted a better enzymatic reaction. GlcCer is embedded in the lipid bilayer and Triton X-100 is a surfactant, working as a detergent and emulsifier, making GlcCer more accessible to imiglucerase.

Different enzyme concentrations were tested by changing the volume of buffer (**Figure 3.4**) or the volume of enzyme (**Figure 3.5**). The effect of different concentrations

of imiglucerase to digest GlcCer from various amounts of wet tissue was also tested (**Figure 3.7**). At this point, the GlcCer enzymatic digestion by imiglucerase seemed to be more efficient when extracted GSLs from 1.25 mg of wet tissue were incubated at 37°C with 15 µL of enzyme and 10 µL of buffer containing 50 mM sodium acetate, 0.6 % Triton X-100, pH 5.0. But GlcCer degradation by imiglucerase was even more efficient when occurring at pH 5.2, using the same buffer but at pH 4.5 (**Figure 3.10**, **Figure 3.11** and **Figure 3.12**).

Even when using optimal conditions, the enzymatic reaction was still very slow and inefficient (2-3 days, **Figure 3.8**). In lysosomes, *in vivo*, GCase requires the presence of saposin C and a specific lipidic environment for optimal activity[233,246]. Accordingly, when saposin C was added to the assay, the presence of saposin C improved the enzymatic reaction efficiency, but surprisingly the addition of liposomes prepared with cholesterol and di-oleoyl phosphatidyl choline showed no further benefit (**Figure 3.10**). However, when different incubation times were tested in the presence vs. absence of saposin C, the full GlcCer digestion was not accomplished in 2-3 days (the values continuously increased until the 4th day of incubation time, **Figure 3.9**).

Lastly, the change of the pH of the buffer to pH 4.5 and of the reaction to pH 5.2 reduced the minimum incubation time to 1 day (**Figure 3.11**). Therefore, for a full GlcCer enzymatic digestion by imiglucerase to occur, GSLs extracted from 1.25 mg of wet tissue incubated at 37°C, for 48 h, with 15 µL of enzyme and 10 µL of buffer containing 50 mM sodium acetate, 0.6 % Triton X-100, pH 4.5 were considered the most efficient and effective conditions. This is still quite a slow enzymatic reaction and additional experiments would be necessary to understand how to better mimic this reaction to what happens *in vivo*.

4. GSL metabolism in the SOD1^{G86R} and the SOD1^{G93A} mouse models

4.1. Introduction

4.1.1. SOD1 mutations in MND

While the causes of MND are largely unknown, (approximately 90 % of cases are sporadic), about 10 % of patients have a family history of MND which has helped identify genes associated with MND, later found to be present in both familial and sporadic cases (https://alsod.ac.uk/). Sporadic and familial cases are, however, clinically indistinguishable. One of the most prevalent and first established genetic cause of MND is mutations in the Cu/Zn superoxide dismutase gene, *SOD1*. Mutations in *SOD1* are now thought to account for about 20 % of the familial cases and some sporadic cases[147,148]. These are usually autosomal dominant mutations that cause, not a loss of function of the free radical scavenger, but a toxic gain of function of the SOD1 protein[146]. Mutant SOD1 proteins are prone to misfolding, consequently aggregating, and becoming toxic to cells and promoting motor neuron degeneration. Notably, it was recently demonstrated that misfolded wild-type SOD1 was found to aggregate in the CSF of patients without *SOD1* mutations, giving evidence that this is a pathological process of ALS independent of mutations[150].

The SOD1^{G93A} mouse was the first and most widely investigated mouse model of ALS. It expresses a mutant form of human SOD1 and develops progressive motor neuron degeneration similar to what happens in patients, without affecting SOD1 activity[151,152].

The first symptoms appear at about 90 days, when mice become paralysed in one or more limbs due to motor neuron death in the spinal cord, and humane endpoint is reached at around 140 days of age[151]. This mouse has been broadly used since it was created in 1993 and several drugs have been tested in this model, nevertheless, only one has had positive clinical trials and been granted FDA approval (edaravone in 2017)[194]. Interestingly, studies with the SOD1^{G93A} mouse suggest that altered lysosomal activity might be involved in MND pathology, particularly in the presence of *SOD1* mutations. For instance, levels of LC3 were found to be increased in the spinal cord of SOD1^{G93A} mice, suggesting autophagosome formation is increased possibly via enhancement of mTORC1 signalling[202]. Expression of TFEB and beclin1 was also found to be increased in motor neurons of this mouse model[204]. On the other hand, SOD1 aggregates have been shown to interfere with dynein-mediated endo-lysosomal trafficking, causing lysosomal deficits and reducing autophagic clearance specifically in motor neurons of asymptomatic SOD1^{G93A} mouse mice, causing axonal degeneration as the disease progresses[207,208].

The SOD1^{G86R} mouse is another mouse model of ALS which expresses a missense mutation in the *SOD1* gene, without reducing SOD1 activity[223]. Similarly to the SOD1^{G93A} mouse, progressive loss of motor function appears around 3-4 months and premature death happens at 4 months of age[223]. SOD1^{G86R} mice have been used to study energy and lipid metabolism in MND and, particularly, the role of GSLs in MND (as discussed in this chapter)[215,217,257].

4.1.2. GSLs in MND and SOD1 mouse models: a review

Dysregulated lipid metabolism affects neurons in MND in several different ways[212]. Particularly for GSL metabolism, a few recent studies gave evidence of an essential role for this group of lipids in MND (**Table 4.1**). Significantly elevated levels of ceramide (Cer), GlcCer and more complex GSLs including galactocerebroside (GalCer, particularly abundant in myelin), lactosylceramide (LacCer), globotriaosylceramide (GL3 or Gb3) and the gangliosides GM3 and GM1, and increased activity of the hydrolases GBA1, GBA2, hexosaminidase, galactosylceramidase, α-galactosidase and β-galactosidase were detected in the spinal cord of ALS patients, when compared to healthy controls[214]. High levels of GlcCer, sphingomyelin (SM) and GM1a were also found in the CSF of ALS patients and, importantly, the levels of GM1a positively correlated with disease severity measured by the ALS functional rating scale (revised, ALSFRS-R) score per month[216,220]. Finally, increased expression of GCS was also found in skeletal muscle of ALS patients[215].

Significantly elevated levels of GM1a and GBA2 (the non-lysosomal GCase, but not GBA1) activity were also found in spinal cord of symptomatic SOD1^{G86R} mice (**Table 4.1** and **Figure 4.1**)[215,218]. Likewise, GlcCer, GM3 and GM2 levels and GCS expression were increased in skeletal muscle of these mice (**Table 4.1** and **Figure 4.1**)[215]. Pharmacological inhibition of GlcCer degradation with conduritol B epoxide, which inhibits both GBA1 and GBA2, delayed disease onset by improving the integrity of motor units and motor function in early symptomatic SOD1^{G86R} mice[216]. Additionally, inhibition of only GBA2 with ambroxol hydrochloride also delayed disease onset by protecting the neuromuscular junctions (NMJs) and integrity of motor units in the spinal cord when administered in

pre-symptomatic mice, and improved survival when administered at onset of symptoms[218].

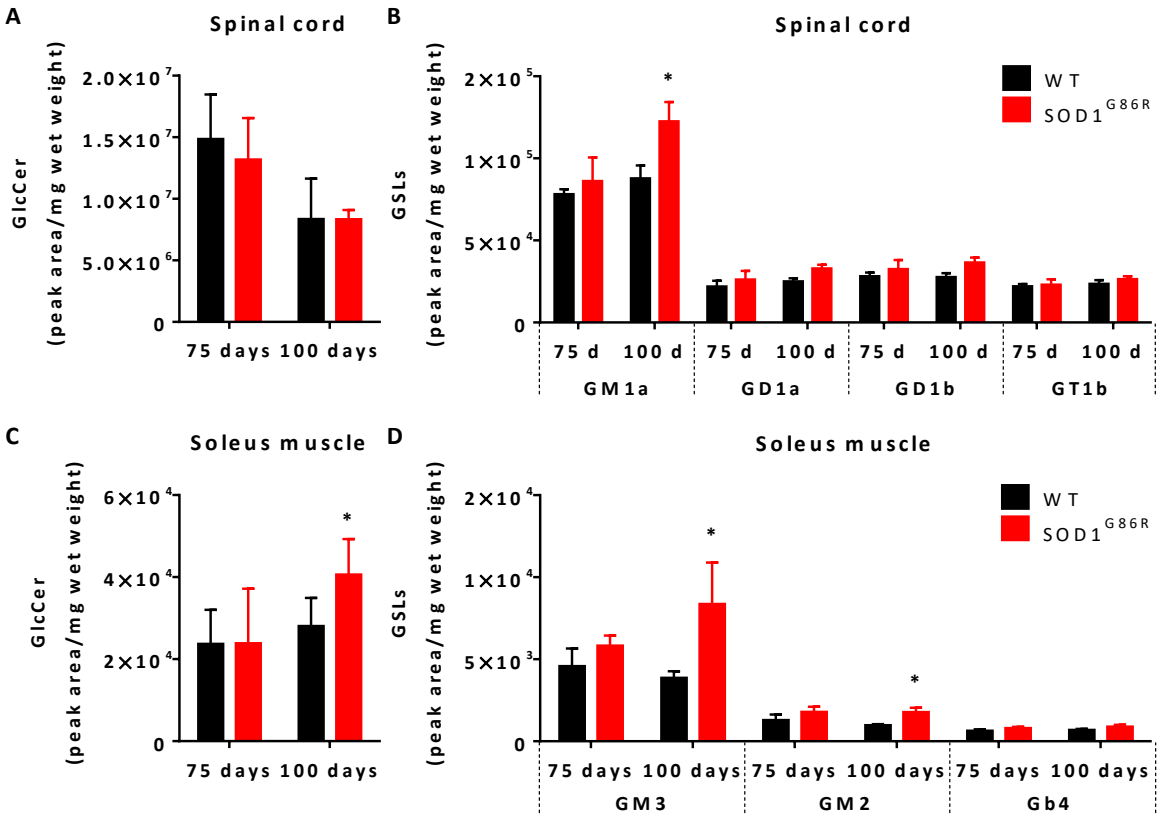


Figure 4.1. Diseased SOD1^{G86R} mice show high levels of GM1a in spinal cord and GlcCer, GM3 and GM2 in soleus muscle when compared to age-matched WT controls.
NP-HPLC quantification of GlcCer and other GSLs in lumbar spinal cord **(A-B)** and soleus muscle **(C-D)** of pre-symptomatic (75 days old) and symptomatic (100 days old) SOD1^{G86R} mice (red) and corresponding WT littermates (black). Significantly increased levels of GM1a in spinal cord and GlcCer, GM3 and GM2 in soleus muscle were found on symptomatic 100 days old SOD1^{G86R} mice, when compared to age-matched WT littermates. Only detected main peaks of gangliosides are shown in each tissue. Data are presented as the mean ±SD for each ganglioside. Data were analysed using student's *t*-test. * $p < 0.05$ versus corresponding WT controls, n = 6 mice per group. Data kindly provided by Mylene Huebecker and adapted from[215].

Interestingly, GSL metabolism was investigated in different stages of disease development on the spinal cord of SOD1^{G93A} mice[214]. Similarly to what was observed in the spinal cord of ALS patients, levels of GlcCer and hexosaminidase activity were elevated at the end stage of the disease. However, levels of Cer, SM, LacCer, Gb3 and

GM1 were significantly reduced at symptoms onset and then recovered, showing higher levels when comparing symptom onset with humane endpoint. Also, the activity of α-galactosidase and β-galactosidase was not significantly changed in the spinal cord of $SOD1^{G93A}$ mice, but the activity of GBA1, GBA2 and galactosylceramidase was reduced both at onset of paralysis and end stage. On the other hand, inhibition of GlcCer synthesis (with GENZ-667161 60 mg/kg/day, an inhibitor of GCS) in $SOD1^{G93A}$ mice accelerated disease progression, while chronic intracerebroventricular infusion (12 μg/day) of GM3 slowed disease progression[214].

In line with what was seen in patients and $SOD1^{G86R}$ mice, GCS expression and GlcCer were significantly higher in mice after surgically induced peripheral nerve injury. However, when GCS activity was inhibited (with *N*-(5-adamantane-1-yl-methoxy-pentyl)-deoxynojirimycin or AMP-DNM) after surgical injury, GlcCer content in muscle was reduced and motor recovery delayed[215]. Interestingly, in a different study, GBA2 inhibition (with ambroxol hydrocloride) after sciatic nerve injury improved motor recovery and muscle re-enervation[218].

Overall, these changes suggest that GSLs might have a protective role or constitute a compensatory mechanism in MND pathogenesis.

 **ALS patients**	**CSF**	↑ GlcCer, SM[220] and GM1a[216]
	Spinal cord	↑ Cer, GlcCer, GalCer, LacCer, Gb3, GM3 and GM1 ↑ GBA1, GBA2, hexosaminidase, galactosylceramidase, α-galactosidase and β-galactosidase activities[214]
	Muscle	↑ GCS expression[215]
 **SOD1^{G86R} mice**	**Spinal cord**	↑ GM1a[215] & GBA2 activity[218]
	Muscle	↑ GlcCer, GM3, GM2 & GCS expression[215]
		GBA2 inhibition ↑ motor units integrity ↑ neuroprotection and ↓ disease progression[216,218]
 **SOD1^{G93A} mice**	**Spinal cord**	↑ GlcCer (end stage) ↓ Cer, SM, LacCer, Gb3 and GM1 at symptom onset and ↑ when moribund ↑ hexosaminidase (at onset of paralysis and end stage) ↓ GBA1, GBA2 and galactosylceramidase activity (at onset of paralysis and end stage)[214]
		GCS inhibition ↑ disease progression GM3 intracerebroventricular infusion ↓ disease progression[214]
 **WT mice**	**Spinal cord**	Peripheral nerve injury ↑ GCS expression and GlcCer levels Peripheral nerve injury & GCS inhibition ↓ GlcCer levels & motor function recovery[215] Peripheral nerve injury & GBA2 inhibition ↑ motor function recovery[218]

⇨ GlcCer seems to modulate disease progression and changes in GBA activity appear to work as a compensatory mechanism, slowing it down.
⇨ GSLs might have a protective or a compensatory role in MND pathogenesis.

Table 4.1. GSL metabolism in MND and the SOD1 mutation: a summary of what is known so far.

To better understand the role of the reported changes of GSL metabolism in MND pathology, GSL levels and hydrolase activities were measured in different relevant tissues (spinal cord and muscle) at different stages of disease. The study of pre-symptomatic and early stages of disease are particularly relevant for clinical purposes, in order to find potential biomarkers or therapeutic targets.

4.1.3. Aims

In this chapter, in order to fully characterise GSL metabolism in tissues from SOD1 mouse models of MND in different stages of disease development, changes in the levels of GlcCer and downstream GSLs with disease progression were measured in spinal cord and muscle of the $SOD1^{G86R}$ mouse and in muscle of the $SOD1^{G93A}$ mouse models of MND. Differences between the $SOD1^{G86R}$ and the $SOD1^{G93A}$ mouse models were also evaluated considering the GSL changes previously characterised.

4.2. Results

According to previous studies, GSL metabolism is affected in both ALS patients and symptomatic $SOD1^{G86R}$ and $SOD1^{G93A}$ mice. However, little is known about when these changes occur, and further studies are necessary to better understand what happens during the early stages of disease. Reported quantification of GSLs on tissues from pre-symptomatic (75 days old) and diseased (100 days) $SOD1^{G86R}$ mice and corresponding age-matched wild-type (WT) controls revealed significantly higher levels of GM1a in the spinal cord (A and B, **Figure 4.1**) and of GlcCer, GM3 and GM2 in soleus muscle (C and D, **Figure 4.1**) of diseased or symptomatic mice[215]. HPLC analysis of spinal cord and tibialis anterior muscle from 90 days old $SOD1^{G86R}$ mice was performed in order to characterise the levels of GSLs at the time of onset of symptoms. Both tissues showed no significant changes in the levels of GSLs when compared with corresponding WT controls (**Figure 4.2**, spinal cord (A): GM1a p = 0.7984, GD1a p = 0.5737, GD1b p = 0.8785, GT1b p = 0.1304, total GSLs p = 0.7209; tibialis anterior (B): LacCer p = 0.8785, GM3 p = 0.1049, GM2 p = 0.7984, total GSLs p = 0.3823).

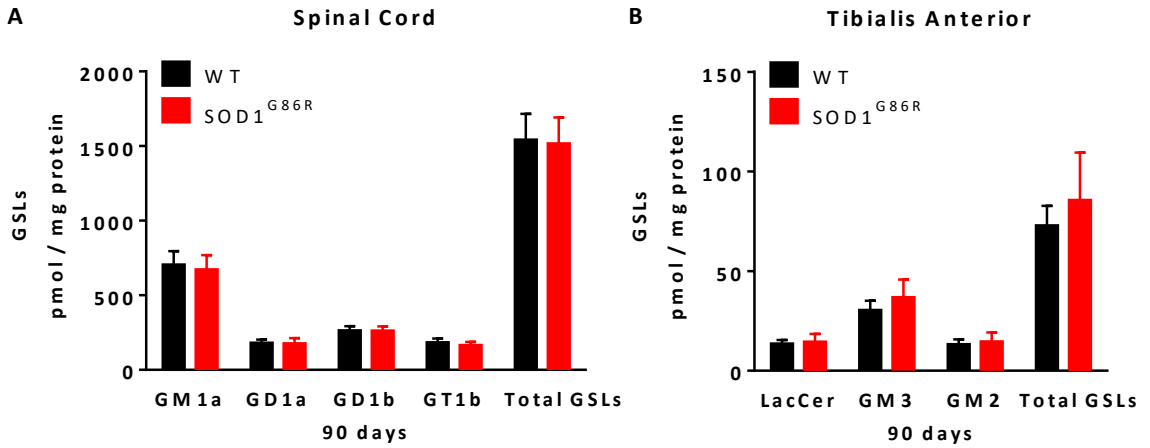


Figure 4.2. No changes were found in the GSL levels of spinal cord or tibialis anterior (TA) muscle of 90 days old SOD1^{G86R} mice when compared to WT littermates.
NP-HPLC quantification of GSLs in spinal cord **(A)** and tibialis anterior **(B)** of 90 days old SOD1^{G86R} mice (red) and aged matched WT controls (black). No changes in GSL levels were observed in the spinal cord or tibialis anterior of SOD1^{G86R} mice at the age of onset of symptoms when compared to matched WT controls. Only main peaks of GSLs are shown. Data are presented as the mean ±SD for each GSL. Data were analysed using Mann-Whitney *t*-test. No statistically significant differences were observed, n = 8 mice per group.

Therefore, SOD1^{G86R} mice only show changes in levels of GSLs when already symptomatic, at 100 days of age. GM1a levels were higher at 100 days in the spinal cord, while GlcCer, GM3 and GM2 levels were significantly increased in soleus muscle of SOD1^{G86R} mice when compared to age-matched WT controls[215].

Pathology in SOD1 mouse models is largely determined by the loss of function in one of the limbs. Despite GSL metabolism being thoroughly studied in the spinal cord of SOD1^{G93A} mice, and changes in the levels of GlcCer and downstream GSLs being described[214], GSL changes in muscle tissues have not been thoroughly examined. Therefore, SOD1^{G93A} muscle tissue was examined during different stages of disease progression to better understand where the changes in GSL metabolism start and what possibly causes them. Quantification of GlcCer on tibialis anterior muscle of SOD1^{G93A} mice at 30 days of age (pre-symptomatic), 84 days (age of onset of symptoms) and 140

days (humane endpoint) revealed no significant changes over time, with disease development, when compared to WT age-matched controls (**Figure 4.3**; WT vs. SOD1^{G93A}: 30 days p > 0.9999, 84 days p = 0.9996, 140 days p = 0.1579; WT: 30 vs. 84 days p = 0.9949, 30 vs. 140 days p = 0.9828, 84 vs. 140 days p > 0.9999; SOD1^{G93A}: 30 vs. 84 days p > 0.9999, 30 vs. 140 days p = 0.2829, 84 vs. 140 days p = 0.2432). Nevertheless, when performing a Pearson correlation analysis, GlcCer levels presented a trend showing an increase on GSL levels for SOD1^{G93A} mice which contrasted with a decrease on GSL levels for WT mice with age (**Figure 4.3** A).

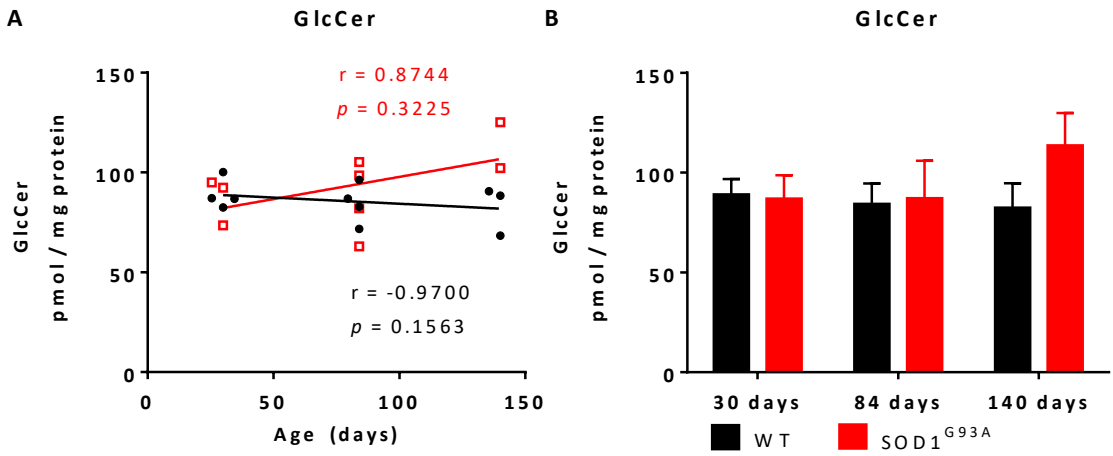


Figure 4.3. No significant changes were found in the GlcCer levels in tibialis anterior muscle of SOD1^{G93A} mice at asymptomatic, onset and symptomatic stages of disease progression and age-matched WT controls.
Changes in GlcCer levels in tibialis anterior of SOD1^{G93A} mice at different ages, corresponding to progressive stages of disease (30 days for pre-symptomatic, 84 days for age of onset and 140 days for humane endpoint, red) and aged matched WT controls (black), measured by NP-HPLC. (A) Data were analysed using Pearson correlation analysis and (B) 2-way ANOVA, with Tukey's multiple comparisons test. Bar graph is presented as the mean ±SD. No statistically significant differences were observed, n = 4 mice per group, with the exception of n = 2 for 140 days old SOD1^{G93A} mice and n = 3 for 140 days old WT mice.

However, quantification of more complex downstream GSLs on tibialis anterior of SOD1^{G93A} mice revealed a significant increase in the total amount of GSLs and,

specifically, in the levels of the main GSLs detected (LacCer, GM3 and GM2) for 140 days old mice when compared to WT controls (**Figure 4.4**, WT vs. $SOD1^{G93A}$ total GSLs (B): 30 days $p = 0.9817$, 84 days $p = 0.4423$, 140 days $p < 0.0001$; **Figure 4.5**, WT vs. $SOD1^{G93A}$ LacCer (B): 30 days $p > 0.9999$, 84 days $p = 0.5641$, 140 days $p < 0.0001$; GM3 (D): 30 days $p = 0.9764$, 84 days $p = 0.5645$, 140 days $p < 0.0001$; GM2 (F): 30 days $p = 0.9990$, 84 days $p = 0.3635$, 140 days $p < 0.0001$). As observed with GlcCer, there is a clear trend showing a general decrease in GSL levels in WT mice over time, which contrasts with the increase in GSL levels for $SOD1^{G93A}$ mice over their lifespan (**Figure 4.4** A and **Figure 4.5** A, C and E; WT: values of r near -1; $SOD1^{G93A}$: values of r near 1). However, these changes are only significant on the tibialis anterior of 140 days old $SOD1^{G93A}$ mice, in line with muscle and spinal cord results in the $SOD1^{G86R}$ mouse (**Figure 4.1**) where significantly altered GSL levels were only observed at end stage[215]. Levels of total GSLs, LacCer, GM3 or GM2 are similar for 30 and 84 days old $SOD1^{G93A}$ mice (**Figure 4.4** and **Figure 4.5**).

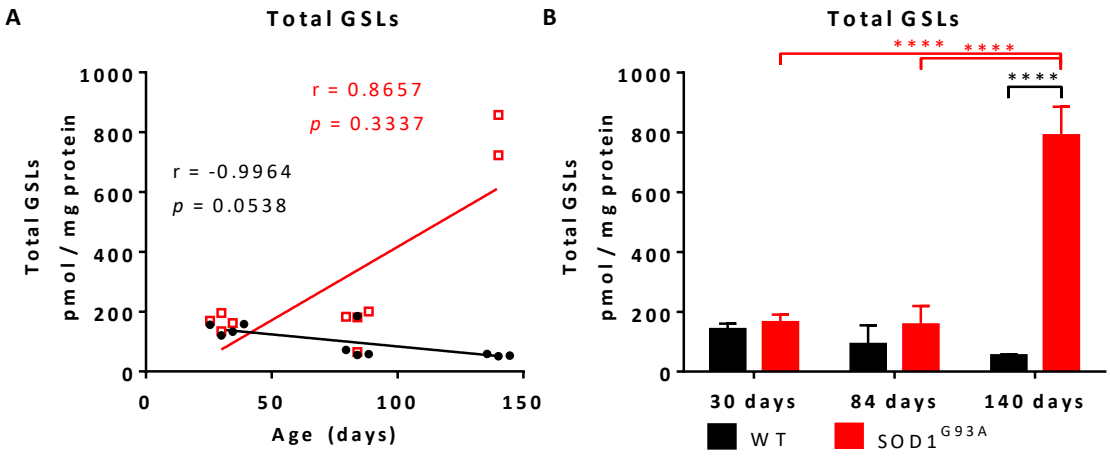


Figure 4.4. Diseased (140 days old) SOD1^{G93A} mice showed high levels of total GSLs in tibialis anterior muscle when compared to age-matched WT littermates.
Changes in the levels of total GSLs in tibialis anterior of SOD1^{G93A} mice at different ages, corresponding to progressive stages of disease (30 days for pre-symptomatic, 84 days for age of onset and 140 days for humane endpoint, red) and aged matched WT controls (black), measured by NP-HPLC. (A) Data were analysed using Pearson correlation analysis and (B) 2-way ANOVA, with Tukey's multiple comparisons test. Bar graph is presented as the mean ±SD. **** $p < 0.0001$, n = 4 mice per group, with the exception of n = 2 for 140 days old SOD1^{G93A} mice and n = 3 for 140 days old WT mice.

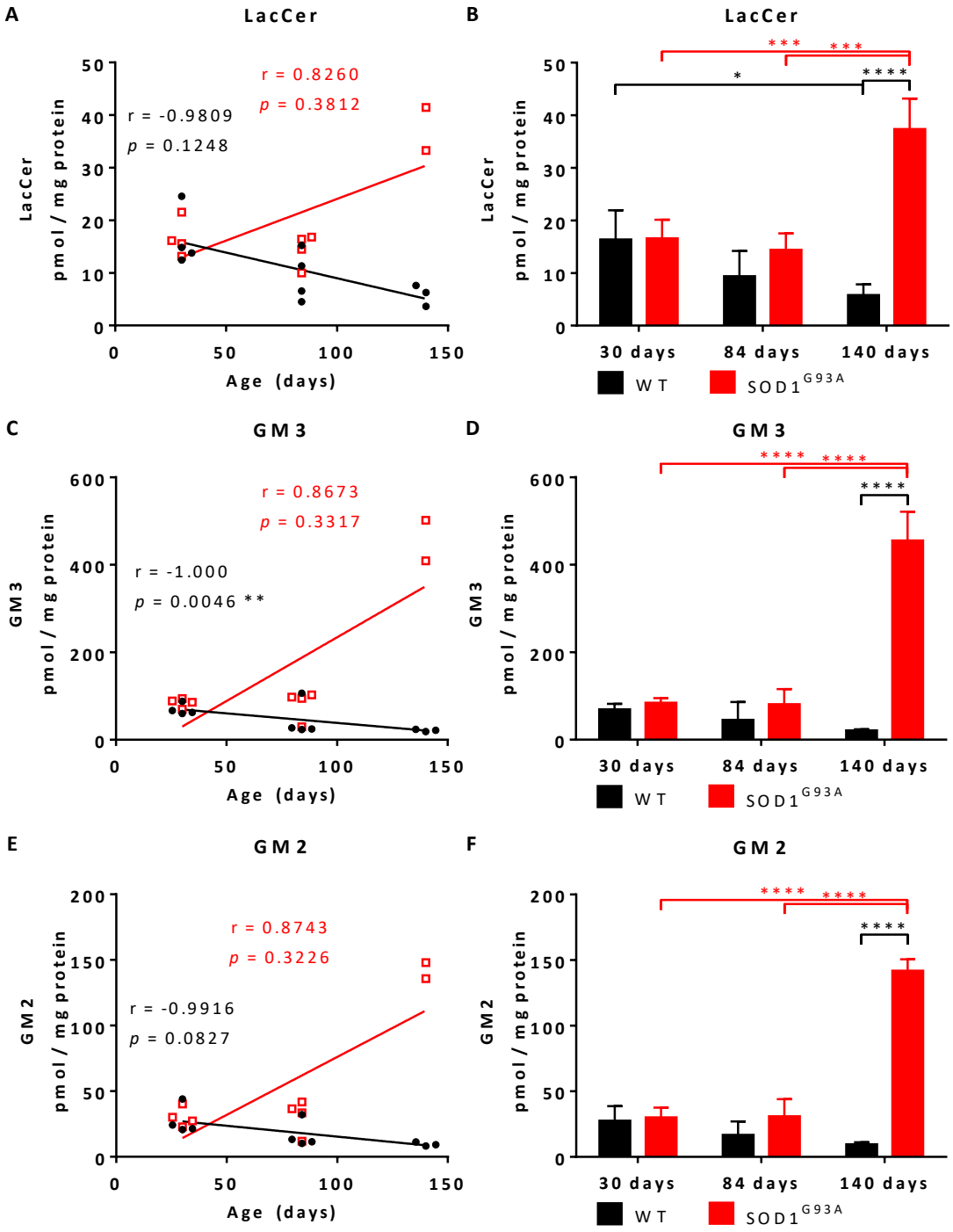


Figure 4.5. Diseased (140 days old) SOD1^{G93A} mice showed high levels of LacCer, GM3 and GM2 in tibialis anterior muscle when compared to age-matched WT littermates. Changes in LacCer, GM3 and GM2 (main peaks of GSLs) levels in tibialis anterior of SOD1^{G93A} mice at different ages, corresponding to progressive stages of disease (30 days for pre-symptomatic, 84 days for age of onset and 140 days for humane endpoint, red) and aged matched WT controls (black), measured by NP-HPLC. (A,C,E) Data were analysed using Pearson correlation analysis and (B,D,F) 2-way ANOVA, with Tukey's multiple comparisons test. Bar graph is presented as the mean ±SD. * $p < 0.05$, ** $p < 0.01$, *** $p < 0.001$, **** $p < 0.0001$, n = 4 mice per group, with the exception of n = 2 for 140 days old SOD1^{G93A} mice and n = 3 for 140 days old WT mice.

Likewise, GlcCer quantification on gastrocnemius muscle of SOD1^{G93A} mice at 30, 84 and 140 days of age, corresponding to asymptomatic, age of onset of symptoms and humane endpoint respectively, showed no significant changes in the levels of GlcCer over time when compared to age-matched WT controls (**Figure 4.6**; WT vs. SOD1^{G93A}: 30 days p = 0.9990, 84 days p = 0.9688, 140 days p = 0.1913; WT: 30 vs. 84 days p = 0.9614, 30 vs. 140 days p = 0.9794, 84 vs. 140 days p > 0.9999; SOD1^{G93A}: 30 vs. 84 days p = 0.9994, 30 vs. 140 days p = 0.2608, 84 vs. 140 days p = 0.4131).

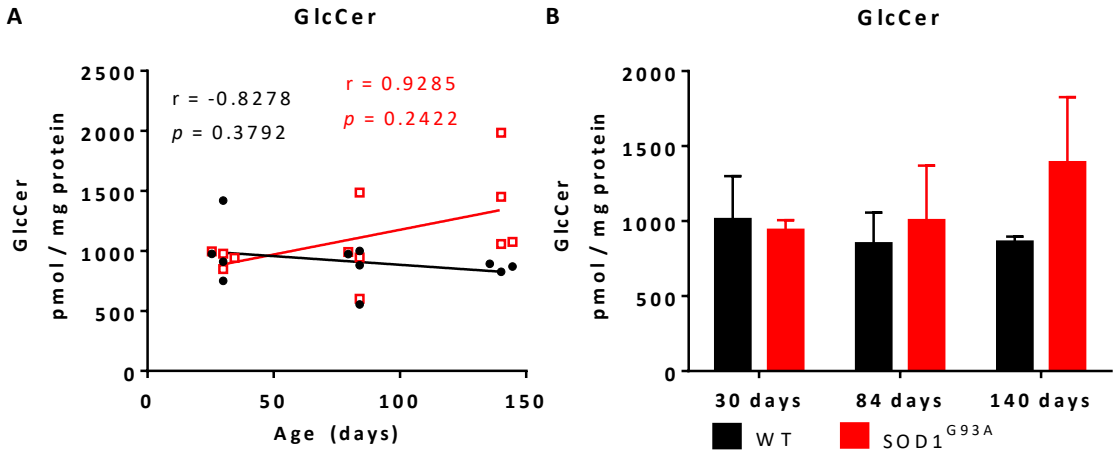


Figure 4.6. No significant changes were found in the GlcCer levels in gastrocnemius of SOD1^{G93A} mice at asymptomatic, onset and symptomatic stages of disease progression and age-matched WT controls.
Changes in GlcCer levels in gastrocnemius muscle of SOD1^{G93A} mice at different ages, corresponding to progressive stages of disease (30 days for pre-symptomatic, 84 days for age of onset and 140 days for humane endpoint, red) and aged matched WT controls (black), measured by NP-HPLC. (A) Data were analysed using Pearson correlation analysis and (B) 2-way ANOVA, with Tukey's multiple comparisons test. Bar graph is presented as the mean ±SD. No statistically significant differences were observed, n = 4 mice per group, with the exception of n = 3 for 140 days old WT mice.

Similar to tibialis anterior, GSLs quantification in gastrocnemius of SOD1^{G93A} mice by NP-HPLC showed a significant increase in the total levels of GSLs and, specifically, in the levels of LacCer, GM3 and GM2, reaching statistical significance at 140 days of age (humane endpoint) when compared to WT controls (**Figure 4.7**, WT vs. SOD1^{G93A} total

GSLs (B): 30 days $p > 0.9999$, 84 days $p = 0.5073$, 140 days $p = 0.0004$; **Figure 4.8**, WT vs. $SOD1^{G93A}$ LacCer (B): 30 days $p > 0.9999$, 84 days $p = 0.8276$, 140 days $p = 0.0468$; GM3 (D): 30 days $p > 0.9999$, 84 days $p = 0.4261$, 140 days $p = 0.0003$; GM2 (F): 30 days $p > 0.9999$, 84 days $p = 0.4735$, 140 days $p = 0.0006$). Pearson correlation analysis of these results showed again a clear trend of a gradual decrease on GSL levels for WT mice and an increase for the gastrocnemius of $SOD1^{G93A}$ mice over time. (**Figure 4.7** A and **Figure 4.8** A, C and E; WT: values of r near -1; $SOD1^{G93A}$: values of r near 1). This trend reached or was near statistical significance for the levels of GM3 and total GSLs of WT mice with age, on both tibialis anterior and gastrocnemius (**Figure 4.4** A, **Figure 4.5** A, C and E, **Figure 4.7** A and **Figure 4.8** A, C and E). Importantly, LacCer (for tibialis anterior), GM3, GM2 and total GSLs levels were similar for 30 and 84 days old $SOD1^{G93A}$ mice, only increasing at the humane endpoint (**Figure 4.4** B, **Figure 4.5** B, D and F, **Figure 4.7** B and **Figure 4.8** B, D and F).

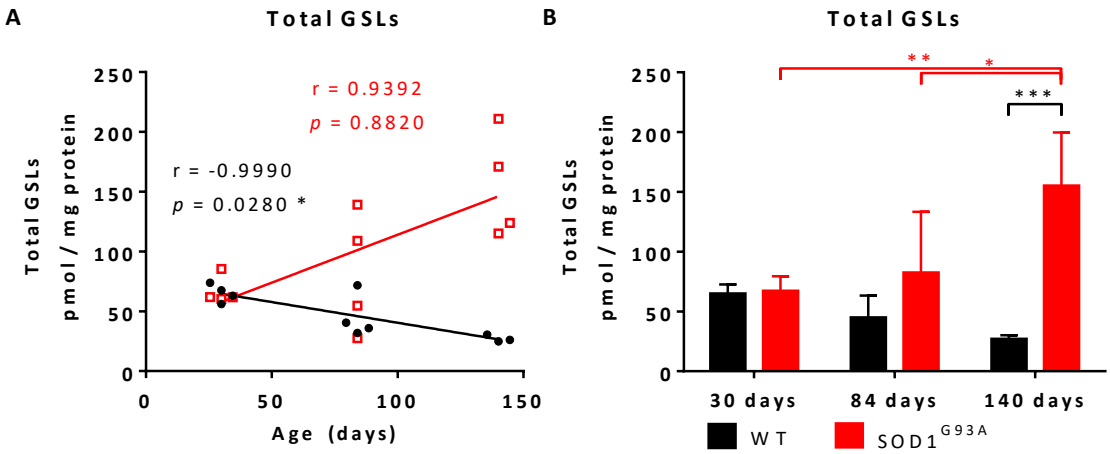


Figure 4.7. Symptomatic (140 days old) SOD1^{G93A} mice showed high levels of total GSLs in gastrocnemius when compared to age-matched WT controls.

Changes in levels of total GSLs in gastrocnemius muscle of SOD1^{G93A} mice at different ages, corresponding to progressive stages of disease (30 days for pre-symptomatic, 84 days for age of onset and 140 days for humane endpoint, red) and aged matched WT controls (black), measured by NP-HPLC. (A) Data were analysed using Pearson correlation analysis and (B) 2-way ANOVA, with Tukey's multiple comparisons test. Bar graph is presented as the mean ±SD. * $p < 0.05$, ** $p < 0.01$, *** $p < 0.001$, n = 4 mice per group, with the exception of n = 3 for 140 days old WT mice.

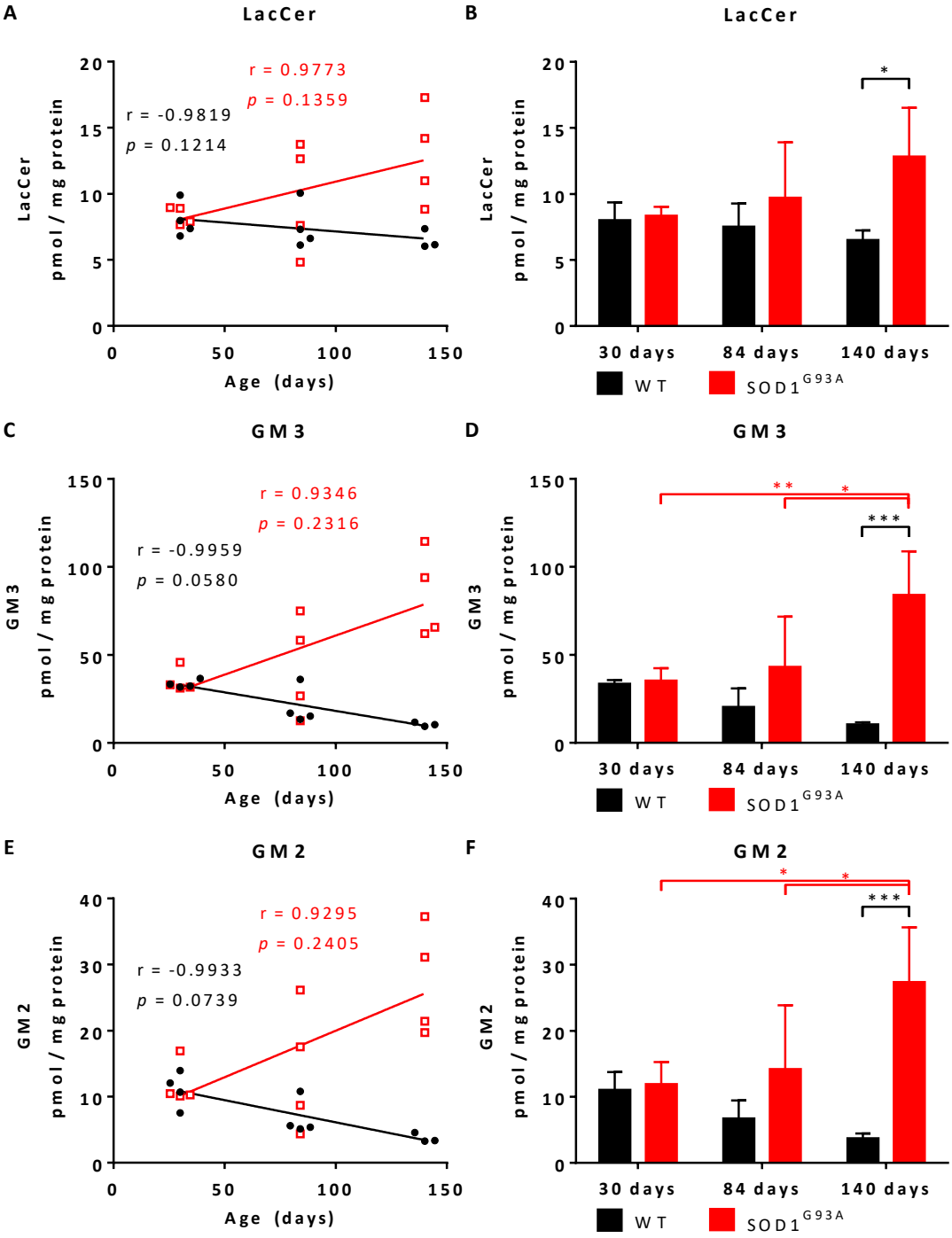


Figure 4.8. Symptomatic (140 days old) SOD1^{G93A} mice showed high levels of LacCer, GM3 and GM2 in gastrocnemius when compared to age-matched WT controls.
Changes in LacCer, GM3 and GM2 (main peaks of GSLs) levels in gastrocnemius muscle of SOD1^{G93A} mice at different ages, corresponding to progressive stages of disease (30 days for pre-symptomatic, 84 days for age of onset and 140 days for humane endpoint, red) and aged matched WT controls (black), measured by NP-HPLC. (A,C,E) Data were analysed using Pearson correlation analysis and (B,D,F) 2-way ANOVA, with Tukey's multiple comparisons test. Bar graph is presented as the mean ±SD. * $p < 0.05$, ** $p < 0.01$, *** $p < 0.001$, n = 4 mice per group, with the exception of n = 3 for 140 days old WT mice.

Finally, in order to better understand if the changes in GSL levels described above are due to changes in GSL catabolism, the activity of the lysosomal enzymes GBA, α-galactosidase, β-galactosidase, β-hexosaminidase and sialidase (neuraminidases Neu1, Neu3 and Neu4) was measured in gastrocnemius muscle of $SOD1^{G93A}$ mice at 30, 84 and 140 days of age and age-matched WT controls (**Figure 4.9** and **Figure 4.10**). No changes were found in the activity of GBA, α-galactosidase or sialidase when comparing $SOD1^{G93A}$ mice with the WT controls (**Figure 4.9**, WT vs. $SOD1^{G93A}$ GBA (A-B): 30 days $p > 0.9999$, 84 days $p = 0.9510$, 140 days $p = 0.9996$; α-galactosidase (C-D): 30 days $p > 0.9999$, 84 days $p = 0.9988$, 140 days $p = 0.9606$; sialidase (E-F): 30 days $p > 0.9999$, 84 days $p > 0.9999$, 140 days $p = 0.9989$). However, the activity of β-galactosidase and β-hexosaminidase showed a similar pattern to the one observed in the levels of GSLs in muscle: the activity of the enzymes in the WT mice showed a tendency to gradually decrease with time; while for the gastrocnemius of $SOD1^{G93A}$ mice the enzymatic activity remained the same at 30 and 84 days of age but increased significantly at 140 days of age, when reaching humane endpoint (**Figure 4.10**, WT vs. $SOD1^{G93A}$ β-galactosidase (A-B): 30 days $p = 0.9992$, 84 days $p = 0.6496$, 140 days $p < 0.0001$; β-hexosaminidase (C-D): 30 days $p = 0.9791$, 84 days $p > 0.9999$, 140 days $p = 0.0006$).

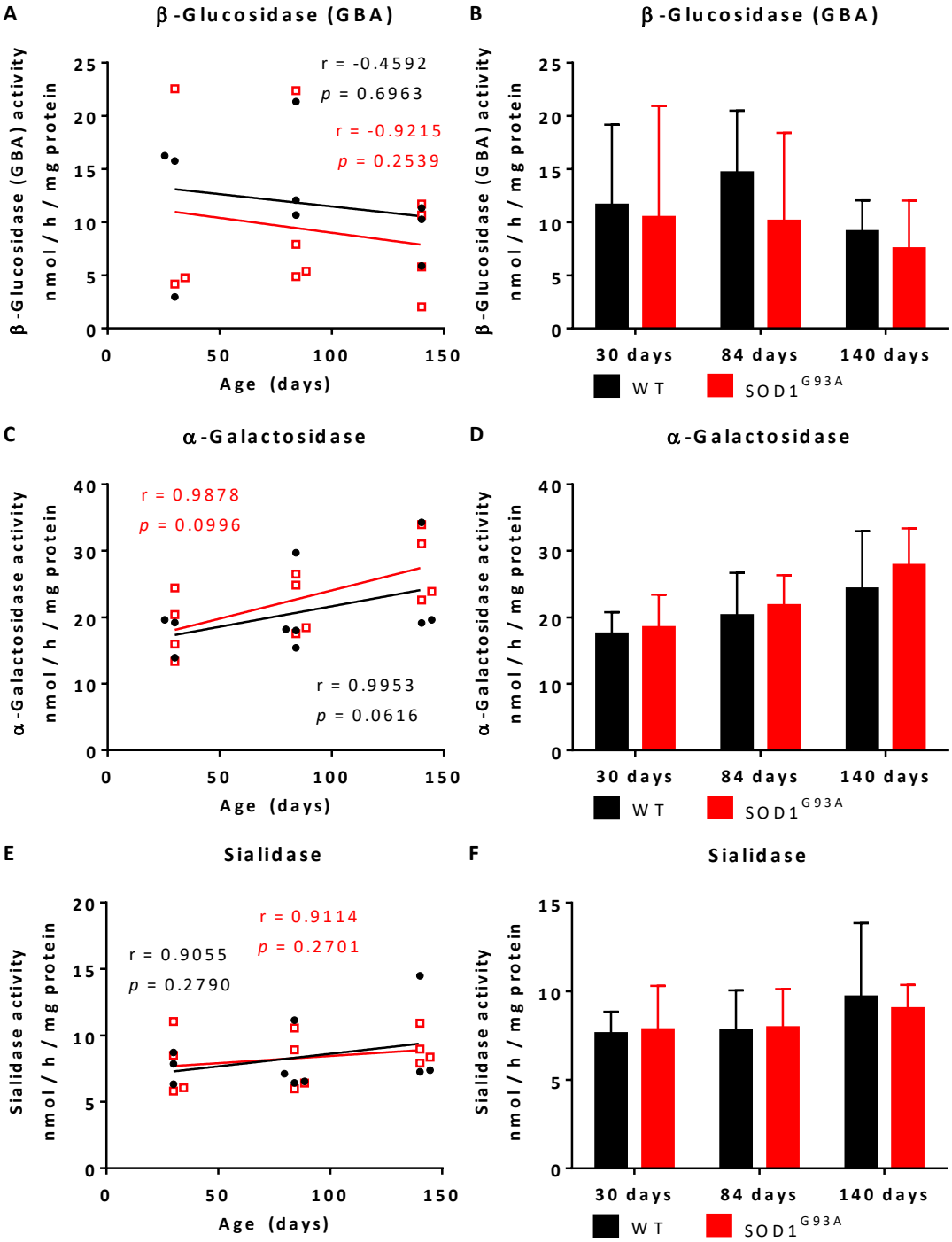


Figure 4.9. No significant changes were found in the activity of GBA, α-galactosidase or sialidase in gastrocnemius muscle of symptomatic (140 days old) SOD1^{G93A} mice when compared to age-matched WT controls.

Changes in β-glucosidase (GBA), α-galactosidase and sialidase activities in gastrocnemius muscle of SOD1^{G93A} mice at different ages, corresponding to progressive stages of disease (30 days for pre-symptomatic, 84 days for age of onset and 140 days for humane endpoint, red) and aged matched WT controls (black). (A,C,E) Data were analysed using Pearson correlation analysis and (B,D,F) 2-way ANOVA, with Tukey's multiple comparisons test. Bar graph is presented as the mean ±SD. No statistically significant differences were observed, n = 4 mice per group, with the exception of n = 3 for 140 days old WT mice.

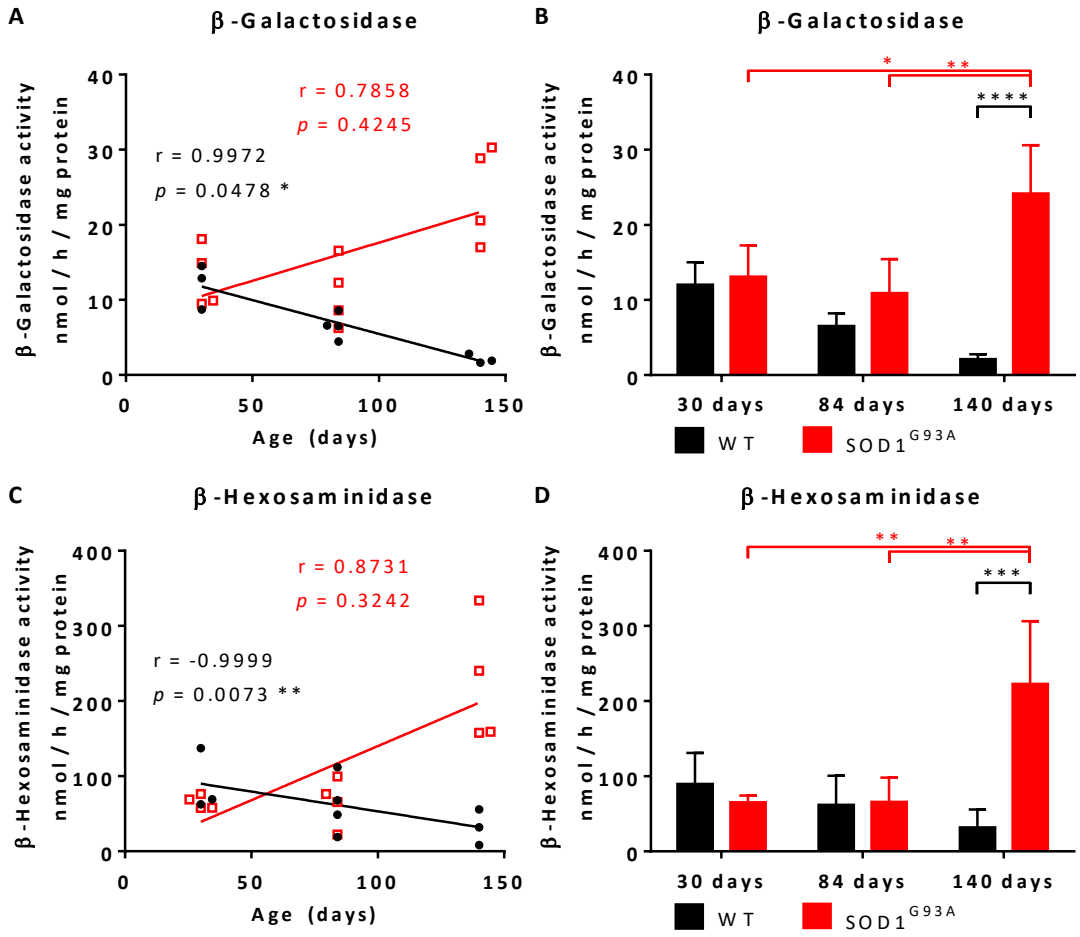


Figure 4.10. Increased β-galactosidase and β-hexosaminidase activity was measured in gastrocnemius muscle of symptomatic (140 days old) SOD1^{G93A} mice when compared to age-matched WT controls.

Changes in β-galactosidase and β-hexosaminidase activities in gastrocnemius muscle of SOD1^{G93A} mice at different ages, corresponding to progressive stages of disease (30 days for pre-symptomatic, 84 days for age of onset and 140 days for humane endpoint, red) and aged matched WT controls (black). (A,C) Data were analysed using Pearson correlation analysis and (B,D) 2-way ANOVA, with Tukey's multiple comparisons test. Bar graph is presented as the mean ±SD. * $p < 0.05$, ** $p < 0.01$, *** $p < 0.001$, **** $p < 0.0001$, n = 4 mice per group, with the exception of n = 3 for 140 days old WT mice.

In summary, levels of LacCer and the main gangliosides in the spinal cord and muscles of SOD1^{G86R} and SOD1^{G93A} mice were acutely elevated at symptomatic or humane endpoint stages of disease development, but not at the time of onset of symptoms and, in gastrocnemius muscle of SOD1^{G93A} mice, β-galactosidase and

β-hexosaminidase activities were also elevated when compared to 30 or 84 days old SOD1^{G93A} mice or age-matched WT controls (**Figure 4.11**).

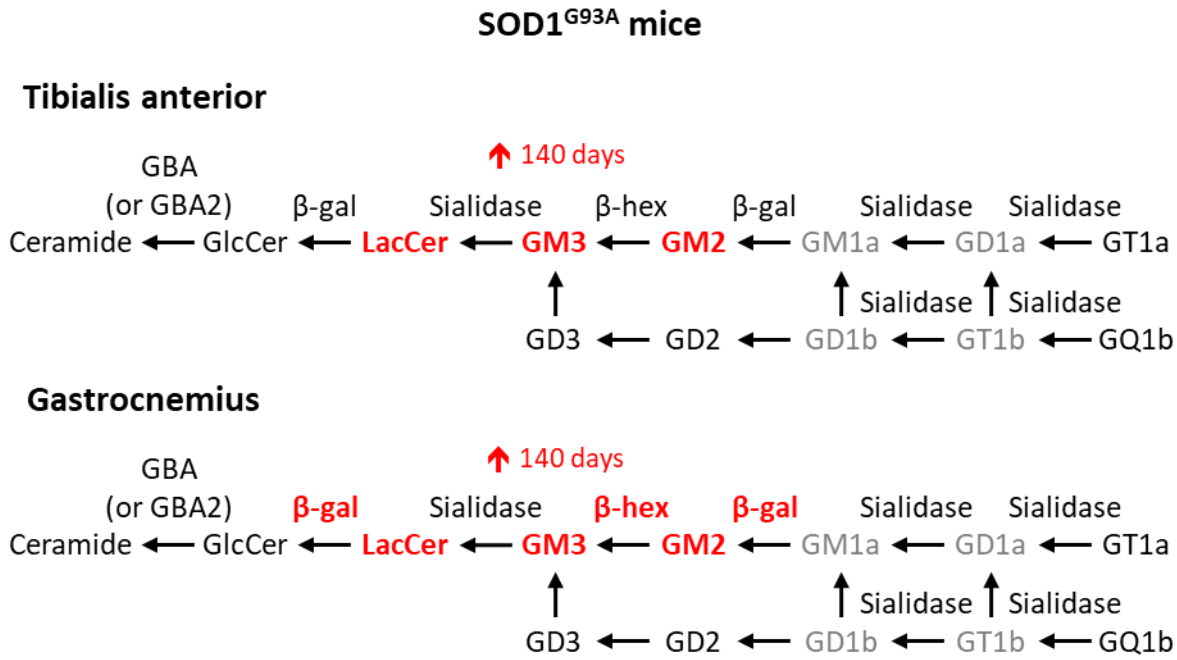


Figure 4.11. Outline of the changes found in GSL levels in tibialis anterior and gastrocnemius of SOD1^{G93A} mice when looking at pre-symptomatic, onset of symptoms and symptomatic stages of disease progression.
Significant changes were found in tibialis anterior and gastrocnemius muscles of 140 days old symptomatic/morbid SOD1^{G93A} mice , when compared to age-matched WT controls. Statistically sifgnificant changes in levels of GSLs or lysosomal hydrolases (GBA, β-galactosidase (β-gal), β-hexosaminidase (β-hex) and sialidase) activity are marked in red. All major changes were found when the mice were 140 days-old. Major gangliosides in the central nervous system (GM1a, GD1a, GD1b and GT1b) are shown in grey.

4.3. Discussion

GSL metabolism has been shown to be dysregulated in MND and disease progression can be attenuated by manipulating the levels of GSLs or the activity of enzymes that regulate their catabolism[214,216,218]. However, it is still unclear when changes in GSL metabolism occur and how they contribute to disease pathology, particularly in the initial stages of the disease. Previous studies indicated a significant increase in GM1a

levels in lumbar spinal cord tissue and GlcCer, GM3 and GM2 levels in soleus muscle of SOD1^{G86R} mice, when compared to the age-matched WT controls, at 100 days old (symptomatic, with paralysis seen at least on one hind limb), but not at 75 days old (pre-symptomatic, **Figure 4.1**)[215]. In this study, HPLC analysis of tibialis anterior and spinal cord of 90 days old (early symptomatic) SOD1^{G86R} mice showed no significant changes in levels of GSLs, when compared with corresponding WT controls (**Figure 4.2**). Therefore, changes in the levels of GSLs in the spinal cord or skeletal muscle of SOD1^{G86R} mice only seem to occur when the mice are already symptomatic, when there is already NMJ and motor neuron degeneration and mice lost function in at least one of the limbs. Also, it has been shown that disease progression in the fast-twitch tibialis anterior happens earlier than in the slow-twitch soleus muscle, in SOD1^{G93A} mice[258,259]. So, small but significant changes could have been expected in tibialis anterior muscle at 90 days of age, but this difference might not be clear because the mice were at the age of onset.

Changes in GSL levels on spinal cord samples from SOD1^{G93A} mice have also been reported[214]. GlcCer was significantly increased in SOD1^{G93A} mice at about 122 days (when moribund), while interestingly almost all GSLs downstream of GlcCer, i.e. LacCer, GM1 and GM3 levels were decreased at onset of symptoms and increased again when the mice were near humane endpoint[214]. Here, HPLC analysis of tibialis anterior and gastrocnemius muscle of SOD1^{G93A} mice revealed a significant increase in the total amount of GSLs in the symptomatic/morbid age group, alongside a significant increase in levels of several GSLs, including LacCer, GM3 and GM2, but no changes were observed at age of onset (**Figure 4.4**, **Figure 4.5**, **Figure 4.7** and **Figure 4.8**). When looking into the activity of the hydrolases which regulate GSLs catabolism, hexosaminidase activity was elevated while GBA1, GBA2 and galactosylceramidase activities were reduced in the

spinal cord of symptomatic SOD1^{G93A} mice at disease end stage[214]. In the gastrocnemius muscle, both β-hexosaminidase and β-galactosidase activities were found to be increased only at morbid stage (**Figure 4.10**). Therefore, despite the reported changes at the age of onset in the spinal cord[214], no changes were found at the age of onset in muscle tissue of SOD1^{G93A} mice. An updated summary of the known changes on GSL metabolism is shown on **Table 4.2**.

 **ALS patients**	**CSF**	↑ GlcCer, SM[220] and GM1a[216]
	Spinal cord	↑ Cer, GlcCer, GalCer, LacCer, Gb3, GM3 and GM1 ↑ GBA1, GBA2, hexosaminidase, galactosylceramidase, α-galactosidase and β-galactosidase activities[214]
	Muscle	↑ GCS expression[215]
 **SOD1^{G86R} mice**	**Spinal cord**	↑ GM1a (when symptomatic)[215] & GBA2 activity[218]
	Muscle	↑ GlcCer, GM3, GM2 (when symptomatic) & GCS expression[215]
		GBA2 inhibition ↑ motor units integrity ↑ neuroprotection and ↓ disease progression[216,218]
 **SOD1^{G93A} mice**	**Spinal cord**	↑ GlcCer (end stage) ↓ Cer, SM, LacCer, Gb3 and GM1 at symptom onset and ↑ when moribund ↑ hexosaminidase (at onset of paralysis and end stage) ↓ GBA1, GBA2 and galactosylceramidase activity (at onset of paralysis and end stage)[214]
		GCS inhibition ↑ disease progression GM3 intracerebroventricular infusion ↓ disease progression[214]
	Muscle	↑ LacCer, GM3 and GM2 (at end stage) ↑ β-hexosaminidase and and β-galactosidase activities (at end stage)
 **WT mice**	**Spinal cord**	Peripheral nerve injury ↑ GCS expression and GlcCer levels Peripheral nerve injury & GCS inhibition ↓ GlcCer levels & motor function recovery[215] Peripheral nerve injury & GBA2 inhibition ↑ motor function recovery[218]

Table 4.2. GSL metabolism in MND: a summary of what is known so far (updated). New acquired data is shown in blue.

The age of onset for the SOD1^{G86R} mice used in this chapter was 90 days and no difference was found in the spinal cord levels of GSLs between WT and mutant mice, while the age of onset for the SOD1^{G93A} mice reported in the literature was 100 days (showing the differences summarised in **Table 4.2**)[214]. Both SOD1^{G86R} mice and SOD1^{G93A} mice show symptoms at around 95 to 110 days[214,216], however, the different results found might be explained by different cohorts and age groups being used in each study. Also, despite having been thoroughly studied over the past almost 30 years, the actual age of onset of the SOD1^{G93A} mouse is still under discussion, as motor neuron and NMJ degeneration can be found weeks before loss of motor function[260,261]. It is also possible that the two mutations have some differences in the way or rate with which they promote neurodegeneration.

Overall, the presented data suggests that changes in GSL metabolism are detected first in the spinal cord and only later in muscle tissues, in the presence of mutant SOD1. This is in line with the literature, suggesting that asymptomatic SOD1^{G93A} mice show gradual impairment of the endo-lysosomal trafficking and autophagic clearance[207,208]. As GSL catabolism occurs mainly in the lysosome and lysosomal enzymes require efficient endo-lysosomal maturation, it is likely that these deficiencies result in changes in the levels of GSLs and on the activity of the lysosomal enzymes that regulate their metabolism.

Further experiments are necessary to understand how the age of the mice and the stage of disease progression in each model influence the described results and, more importantly, if this order of events also happens in cases of MND in the absence of mutant SOD1. Analysis of tissues in more timepoints throughout disease progression would allow a better understanding of the GSL metabolic changes occurring with disease

progression. The study of GSL metabolism in different models of MND (for different aspects of the disease other than SOD1 mutations) would clarify if these results are only caused by SOD1 mutations or if it is part of general MND pathology.

5. GSL metabolism in the TDP-43^{M337V} BAC mouse model

5.1. Introduction

5.1.1. TDP-43 pathology in MND

TDP-43 is a ubiquitously expressed protein encoded by the *TARDBP* gene, with various domains including two highly conserved RNA recognition motifs and a glycine-rich C-terminal domain[154,165]. TDP-43 is primarily localized in the nucleus of cells where it is responsible for several physiological roles through the regulation of various genes by DNA/RNA binding, splicing and protein-protein interactions[166–171]. About 95 % of all sporadic and familiar cases of MND show a redistribution of TDP-43 to the cytoplasm in the affected motor neurons, where it forms insoluble ubiquitinated aggregates, making TDP-43 proteinopathy a pathological hallmark of the disease[135,174,175].

More than 50 mutations in *TARDBP* have been identified in MND patients, mainly in its C-terminal region, which is thought to be responsible for RNA-protein and protein-protein interactions and for the tendency of TDP-43 to aggregate[172,173]. *TARDBP* mutations directly associate with neurodegeneration, but it is still unclear what causes the pathology downstream of the mutation. It has been suggested that it is caused by the mislocalisation of the protein from the nucleus to the cytoplasm affecting its normal nuclear function, an acquired toxic effect or a combination of factors[135,262]. While *TARDBP* mutations are associated with only a small percentage of cases, TDP-43 aggregates are found in the brain and spinal cord of the majority of MND patients. Importantly, TDP-43

pathology has also been found in frontotemporal dementia (FTD, the second most common cause of dementia) and ALS/FTD patients, suggesting these diseases might share common molecular pathways mediated by changes in TDP-43[135,177,263].

With the finding of SOD1 mutations in MND, the first models for MND were based on SOD1 genetics[151,152]. However, SOD1 mutations are only responsible for a small percentage of MND cases and it is still under debate if patients with SOD1 mutations exhibit TDP-43 pathology[264–267]. Therefore, new mouse models were developed to study how TDP-43 pathology contributes to MND. However, the *TARDBP* general knockout mouse is embryonic lethal and mice with only one copy of TDP-43 (*TARDBP*$^{+/-}$) show normal levels of TDP-43 and no pathology (**Table 5.1**)[268–270]. Thus, many researchers have instead used models that express the human form of the TDP-43 gene, with different models expressing different transgenes (and different promotors, to regulate their expression). Overexpression of both mutant and WT human TDP-43 causes motor deficits, partially recapitulating human MND pathology[271–273]. However, TDP-43 overexpression in models also can have a non-specific toxic effect, which makes it difficult to distinguish from the motor neuron degeneration effects (**Table 5.1**)[227,274–280].

TARDBP mutation	Outcome
Complete knockout ($TARDBP^{-/-}$)	Embryonic lethal[268–270]
Partial knockout ($TARDBP^{+/-}$)	Normal levels of TDP-43 and no pathology[268]
Partial knockdown	Directly impairs endosomal pathways, necessary to regulate dendrite growth and neuronal signalling[281]
Overexpression of WT or mutant forms, or C-terminal fragments of the gene	Partially recapitulates MND pathology and mice develop motor deficits, but disease phenotypes are variable, meaning these might be due to non-specific toxicity from TDP-43 overexpression[274–280]
TDP-43^{M337V} BAC mouse	Recapitulates MND pathology and mice develop progressive motor deficits without the formation of TDP-43 insoluble aggregates. The expression of human mutant TDP-43 occurs under physiological levels, avoiding non-specific toxicity[227]

Table 5.1. Some of the outcomes of *TARDBP* mutations in mouse models.

To address the complications and limitations of the previous models, David Gordon and colleagues (Nuffield Department of Clinical Neurosciences, University of Oxford) generated a mouse expressing a single copy of a bacterial artificial chromosome (BAC) construct containing the full length human *TARDBP* gene, WT or with the M337 V mutation that has been associated with MND, and a C-terminal Ypet tag, specifically inserted into the mouse *Rosa26 (Gt(ROSA26)Sor* locus[227,228]. These TDP-43^{M337V} BAC mice express low levels of human TDP-43, avoiding possible overexpression toxic effects, and replicate human ALS/FTD pathology by developing progressive neuromuscular abnormalities and motor deficits with age and reduced survival[227]. Homozygous (TDP-$43^{M337V/M337V}$) mice perform significantly worse than their heterozygous (TDP-$43^{M337V/-}$) littermates in grip strength and accelerating rotarod tests for motor function and, consequently, show significantly reduced survival (homozygotes live approximately 500 days and heterozygotes 650 days)[227]. Interestingly, despite the loss of neuromuscular junction integrity and development of motor deficits, no TDP-43 cytoplasmic aggregates were found in TDP-43^{M337V} mice at any age, and no significant

neuronal death or macrophage/microglial involvement was found at 12 months of age (symptomatic)[227]. However, this mouse model of MND did show impaired axonal transport of signalling endosomes, before symptoms onset (between 1.5 and 3 months of age, not seen this early in mice carrying mutant FUS)[282]. On the other hand, primary motor neurons from TDP-43^{M337V} mice displayed increased TDP-43 cytoplasmic mislocalisation, associated with reduced endoplasmic reticulum Ca^{2+} stores and altered stress granule dynamics[227,228]. TDP-43^{M337V} mice are phenotypically normal until they are 6 months-old, making this a great model to study early stages of MND pathology[227].

5.1.2. GSL metabolism and TDP-43 pathology

A lot of what is known about GSL metabolism in ALS came from studies of the SOD1 models or from CSF samples from MND patients (see **Chapter 4**)[212]. However, as stated previously, SOD1 mutations are only responsible for a small percentage of MND cases and the relevance of TDP proteinopathy in patients with these mutations is still under discussion[264–267]. In normal physiological conditions, TDP-43 aggregates are degraded by autophagy and it has been suggested that in MND TDP-43 interferes with endosomal maturation and lysosomal function, the organelle responsible for GSL catabolism[283–288]. Also, TDP-43 alterations and aggregation have been reported in the neurodegenerative, lysosomal storage disease Niemann-Pick disease Type C[289]. Yet, the effect of TDP-43 pathology specifically in terms of GSL metabolism remains unexplored (Error! Reference s ource not found.).

TDP 43$^{M337V/M337V}$ mice			TDP 43$^{M337V/-}$ mice
3 months	6 months	9 months	12 months
pre-symptomatic	early onset of symptoms	late onset of symptoms	early symptomatic

Table 5.2. Different cohorts of TDP-43 mice were studied in this thesis. The study of GSL metabolism in TDP-43$^{M337V/M337V}$ mice is presented in Chapter 5.2.1 and in TDP-43$^{M337V/-}$ mice in Chapter 5.2.2.

5.1.3. Aims

In this chapter, the effect of TDP-43 pathology on GSL metabolism was investigated by evaluating the changes in levels of GlcCer and downstream GSLs, as well as measuring GSL lysosomal hydrolase activities in spinal cord and brain of the TDP-43$^{M337V/M337V}$ mouse model. These changes were also evaluated in spinal cord and brain of early symptomatic 12 months TDP-43$^{M337V/-}$ (heterozygous) mice (Error! Reference source not found.).

5.2. Results

5.2.1. GSL metabolism in the TDP-43$^{M337V/M337V}$ mouse

GSL metabolism was shown to play a significant role in MND in studies using SOD1 mouse models and CSF of patients with MND, but the involvement of GSL metabolism on TDP pathology remains unexplored. Therefore, TDP-43$^{M337V/M337V}$ BAC mice and age-matched C57BL/6J (NTg) littermates (males and females) were aged to 3, 6 months and 9 months, which corresponds to pre-symptomatic, early onset and late onset of symptoms, respectively.

On average, NTg mice gained weight as they aged but TDP-43$^{M337V/M337V}$ BAC mice did not (**Figure 5.1** NTg vs. TDP-43$^{M337V/M337V}$: 3 months p>0.9999, 6 months p=0.4724, 9 months p=0.1410; NTg: 3 vs. 6 months p=0.3625, 3 vs. 9 months p=0.0076, 6 vs. 9 months p=0.4871; TDP-43$^{M337V/M337V}$: 3 vs. 6 months p=0.9945, 3 vs. 9 months p=0.7129, 6 vs. 9 months p=0.9373, n=10-15 mice per group).

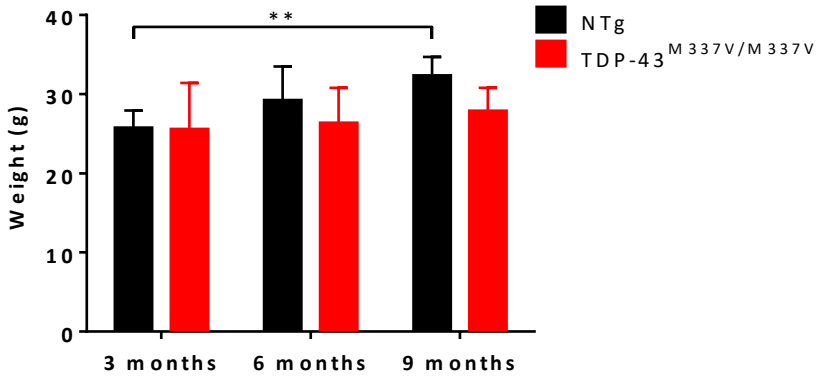


Figure 5.1. No significant changes were found in the average weight of TDP-43$^{M337V/M337V}$ mice at 3, 6 or 9 months of age when compared to age-matched NTg controls.
Average weight of 3, 6 and 9 months-old TDP-43$^{M337V/M337V}$ BAC mice (red), corresponding to progressive stages of disease (pre-symptomatic, age of early onset and late onset of symptoms, respectively), and age-matched NTg controls (black). Data are presented as the mean ±SD. Data were analysed using 2-way ANOVA, with Tukey's multiple comparisons test. **p < 0.01, n = 10-15 mice per group.

GlcCer and downstream GSL levels were measured by NP-HPLC. GlcCer levels in the spinal cord of NTg mice showed a tendency to increase with age, reaching statistical significance when comparing levels at 3 months with the levels at 9 months (**Figure 5.2**, black, NTg: 3 vs. 6 months p=0.2627, 3 vs. 9 months p=0.0038, 6 vs. 9 months p=0.4388; n=5-6 mice per group). Levels of GlcCer in the spinal cord of TDP-43$^{M337V/M337V}$ mice were not significantly different from their NTg littermates (**Figure 5.2**, red; NTg vs. TDP-43$^{M337V/M337V}$: 3 months p=0.3442, 6 months p=0.9388, 9 months p=0.9914;

TDP-43$^{M337V/M337V}$: 3 vs. 6 months p=0.8825, 3 vs. 9 months p=0.1224, 6 vs. 9 months p=0.6444; n=5-6 mice per group).

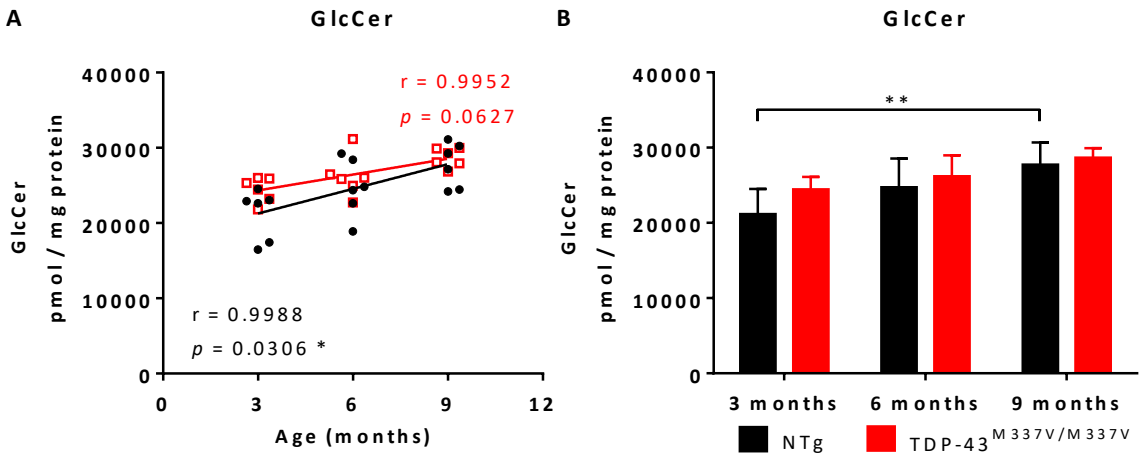


Figure 5.2. No significant differences in GlcCer levels were found in spinal cord of TDP-43$^{M337V/M337V}$ mice at pre-symptomatic or onset stages of disease progression when compared to age-matched NTg controls.
Changes in GlcCer levels in spinal cord of TDP-43$^{M337V/M337V}$ BAC mice at different ages, corresponding to progressive stages of disease (3 months for pre-symptomatic, 6 months for early onset and 9 months for late onset of symptoms, red) and aged matched NTg controls (black), measured by NP-HPLC. Data were analysed using (A) Pearson correlation analysis and (B) 2-way ANOVA, with Tukey's multiple comparisons test. Bar graph is presented as the mean ±SD. *p < 0.05, **p < 0.01, n = 5-6 mice per group.

When evaluating the levels of total GSLs and the major gangliosides (GM1a, GD1a, GD1b and GT1b) in the spinal cord, TDP-43$^{M337V/M337V}$ mice and NTg mice showed equivalent changes in the levels of GSLs over time, which is visible on the parallel and almost overlapping lines of linear regression and Pearson correlation analysis shown on panels A and C of **Figure 5.3** and panels A, C and E of **Figure 5.4**. GM1a levels increased significantly with age, while levels of GD1a, GD1b and GT1b decreased with time in the spinal cord of both TDP-43$^{M337V/M337V}$ and NTg mice (**Figure 5.3** B, GM1a, NTg vs. TDP-43$^{M337V/M337V}$: 3 months p=0.9007, 6 months p=0.0743, 9 months p=0.9746; NTg: 3 vs. 6 months p=0.0122, 3 vs. 9 months p<0.0001, 6 vs. 9 months p=0.0023;

TDP-43$^{M337V/M337V}$: 3 vs. 6 months p=0.0002, 3 vs. 9 months p<0.0001, 6 vs. 9 months p=0.3917; n=5-6 mice per group; **Figure 5.3** D, GD1a, NTg vs. TDP-43$^{M337V/M337V}$: 3 months p=0.9968, 6 months p>0.9999, 9 months p=0.9962; NTg: 3 vs. 6 months p=0.0033, 3 vs. 9 months p<0.0001, 6 vs. 9 months p=0.1136; TDP-43$^{M337V/M337V}$: 3 vs. 6 months p=0.0090, 3 vs. 9 months p<0.0001, 6 vs. 9 months p=0.0507; n=5-6 mice per group; **Figure 5.4** B, GD1b, NTg vs. TDP-43$^{M337V/M337V}$: 3 months p=0.5109, 6 months p>0.9999, 9 months p>0.9999; NTg: 3 vs. 6 months p=0.0007, 3 vs. 9 months p<0.0001, 6 vs. 9 months p=0.0765; TDP-43$^{M337V/M337V}$: 3 vs. 6 months p=0.0330, 3 vs. 9 months p<0.0001, 6 vs. 9 months p=0.1065; n=5-6 mice per group; **Figure 5.4** D, GT1b, NTg vs. TDP-43$^{M337V/M337V}$: 3 months p=0.9258, 6 months p=0.8573, 9 months p=0.9992; NTg: 3 vs. 6 months p=0.3820, 3 vs. 9 months p=0.0021, 6 vs. 9 months p=0.2021; TDP-43$^{M337V/M337V}$: 3 vs. 6 months p=0.4651, 3 vs. 9 months p=0.0334, 6 vs. 9 months p=0.6238; n=5-6 mice per group).

However, levels of GD1a and GD1b did not reach statistical significance when comparing the levels at 6 and 9 months of age, which shows that the major changes observed occurred between the ages of 3 and 6 months (**Figure 5.3** C-D and **Figure 5.4** A-B). The altered expression of GD1a and GD1b in the spinal cord of both the NTg and TDP-43$^{M337V/M337V}$ mice were not reflected in the total amount of GSLs, which did not change with age or the TDP-43$^{M337V/M337V}$ mutation (**Figure 5.4** F, NTg vs. TDP-43$^{M337V/M337V}$: 3 months p=0.9895, 6 months p=0.9521, 9 months p>0.9999; NTg: 3 vs. 6 months p=0.9981, 3 vs. 9 months p=0.5472, 6 vs. 9 months p=0.3073; TDP-43$^{M337V/M337V}$: 3 vs. 6 months p>0.9999, 3 vs. 9 months p=0.8220, 6 vs. 9 months p=0.7317; n=5-6 mice per group).

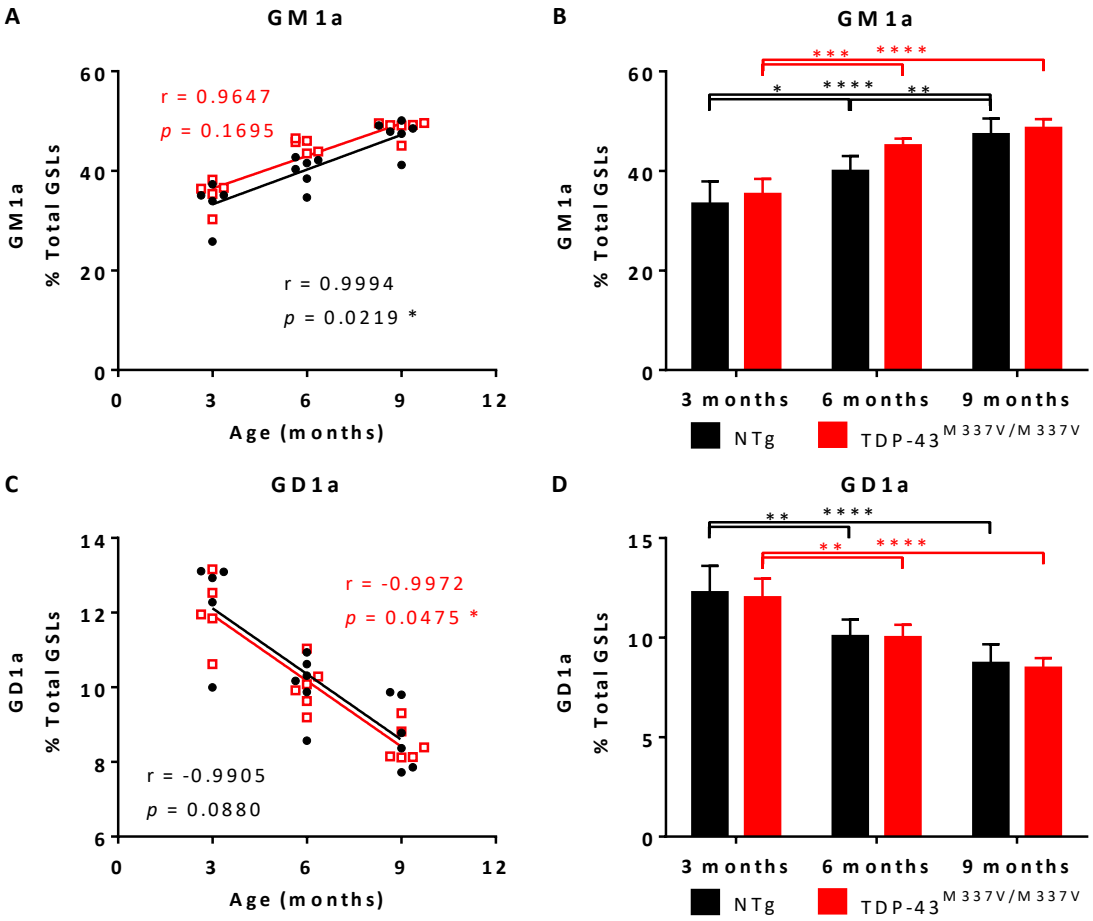


Figure 5.3. No significant changes were found in the levels of GM1a and GD1a in spinal cord of TDP-43$^{M337V/M337V}$ mice at pre-symptomatic or onset stages of disease progression when compared to age-matched NTg controls.

Changes in levels of GM1a (A-B) and GD1a (C-D) in spinal cord of TDP-43$^{M337V/M337V}$ BAC mice at different ages, corresponding to progressive stages of disease (3 months for pre-symptomatic, 6 months for early onset and 9 months for late onset of symptoms, red) and aged matched NTg controls (black), measured by NP-HPLC. Data were analysed using (A,C) Pearson correlation analysis and (B,D) 2-way ANOVA, with Tukey's multiple comparisons test. Bar graph is presented as the mean ±SD. *p < 0.05, **p < 0.01, ***p < 0.001, ****p < 0.0001, n = 5-6 mice per group.

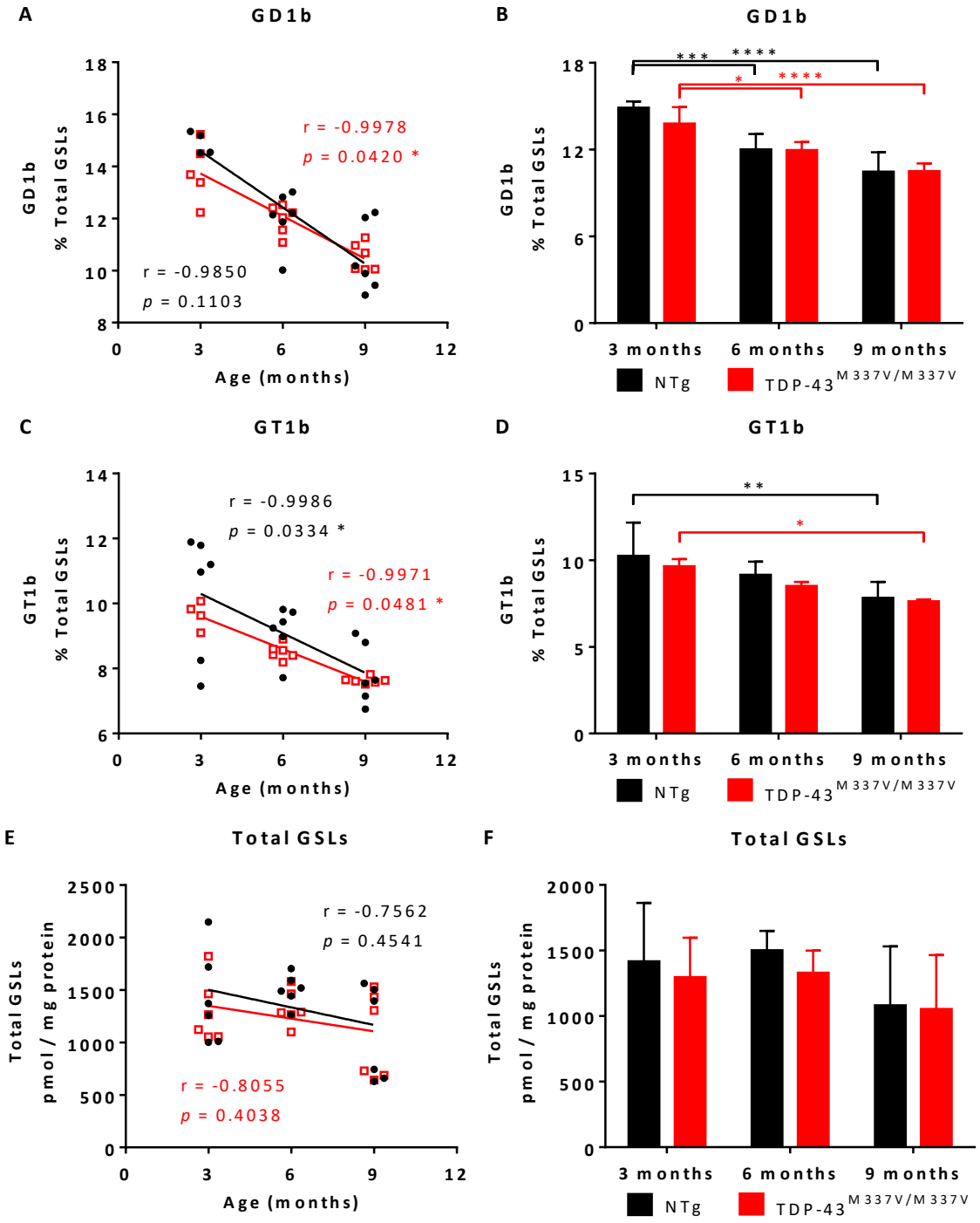


Figure 5.4. No significant changes were found in the levels of GD1b, GT1b and total GSLs in spinal cord of TDP-43$^{M337V/M337V}$ mice at pre-symptomatic or onset stages of disease progression when compared to age-matched NTg controls.

Changes in levels of GD1b (A-B), GT1b (C-D) and total GSLs (E-F) in spinal cord of TDP-43$^{M337V/M337V}$ BAC mice at different ages, corresponding to progressive stages of disease (3 months for pre-symptomatic, 6 months for early onset and 9 months for late onset of symptoms, red) and aged matched NTg controls (black), measured by NP-HPLC. Data were analysed using (A,C,E) Pearson correlation analysis and (B,D,F) 2-way ANOVA, with Tukey's multiple comparisons test. Bar graph is presented as the mean ±SD. *$p < 0.05$, **$p < 0.01$, ***$p < 0.001$, ****$p < 0.0001$, n = 5-6 mice per group.

The activity of the GSL hydrolases GBA, GBA2, α-galactosidase, β-galactosidase, β-hexosaminidase and sialidase (neuraminidases Neu1, Neu3 and Neu4) in the spinal cord of the same 3, 6 and 9 months-old TDP-43$^{M337V/M337V}$ mice and age-matched NTg controls revealed more complex results (**Figure 5.5** and **Figure 5.6**). GBA activity decreased with age similarly on NTg and TDP-43$^{M337V/M337V}$ mice, with a statistically significantly lower value at 9 months, when compared to both 3 or 6 months-old mice (**Figure 5.5** A-B, NTg vs. TDP-43$^{M337V/M337V}$: 3 months p=0.6350, 6 months p=0.7120, 9 months p=0.8934; NTg: 3 vs. 6 months p=0.2058, 3 vs. 9 months p<0.0001, 6 vs. 9 months p=0.0051; TDP-43$^{M337V/M337V}$: 3 vs. 6 months p=0.1854, 3 vs. 9 months p<0.0001, 6 vs. 9 months p=0.0095; n=5-6 mice per group). GBA2 activity also tended to decrease with time for the TDP-43$^{M337V/M337V}$ mice, but more consistently and significantly for the NTg controls (r values near -1, specially for the spinal cord of NTg mice, **Figure 5.5** C). Notably, GBA2 activity in the spinal cord of TDP-43$^{M337V/M337V}$ mice was higher than that of NTg mice at both 6 and 9 months of age – a small difference on average but statistically significant (**Figure 5.5** D, NTg vs. TDP-43$^{M337V/M337V}$: 3 months p=0.5019, 6 months p=0.0234, 9 months p=0.5882; NTg: 3 vs. 6 months p=0.8018, 3 vs. 9 months p=0.0798, 6 vs. 9 months p=0.6227; TDP-43$^{M337V/M337V}$: 3 vs. 6 months p=0.9963, 3 vs. 9 months p=0.0590, 6 vs. 9 months p=0.0265; n=5-6 mice per group). These results are in agreement with previous reports of reduced GBA and GBA2 activity in the brain of aged mice[249]. α-galactosidase and sialidase activities were similar in TDP-43$^{M337V/M337V}$ and NTg mice and did not change significantly with time, even though they had a tendency to decrease with age (**Figure 5.5** F, α-galactosidase: NTg vs. TDP-43$^{M337V/M337V}$: 3 months p=0.9991, 6 months p>0.9999, 9 months p=0.9976; NTg: 3 vs. 6 months p=0.8902, 3 vs. 9 months p=0.7951, 6 vs. 9 months p>0.9999; TDP-43$^{M337V/M337V}$: 3 vs. 6 months

p=0.9949, 3 vs. 9 months *p*=0.7476, 6 vs. 9 months *p*=0.9567; n=5-6 mice per group; **Figure 5.6** F, sialidase: NTg vs. TDP-43$^{M337V/M337V}$: 3 months *p*=0.6008, 6 months *p*>0.9999, 9 months *p*=0.8927; NTg: 3 vs. 6 months *p*=0.8101, 3 vs. 9 months *p*=0.1897, 6 vs. 9 months *p*=0.8568; TDP-43$^{M337V/M337V}$: 3 vs. 6 months *p*=0.9987, 3 vs. 9 months *p*=0.4504, 6 vs. 9 months *p*=0.2495; n=5-6 mice per group). The average activity of β-galactosidase also tended to decrease with age (**Figure 5.6** A) and was lower on the spinal cord of TDP-43$^{M337V/M337V}$ mice when compared to NTg mice, but only reached statistical significance at 3 months of age (**Figure 5.6** B, NTg vs. TDP-43$^{M337V/M337V}$: 3 months *p*=0.0348, 6 months *p*=0.1463, 9 months *p*=0.1067; NTg: 3 vs. 6 months *p*=0.6400, 3 vs. 9 months *p*=0.1436, 6 vs. 9 months *p*=0.9144; TDP-43$^{M337V/M337V}$: 3 vs. 6 months *p*=0.9487, 3 vs. 9 months *p*=0.3468, 6 vs. 9 months *p*=0.853; n=5-6 mice per group). Finally, β-hexosaminidase was the most active enzyme in the spinal cord of both NTg and TDP-43$^{M337V/M337V}$ mice and its activity did not change with age (as previously reported in the aged mouse brain[249]) or in the presence of the TDP-43$^{M337V/M337V}$ mutation (**Figure 5.6** C-D, NTg vs. TDP-43$^{M337V/M337V}$: 3 months *p*=0.9997, 6 months *p*>0.9999, 9 months *p*=0.9951; NTg: 3 vs. 6 months *p*>0.9999, 3 vs. 9 months *p*>0.9999, 6 vs. 9 months *p*>0.9999; TDP-43$^{M337V/M337V}$: 3 vs. 6 months *p*>0.9999, 3 vs. 9 months *p*=0.9990, 6 vs. 9 months *p*>0.9999; n=5-6 mice per group).

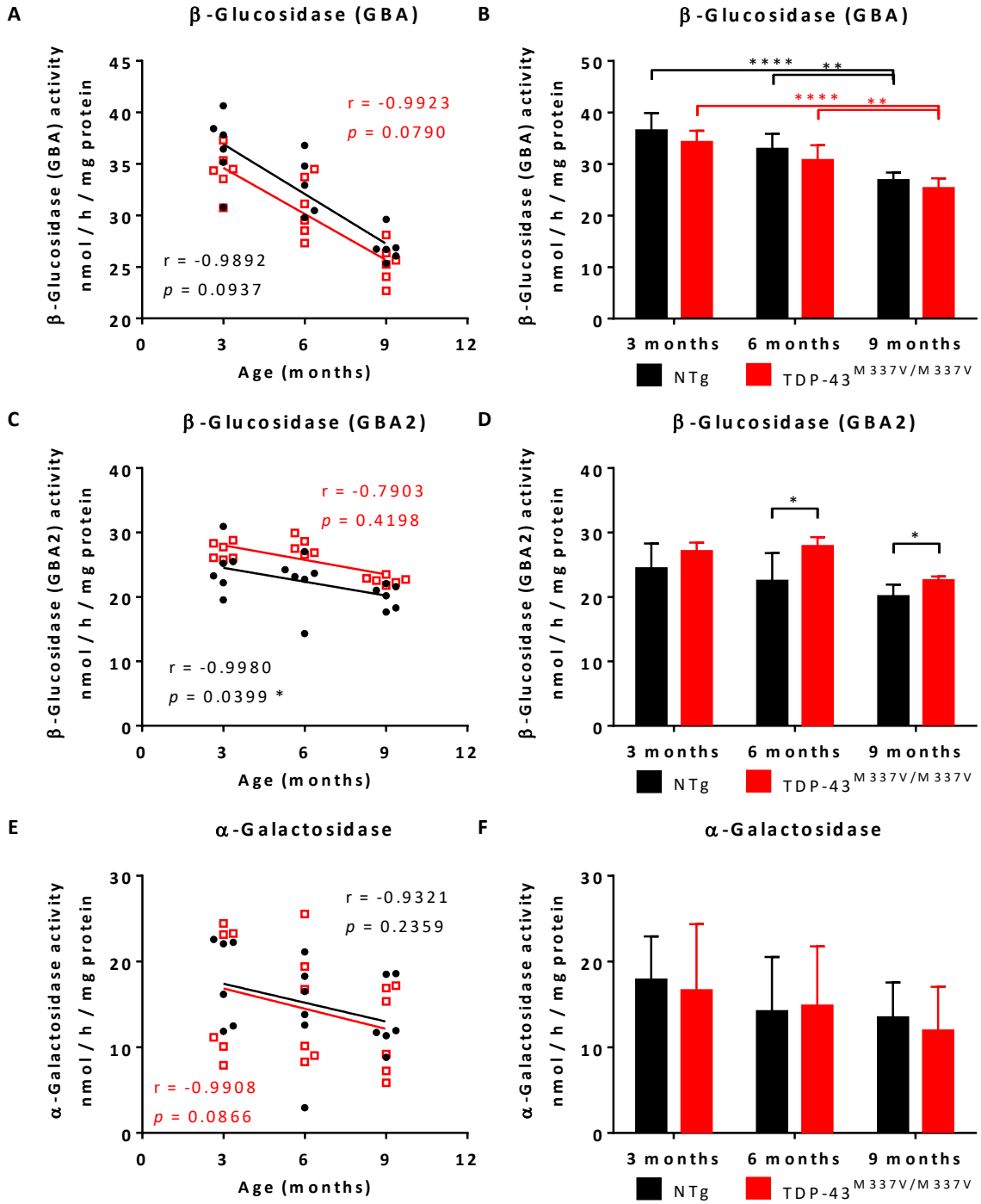


Figure 5.5. No significant changes were found in the activity of GBA, GBA2 or α-galactosidase in spinal cord of TDP-43$^{M337V/M337V}$ mice at pre-symptomatic or onset stages of disease progression when compared to age-matched NTg controls.

Changes in GBA, GBA2 and α-galactosidase activities in spinal cord of TDP-43$^{M337V/M337V}$ mice at different ages, corresponding to progressive stages of disease (3 months for pre-symptomatic, 6 months for early onset and 9 months for late onset of symptoms, red) and aged matched NTg controls (black). Data were analysed using (A,C,E) Pearson correlation analysis and (B,D,F) 2-way ANOVA, with Tukey's multiple comparisons test. Bar graph is presented as the mean ±SD. *$p < 0.05$, **$p < 0.01$, ****$p < 0.0001$, n = 5-6 mice per group.

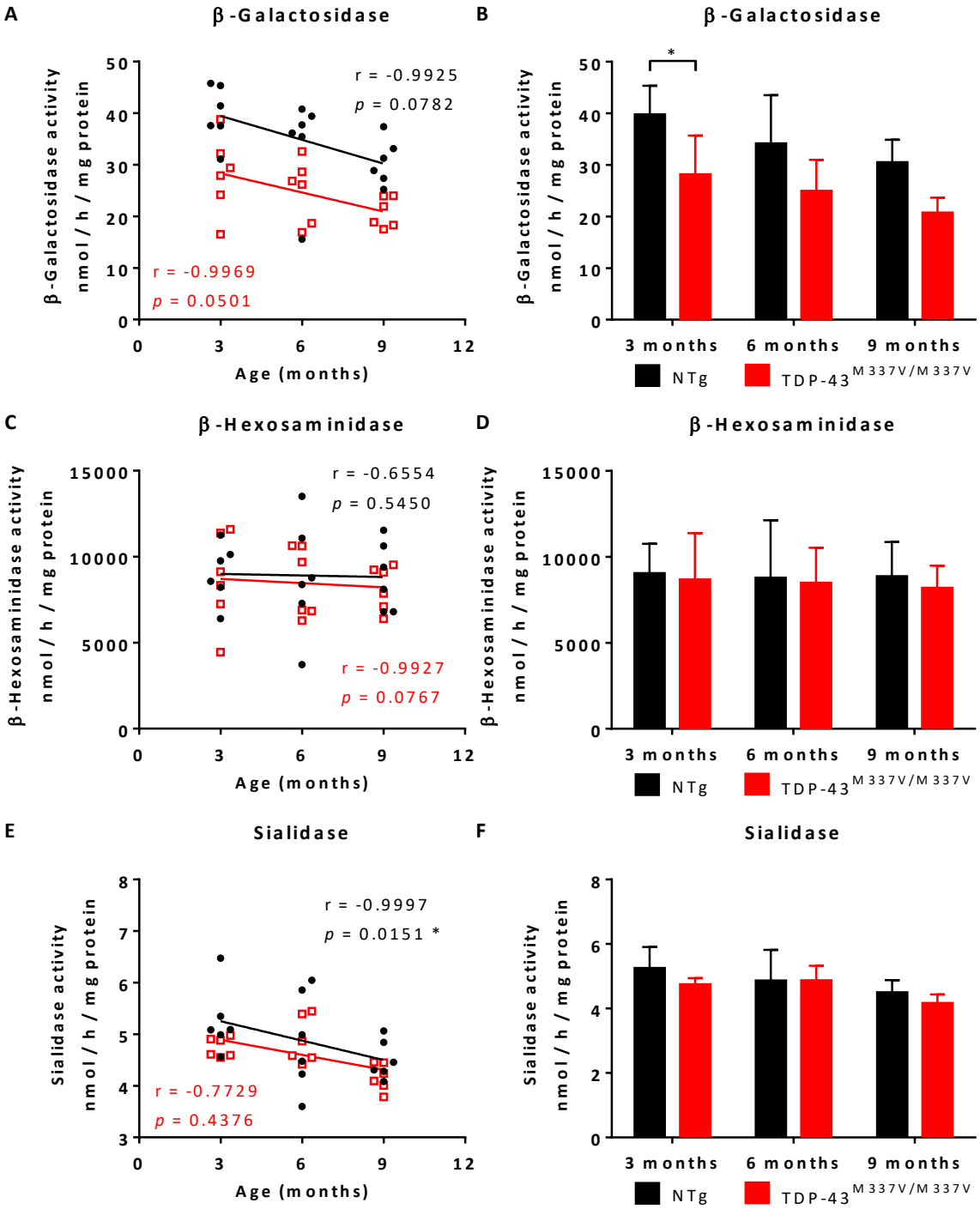


Figure 5.6. β-galactosidase activity was reduced in spinal cord of pre-symptomatic TDP-43$^{M337V/M337V}$ mice, but no significant changes were found in the activity of β-hexosaminidase or sialidase at pre-symptomatic or onset stages of disease progression, when compared to age-matched NTg controls.

Changes in β-galactosidase, β-hexosaminidase and sialidase activities in spinal cord of TDP-43$^{M337V/M337V}$ mice at different ages, corresponding to progressive stages of disease (3 months for pre-symptomatic, 6 months for early onset and 9 months for late onset of symptoms, red) and aged matched NTg controls (black). Data were analysed using (A,C,E) Pearson correlation analysis and (B,D,F) 2-way ANOVA, with Tukey's multiple comparisons test. Bar graph is presented as the mean ±SD. *p < 0.05, n = 5-6 mice per group.

GSL metabolism was also studied in whole brain tissue of TDP-43$^{M337V/M337V}$ BAC mice. GlcCer levels in the brain of TDP-43$^{M337V/M337V}$ mice were found to be significantly higher at 9 months of age when compared to levels at 3 or 6 months. However, these levels were not significantly different from those observed in the NTg mice (**Figure 5.7**, NTg vs. TDP-43$^{M337V/M337V}$: 3 months p=0.9138, 6 months p=0.9983, 9 months p=0.3718; NTg: 3 vs. 6 months p>0.9999, 3 vs. 9 months p=0.0838, 6 vs. 9 months p=0.0918; TDP-43$^{M337V/M337V}$: 3 vs. 6 months p=0.9938, 3 vs. 9 months p=0.0100, 6 vs. 9 months p=0.0026; n=5-6 mice per group).

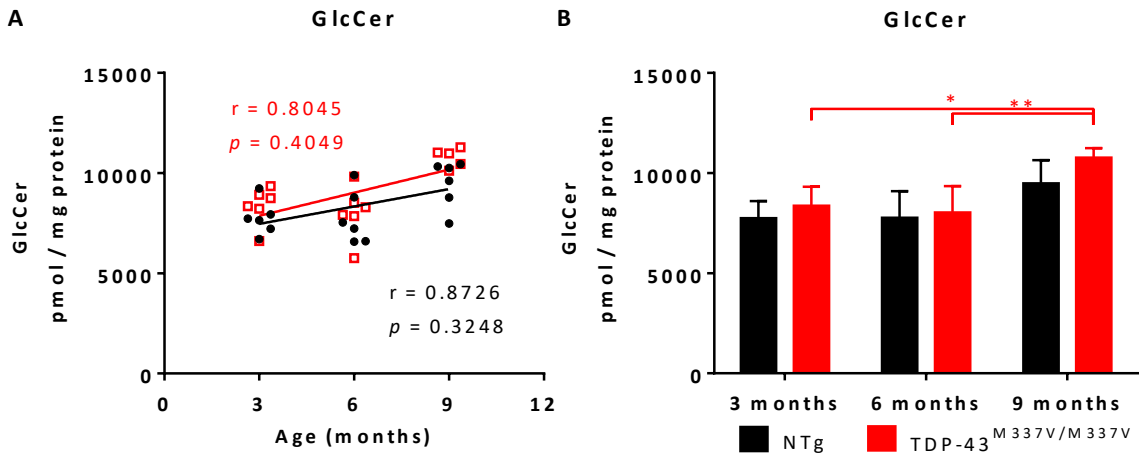


Figure 5.7. No significant differences in GlcCer levels were found in brain of TDP-43$^{M337V/M337V}$ mice at pre-symptomatic or onset stages of disease progression when compared to age-matched NTg controls.
Changes in GlcCer levels in brain of TDP-43$^{M337V/M337V}$ BAC mice at different ages, corresponding to progressive stages of disease (3 months for pre-symptomatic, 6 months for early onset and 9 months for late onset of symptoms, red) and aged matched NTg controls (black), measured by NP-HPLC. Data were analysed using (A) Pearson correlation analysis and (B) 2-way ANOVA, with Tukey's multiple comparisons test. Bar graph is presented as the mean ±SD. *p < 0.05, **p < 0.01, n = 5-6 mice per group.

The amount of total GSLs in the brain did not change apart from a small reduction at 9 months in the TDP-43$^{M337V/M337V}$ mice when compared to 6 months-old transgenic mice (**Figure 5.9** E-F, NTg vs. TDP-43$^{M337V/M337V}$: 3 months p=0.1449, 6 months p=0.9666,

9 months p=0.2335; NTg: 3 vs. 6 months p=0.4387, 3 vs. 9 months p=0.5294, 6 vs. 9 months p>0.9999; TDP-43$^{M337V/M337V}$: 3 vs. 6 months p>0.9999, 3 vs. 9 months p=0.0503, 6 vs. 9 months p=0.0374; n=5-6 mice per group). However, when looking into the levels of individual gangliosides in brain, contrary to what was seen in spinal cord, TDP-43$^{M337V/M337V}$ mice and NTg mice do not change in the same manner with time (intersecting lines on **Figure 5.8** A and C and **Figure 5.9** A and C). GD1b and GT1b levels are significantly higher in TDP-43$^{M337V/M337V}$ mice when compared to NTg mice at 3 months of age (**Figure 5.9** B, GD1b: NTg vs. TDP-43$^{M337V/M337V}$: 3 months p=0.0227, 6 months p=0.9999, 9 months p>0.9999; n=5-6 mice per group; **Figure 5.9** D, GT1b: NTg vs. TDP-43$^{M337V/M337V}$: 3 months p=0.0277, 6 months p=0.8978, 9 months p=0.9858; n=5-6 mice per group). GM1a levels increase in brain of NTg mice from 3 to 6 months of age, but do not change over time in the TDP-43$^{M337V/M337V}$ mice (**Figure 5.8** A-B, NTg vs. TDP-43$^{M337V/M337V}$: 3 months p=0.0541, 6 months p=0.9699, 9 months p=0.4925; NTg: 3 vs. 6 months p=0.0187, 3 vs. 9 months p=0.0003, 6 vs. 9 months p=0.6315; TDP-43$^{M337V/M337V}$: 3 vs. 6 months p=0.8207, 3 vs. 9 months p>0.9999, 6 vs. 9 months p=0.9026; n=5-6 mice per group). GD1a, GD1b and GT1b levels do not change for NTg mice, but decrease with disease progression in the brain of TDP-43$^{M337V/M337V}$ mice, with significantly reduced levels by 9 months when compared to levels at 3 months of age (**Figure 5.8** C-D, GD1a: NTg vs. TDP-43$^{M337V/M337V}$: 3 months p=0.2037, 6 months p>0.9999, 9 months p=0.5756; NTg: 3 vs. 6 months p>0.9999, 3 vs. 9 months p=0.8685, 6 vs. 9 months p=0.8519; TDP-43$^{M337V/M337V}$: 3 vs. 6 months p=0.2686, 3 vs. 9 months p=0.0002, 6 vs. 9 months p=0.0644; n=5-6 mice per group; **Figure 5.9** A-B, GD1b: NTg: 3 vs. 6 months p=0.9719, 3 vs. 9 months p>0.9999, 6 vs. 9 months p=0.9997; TDP-43$^{M337V/M337V}$: 3 vs. 6 months p=0.9208, 3 vs. 9 months p=0.0245, 6 vs. 9 months

p=0.5692; n=5-6 mice per group; **Figure 5.9** C-D, GT1b: NTg: 3 vs. 6 months *p*=0.5210, 3 vs. 9 months *p*=0.9679, 6 vs. 9 months *p*=0.9301; TDP-43$^{M337V/M337V}$: 3 vs. 6 months *p*=0.9953, 3 vs. 9 months *p*=0.0381, 6 vs. 9 months *p*=0.1167; n=5-6 mice per group).

Interestingly, the levels of the major gangliosides present in spinal cord of NTg mice reduced with age but remained constant in brain (except for GM1a which increased with age). On the other hand, GD1a, GD1b and GT1b levels in spinal cord and brain of TDP-43$^{M337V/M337V}$ mice seem to change similarly with aging (**Figure 5.3**, **Figure 5.4**, **Figure 5.8** and **Figure 5.9**).

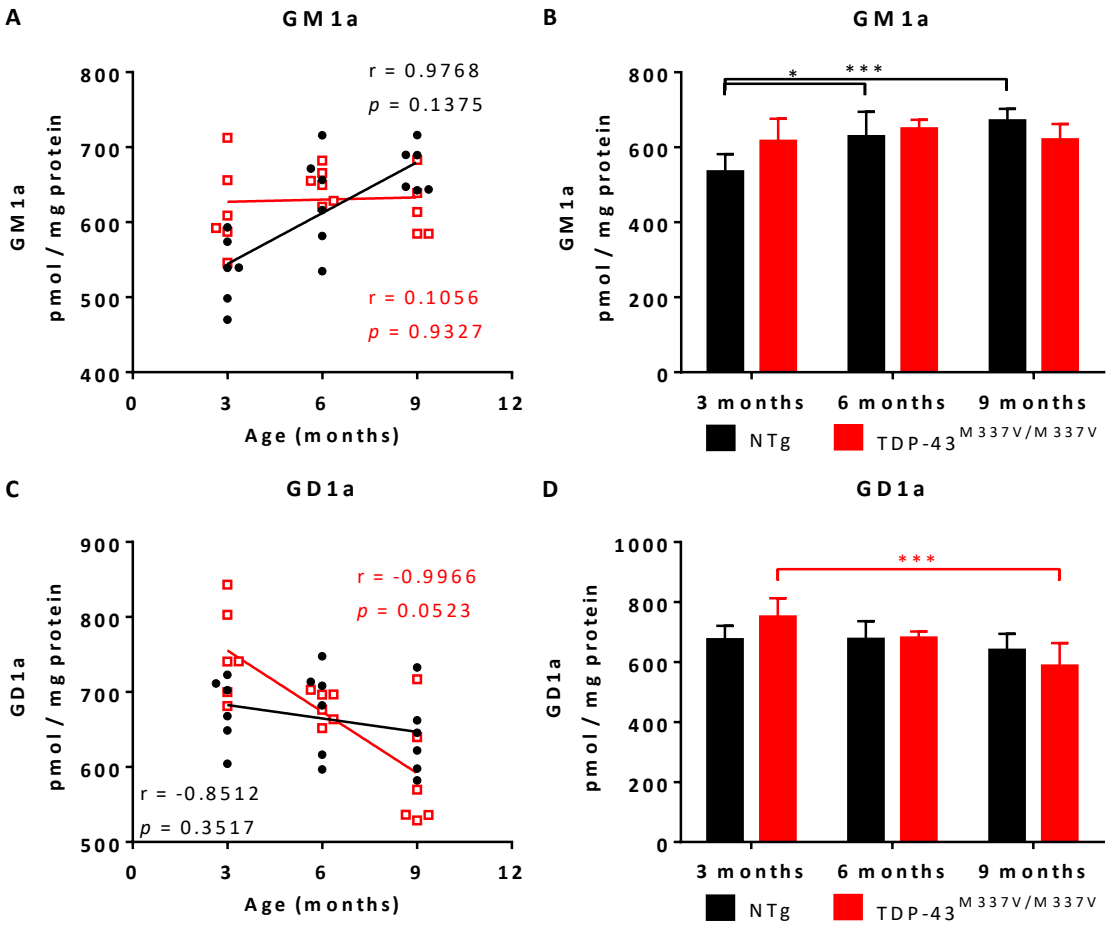


Figure 5.8. No significant changes were found in the levels of GM1a or GD1a in brain of TDP-43$^{M337V/M337V}$ mice mice at pre-symptomatic or onset stages of disease progression when compared to age-matched NTg controls.

Changes in levels of GM1a and GD1a in brain of TDP-43$^{M337V/M337V}$ BAC mice at different ages, corresponding to progressive stages of disease (3 months for pre-symptomatic, 6 months for early onset and 9 months for late onset of symptoms, red) and aged matched NTg controls (black), measured by NP-HPLC. Data were analysed using (A,C) Pearson correlation analysis and (B,D) 2-way ANOVA, with Tukey's multiple comparisons test. Bar graph is presented as the mean ±SD. *$p < 0.05$, ***$p < 0.001$, n = 5-6 mice per group.

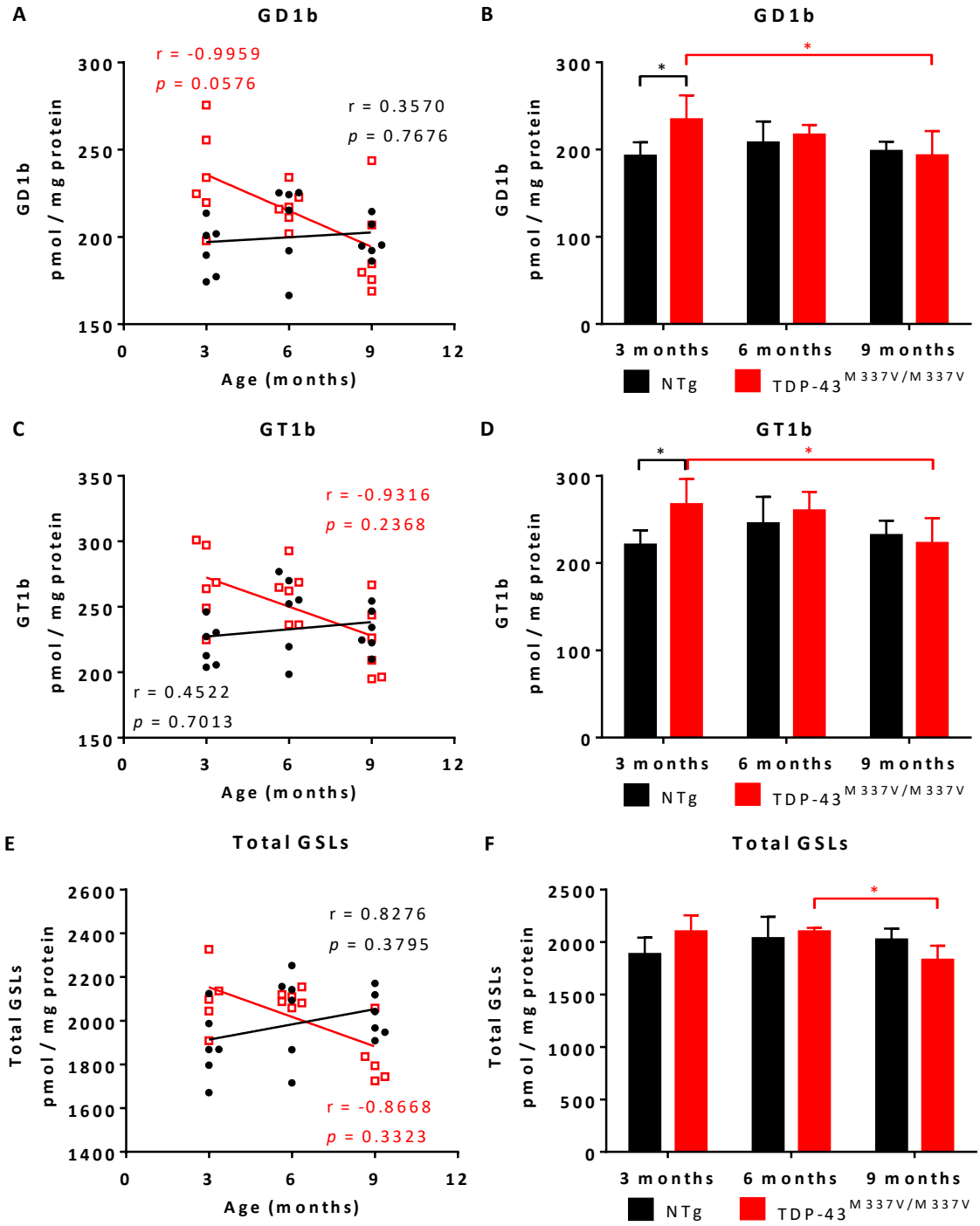


Figure 5.9. Increased levels of GD1b and GT1b were found in brain of pre-symptomatic (3 months-old) TDP-43$^{M337V/M337V}$ mice, but no significant changes were found in the levels of total GSLs at pre-symptomatic or onset stages of disease progression, when compared to age-matched NTg controls.

Changes in levels of GD1b, GT1b and total GSLs in brain of TDP-43$^{M337V/M337V}$ BAC mice at different ages, corresponding to progressive stages of disease (3 months for pre-symptomatic, 6 months for early onset and 9 months for late onset of symptoms, red) and aged matched NTg controls (black), measured by NP-HPLC. Data were analysed using (A,C,E) Pearson correlation analysis and (B,D,F) 2-way ANOVA, with Tukey's multiple comparisons test. Bar graph is presented as the mean ±SD. *p < 0.05, n = 5-6 mice per group.

When looking at the activity of some of the hydrolases responsible for GSL catabolism in brain, some similarities could be found to what was previously measured in spinal cord (**Figure 5.10** and **Figure 5.11**). GBA activity decreased with age similarly in TDP-43$^{M337V/M337V}$ mice and NTg mice, but the activity in the brain of TDP-43$^{M337V/M337V}$ mice was significantly higher than of NTg mice at 6 months of age. This is explained by a later decrease on GBA activity on TDP-43$^{M337V/M337V}$ mice, from 6 to 9 months, when compared to NTg mice, from 3 to 6 months of age (**Figure 5.10** A-B, NTg vs. TDP-43$^{M337V/M337V}$: 3 months p=0.4579, 6 months p=0.0382, 9 months p=0.9979; NTg: 3 vs. 6 months p=0.0043, 3 vs. 9 months p=0.0010, 6 vs. 9 months p=0.9936; TDP-43$^{M337V/M337V}$: 3 vs. 6 months p=0.1031, 3 vs. 9 months p<0.0001, 6 vs. 9 months p=0.0291; n=5-6 mice per group). GBA2 activity in the brain of TDP-43$^{M337V/M337V}$ mice was higher than that of NTg mice at 6 months of age (but not at 9 months of age, like measured in spinal cord) (**Figure 5.10** C-D, NTg vs. TDP-43$^{M337V/M337V}$: 3 months p=0.9951, 6 months p=0.0271, 9 months p=0.5615; NTg: 3 vs. 6 months p=0.3331, 3 vs. 9 months p=0.2190, 6 vs. 9 months p=0.9998; TDP-43$^{M337V/M337V}$: 3 vs. 6 months p=0.9773, 3 vs. 9 months p=0.8502, 6 vs. 9 months p=0.4281; n=5-6 mice per group). α-galactosidase activity did not change with age in brain of NTg mice, but tended to decrease with age in TDP-43$^{M337V/M337V}$ mice, reaching statistical significance when comparing 3 to 9 months-old mice (**Figure 5.10** E-F, NTg vs. TDP-43$^{M337V/M337V}$: 3 months p=0.7788, 6 months p=0.9989, 9 months p=0.9707; NTg: 3 vs. 6 months p=0.1125, 3 vs. 9 months p=0.2307, 6 vs. 9 months p=0.9989; TDP-43$^{M337V/M337V}$: 3 vs. 6 months p=0.4212, 3 vs. 9 months p=0.0018, 6 vs. 9 months p=0.1679; n=5-6 mice per group). Similarly to spinal cord, the average activity of β-galactosidase was significantly lower in the brain of TDP-43$^{M337V/M337V}$ mice when compared to NTg mice at 3, 6 and 9 months of age (**Figure**

5.11 A-B, NTg vs. TDP-43$^{M337V/M337V}$: 3 months p=0.0002, 6 months p=0.0182, 9 months p=0.0003; NTg: 3 vs. 6 months p=0.4649, 3 vs. 9 months p=0.5900, 6 vs. 9 months p>0.9999; TDP-43$^{M337V/M337V}$: 3 vs. 6 months p>0.9999, 3 vs. 9 months p=0.6584, 6 vs. 9 months p=0.7800; n=5-6 mice per group). β-hexosaminidase was the most active enzyme also in the spinal cord of NTg and TDP-43$^{M337V/M337V}$ mice and its activity did not change with age or the TDP-43$^{M337V/M337V}$ mutation (**Figure 5.11** C-D, NTg vs. TDP-43$^{M337V/M337V}$: 3 months p=0.9998, 6 months p=0.8946, 9 months p=0.9997; NTg: 3 vs. 6 months p=0.9718, 3 vs. 9 months p=0.9076, 6 vs. 9 months p=0.9998; TDP-43$^{M337V/M337V}$: 3 vs. 6 months p>0.9999, 3 vs. 9 months p=0.9188, 6 vs. 9 months p=0.9067; n=5-6 mice per group). Lastly, sialidase activity decreased in the brain of NTg mice from 3 to 6 months but remained constant in the brain of TDP-43$^{M337V/M337V}$ mice, which resulted in higher sialidase activity for TDP-43$^{M337V/M337V}$ mice at 6 months compared to their NTg littermates (**Figure 5.11** E-F, NTg vs. TDP-43$^{M337V/M337V}$: 3 months p=0.0707, 6 months p=0.0280, 9 months p=0.7372; NTg: 3 vs. 6 months p<0.0001, 3 vs. 9 months p=0.0235, 6 vs. 9 months p=0.1607; TDP-43$^{M337V/M337V}$: 3 vs. 6 months p=0.9994, 3 vs. 9 months p=0.4459, 6 vs. 9 months p=0.2734; n=5-6 mice per group).

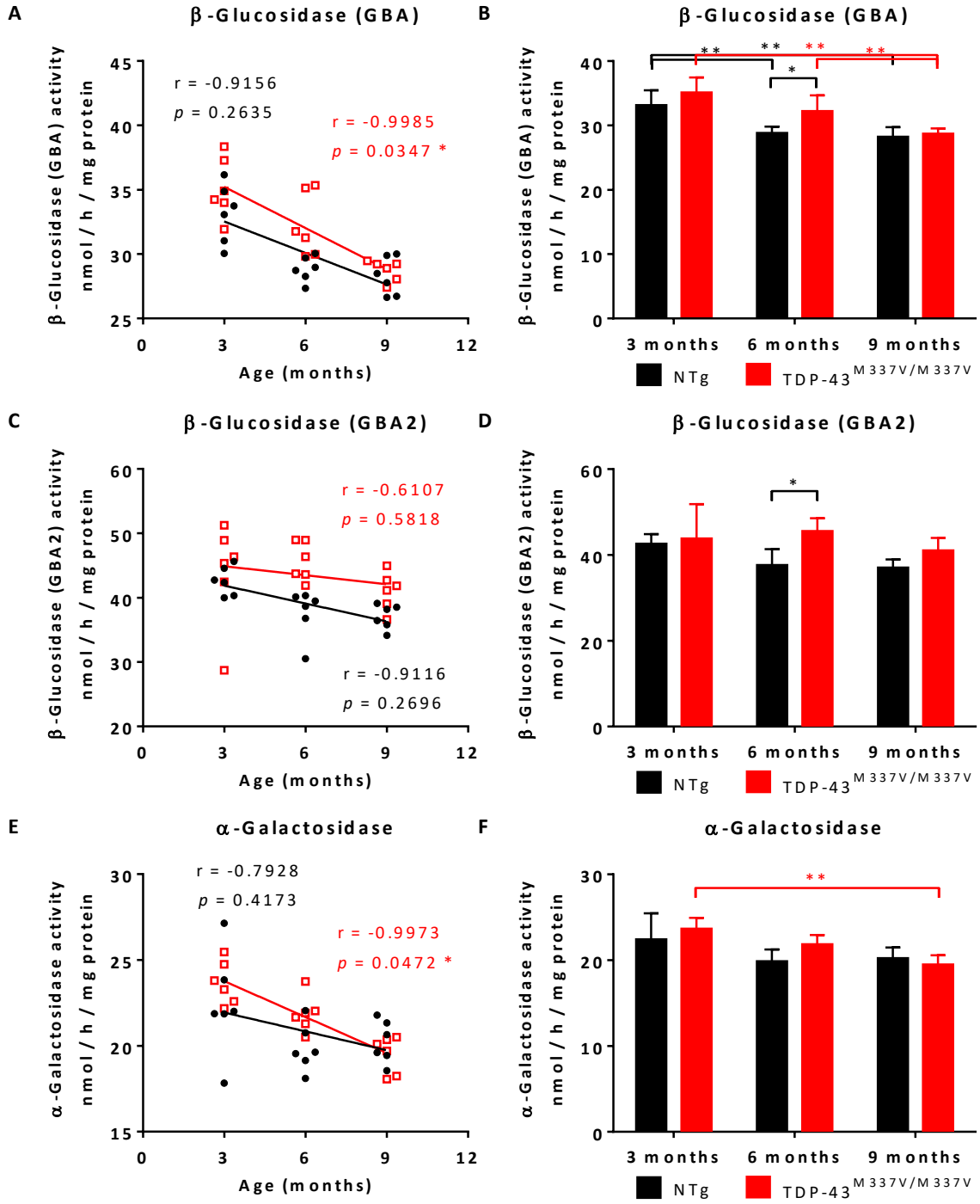


Figure 5.10. Increased GBA and GBA2 activity was measured in brain of 6 months-old (early onset) TDP-43$^{M337V/M337V}$ mice, but no significant changes were found in the activity of α-galactosidase at pre-symptomatic or onset stages of disease progression, when compared to age-matched NTg controls.

Changes in GBA, GBA2 and α-galactosidase activities in brain of TDP-43$^{M337V/M337V}$ mice at different ages, corresponding to progressive stages of disease (3 months for pre-symptomatic, 6 months for early onset and 9 months for late onset of symptoms, red) and aged matched NTg controls (black). Data were analysed using (A,C,E) Pearson correlation analysis and (B,D,F) 2-way ANOVA, with Tukey's multiple comparisons test. Bar graph is presented as the mean ±SD. *$p < 0.05$, **$p < 0.01$, n = 5-6 mice per group.

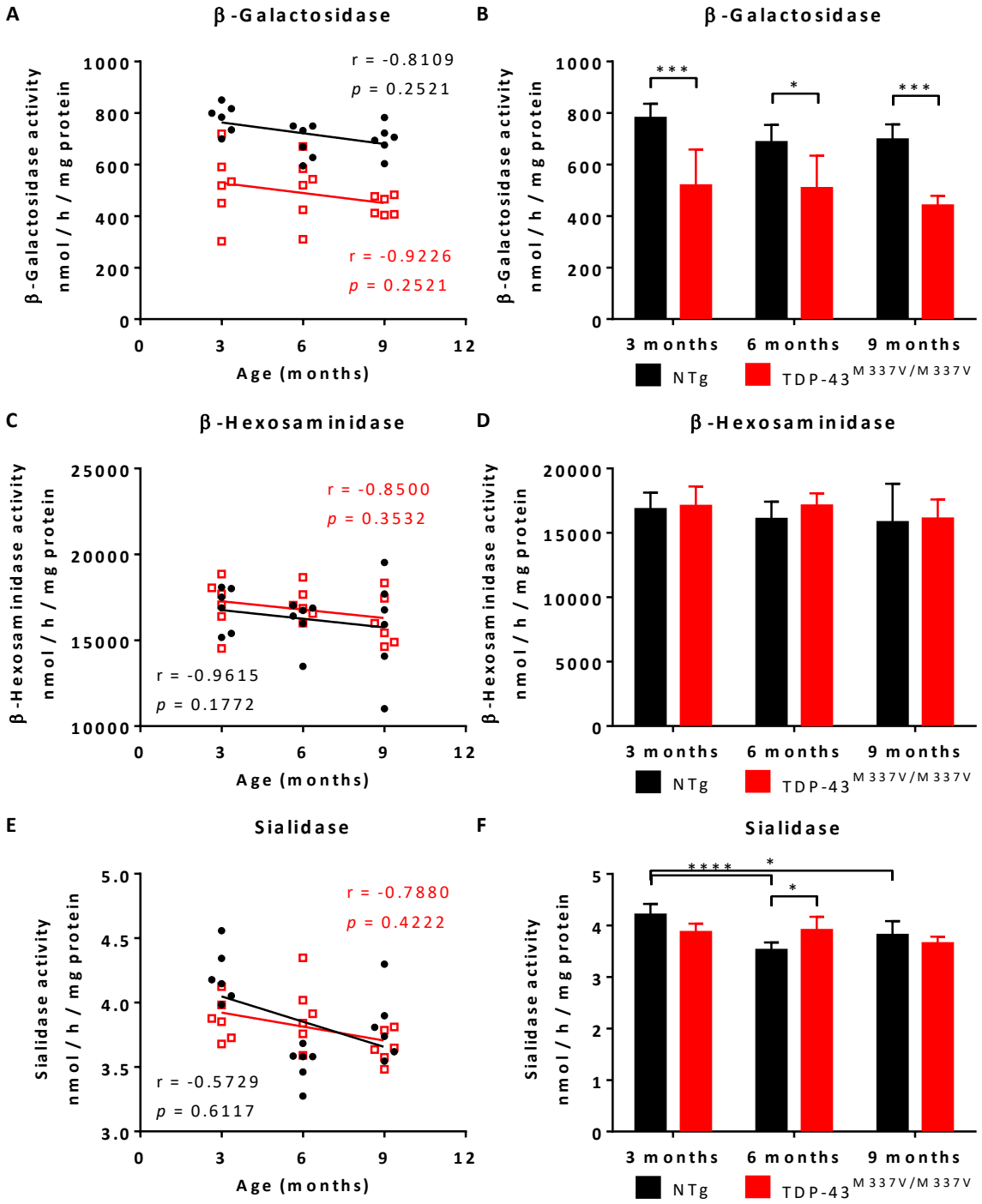


Figure 5.11. Sialidase activity was increased in brain of 6 months-old (early onset) TDP-43$^{M337V/M337V}$ mice, while β-galactosidase activity was reduced at pre-symptomatic and onset stages of disease progression, but no significant changes were found in the activity of β-hexosaminidase, when compared to age-matched NTg controls.

Changes in β-galactosidase, β-hexosaminidase and sialidase activities in brain of TDP-43$^{M337V/M337V}$ mice at different ages, corresponding to progressive stages of disease (3 months for pre-symptomatic, 6 months for early onset and 9 months for late onset of symptoms, red) and aged matched NTg controls (black). Data were analysed using (A,C,E) Pearson correlation analysis and (B,D,F) 2-way ANOVA, with Tukey's multiple comparisons test. Bar graph is presented as the mean ±SD. *p < 0.05, ***p < 0.001, ****p < 0.0001, n = 5-6 mice per group.

In summary, several changes were found in GSL metabolism of brain and spinal cord of TDP-43$^{M337V/M337V}$ mice with age when compared to age-matched NTg mice (**Table 5.3**). In spinal cord, no major changes were found in the levels of GlcCer or any of the major gangliosides in this tissue (**Figure 5.2**, **Figure 5.3** and **Figure 5.4**). However, β-galactosidase activity, the enzyme responsible for hydrolysis of GM1a and LacCer, was lower in TDP-43$^{M337V/M337V}$ mice spinal cord than on the NTg cohort but only at 3 months of age, when TDP-43$^{M337V/M337V}$ mice were still asymptomatic (**Figure 5.6**). At the age of onset of symptoms 6 (early) and 9 (late) months GBA2 activity (a non-lysosomal enzyme which degrades GlcCer into glucose and ceramide) was increased on the TDP-43$^{M337V/M337V}$ mice compared to NTg (**Figure 5.5**). Importantly, none of the changes found in enzymatic activity results in changes in the levels of GSLs in the spinal cord of the TDP-43$^{M337V/M337V}$ mice. Further changes were observed in brain, including increased levels of GD1b and GT1b in pre-symptomatic TDP-43$^{M337V/M337V}$ mice when compared to age-matched NTg controls (**Figure 5.9**). β-galactosidase activity was not only reduced at 3 months but also at 6 and 9 months of age and, besides GBA2, GBA and sialidase activities were also higher at 6 months of age (early onset), when comparing TDP-43$^{M337V/M337V}$ with NTg mice (**Figure 5.10** and **Figure 5.11**). Again, the changes found in enzymatic activity in the brain of TDP-43$^{M337V/M337V}$ mice do not directly associate with the measured changes in the levels of GSLs (**Table 5.3**).

	3 months (pre-symptomatic)	6 months (early symptoms onset)	9 months (late symptoms onset)
Spinal cord	↓ β-galactosidase	↑ GBA2	↑ GBA2
Brain	↑ GD1b and GT1b ↓ β-galactosidase	↑ GBA, GBA2 and sialidase ↓ β-galactosidase	↓ β-galactosidase

Table 5.3. Summary of the changes found in GSL metabolism in spinal cord and brain of TDP-43$^{M337V/M337V}$ mice at pre-symptomatic, early onset and late onset of symptoms stages of disease progression.

5.2.2. GSL metabolism in the 12 months TDP-43$^{M337V/-}$ mouse

In parallel to studying TDP-43$^{M337V/M337V}$ BAC mice at pre-symptomatic (3 months), early onset (6 months) and late onset of symptoms (9 months), GSL metabolism of 12 months-old TDP-43$^{M337V/-}$ BAC mice (early symptomatic heterozygote mice) was also evaluated and compared to 12-15 months-old NTg mice. No difference was found in the average weight of TDP-43$^{M337V/-}$ BAC mice when compared to NTg controls (**Figure 5.12**, *p*=0.8112, n=3 mice per group).

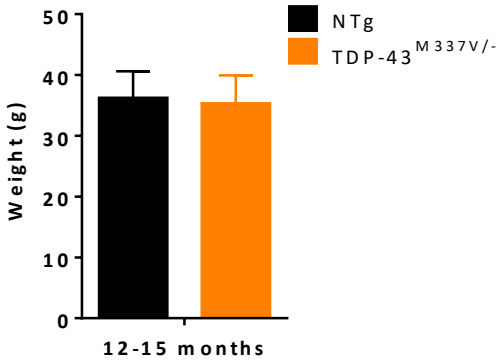


Figure 5.12. No significant differences were found in the average weight of 12 months symptomatic TDP-43$^{M337V/-}$ mice when compared to 12-15 months-old NTg controls.
Average weight of 12 months-old symptomatic TDP-43$^{M337V/-}$ mice (orange) and 12-15 months NTg controls (black). Data are presented as the mean ±SD. Data were analysed using two-tailed unpaired *t*-test. No statistically significant differences were observed, n = 3 mice per group.

Levels of GlcCer and downstream GSLs were measured by NP-HPLC. No difference was found in the levels of GlcCer in spinal cord of TDP-43$^{M337V/-}$ mice when compared to their age-matched NTg controls (**Figure 5.13**, *p*=0.9302, n=3 mice per group).

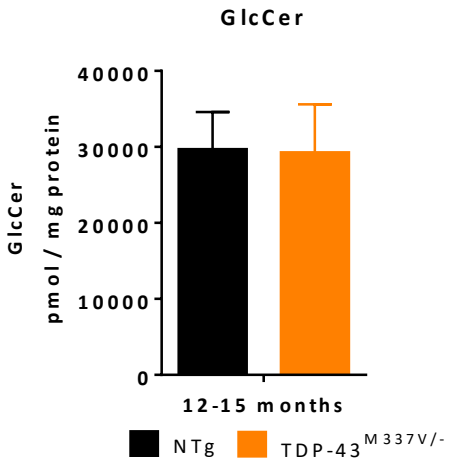


Figure 5.13. No changes were found in the levels of GlcCer in spinal cord of 12 months symptomatic TDP-43$^{M337V/-}$ mice when compared to 12-15 months-old NTg controls.
Changes in GlcCer levels in spinal cord of 12 months-old symptomatic TDP-43$^{M337V/-}$ mice (orange) and 12-15 months NTg controls (black). Data are presented as the mean ±SD. Data were analysed using two-tailed unpaired *t*-test. No statistically significant differences were observed, n = 3 mice per group.

When looking into the levels of total GSLs and the main ganglioside species found in the spinal cord (GM1a, GD1a, GD1b and GT1b), there was a small but significant increase in GD1b, but no changes in GM1a, GD1a and GT1b, when comparing 12-15 months-old TDP-43$^{M337V/-}$ and NTg mice (**Figure 5.14** A, GM1a *p*=0.5111; B, GD1a *p*=0.7377; C, GD1b *p*=0.0167; D, GT1b *p*=0.2794; E, total GSLs *p*=0.9836; n=3 mice per group).

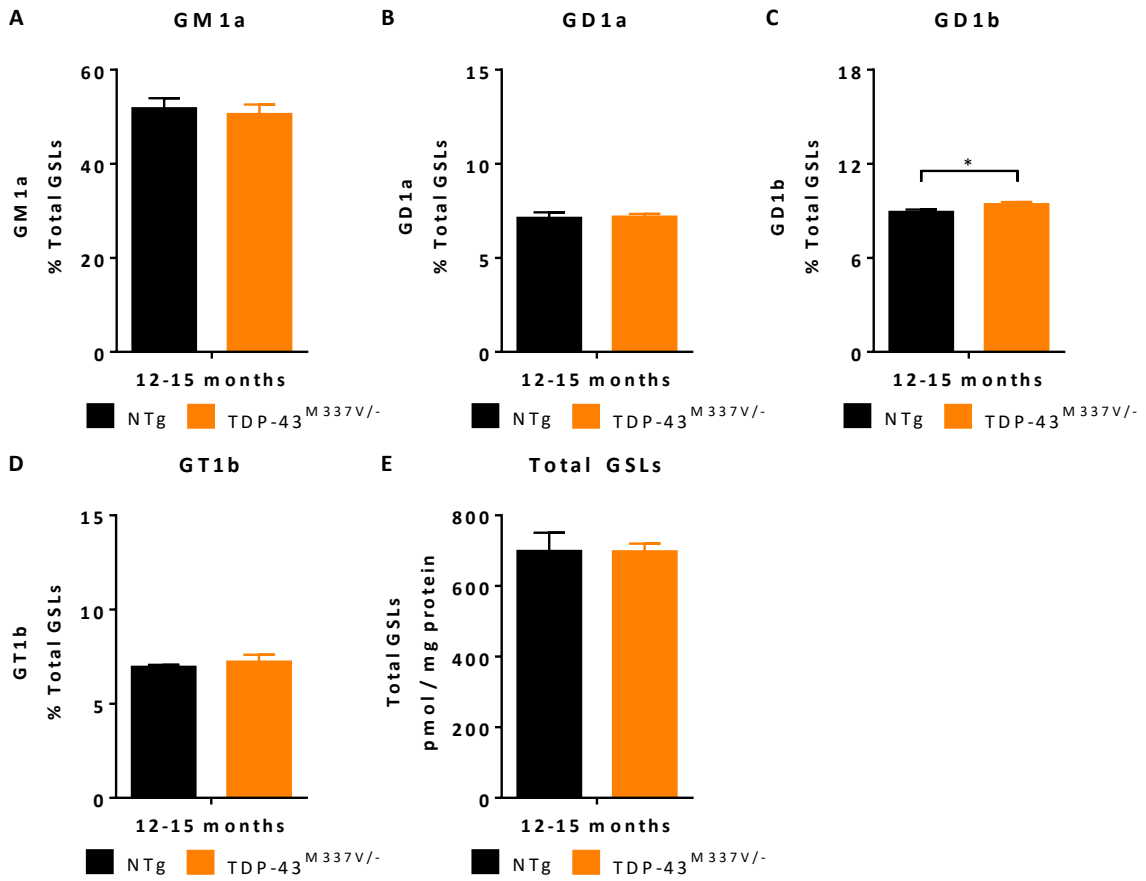


Figure 5.14. Increased levels of GD1b were found in spinal cord of 12 months symptomatic TDP-43$^{M337V/-}$ mice when compared to 12-15 months-old NTg controls, but no significant changes were found in the levels of GM1a, GD1a, GT1b or total GSLs.
Changes in levels of GM1a (A), GD1a (B), GD1b (C), GT1b (D) and total GSLs (E) in spinal cord of 12 months-old symptomatic TDP-43$^{M337V/-}$ mice (orange) and 12-15 months NTg controls (black). Data are presented as the mean ±SD. Data were analysed using two-tailed unpaired *t*-test. Only major gangliosides are presented. *$p < 0.05$, n = 3 mice per group.

Also, when measuring the activity of the main hydrolases responsible for GSL catabolism in spinal cord, no changes were found for the activity of GBA, GBA2, α-galactosidase, β-hexosaminidase and sialidase (**Figure 5.15** A, GBA p=0.0759; B, GBA2 p=0.1260; C, α-galactosidase p=0.8680; E, β-hexosaminidase p=0.9352; F, sialidase p=0.7830; n=3 mice per group). β-galactosidase, responsible for the degradation of GM1a, was the only enzyme analysed which showed a statistically significant decrease in

activity on 12 months-old symptomatic TDP-43$^{M337V/-}$ mice when compared to the NTg controls (**Figure 5.15** D, *p*=0.0223, n=3 mice per group).

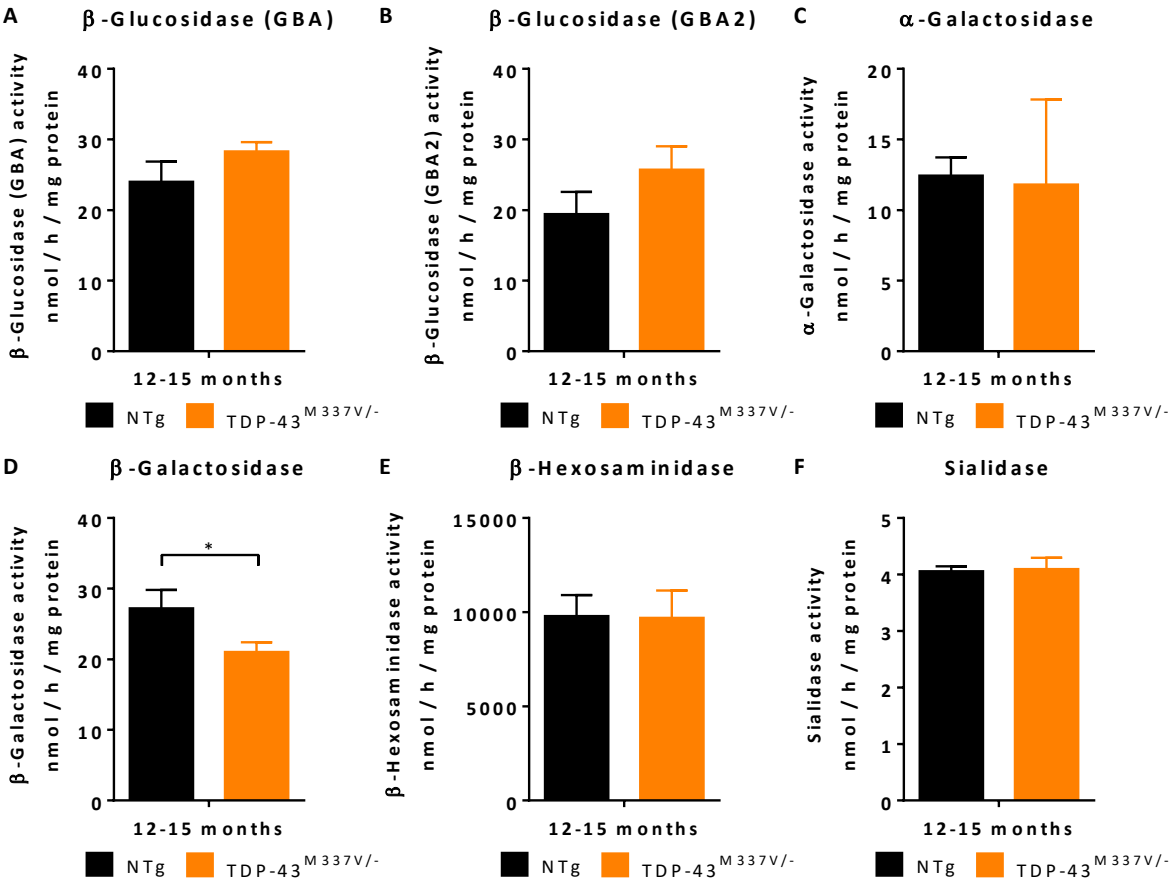


Figure 5.15. Decreased β-galactosidase activity was measured in spinal cord of 12 months symptomatic TDP-43$^{M337V/-}$ mice when compared to 12-15 months-old NTg controls, no changes were found in the activity of GBA, GBA2, α-galactosidase, β-hexosaminidase and sialidase.
GBA (A), GBA2 (B), α-galactosidase (C), β-galactosidase (D), β-hexosaminidase (E) and sialidase (F) activities in spinal cord of 12 months-old symptomatic TDP-43$^{M337V/-}$ mice (orange) and 12-15 months NTg controls (black). Data are presented as the mean ±SD. Data were analysed using two-tailed unpaired *t*-test. *$p < 0.05$, n = 3 mice per group.

Similarly to what was found in spinal cord, no significant difference was found in the levels of GlcCer in brain of TDP-43$^{M337V/-}$ mice when compared to their age-matched NTg controls (**Figure 5.16**, *p*=0.0730, n=3 mice per group).

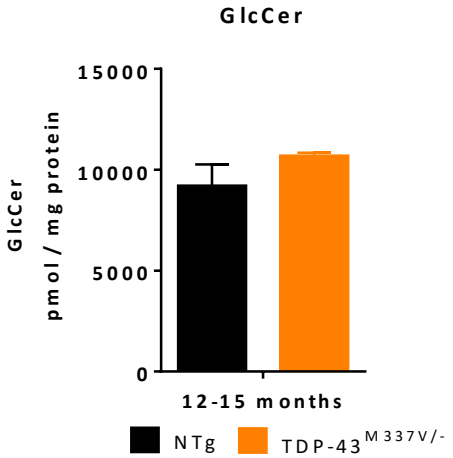


Figure 5.16. No changes were found in the levels of GlcCer in brain of 12 months symptomatic TDP-43$^{M337V/-}$ mice when compared to 12-15 months-old NTg controls. Changes in GlcCer levels in brain of 12 months-old symptomatic TDP-43$^{M337V/-}$ mice (orange) and 12-15 months NTg controls (black). Data are presented as the mean ±SD. Data were analysed using two-tailed unpaired *t*-test. No statistically significant differences were observed, n = 3 mice per group.

No significant changes were also found in the total levels of GSL and major gangliosides in the brain GD1b, GM1a, GD1a and GT1b, when comparing early symptomatic TDP-43$^{M337V/-}$ mice with age-matched NTg mice (**Figure 5.17** A, GM1a p=0.1392; B, GD1a p=0.1153; C, GD1b p=0.0822; D, GT1b p=0.4260; E, total GSLs p=0.0971; n=3 mice per group).

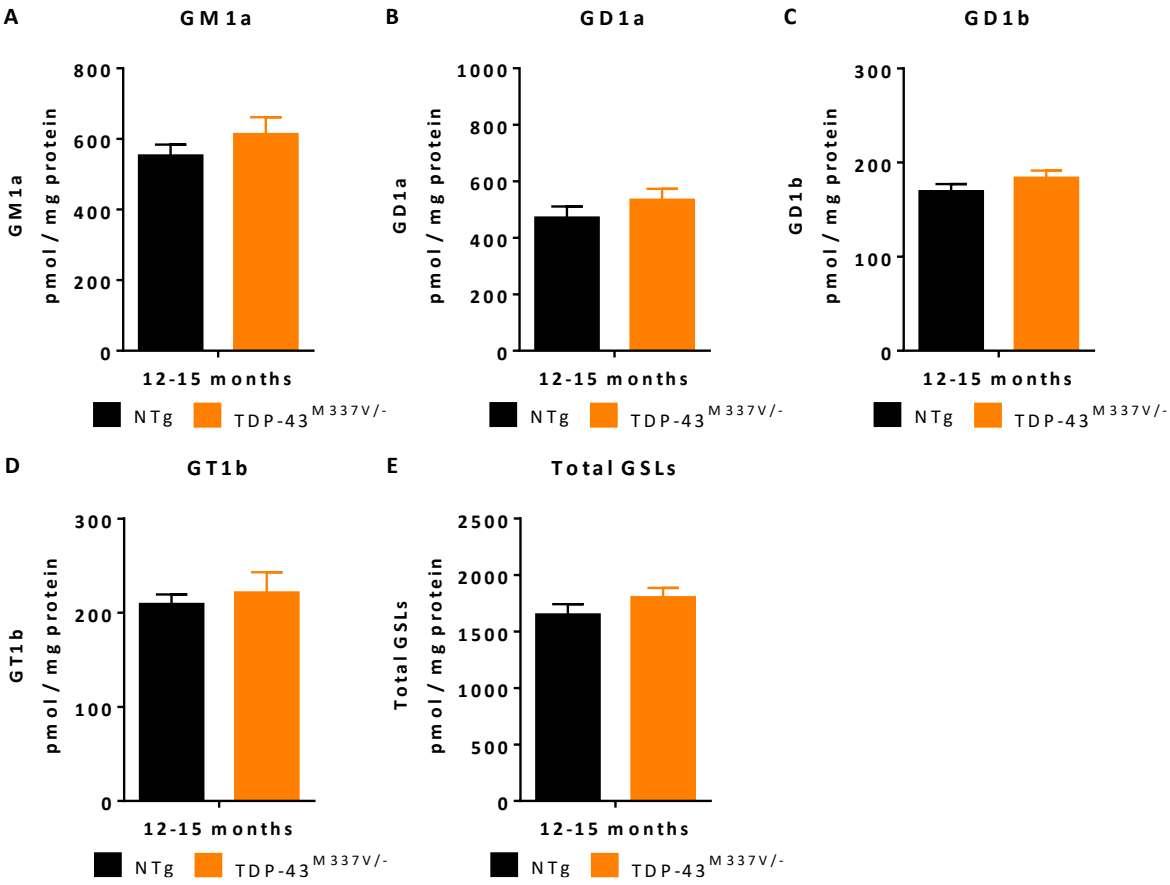


Figure 5.17. No significant changes were found in the levels of GM1a, GD1a, GD1b, GT1b and total GSLs in brain of 12 months symptomatic TDP-43$^{M337V/-}$ mice when compared to 12-15 months-old NTg controls.
Changes in levels of GM1a (A), GD1a (B), GD1b (C), GT1b (D) and total GSLs (E) in brain of 12 months-old symptomatic TDP-43$^{M337V/-}$ mice (orange) and 12-15 months NTg controls (black). Data are presented as the mean ±SD. Data were analysed using two-tailed unpaired *t*-test. Only major gangliosides are presented. No statistically significant differences were observed, n = 3 mice per group.

Finally, when measuring hydrolases activity in the brain of TDP-43$^{M337V/-}$ mice, the activity of both GBA and GBA2 was higher on the TDP-43$^{M337V/-}$ mice when compared to NTg controls (**Figure 5.18** A, GBA p=0.0439; B, GBA2 p=0.0301; n=3 mice per group). Similarly to what was measured in spinal cord, β-galactosidase activity was reduced on the TDP-43$^{M337V/-}$ mice when compared to the NTg (**Figure 5.18** D, p=0.0251, n=3 mice per group). No significant changes were found in the activity of α-galactosidase,

β-hexosaminidase and sialidase (**Figure 5.18** C, α-galactosidase p=0.0541; E, β-hexosaminidase p=0.9816; F, sialidase p=0.0997; n=3 mice per group).

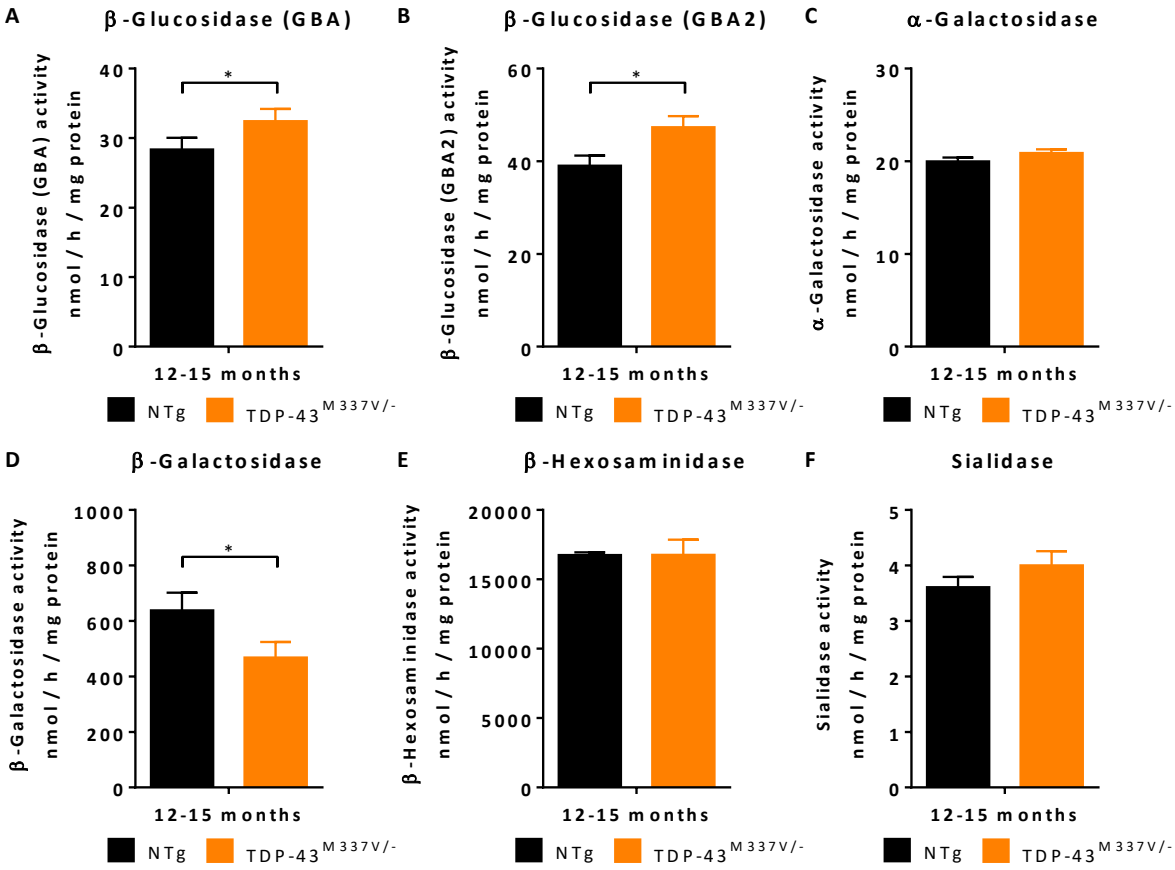


Figure 5.18. Increased GBA and GBA2 activity and decreased β-galactosidase activity were measured in brain of 12 months symptomatic TDP-43$^{M337V/-}$ mice when compared to 12-15 months-old NTg controls, no changes were found in the activity of α-galactosidase, β-hexosaminidase and sialidase.
GBA (A), GBA2 (B), α-galactosidase (C), β-galactosidase (D), β-hexosaminidase (E) and sialidase (F) activities in brain of 12 months-old symptomatic TDP-43$^{M337V/-}$ mice (orange) and 12-15 months NTg controls (black). Data are presented as the mean ±SD. Data were analysed using two-tailed unpaired *t*-test. *$p < 0.05$, n = 3 mice per group.

In conclusion, not many changes were found in the GSL metabolism of brain and spinal cord of early symptomatic (12 months-old) TDP-43$^{M337V/-}$ mice when compared to age-matched NTg controls (**Table 5.4**). No major changes were found in the levels of GlcCer or any of the major gangliosides, both in spinal cord and brain of TDP-43$^{M337V/-}$ mice, with the exception of a significant but small increase on GD1b levels in spinal cord,

when compared to NTg (**Figure 5.13**, **Figure 5.14**, **Figure 5.16** and **Figure 5.17**). Nevertheless, GBA and GBA2 activities were significantly higher in the brain, and β-galactosidase activity was significantly reduced in both the spinal cord and brain of TDP-43$^{M337V/-}$ 12 months-old mice (**Figure 5.15** and **Figure 5.18**).

	12 months (early symptomatic)
Spinal cord	↓ β-galactosidase
	↑ GD1b
Brain	↓ β-galactosidase
	↑ GBA and GBA2

Table 5.4. Summary of the changes found in GSL metabolism in spinal cord and brain of early symptomatic TDP-43$^{M337V/-}$ mice.

5.3. Discussion

Lipid and GSL metabolism has been thoroughly studied in SOD1 models and also in CSF and spinal cord of MND patients (as discussed in **Chapter 3** and summarised in **Table 5.5**)[212]. Nevertheless, while SOD1 mutations represent only 20 % of the familial cases and some sporadic cases[147,148], about 95 % of all cases of MND present TDP-43 proteinopathy, with mislocalisation of TDP-43 to the cytoplasm and formation of ubiquitinated insoluble aggregates in diseased motor neurons[135,174,175]. In this chapter, the effect of TDP pathology on GSL metabolism was investigated in early stages of disease progression by measuring the changes in GSL levels and lysosomal hydrolase activities in the spinal cord and brain of the TDP-43$^{M337V/M337V}$ BAC mouse model[227,228].

Male TDP-43$^{M337V/M337V}$ mice were described to show a small but significant reduction in weight from 5 months of age, while females only display weight loss after 12 months, when compared to TDP-43^{WT} or NTg mice[227]. Accordingly, on average, the

mixed cohort of male and female TDP-43$^{M337V/M337V}$ mice used in this study did not show the gradual weight gain associated with aging observed in the NTg mice. (**Figure 5.1**).

No significant changes were found in the levels of GlcCer, the GSL precursor required for the biosynthesis of complex GSLs, or the major gangliosides in the central nervous system (GM1a, GD1a, GD1b and GT1b) or in total GSL levels in the spinal cord of TDP-43$^{M337V/M337V}$ mice when compared to NTg controls, at pre-symptomatic (3 months) or at early or late onset of symptoms (6 and 9 months) timepoints (**Figure 5.2**, **Figure 5.3** and **Figure 5.4**). However, when measuring hydrolase activities in the spinal cord of TDP-43$^{M337V/M337V}$ mice compared to NTg age-matched controls, GBA2 activity was significantly increased at both 6 and 9 months of age (early and late onset of symptoms stages), similar to what was reported in the spinal cord of ALS patients and of SOD1^{G86R} mice, but not of SOD1^{G93A} mice[214,218]. On the other hand, β-galactosidase activity was reduced in the spinal cord of TDP-43$^{M337V/M337V}$ mice, but only reached statistical significance at 3 months of age (pre-symptomatic) (**Figure 5.6**), which contrasts to the significant increase found in the spinal cord of ALS patients (**Table 5.5**)[214].

The levels of GlcCer in the brain of the TDP-43$^{M337V/M337V}$ mice also did not show any differences when compared to age-matched 3, 6 or 9 months-old NTg C57BL/6J mice (**Figure 5.7**). Nevertheless, while the levels of GM1a increased with age and GD1a, GD1b and GT1b decreased with age in the spinal cord of both TDP-43$^{M337V/M337V}$ and NTg mice (as seen on the Pearson correlation analysis, **Figure 5.3** and **Figure 5.4**), the same trends were not observed in the brain (**Figure 5.8** and **Figure 5.9**). No significant changes were found in the levels of GM1a in the brain of TDP-43$^{M337V/M337V}$ mice when compared to NTg, but while GM1a levels tended to increase in NTg mice, no changes were found in the brain of TDP-43$^{M337V/M337V}$ mice with age. Correspondingly, levels of GD1a, GD1b and

GT1b remained unchanged in NTg mice, but showed a tendency to decrease with age in TDP-43$^{M337V/M337V}$ mice, starting at 3 months from significantly higher levels of GD1b and GT1b in the TDP-43$^{M337V/M337V}$ mice when compared to the age-matched controls (**Figure 5.8**, **Figure 5.9** and **Table 5.5**). Changes were also found in the activity of hydrolases in the brain of TDP-43$^{M337V/M337V}$ mice. Not only the activity of GBA2, but also of GBA1 and sialidase were significantly increased in the brain of TDP-43$^{M337V/M337V}$ mice at 6 months (early onset of symptoms), when compared to NTg mice. Similarly to what was seen in spinal cord, the activity of β-galactosidase was significantly lower at all measured timepoints (3, 6 and 9 months) in the brain of TDP-43$^{M337V/M337V}$ mice when compared to their age-matched NTg controls (**Figure 5.10**, **Figure 5.11** and **Table 5.5**).

These results are generally in agreement with previously reported changes in GSL metabolism in the normal aging mouse brain, including increased levels of GlcCer, LacCer, and GM1a, reduced levels of more complex gangliosides (GD1a, GD1b and GT1b) and lower GBA, GBA2 and β-galactosidase activity with age (**Table 5.5**)[249]. Importantly, the increased levels of GD1b and GT1b found in the brain of pre-symptomatic TDP-43$^{M337V/M337V}$ mice followed by a reduction with ageing are consistent to what was reported in normal ageing, suggesting the measured changes in the levels of GSLs in TDP-43$^{M337V/M337V}$ mice might not be due to the mutation (but to the controls used). Also, despite the increase found in the activity of GBA and GBA2 in the brain of TDP-43$^{M337V/M337V}$ mice at early symptoms onset, their activity still tends to decrease with ageing (**Figure 5.10**).

 **ALS patients**	**CSF**	↑ GlcCer, SM[220] and GM1a[216]
	Spinal cord	↑ Cer, GlcCer, GalCer, LacCer, Gb3, GM3 and GM1 ↑ GBA1, GBA2, hexosaminidase, galactosylceramidase, α-galactosidase and β-galactosidase activities[214]
	Muscle	↑ GCS expression[215]
 **SOD1^{G86R} mice**	**Spinal cord**	↑ GM1a (when symptomatic)[215] & GBA2 activity[218]
	Muscle	↑ GlcCer, GM3, GM2 (when symptomatic) & GCS expression[215]
		GBA2 inhibition ↑ motor units integrity ↑ neuroprotection and ↓ disease progression[216,218]
 **SOD1^{G93A} mice**	**Spinal cord**	↑ GlcCer (end stage) ↓ Cer, SM, LacCer, Gb3 and GM1 at symptom onset and ↑ when moribund ↑ hexosaminidase (at onset of paralysis and end stage) ↓ GBA1, GBA2 and galactosylceramidase activity (at onset of paralysis and end stage)[214]
		GCS inhibition ↑ disease progression GM3 intracerebroventricular infusion ↓ disease progression[214]
	Muscle	↑ LacCer, GM3 and GM2 (at end stage) ↑ β-hexosaminidase and β-galactosidase activities (at end stage)
 **TDP-43^{M337V} mice**	**Spinal cord**	↓ β-galactosidase activity (when pre-symptomatic) ↑ GBA2 activity (early and late onset of symptoms)
	Brain	↑ GD1b and GT1b (when pre-symptomatic) ↓ β-galactosidase activity (when pre-sypmtomatic and at early and late onset of symptoms) ↑ GBA, GBA2 and sialidase activities (early onset of symptoms)
 **WT mice**	**Spinal cord**	Peripheral nerve injury ↑ GCS expression and GlcCer levels Peripheral nerve injury & GCS inhibition ↓ GlcCer levels & motor function recovery[215] Peripheral nerve injury & GBA2 inhibition ↑ motor function recovery[218]
	Brain	↑ GlcCer, glucosylsphingosine, LacCer and GM1a with ageing ↓ GD1a, GD1b and GT1b with ageing ↓ GBA, GBA2 and β-galactosidase activities with ageing ↑ Sialidase activity with ageing[249]

Table 5.5. GSL metabolism in MND: a summary of what is known so far (updated, part II). New acquired data is shown in blue.

Besides investigating changes in GSL metabolism in pre-symptomatic, early onset and late onset of symptoms (3, 6 and 9 months, respectively) TDP-43$^{M337V/M337V}$ mice, spinal cord and brain of early symptomatic (12 months-old) TDP-43$^{M337V/-}$ mice were also studied. No changes were found in the levels of GlcCer and downstream GSLs in both spinal cord and brain, with the exception of a very small but significant increase of GD1b levels in the spinal cord of TDP-43$^{M337V/-}$ mice when compared to NTg (**Figure 5.13**, **Figure 5.14**, **Figure 5.16** and **Figure 5.17**). When looking into hydrolases activity, as in the early stages of disease progression in TDP-43$^{M337V/M337V}$ mice, β-galactosidase activity was reduced in both spinal cord and brain of 12 months TDP-43$^{M337V/-}$ mice when compared to age-matched NTg mice. Also GBA and GBA2 activities were higher in the early symptomatic TDP-43$^{M337V/-}$ mice when compared to NTg (**Figure 5.15** and **Figure 5.18**). These results are consistent with a reported genetic dose-dependent effect, with homozygous mice performing significantly worse in the grip strength and accelerating rotarod tests and showing reduced survival when compared to their heterozygous littermates[227].

Overall, the changes found in the GSL metabolism of TDP-43^{M337V} BAC mice at pre-symptomatic and early symptomatic timepoints is quite different from what was measured in ALS patients or in SOD1 models. Additionally, in TDP-43^{M337V} mice, none of the changes found in lysosomal hydrolases is reflected in specific substrate level changes (**Table 5.5**). SOD1 models are altogether very different from this TDP-43 model. The most obvious difference lies in their pathology: this TDP-43^{M337V} mouse model develops motor function deficits and pathology without forming TDP-43 insoluble aggregates or neuroinflammation; while in most SOD1 mouse models neuroinflammation is a major feature of disease development[227,290]. This is highlighted by the current debate on

whether or not SOD1 MND patients show TDP-43 pathology[264–267]. Another issue, as with other neurodegenerative diseases, is the difficulty to finding a good model for a complex and varied group of diseases like MND. The SOD1 models have been useful for understanding the pathways involved in motor neuron degeneration, but 25 years later no disease modifying drug has been developed for MND. Only two drugs have received FDA approval and those have their limitations: riluzole, an inhibitor of glutamatergic neurotransmission that prolongs survival at the latest stage of MND; and edaravone, an antioxidant which mildly delays disease progression in early disease stages[181,182,186,196]. In addition, both SOD1^{G93A} and SOD1^{G86R} mice express mutant forms of the SOD1 protein in supraphysiological levels, which can lead to toxicity. Whereas the TDP-43^{M337V} BAC mice show low expression levels of a mutated form of human TDP-43 which leads to progressive motor weakness and disfunction in the absence of TDP-43 aggregates or neuroinflammation, allowing for a more reliable study of what drives the initiation of pathology in the presence of TDP-43 mutations[227,228,282].

Interestingly, the existing data from the spinal cord of ALS patients is from post-mortem tissue[214], so it is from end stage disease, much later than the time points studied in this chapter in mice. Further experiments are therefore needed to better understand what happens in later stages of disease pathology in the TDP-43^{M337V} BAC mice (e.g. 12 or 16 months of age) and if it correlates with what has been reported in patients. Also, a thorough study of GSL metabolism in muscle tissues from TDP-43$^{M337V/M337V}$ mice and ALS patients might be relevant from a clinical point of view, as it is more easily accessible and might provide equally relevant information when compared to spinal cord. The detected changes in the activity of hydrolases in early stages of disease development of the TDP-43^{M337V} mice suggest that changes in GSL

metabolism are not just a consequence of pathology. The aforementioned additional studies would give a better understanding of the changes in GSL metabolism in MND and reveal if they are involved in disease pathology or if they are playing a protective or compensatory role.

6. A pilot study of the effects of edaravone on the TDP-43$^{M337V/M337V}$ and *Hexb*$^{-/-}$ mouse models

6.1. Introduction

6.1.1. Edaravone and MND

Edaravone (3-methyl-1-phenyl-4,5-dihydro-1H-pyrazol-5-one, Radicut® or Radicava®) is a free radical scavenger and inhibitor of lipid peroxidation[187] primarily used in Japan to help with recovery following an acute ischemic stroke[188,189]. As oxidative stress is a feature of motor neuron degeneration in ALS[190–192], edaravone was tested and approved for the treatment of MND in Japan in 2015[193], and subsequently approved in South Korea, the United States (FDA approved in 2017, 22 years after approval of Riluzole[194]), Canada, Switzerland and China.

Edaravone's antioxidant and neuroprotective properties have been studied in only a few models of MND (see **Table 6.1**). In SOD1^{G93A} mice, the classic familial model of MND, edaravone treatment started post-symptom onset reduced the accumulation of mutant SOD1 in the anterior horns of the spinal cord, and significantly slowed motor neuron degeneration and slowed disease progression[291]. The treatment of the SOD1^{H46R} rat, exhibiting a milder form of MND, also resulted in motor function improvement, with significantly better performance in the landing foot-splay test[292]. The Wobbler mouse, a model of motor neuron degeneration and sporadic MND, also showed reduced muscle weakness and contracture, muscle atrophy in the forelimbs, astrocyte proliferation and

spinal motor neuron degeneration, when treatment with edaravone started after the onset of symptoms[293]. More recently, edaravone was shown to also reduce motor neuron degeneration and motor function, along with reduction in oxidative stress in both spinal motor neurons and lower limb muscles in the Nrf2/G93A mouse, a model overexpressing the oxidative stress sensor nuclear erythroid 2-related factor 2 (Nrf2) and the G93A-human SOD1 (**Table 6.1**)[294]. Cellular and molecular targets of edaravone still remain unknown, but, along with the studies performed in rodents, clinical trials showed that edaravone is effective in delaying MND progression during early stages of disease by slowing decline in muscle strength and progressive muscle atrophy[196,295].

MND pathophysiology is highly heterogeneous and oxidative stress is well known to affect motor neuron energy balance and function[296,297]. Oxidative stress promotes TDP-43 mislocalization from the nucleus to the cytoplasm and its phosphorylation, increasing its tendency to aggregate in MND motor neurons[198,262]. Also, pathological aggregation of TDP-43 was shown to be triggered by the stress granules pathway[298–301]. More recently it was reported that modulation of TDP-43 recruitment to stress granules prevents its accumulation in the cytoplasm of ALS induced pluripotent stem (iPS) motor neurons[302]. Likewise, neuronal overexpression of the oxidation resistance 1 (Oxr1) protein prevents mutant TDP-43 mislocalization in primary motor neurons from TDP-43$^{M337V/-}$ mice and improves motor function, muscle denervation and neuron muscular junction (NMJ) degeneration in TDP-43$^{M337V/M337V}$ mice[303]. Thus, there is evidence that TDP-43 pathology is closely related to oxidative stress, but the effect of the antioxidant edaravone in TDP-43 proteinopathies or in TDP-43 transgenic animals has not been reported and merits further examination.

Animal model	Dose and length of edaravone treatment	Effect
$SOD1^{G93A}$ mouse	5 or 15 mg/kg/day vs. vehicle. IP injections started at symptoms onset (~100 days of age) until loss of righting reflex.	Significantly reduced accumulation of mutant SOD1 in the spinal cord and slowed motor decline, neuron degeneration and disease progression[291].
Nrf2/G93A mouse	15 mg/kg/day vs. vehicle. IP injections started at 91 days of age (average symptoms onset) over a period of 28 days.	Significantly reduced oxidative stress in both spinal motor neurons and lower limb muscles, reduced motor neuron degeneration, motor function loss and reduced muscle atrophy[294].
Wobbler mouse	1 or 10 mg/kg/day vs. vehicle. IP injections started at symptoms onset (3-4 weeks) for 4 weeks.	Reduced muscle weakness, contracture and muscle atrophy in the forelimbs, reduced astrocyte proliferation and spinal motor neuron degeneration[293].
$SOD1^{H46R}$ rat	1.5 or 3.0 mg/kg/h vs. vahicle. Continuous infusion (1 h per day) for 2 days followed by a 2-day holiday, started at 18 weeks of age until loss of righting reflex.	Improved motor function, with significantly better performance in the landing foot-splay test[292].

Table 6.1. Effect of the treatment with edaravone on rodent models of MND reported in the literature.

6.1.2. Edaravone and GM2 gangliosidoses

The GM2 (monosialoganglioside 2) gangliosidoses are a group of LSDs caused by mutations in β-hexosaminidase and includes Tay-Sachs disease, Sandhoff disease and GM2 activator deficiency. They are rare autosomal recessive disorders, caused by mutations in the α (*HEXA*) or β (*HEXB*) subunits of β-hexosaminidase or in the GM2 activator protein (a protein that presents insoluble GM2 to soluble β-hexosaminidase), respectively[5,74,75]. β-hexosaminidase is an enzyme responsible for the catabolism of GM2 ganglioside. Mutations in β-hexosaminidase result in reduced enzymatic activity, with consequent inability to efficiently degrade GM2 leading to its accumulation. The storage of GM2 in the central nervous system (CNS) causes progressive neurodegeneration, inflammation and premature death[73,76]. Onset of symptoms can occur from early in infancy until later in adulthood, typically with rapid disease progression in the early onset

cases and slower disease progression in the less common late onset forms of the disease. The general pathology of infantile Tay-Sachs disease and Sandhoff disease is very similar and positive diagnosis is only possible after enzymatic assays of HEXA and HEXB activities in plasma or white blood cells. Some adult-onset cases share both clinical and pathological features with MND to such an extent it can lead to mis-diagnosis[304,305].

No therapies have yet been approved for GM2 gangliosidoses, but several approaches have been tested over the years in animal models, mainly to prevent or correct the accumulation of GM2 ganglioside[73,79]. A few examples are enzyme replacement therapies, substrate reduction therapies (e.g. miglustat), BMT, chaperone therapy, stem cell and gene therapies[93–97]. Anti-inflammatory and antioxidant therapies have also been evaluated[98]. Importantly, N-acetyl-L-leucine, a derivative of the amino acid leucine that has been used for decades to treat acute vertigo and vertiginous symptoms (Tanganil®), is now on phase 2 clinical trials for the treatment of the GM2 gangliosidoses (clinicaltrials.gov NCT03759665 and EudraCT 2018-004406-25). Its mechanism of action remains unknown, but acetyl-DL-leucine was shown to delay the onset of motor dysfunction, to reduce GA2 and GM2 storage in the brain and to increase survival on the Sandhoff mouse model[306]. Furthermore, when used in combination with miglustat, acetyl-DL-leucine significantly increased autophagy and the levels of SOD1 in Sandhoff mice cerebellum, suggesting it might be indirectly providing antioxidant support[306]. Likewise, edaravone acts primarily as an antioxidant and has shown to slow motor neuron degeneration in some animal models, making it another interesting therapy to test in the GM2 gangliosidoses.

Spontaneous mutations in β-hexosaminidase have been reported in a variety of animal species and engineered mouse models of Tay-Sachs disease, Sandhoff disease and

GM2 protein activator deficiency have been generated[230,307–310]. Surprisingly, despite storing GM2, Tay-Sachs (*Hexa*$^{-/-}$) mice exhibit no behavioural or neurologic defects and therefore are not a good representative model for evaluating therapies. This is because they can bypass the catabolic block by having higher expression levels of neuraminidases that can convert GM2 to GA2, which is then a substrate for HEXB allowing the mouse to escape the disease[311,312]. However, Sandhoff (*Hexb*$^{-/-}$) mice develop symptoms reflective of the human disease, including abnormal motor function and coordination at 3 months of age, bradykinesia, tremors and muscular atrophy, with consequent weight loss at 4 to 5 months of age, and premature death[230,308]. These characteristics make the Sandhoff mouse ideal for examining the effect of edaravone in a GM2 gangliosidosis model.

6.1.3. Aims

Edaravone improved motor function and delayed disease progression in SOD1 models and on the Wobbler mouse model of MND. In this chapter, the effect of edaravone on the TDP-43$^{M337V/M337V}$ BAC mouse was investigated (**Chapter 6.2.1**). Additionally, antioxidants have been shown to be promising candidates for the treatment of GM2 gangliosidosis, so the effect of edaravone on the Sandhoff mouse model was also examined (**Chapter 6.2.2**).

6.2. Results

6.2.1. Edaravone and the TDP-43$^{M337V/M337V}$ mouse model

To evaluate the effect of edaravone on the TDP-43$^{M337V/M337V}$ BAC mouse, mice were injected intraperitoneally daily, Monday to Friday (15 mg/kg/day of edaravone 1.5 mg/mL solution or PBS) for 5 weeks following disease onset (6 months of age, **Figure 6.1**). Weight measurements, behavioural testing and tissues collection were also performed on a group of untreated NTg (C57BL/6J) mice, at 6 months of age.

No significant weight changes were observed between the treated and untreated groups over the 5 weeks of treatment (week 0 p = 0.1702, week 1 p = 0.1831, week 2 p = 0.1040, week 3 p = 0.3003, week 4 p = 0.2876, week 5 p = 0.1451; **Figure 6.1**). Also, no significant changes between the TDP-43$^{M337V/M337V}$ BAC mice and the untreated C57BL/6J mice were observed, as previously reported[227].

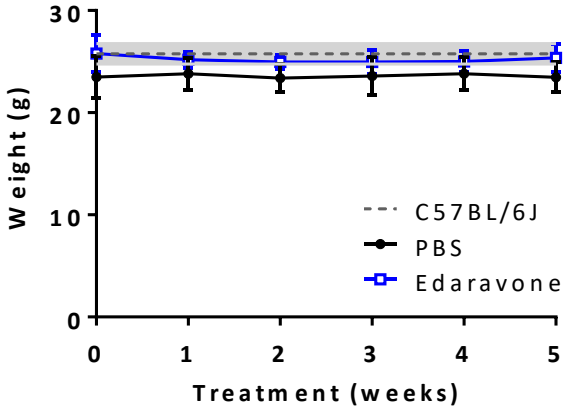


Figure 6.1. Treatment with edaravone did not alter the average weight of TDP-43$^{M337V/M337V}$ BAC mice during the 5 weeks of treatment, from 6 months of age.
Average weight of TDP-43$^{M337V/M337V}$ mice treated with edaravone (blue) or PBS (controls, black), for 5 weeks starting from 6 months of age. The weight of untreated non-transgenic C57BL/6J mice was measured at 6 months of age and is shown as a gray dashed line for reference (±SD as a gray area). Data are presented as the mean ±SD at each time point. Data were analysed using multiple *t*-tests, with Holm-Sidak multiple comparisons correction. No significant changes were found, n = 3-4 mice per group.

Muscle strength and coordination were measured by rotarod (**Figure 6.2**). TDP-43$^{M337V/M337V}$ mice were reported to progressively lose motor function, the ability to stay on the accelerating rotarod and grip strength from between 6 and 9 months until 18 months of age, when compared to non-transgenic controls[227]. Accordingly, at 6 months of age this cohort of vehicle treated TDP-43$^{M337V/M337V}$ mice still performed as well as the non-transgenic C57BL/6J mice (dashed vs black line, **Figure 6.2**). Edaravone treated TDP-43$^{M337V/M337V}$ mice also performed as well as the vehicle treated controls on all the parameters measured on the rotarod: latency or time to fall, speed of the rotarod at the time of the fall, total number of revolutions and distance travelled (week 0 p = 0.2680, week 1 p = 0.7945, week 2 p = 0.1770, week 3 p = 0.1280, week 4 p = 0.2001, week 5 p = 0.2605; **Figure 6.2**). However, there was a non-significant trend for the edaravone treated mice to have reduced performance than the controls, with the edaravone treated mice not following the expected long-term learning/improved performance on the rotarod, as observed in the PBS injected group (**Figure 6.2**).

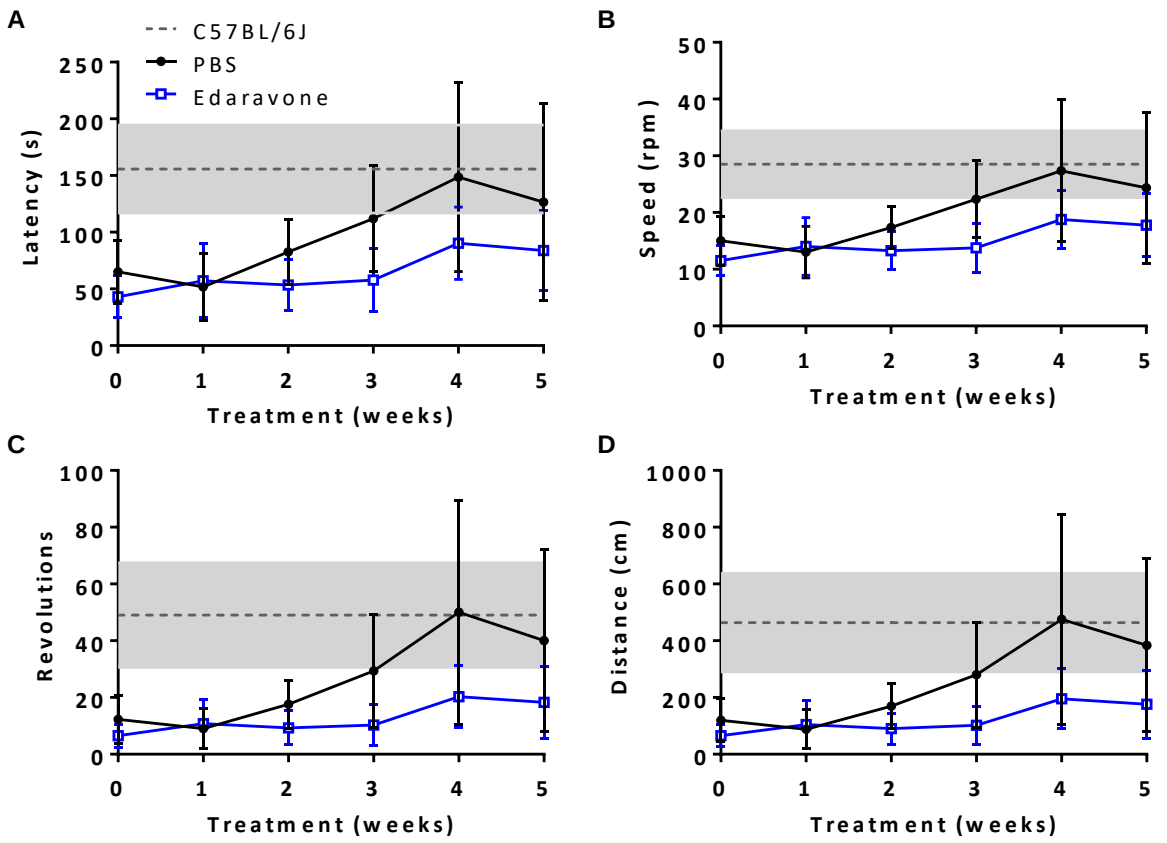


Figure 6.2. Treatment with edaravone did not change the motor function of TDP-43$^{M337V/M337V}$ BAC mice measured by their performance on the rotarod.
Latency (or time to fall, **A**), speed of the rotarod at the time of the fall (**B**), number of revolutions (**C**) and travelled distance (**D**) were recorded once a week for TDP-43$^{M337V/M337V}$ mice treated with edaravone (blue) or PBS (controls, black), for 5 weeks starting from 6 months of age. Performance on the rotarod of untreated non-transgenic C57BL/6J mice was measured at 6 months of age and is shown as a grey dashed line for reference (±SD as a gray area). Data are presented as the mean ±SD at each time point. Data were analysed using multiple *t*-tests, with Holm-Sidak multiple comparisons correction. No significant changes were found, n = 3-4 mice per group.

After 5 weeks of treatment, each mouse was put individually in an open field and rearing events manually counted. Side rears were recorded when mice reared on hind legs using the walls of the cage as support and centre rears were counted when mice reared un-aided (**Figure 6.3**). Although no significant changes were observed, edaravone treated mice reared less in the centre, when compared with the PBS injected mice or the non-transgenic C57BL/6J mice (C57BL/6J vs. PBS side $p = 0.1777$, centre $p = 0.9359$; PBS vs. edaravone side $p = 0.6460$, centre $p = 0.8787$; **Figure 6.3**).

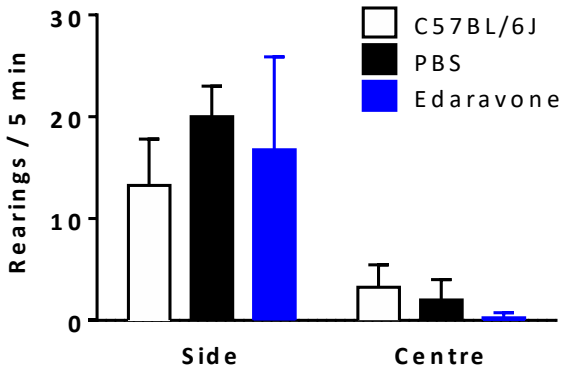


Figure 6.3. Treatment with edaravone did not alter the manual scores of side or centre rearing per 5 min of the TDP-43$^{M337V/M337V}$ BAC mice compared to untreated mice.
Side and centre rearing events averages of TDP-43$^{M337V/M337V}$ mice after 5 weeks of treatment with edaravone (blue) or PBS (controls, black). Rearing events of untreated non-transgenic C57BL/6J mice were also counted at 6 months of age (white). Data are presented as the mean ±SD at each time point. Data were analysed using 2-way ANOVA, with Tukey's multiple comparisons test. No significant changes were found, n = 3-4 mice per group.

In addition to manual rearing, motor coordination and gait of the TDP-43$^{M337V/M337V}$ mice treated with edaravone was also measured using the footprint pattern test (**Figure 6.4**). The front paws were painted blue and hind paws were painted red, and each mouse was put at the end of an open-roofed tunnel lined with white paper and facing a dark enclosure at the far end. The distance between each stride on the same side (A), or from paws on opposite sides (B), hindbase width (C), frontbase width (D) and forepaw/hindpaw overlap (E, **Figure 6.4**) was measured and mean values calculated per group. Representative images of each group are shown in panel A of **Figure 6.4**and quantitative analysis is shown in panel B. PBS treated TDP-43$^{M337V/M337V}$ mice showed no changes in gait when compared to non-transgenic mice (PBS vs. C57BL/6J, A p = 0.8515, B p = 0.9605, C p = 0.2059, D p = 0.4814, E p = 0.5138, **Figure 6.4**). No changes on the footprint pattern were also found for the edaravone treated TDP-43$^{M337V/M337V}$ mice, which demonstrates the drug did not worsen gait (edaravone treated vs. PBS control, A p = 0.7144, B p = 0.9241, C p = 0.7783, D p = 0.9804, E p = 0.2260, **Figure 6.4**).

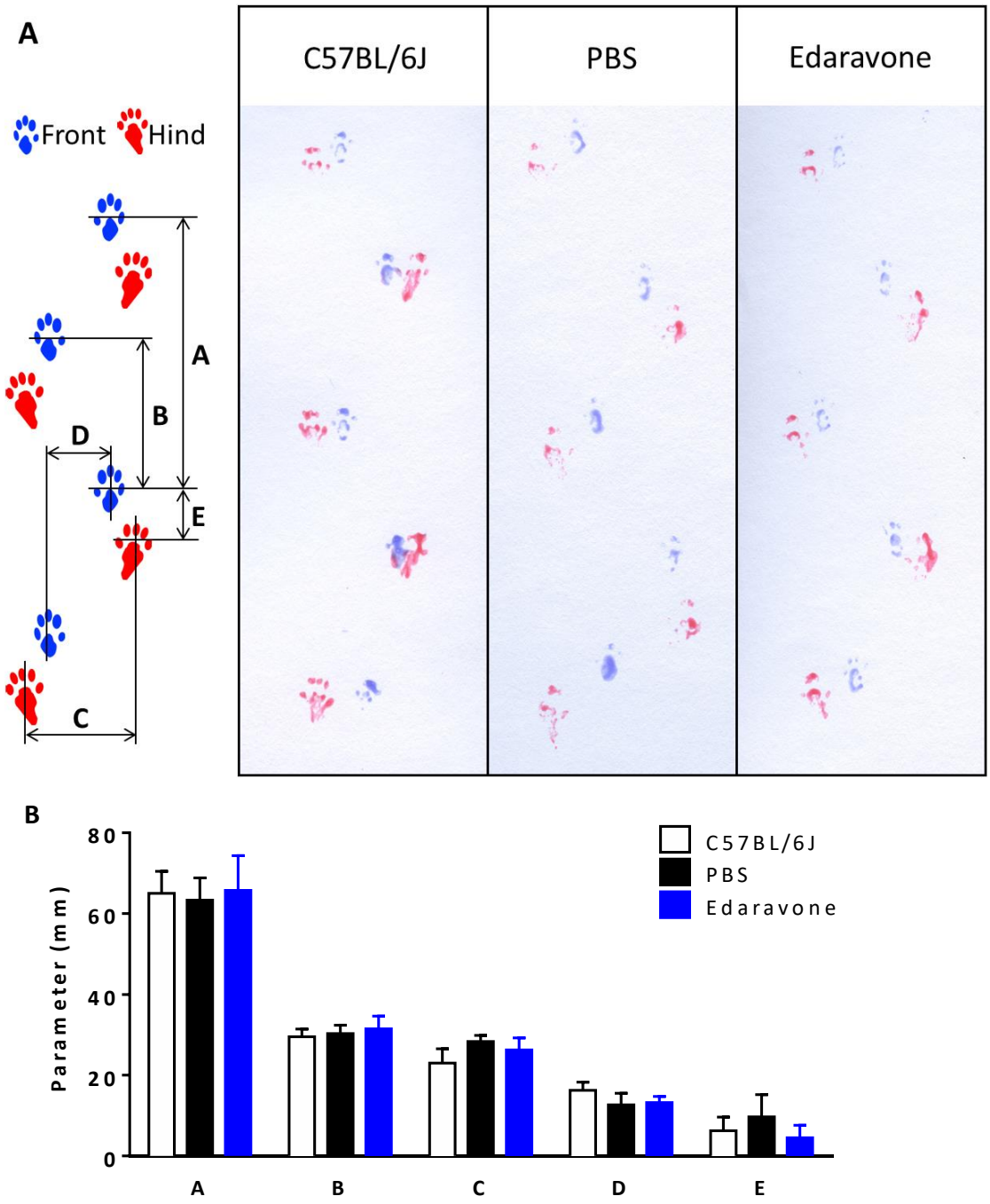


Figure 6.4. Treatment with edaravone did not change motor coordination or gait of TDP-43$^{M337V/M337V}$ mice measured using the footprint pattern test, when compared to untreated TDP-43$^{M337V/M337V}$ or C57BL/6J non-transgenic mice.

The front and hind paws of 4 untreated non-transgenic C57BL/6J mice at 6 months of age (white bars), 3 untreated TDP-43$^{M337V/M337V}$ BAC mice (black) and 4 TDP-43$^{M337V/M337V}$ BAC mice treated with edaravone for 5 weeks (blue) at 7 months and 1 week of age, were painted red and blue, respectively. The distance between each stride from paws on the same side (A), each stride from paws on opposite sides (B), hindbase width (C), frontbase width (D) and forepaw/hindpaw overlap (E) was measured. Panel **A** shows representative images for each group and panel **B** the corresponding quantification, presented as the mean ±SD for each group. Data were analysed using 2-way ANOVA, with Tukey's multiple comparisons test. No significant changes were found, n = 3-4 mice per group.

Finally, the biochemical effect of edaravone was evaluated by measuring the levels of GSLs in the brain and liver of the TDP-43$^{M337V/M337V}$ mice by NP-HPLC (**Figure 6.5** and **Figure 6.6**). Normal lipid profile of GSLs in the brain of mice with C57BL/6J background was observed in the three groups, including the precursor GlcCer and the downstream GSLs GM1a, GD1a, GD1b and GT1b. No changes in the accumulation of GSLs was observed as a result of the treatment with edaravone, even for total levels of GSLs (GlcCer p = 0.6206, GSLs p = 0.6271; **Figure 6.5**).

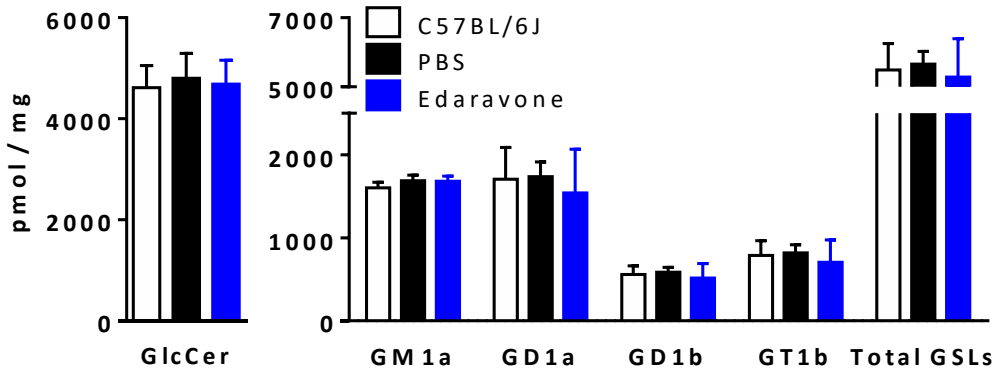


Figure 6.5. Treatment with edaravone did not alter the accumulation of GSLs in the TDP-43$^{M337V/M337V}$ BAC mouse brain.
NP-HPLC quantification of GSLs in brain of 6 months-old untreated non-transgenic C57BL/6J mice (white), 7 months and 1 week old TDP-43$^{M337V/M337V}$ BAC mice treated with edaravone for 5 weeks (blue) or PBS (controls, black). No changes in GSL levels were observed in the brain of edaravone treated mice when compared to PBS treated or non-transgenic matched controls. Only main peaks of gangliosides are shown. Data are presented as the mean ±SD for each ganglioside. GlcCer data were analysed using mustiple *t*-tests, with Holm-Sidak's multiple comparisons correction. Downstream GSLs data were analysed using 2-way ANOVA, with Tukey's multiple comparisons test. No significant changes were found, n = 3-4 mice per group.

No changes in the accumulation of GSLs were found also in the liver of these mice, an organ that typically accumulates GSLs in many of the LSDs. Typical GSL profile was measured in the three groups, including GlcCer and the downstream GSLs GA2, GM3, GM3Gc and GM2Gc (GlcCer p = 0.3586, GSLs p = 0.7372; **Figure 6.6**).

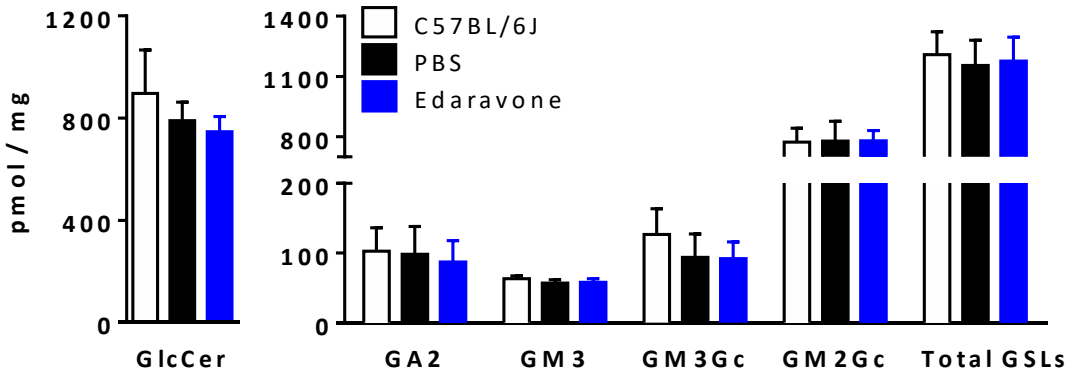


Figure 6.6. Treatment with edaravone did not change the accumulation of GSLs in the TDP-43$^{M337V/M337V}$ BAC mouse liver.
NP-HPLC quantification of GSLs in liver of 6 months-old untreated non-transgenic C57BL/6J mice (white), 7 months and 1 week old TDP-43$^{M337V/M337V}$ BAC mice treated with edaravone for 5 weeks (blue) or PBS (controls, black). No changes in GSL levels were observed in the liver of edaravone treated mice when compared to PBS treated or non-transgenic matched controls. Only main peaks of gangliosides are shown. Data are presented as the mean ±SD for each ganglioside. GlcCer data were analysed using multiple *t*-tests, with Holm-Sidak's multiple comparisons correction. Downstream GSLs data were analysed using 2-way ANOVA, with Tukey's multiple comparisons test. No significant changes were found, n = 3-4 mice per group.

Despite not showing any significant changes on the behavioural tests performed, the data gathered indicates a trend that the administered dose of edaravone mildly worsened motor function and coordination of the TDP-43$^{M337V/M337V}$ mice, in contrast to the beneficial effects observed in the other models of MND.

6.2.2. Edaravone and the *Hexb*$^{-/-}$ mouse model

In order to assess the effect of edaravone on the development of symptoms associated with Sandhoff disease, Sandhoff mice were injected daily, from Monday to Friday, intraperitoneally with 15 mg/kg/day edaravone (or PBS for the controls) from weaning until the mice reached end-stage at 15-16 weeks (**Figure 6.7**).

The administration of edaravone did not change survival, as all animals reached end stage or were close to it at 16 weeks of age when tissues were collected for biochemical

analysis. However, Sandhoff mice treated with edaravone put on weight at a slower rate and, after 4 weeks of treatment, the mice injected with edaravone weighed significantly less than the vehicle injected Sandhoff mice (4 weeks $p = 0.1833$, 5 weeks $p = 0.4125$, 6 weeks $p = 0.0560$, 7 weeks $p = 0.0149$, 8 weeks $p = 0.0056$, 9 weeks $p = 0.0128$, 10 weeks $p = 0.0059$, 11 weeks $p = 0.0232$, 12 weeks $p = 0.1106$, 13 weeks $p = 0.0740$, 14 weeks $p = 0.0478$, 15 weeks $p = 0.0316$; **Figure 6.7**).

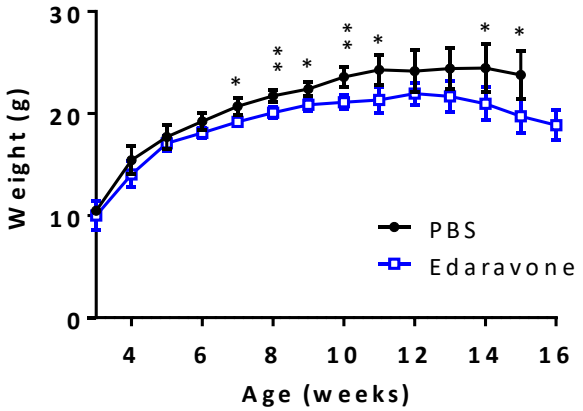


Figure 6.7. Treatment with edaravone significantly decreased the average weight of Sandhoff mice after the appearance of symptoms at 7 weeks.
Average weight of Sandhoff mice treated with edaravone (blue) or PBS (controls, black), starting from 3 weeks of age to end-stage at 15-16 weeks. Data are presented as the mean ±SD at each time point. Data were analysed using multiple *t*-tests, with Holm-Sidak multiple comparisons correction. *$p < 0.05$, **$p < 0.01$ versus corresponding controls, n = 4 mice per group.

Muscular strength and motor coordination were measured by bar crossing (**Figure 6.8**) and rotarod (**Figure 6.9**) tests. Edaravone treated Sandhoff mice performed as well as the PBS injected controls on the bar-crossing test, having a slight tendency to perform (non-statistically significantly) worse near the end stage, at 14-15 weeks (6 weeks $p = 0.5705$, 7 weeks $p = 0.5831$, 8 weeks $p = 0.0773$, 9 weeks $p = 0.1109$, 10 weeks $p = 0.4017$, 11 weeks $p = 0.0536$, 12 weeks $p = 0.3742$, 13 weeks $p = 0.9311$, 14 weeks $p = 0.2512$, 15 weeks $p = 0.3598$; **Figure 6.8**).

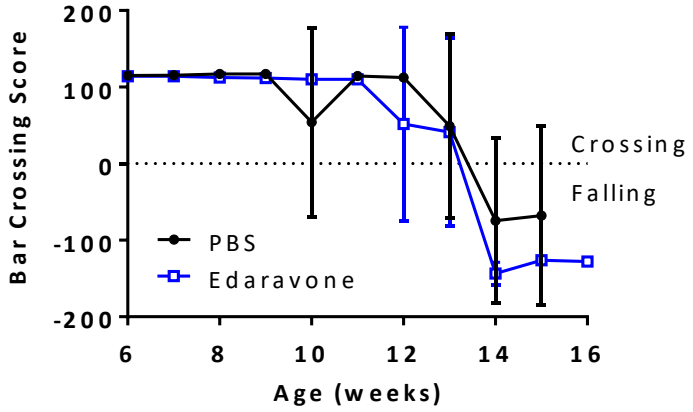


Figure 6.8. Treatment with edaravone did not have an impact on the bar crossing performance of Sandhoff mice.
Performance of Sandhoff mice treated with edaravone (blue) or PBS (controls, black) in bar-crossing test was measured from 6 weeks of age by the latency to cross or fall from the bar, with 120 s maximum, to termination of each trial. If crossing time (CT) was greater than 0, then score = 120 - CT. If falling time (FT) was greater than 0, then score = FT - 120. Data are presented as the mean ±SD at each time point. Data were analysed using multiple *t*-tests, with Holm-Sidak multiple comparisons correction. No significant changes were found, n = 4 mice per group.

Sandhoff mice treated with edaravone also had a trend to perform worse on the rotarod than the controls, from 6 weeks of age to end stage, but the difference is not statistically significant for either the latency to fall, the speed of the rod at the time of the fall, the number of revolutions and the distance travelled (**Figure 6.9**).

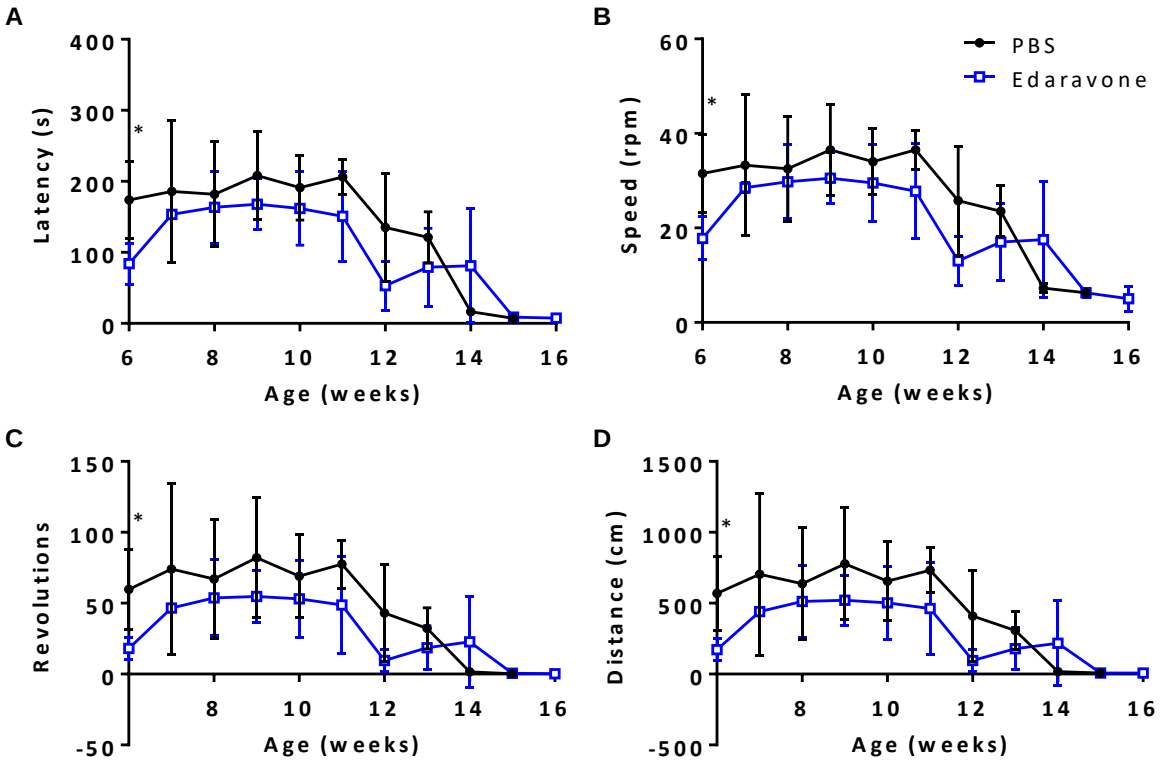


Figure 6.9. Edaravone did not change the performance of Sandhoff mice on the rotarod. Latency (or time to fall, **A**), speed of the rotarod at the time of the fall (**B**), number of revolutions (**C**) and travelled distance (**D**) were recorded once a week for Sandhoff mice treated with edaravone (blue) or PBS (controls, black), starting from 6 weeks of age to end-stage (15-16 weeks). Data are presented as the mean ±SD at each time point. Data were analysed using multiple *t*-tests, with Holm-Sidak multiple comparisons correction. *$p < 0.05$ versus corresponding controls, n = 4 mice per group.

In summary, despite the Sandhoff mice treated with 15 mg/kg/day of edaravone being lighter than the control group (**Figure 6.7**), no significant changes were observed on the behavioural tests performed, with only a slight worsening of motor function and coordination (**Figure 6.8** and **Figure 6.9**).

Sandhoff mice progressively accumulate GSLs, specially GA2 and GM2 in the CNS and in internal organs, including the liver[306]. Acetyl-DL-leucine, which significantly increased the levels of SOD1 suggesting it might indirectly provide antioxidant support, was shown to reduce the storage of GA2 and GM2 in the brain of Sandhoff mice[306]. Therefore, to assess the impact of edaravone on the accumulation of GSLs, brain and liver

of Sandhoff mice were collected when they reached humane endpoint or at 16 weeks of age, and the level of GlcCer and downstream GSLs was measured by NP-HPLC (**Figure 6.10** and **Figure 6.11**). As previously observed for the TDP-43$^{M337V/M337V}$ BAC mice, typical distribution profile of Sandhoff mouse brain GSLs was measured, including GlcCer and the GSLs GA2, GM2, GM1a, GD1a, GD1b and GT1b, with no changes with the treatment with edaravone (GlcCer p = 0.2587, GSLs p = 0.2618; **Figure 6.10**).

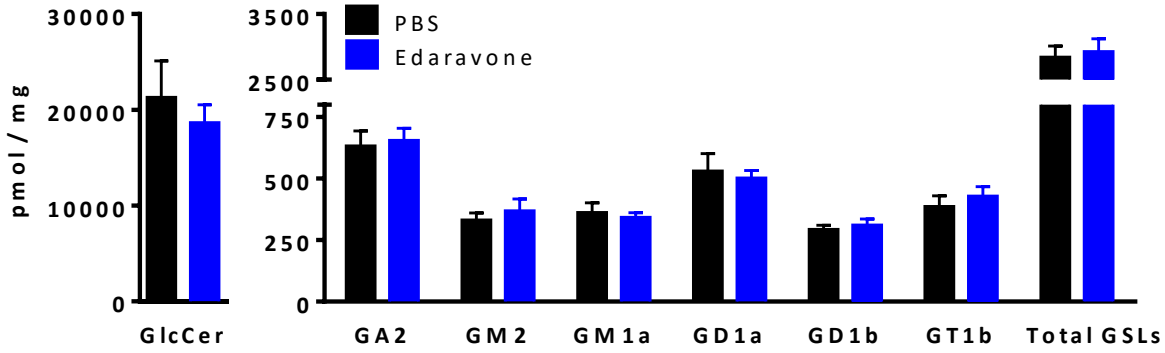


Figure 6.10. Edaravone did not alter the accumulation of GSLs in the Sandhoff mouse brain.
NP-HPLC quantification of GSLs in brain of 15-16 weeks old Sandhoff mice treated with edaravone (blue) or PBS (controls, black). No changes in GSL levels were observed in the brain of edaravone treated mice when compared to PBS treated matched controls. Only main peaks of gangliosides are shown. Data are presented as the mean ±SD for each ganglioside. GlcCer data were analysed using *t*-test, with Holm-Sidak's multiple comparisons correction. Downstream GSLs data were analysed using 2-way ANOVA, with Sidak's multiple comparisons test. No significant changes were found, n = 4 mice per group.

Additionally, no edaravone effect was observed for GSL accumulation in the Sandhoff mouse liver, with the typical lipid profile of GlcCer, GA2, GM2Gc, GM3Gc and GM3 species (GlcCer p = 0.6398, GSLs p = 0.2006; **Figure 6.11**).

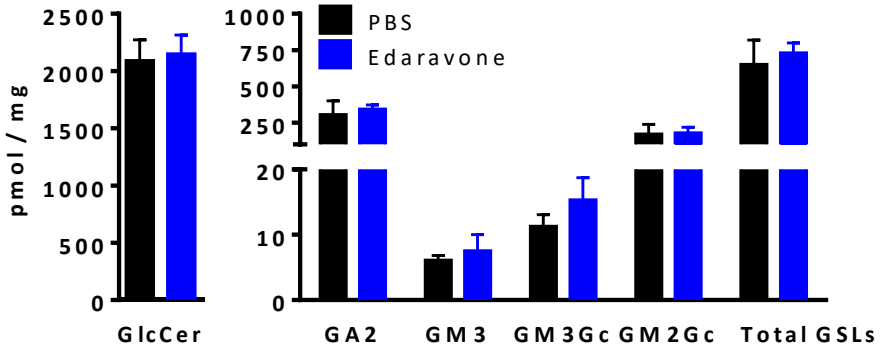


Figure 6.11. Edaravone did not change the accumulation of GSLs in the Sandhoff mouse liver.
NP-HPLC quantification of GSLs in liver of 15-16 weeks old Sandhoff mice treated with edaravone (blue) or PBS (controls, black). No changes in GSL levels were observed in the liver of edaravone treated mice when compared to PBS treated matched controls. Only main peaks of gangliosides are shown. Data are presented as the mean ±SD for each ganglioside. GlcCer data were analysed using *t*-test, with Holm-Sidak's multiple comparisons correction. Downstream GSLs data were analysed using 2-way ANOVA, with Sidak's multiple comparisons test. No significant changes were found, n = 4 mice per group.

In conclusion, edaravone treatment had no effect in the accumulation of GSLs in either the brain or liver of Sandhoff mice when compared to controls (**Figure 6.10** and **Figure 6.11**).

6.3. Discussion

In this chapter, the effect of edaravone on the TDP-43$^{M337V/M337V}$ BAC mouse and on the Sandhoff mouse models was investigated in two pilot studies. When treated with 15 mg/kg/day of edaravone for 5 weeks (see **Table 6.1** for dosage used in other MND rodent models), TDP-43$^{M337V/M337V}$ BAC mice behaviour and health did not change significantly. The weight of these mice was similar to the untreated and the non-transgenic groups and remained constant throughout the 5 weeks of treatment (**Figure 6.1**). Muscular strength and coordination were evaluated by rotarod over the

5 weeks and no statistically significant changes were found (**Figure 6.2**). Locomotor activity, assessed by scoring of rearing (**Figure 6.3**), and motor coordination and gait, measured by footprint pattern testing, after the 5 weeks of treatment (**Figure 6.4**) also didn't show statistically significant changes after treatment with edaravone. Likewise, GSLs storage also remained unchanged in the brain and liver of these mice when compared to PBS controls or non-transgenic untreated mice (**Figure 6.5** and **Figure 6.6**). However, edaravone treated mice showed a tendency to perform less well on the rotarod and a visibly reduced amount of unaided (or centre) rearing, indicating a slight reduction in muscular strength on their hindlimbs, even though this difference was non-statistically significant.

At 6-7 months of age TDP-43$^{M337V/M337V}$ mice are considered early symptomatic, which means the mice are only beginning to show signs of disease and behavioural changes[227]. As a result of this, our data indicating lack of a significant effect by edaravone might not be due to ineffectiveness of the drug, but because it was administered too early in disease development. Alternatively, 5 weeks of treatment in a model that takes 3-6 months to develop symptoms might not be long enough to correctly assess the effect of edaravone on this mouse model, as opposed to administering the drug from the onset of symptoms until end-stage (**Table 6.1**).

Another aspect to take in consideration is the dose administered. The injection of 15 mg/kg of edaravone is quite a high dose, also used on studies on the SOD1^{G93A} and Nrf2/G93A mice[291,294], but other studies have used much lower doses of 10 or 3 mg/kg[292,293] **Table 6.1**). Without a dose-response curve to learn what the optimal dose is to administer to these mice, drawing conclusions from this study is difficult and would require further investigation. In fact, the worsening of motor function and coordination

and mild loss of muscular strength, even though non-statistically significant, might be an indicator of toxicity.

Therefore, the mild worsening of the rotarod and centre rearing performances caused by edaravone is still worth noting. The accelerating rotarod test was initially designed to evaluate maximal gait or motor performance, though it can be influenced by other factors like motor coordination, learning and cardiopulmonary endurance[313]. Nevertheless, it was previously used to assess motor function when describing the TDP-43$^{M337V/M337V}$ mouse model[227]. On the other hand, rearing in the centre of the open field requires more coordination than side rearing, with the support of the side of the cage, because the animal needs to be able to balance itself. Hence, a mild worsening on the performance in rotarod and on the centre rearing scoring shows that edaravone had some negative effects on these mice, contrasting to what was previously reported in other models (**Table 6.1**). Indeed, the TDP-43$^{M337V/M337V}$ BAC mouse develops progressive motor function deficits without showing TDP-43 cytoplasmic aggregation or neuroinflammation, while most SOD1 mouse models show neuroinflammation as an important feature of pathology[227,290]. This, together with the data acquired in this work, adds up to the premise that pathogenesis and respective possible therapies in MND vary depending on the mutations associated[178]. Also, as this was a preliminary experiment, increasing the number of animals used would provide more statistical power and could indicate if this trend is replicable and significance may be reached.

A combination treatment of edaravone with riluzole would also be interesting to explore, as it was previously suggested that riluzole might also have an antioxidant effect and a combined therapy may result in higher efficacy reducing ROS and slowing disease progression in this TDP-43 model of MND[181,185].

For the Sandhoff mice, edaravone treatment (15 mg/kg/day) did not change disease development. Although these mice had significantly less weight than the vehicle treated group (**Figure 6.7**), they performed as well as the controls on the bar crossing test (**Figure 6.8**) and the rotarod (**Figure 6.9**), with only a non-statistically significant tendency to perform worse. Similarly, GlcCer and downstream GSLs storage was the same in the brain and liver of these mice when compared to the corresponding controls (**Figure 6.10** and **Figure 6.11**). Acetyl-DL-leucine was suggested to act indirectly as an antioxidant and reported to improve motor function and strength and coordination, and to significantly reduce the storage of GA2 and GM2 in the brain and liver of Sandhoff mice[306]. However, the cerebellum of Sandhoff mice was shown to have normal levels of SOD1[306], and the lack of an effect by the treatment of this mice with the antioxidant edaravone suggests that, even if upregulation of reductive oxygen species (ROS) like SOD1 is beneficial, oxidative stress is not a driver of disease pathology on this model. Many of the reservations mentioned for the TDP-43$^{M337V/M337V}$ BAC mouse model are also valid for this model. The dose used might have been too high, as indicated by the reduced body weight, and the mild negative effects due to toxicity. Also, the number of animals in the treated and untreated groups were small for an analysis with statistical power and non-transgenic treated and untreated controls would be a valuable addition to the experiment. However, all things considered, the mild changes observed in the Sandhoff mouse model were not beneficial and other treatments should be studied further instead, e.g. the recently published effect of acetyl-DL-leucine[306].

Overall, these data indicate that edaravone does not delay disease progression or the development of the main symptoms associated to MND or Sandhoff's disease in the

TDP-43$^{M337V/M337V}$ or the Sandhoff mouse models, respectively. Further experiments are necessary to calculate the best dose of edaravone to use in each model. These experiments should be done with a higher number of animals in each group and non-transgenic controls, treated and untreated, are essential to include in the study. Also, for the TDP-43$^{M337V/M337V}$ mouse model, it would be interesting to evaluate the effect of edaravone in a later stage of disease development, e.g. 6-12 months or even later, when the mice already show some significant motor deficits, also better mimicking what would happen in a clinical situation.

7. Conclusion and future directions

The work presented in this thesis supports the link between LSDs, as rare, monogenic, early-onset, neurodegenerative disorders, and MND, as more common, late-onset, neurodegenerative diseases[211,213,252]. There is evidence of lysosomal dysfunction and changes in GSL metabolism in MND, but the work here presented demonstrates that their role in the pathology of this heterogeneous disease is complex and requires careful interpretation.

The role of GlcCer in MND

In the beginning of this thesis, a protocol for GlcCer quantification by NP-HPLC was developed to further study the proposed role of GlcCer as a modulator of disease progression in MND (**Chapter 3**). Data from post-mortem tissues of ALS patients and from tissues of the $SOD1^{G86R}$ and $SOD1^{G93A}$ mouse models of MND supported this hypothesis. Not only changes in the levels of GlcCer and GBA activity were reported in diseased tissues[214,215,218,220], but also when inhibiting GCS activity, and consequently the synthesis of GlcCer and all GlcCer-derived GSLs, disease progression was accelerated in $SOD1^{G93A}$ mice; while when administering GM3 disease progression was slowed down[214]. Additionally, in healthy mice, peripheral nerve injury was shown to induce an increase in GCS expression and GlcCer levels, while when after nerve injury GCS activity is inhibited motor function recovery is delayed[215].

However, we observed no changes in the levels of GlcCer or GBA activity in the TA and gastrocnemius muscles of symptomatic/morbid SOD1^{G93A} mice (**Chapter 4**), or in the levels of GlcCer in the spinal cord and brain of pre-symptomatic and symptoms onset TDP^{M337V} mice (**Chapter 5**). Nevertheless, GBA and GBA2 activities were elevated at symptom onset in the brain (GBA and GBA2) and spinal cord (only GBA2) of TDP^{M337V} mice, suggesting not only lysosomal GlcCer degradation has a role in MND, but also its non-lysosomal metabolism (**Chapter 5** and **Table 7.1**).

Recently, a review on the role of sphingolipids in neurodegeneration implicated ceramide as the main sphingolipid contributing to apoptosis in ALS[252]. It also highlighted how further studies are necessary to better understand the specific role of each sphingolipid in the development or the progression to different stages of MND and other neurodegenerative disorders[252]. The work in this thesis supports the need for a better understanding of the specific role of each sphingolipid in the initiation and development of MND is necessary, not only in their lysosomal catabolism but also in non-lysosomal pathways.

GSL metabolism and SOD1 mutations

MND is a heterogeneous group of diseases with poorly understood aetiology. About 5 to 10 % of the patients have a familial history of MND and some genetic mutations have been found to be associated with this pathology. Mutations in the free radical scavenger SOD1 were the first to be found and are present in about 20 % of the familial cases[147,148]. MND is a disease of the motor system, which affects primarily the CNS from the NMJs to the brain and, consequently, the muscular system. Changes in GSL metabolism have been reported both in the CSF and spinal cord (post-mortem tissue) of

patients with ALS[214,216,220]. In **Chapter 4**, GlcCer and GlcCer-derived GSL metabolism was measured in spinal cord and/or in skeletal muscle tissues from SOD1^{G86R} and SOD1^{G93A} mice in different stages of disease development (pre-symptomatic, age of symptoms onset and symptomatic/morbid), to complement and support the data in the literature on GSL metabolism in SOD1 mouse models of MND[214,215].

We found no changes in the levels of GSLs at the age of symptom onset in both spinal cord and muscle of SOD1^{G86R} mice or in muscles of SOD1^{G93A} mice, which contrasts with the reported decrease in GSL levels and changes in GSL hydrolases activity in the spinal cord of SOD1^{G93A} mice at age of symptoms onset[214]. This might be due to the definition of age of onset, which is still under discussion, because motor neuron degeneration can be detected before the loss of motor function[260,261]. However, it has been consistently reported an increase in the levels of GSLs and changes in GSL hydrolases activity, not only in post-mortem spinal cord tissue from ALS patients, but also in the spinal cord and muscle of SOD1^{G86R} mice and the spinal cord of SOD1^{G93A} mice[214,215]. Accordingly, we observed increased levels of GSLs and GSL hydrolases activity in muscle tissues from SOD1^{G93A} mice at morbid stage (**Table 7.1**).

Overall, these data suggest that changes in GSL metabolism appear first in the spinal cord at or near symptoms onset and only later in muscle, in the presence of mutant SOD1. This hypothesis is in agreement with the literature, as pre-symptomatic SOD1^{G93A} mice have shown progressive impairment of the endo-lysosomal trafficking and autophagic clearance[207,208]. Axonal retrograde transport deficits were also found in motor neurons of pre-symptomatic SOD1^{G93A} mice and suggested to promote motor neuron degeneration[209]. The majority of GSL catabolism occurs in the lysosome and lysosomal enzymes require efficient endo-lysosomal maturation, therefore it is likely these

deficiencies result in the measured and reported changes in the levels of GSLs and the activity of the enzymes responsible for their catabolism in the lysosome.

GSL metabolism and TDP-43

Mutations in *TARDBP*, the gene encoding the DNA binding protein TDP-43, are considered rare in MND, but as many as 95 % of all cases show TDP-43 proteinopathy, meaning TDP-43 is mislocalised to the cytoplasm where it forms insoluble aggregates, contributes to the formation of stress granules and promotes motor neuron degeneration[135,174,175]. In **Chapter 5**, the effect of TDP pathology on GSL metabolism was investigated in early stages of disease progression, more clinically relevant for the development of potential biomarkers and therapies that efficiently prevent neurodegeneration. The levels of GSLs and the activity of the enzymes that regulate their catabolism were measured in the spinal cord and brain of TDP-43$^{M337V/M337V}$ mice, in pre-symptomatic, early and late onset of symptoms stages of disease development, and in age-matched WT mice.

We found no changes in the levels of GSLs in the spinal cord of TDP-43$^{M337V/M337V}$ mice in pre-symptomatic or onset of symptoms stages (**Table 7.1**). However, we observed increased levels of GD1b and GT1b in the brain of pre-symptomatic TDP-43$^{M337V/M337V}$ mice, and elevated activity of the GSL hydrolases GBA1, GBA2 and sialidase (neuraminidases Neu1, Neu3 and Neu4) at early symptoms onset, but reduced β-galactosidase activity overall in all the pre-symptomatic and early stages of disease development (**Table 7.1**).

Previously, a partial knockdown of *TARDBP* was shown to directly impair endo-lysosomal pathways, necessary for dendrite growth regulation and neuronal

signalling[281], and TDP-43 mislocalisation was also described in NPC, an early-onset neurodegenerative LSD characterised by the storage of GSLs, SM, sphingosine and cholesterol[289]. Therefore, although the changes we found in lysosomal enzymes are not reflected in alterations to GSL levels, our findings suggest that, in the early stages of disease development of the TDP-43^{M337V} mouse, mutant TDP-43 promotes some changes in GSL and lysosomal metabolism (both in spinal cord and brain). However, further studies are required to investigate the molecular link between them. Importantly, the mouse model studied in this thesis expresses a human mutant form of TDP-43 but in considerably lower levels than the endogenous mouse TDP-43, developing motor function deficits and mimicking human MND pathology without forming TDP-43 insoluble aggregates or neuroinflammation[227]. This is important as it suggests aggregation is not necessary for disease initiation in MND, and contrasts with the SOD1 mouse models where neuroinflammation is a main feature of disease development[227]. Consequently, the relatively mild pathology reported in the TDP-43^{M337V} mouse, showing no neuroinflammation and slow progression of symptoms over months (particularly in the pre-symptomatic and early stages of disease pathology) vs. the severe and rapid development of symptoms reported in SOD1 models, which show severe neuroinflammation, rapidly developing symptoms and reaching morbid stage in only a few days, explains the differences we found in their GSL metabolism (**Table 7.1**).

		Pre-symptomatic	Symptoms onset	Symptomatic/ post-mortem
 **ALS patients**	**CSF**	(undetermined)	(undetermined)	↑ GlcCer, SM[220] and GM1a[216]
	Spinal cord	(undetermined)	(undetermined)	↑ GBA1, GBA2, hexosaminidase, galactosylceramidase, α-galactosidase and β-galactosidase ↑ Cer, GlcCer, GalCer, LacCer, Gb3, GM3 and GM1[214]
	Muscle	(undetermined)	(undetermined)	↑ GCS expression[215]
 **SOD1^{G86R} mice**	**Spinal cord**	=	=	↑ GBA2 activity[218] ↑ GM1a[215]
	Muscle	=	=	↑ GCS expression ↑ GlcCer, GM3 and GM2[215]
 **SOD1^{G93A} mice**	**Spinal cord**	=	↓ GBA1, GBA2 and galactosylceramidase ↑ hexosaminidase ↓ Cer, SM, LacCer, Gb3 and GM1	↓ GBA1, GBA2 and galactosylceramidase ↑ hexosaminidase ↑ GlcCer, Cer, SM, LacCer, GM3, Gb3 and GM1
	Muscle	=	=	↑ β-hexosaminidase and β-galactosidase ↑ LacCer, GM3 and GM2
 **TDP-43^{M337V} mice**	**Spinal cord**	↓ β-galactosidase	↑ GBA2	(undetermined)
	Brain	↑ GD1b and GT1b ↓ β-galactosidase	↑ GBA, GBA2 and sialidase ↓ β-galactosidase	(undetermined)

Table 7.1. Summary of the changes in GSL metabolism (levels of GSLs and activity of GSL catalytic enzymes) reported in the literature and measured in the work of this thesis (shown in blue) in different stages of MND.

The data acquired in the work of this thesis (in blue) shows that changes in GSL metabolism in SOD1 mouse models are different from the ones found in the TDP-43^{M337V} mouse model, highlighting the role of GSL metabolism in MND is complex and requires careful interpretation. The pre-symptomatic changes in GSL metabolism found in tissues from the TDP-43^{M337V} mouse suggest GSLs have a role in disease pathology. Also, changes found in GBA and GBA2 activities in the brain (GBA and GBA2) and spinal cord (GBA2) of early symptomatic TDP-43^{M337V} mice suggest both lysosomal and non-lysosomal GlcCer metabolism have a role in MND.

Edaravone as a therapy for MND and LSDs

Finally, the effect of edaravone in the TDP-43^{M337V} mouse model of MND and the *Hexb*$^{-/-}$ mouse model of Sandhoff disease was evaluated in a pilot study (**Chapter 6**) to investigate the potential common mechanisms between MND and LSDs and contribute for a better understanding of MND pathology. Edaravone is a free radical scavenger and inhibitor of lipid peroxidation[187] and oxidative stress has been shown to be an important feature of motor neuron degeneration in ALS[190–192]. In clinical trials, edaravone was shown to be effective in delaying MND progression during early stages of disease by slowing muscle strength loss and progressive muscle atrophy[196,295]. Edaravone antioxidant and neuroprotective properties were confirmed in a few mouse models of MND[291,293,294], but only tests in SOD1 models are currently required for the pre-clinical approval of therapies for MND. Therefore, the effect of edaravone in MND pathology caused by other mutations remained unexplored.

When we treated TDP-43^{M337V} mice with 15 mg/kg/day of edaravone for 5 weeks at symptoms onset, their behaviour and health did not change. No changes were found in the weight of the mice, in muscle strength and coordination evaluated in the accelerating rotarod, in locomotor activity assessed by scoring of rearing, and in coordination and gait measured by footprint pattern testing after 5 weeks of treatment. Therefore, edaravone doesn't seem to have any effect in the TDP-43^{M337V} mice. Similarly, when we treated *Hexb*$^{-/-}$ mice with edaravone (15 mg/kg/day) from weaning until end-stage at 15-16 weeks, edaravone did not change disease development (**Chapter 6**).

At 6-7 months of age TDP-43$^{M337V/M337V}$ mice are considered early symptomatic, which means the mice are only beginning to show signs of disease and behavioural changes, and this is a model that takes 3-6 months to develop pathological symptoms[227].

Therefore, the lack of a significant effect by edaravone might be due to the treatment being done too early in disease development, or not for long enough to correctly assess the effect of edaravone in this mouse model (as opposed to administering the drug from the onset of symptoms until end-stage). Another aspect to take in consideration is the dose administered, which has been previously used in mice[291,294], but is quite high in comparison with some other studies where doses as low as 10 or 3 mg/kg were used[292,293]. Further experiments are therefore necessary to understand the kinetics of edaravone and trace a dose-response curve, before considering repeating this study in larger scale, with more mice and on a later and longer period through symptoms development (from 6 to 12 months of age), better mimicking what would happen in a clinical setting.

Hexb$^{-/-}$ mice develop symptoms reflective of the Sandhoff human disease, including abnormal motor function and coordination at 3 months of age, bradykinesia, tremors and muscular atrophy, with consequent weight loss and premature death at 4 to 5 months of age[230,308]. No therapies have been approved for the treatment of Sandhoff disease, but acetyl-DL-leucine was shown to delay the onset of motor dysfunction, to reduce GA2 and GM2 storage in the brain and to increase survival on the *Hexb*$^{-/-}$ mouse model[306]. Additionally, when used in combination with miglustat, acetyl-DL-leucine significantly increased autophagy and the levels of SOD1 in *Hexb*$^{-/-}$ mice cerebellum, suggesting it can indirectly provide antioxidant support[306], like edaravone. However, the cerebellum of *Hexb*$^{-/-}$ mice was shown to have normal levels of SOD1[306]. Therefore, the lack of an effect by edaravone in this mouse model suggests that, even if upregulation of ROS (like SOD1) is beneficial, oxidative stress is not a driver of disease pathology and other therapies should be studied instead for Sandhoff disease (e.g. miglustat and acetyl-DL-leucine).

MND is a highly heterogenous group of diseases and the role of GSL and lysosomal metabolism in the mechanisms initiating or contributing for disease progression is not linear. To complete the work described in this thesis, it is relevant to study GSL metabolism in skeletal muscles of TDP-43^{M337V} mice and also in spinal cord in later stages of disease development (at 12-16 months, when the mice are considered symptomatic). Further studies in other models of MND and in different stages of disease progression are also necessary to understand how GSL metabolism contributes to the pathology in the presence of other MND mutations or pathological mechanisms of MND. For example, mutant mice with C9orf72 repeat expansions, the most common cause of familial MND and FTD, have recently been linked to lysosomal dysfunction and impaired exocytosis (and consequent overactivation of MTORC1 signalling), resulting in splenomegaly and lymphadenopathy in mutant mice[314–316]. Therefore, lysosomal metabolism is affected in models of C9orf72 pathology and it would be relevant to investigate the role of GSL metabolism. Finally, to investigate GSLs as potential biomarkers or GSL metabolism as a therapeutic target for MND, changes in GSL metabolism in the CSF of patients during different stages of disease progression could also be measured, together with GWAS analysis, to find associations with genetic mutations and allow for a more personalised medical approach, as it has recently been proposed[317].

Bibliography

1. Wennekes, T., Van Den Berg, R. J. B. H. N., Boot, R. G., Van Der Marel, G. A., Overkleeft, H. S. & Aerts, J. M. F. G. Glycosphingolipids - Nature, function, and pharmacological modulation. *Angew. Chemie - Int. Ed.* **48**, 8848–8869 (2009).
2. D'Angelo, G., Capasso, S., Sticco, L. & Russo, D. Glycosphingolipids: Synthesis and functions. *FEBS J.* **280**, 6338–6353 (2013).
3. Schnaar, R. L., Gerardy-Schahn, R. & Hildebrandt, H. Sialic acids in the brain: Gangliosides and polysialic acid in nervous system development, stability, disease, and regeneration. *Physiol. Rev.* **94**, 461–518 (2014).
4. Schnaar, R. L. Gangliosides of the Vertebrate Nervous System. *J. Mol. Biol.* **428**, 3325–3336 (2016).
5. Platt, F. M. Sphingolipid lysosomal storage disorders. *Nature* **510**, 68–75 (2014).
6. Gupta, G. & Surolia, A. Glycosphingolipids in microdomain formation and their spatial organization. *FEBS Lett.* **584**, 1634–1641 (2010).
7. Hakomori, S. itiroh. Structure and function of glycosphingolipids and sphingolipids: Recollections and future trends. *Biochim. Biophys. Acta - Gen. Subj.* **1780**, 325–346 (2008).
8. Sillence, D. J. & Platt, F. M. Introduction: Glycosphingolipids in cell biology and disease. *Semin. Cell Dev. Biol.* **15**, 371–373 (2004).
9. Sillence, D. J. & Platt, F. M. Glycosphingolipids in endocytic membrane transport. *Semin. Cell Dev. Biol.* **15**, 409–416 (2004).
10. Chiricozzi, E., Lunghi, G., Di Biase, E., Fazzari, M., Sonnino, S. & Mauri, L. GM1 ganglioside is a key factor in maintaining the mammalian neuronal functions avoiding neurodegeneration. *Int. J. Mol. Sci.* **21**, 1–29 (2020).
11. Snijder, B., Sacher, R., Rämö, P., Damm, E. M., Liberali, P. & Pelkmans, L. Population context determines cell-to-cell variability in endocytosis and virus infection. *Nature* **461**, 520–523 (2009).
12. Varki, A., Freeze, H. H. & Manzi, A. E. Overview of Glycoconjugate Analysis. *Curr. Protoc. Protein Sci.* **57**, 1–7 (2009).
13. Maccioni, H. J. F., Quiroga, R. & Ferrari, M. L. Cellular and molecular biology of glycosphingolipid glycosylation. *J. Neurochem.* **117**, no-no (2011).
14. Merrill, A. H., Schmelz, E. M., Dillehay, D. L., Spiegel, S., Shayman, J. A., Schroeder, J. J., Riley, R. T., Voss, K. A. & Wang, E. Sphingolipids - The enigmatic lipid class: Biochemistry, physiology and pathophysiology. *Toxicol. Appl. Pharmacol.* **142**, 208–225 (1997).
15. Futerman, A. H. & Riezman, H. The ins and outs of sphingolipid synthesis. *Trends Cell Biol.* **15**, 312–318 (2005).
16. Futerman, A. H. Intracellular trafficking of sphingolipids: Relationship to biosynthesis. *Biochim. Biophys. Acta - Biomembr.* **1758**, 1885–1892 (2006).
17. Lahiri, S. & Futerman, A. H. The metabolism and function of sphingolipids and glycosphingolipids. *Cell. Mol. Life Sci.* **64**, 2270–2284 (2007).
18. Pruett, S. T., Bushnev, A., Hagedorn, K., Adiga, M., Haynes, C. A., Sullards, M. C.,

Liotta, D. C. & Merrill, A. H. Biodiversity of sphingoid bases ('sphingosines') and related amino alcohols. *J. Lipid Res.* **49**, 1621–1639 (2008).
19. Pewzner-Jung, Y., Ben-Dor, S. & Futerman, A. H. When do Lasses (longevity assurance genes) become CerS (ceramide synthases)? Insights into the regulation of ceramide synthesis. *J. Biol. Chem.* **281**, 25001–25005 (2006).
20. Mullen, T. D., Hannun, Y. A. & Obeid, L. M. Ceramide synthases at the centre of sphingolipid metabolism and biology. *Biochem. J.* **441**, 789–802 (2012).
21. Funakoshi, T., Yasuda, S., Fukasawa, M., Nishijima, M. & Hanada, K. Reconstitution of ATP- and cytosol-dependent transport of de novo synthesized ceramide to the site of sphingomyelin synthesis in semi-intact cells. *J. Biol. Chem.* **275**, 29938–29945 (2000).
22. Holthuis, J. C. M., Pomorski, T., Raggers, R. J., Sprong, H. & Van Meer, G. The Organizing Potential of Sphingolipids in Intracellular Membrane Transport. *Physiol. Rev.* **81**, 1689–1723 (2001).
23. Hanada, K., Kumagai, K., Yasuda, S., Miura, Y., Kawano, M., Fukasawa, M. & Nishijima, M. Molecular machinery for non-vesicular trafficking of ceramide. *Nature* **426**, 803–809 (2003).
24. Gault, C. R., Obeid, L. M. & Hannun, Y. A. An Overview of Sphingolipid Metabolism: From Synthesis to Breakdown. in *Sereal Untuk* vol. 51 1–23 (2010).
25. D'Angelo, G., Polishchuk, E., Tullio, G. Di, Santoro, M., Campli, A. Di, Godi, A., West, G., Bielawski, J., Chuang, C. C., Van Der Spoel, A. C., Platt, F. M., Hannun, Y. A., Polishchuk, R., Mattjus, P. & De Matteis, M. A. Glycosphingolipid synthesis requires FAPP2 transfer of glucosylceramide. *Nature* **449**, 62–67 (2007).
26. Halter, D., Neumann, S., Van Dijk, S. M., Wolthoorn, J., De Mazière, A. M., Vieira, O. V., Mattjus, P., Klumperman, J., Van Meer, G. & Sprong, H. Pre- and post-Golgi translocation of glucosylceramide in glycosphingolipid synthesis. *J. Cell Biol.* **179**, 101–115 (2007).
27. De Matteis, M. A. & Luini, A. Exiting the Golgi complex. *Nat. Rev. Mol. Cell Biol.* **9**, 273–284 (2008).
28. D'Angelo, G., Uemura, T., Chuang, C. C., Polishchuk, E., Santoro, M., Ohvo-Rekilä, H., Sato, T., Di Tullio, G., Varriale, A., D'Auria, S., Daniele, T., Capuani, F., Johannes, L., Mattjus, P., Monti, M., Pucci, P., Williams, R. L., Burke, J. E., Platt, F. M., Harada, A. & De Matteis, M. A. Vesicular and non-vesicular transport feed distinct glycosylation pathways in the Golgi. *Nature* **501**, 116–120 (2013).
29. Kitatani, K., Idkowiak-Baldys, J. & Hannun, Y. A. The sphingolipid salvage pathway in ceramide metabolism and signaling. *Cell. Signal.* **20**, 1010–1018 (2008).
30. Yamashita, T., Wada, R., Sasaki, T., Deng, C., Bierfreund, U., Sandhoff, K. & Proia, R. L. A vital role for glycosphingolipid synthesis during development and differentiation. *Proc. Natl. Acad. Sci.* **96**, 9142–9147 (1999).
31. Wu, Y. P. & Proia, R. L. Deletion of macrophage-inflammatory protein 1 retards neurodegeneration in Sandhoff disease mice. *Proc. Natl. Acad. Sci.* **101**, 8425–8430 (2004).
32. Ichikawa, S., Nakajo, N., Sakiyama, H. & Hirabayashi, Y. A mouse B16 melanoma mutant deficient in glycolipids. *Proc. Natl. Acad. Sci. U. S. A.* **91**, 2703–2707 (1994).
33. Ichikawa, S. & Hirabayashi, Y. Glucosylceramide synthase and glycosphingolipid synthesis. *Trends Cell Biol.* **8**, 198–202 (1998).
34. Simpson, M. A., Cross, H., Proukakis, C., Priestman, D. A., Neville, D. C. A.,

Reinkensmeier, G., Wang, H., Wiznitzer, M., Gurtz, K., Verganelaki, A., Pryde, A., Patton, M. A., Dwek, R. A., Butters, T. D., Platt, F. M. & Crosby, A. H. Infantile-onset symptomatic epilepsy syndrome caused by a homozygous loss-of-function mutation of GM3 synthase. *Nat. Genet.* **36**, 1225–1229 (2004).

35. Boukhris, A., Schule, R., Loureiro, J. L., Lourenço, C. M., Mundwiller, E., Gonzalez, M. A., Charles, P., Gauthier, J., Rekik, I., Acosta Lebrigio, R. F., Gaussen, M., Speziani, F., Ferbert, A., Feki, I., Caballero-Oteyza, A., Dionne-Laporte, A., Amri, M., Noreau, A., Forlani, S., Cruz, V. T., Mochel, F., Coutinho, P., Dion, P., Mhiri, C., Schols, L., Pouget, J., Darios, F., Rouleau, G. A., Marques, W., Brice, A., Durr, A., Zuchner, S. & Stevanin, G. Alteration of ganglioside biosynthesis responsible for complex hereditary spastic paraplegia. *Am. J. Hum. Genet.* **93**, 118–123 (2013).
36. Harlalka, G. V., Lehman, A., Chioza, B., Baple, E. L., Maroofian, R., Cross, H., Sreekantan-Nair, A., Priestman, D. A., Al-Turki, S., McEntagart, M. E., Proukakis, C., Royle, L., Kozak, R. P., Bastaki, L., Patton, M., Wagner, K., Coblentz, R., Price, J., Mezei, M., Schlade-Bartusiak, K., Platt, F. M., Hurles, M. E. & Crosby, A. H. Mutations in B4GALNT1 (GM2 synthase) underlie a new disorder of ganglioside biosynthesis. *Brain* **136**, 3618–3624 (2013).
37. Li, T. A. & Schnaar, R. L. Congenital Disorders of Ganglioside Biosynthesis. *Prog. Mol. Biol. Transl. Sci.* **156**, 63–82 (2018).
38. Mayor, S. & Pagano, R. E. Pathways of clathrin-independent endocytosis. *Nat. Rev. Mol. Cell Biol.* **8**, 603–612 (2007).
39. Singh, R. D., Puri, V., Valiyaveettil, J. T., Marks, D. L., Bittman, R. & Pagano, R. E. Selective Caveolin-1–dependent Endocytosis of Glycosphingolipids. *Mol. Biol. Cell* **14**, 3254–3265 (2003).
40. Kolter, T. & Sandhoff, K. Principles of Lysosomal Membrane Digestion: Stimulation of Sphingolipid Degradation by Sphingolipid Activator Proteins and Anionic Lysosomal Lipids. *Annu. Rev. Cell Dev. Biol.* **21**, 81–103 (2005).
41. Schulze, H., Kolter, T. & Sandhoff, K. Principles of lysosomal membrane degradation. *Biochim. Biophys. Acta - Mol. Cell Res.* **1793**, 674–683 (2009).
42. Sandhoff, K. & Kolter, T. Biochemistry of glycosphingolipid degradation. *Clin. Chim. Acta* **266**, 51–61 (1997).
43. Wilkening, G., Linke, T. & Sandhoff, K. Lysosomal Degradation on Vesicular Membrane Surfaces. *J. Biol. Chem.* **273**, 30271–30278 (1998).
44. Sandhoff, K. & Kolter, T. Biosynthesis and degradation of mammalian glycosphingolipids. *Philos. Trans. R. Soc. B Biol. Sci.* **358**, 847–861 (2003).
45. Kolter, T. & Sandhoff, K. Sphingolipids—Their Metabolic Pathways and the Pathobiochemistry of Neurodegenerative Diseases. *Angew. Chemie Int. Ed.* **38**, 1532–1568 (1999).
46. Kolter, T. & Sandhoff, K. Sphingolipid metabolism diseases. **1758**, 2057–2079 (2006).
47. Stunff, H. Le, Milstien, S. & Spiegel, S. Generation and metabolism of bioactive sphingosine-1-phosphate. *J. Cell. Biochem.* **92**, 882–899 (2004).
48. Platt, F. M., d'Azzo, A., Davidson, B. L., Neufeld, E. F. & Tifft, C. J. Lysosomal storage diseases. *Nat. Rev. Dis. Prim.* **4**, (2018).
49. Trinchera, M., Ghidoni, R., Sonnino, S. & Tettamanti, G. Recycling of glucosylceramide and sphingosine for the biosynthesis of gangliosides and sphingomyelin in rat liver. *Biochem. J.* **270**, 815–820 (1990).

50. Prinetti, A., Chigorno, V., Mauri, L., Loberto, N. & Sonnino, S. Modulation of cell functions by glycosphingolipid metabolic remodeling in the plasma membrane. *J. Neurochem.* **103**, 113–125 (2007).
51. van Weely, S., Brandsma, M., Strijland, A., Tager, J. M. & Aerts, J. M. F. G. Demonstration of the existence of a second, non-lysosomal glucocerebrosidase that is not deficient in Gaucher disease. *Biochim. Biophys. Acta - Mol. Basis Dis.* **1181**, 55–62 (1993).
52. Yildiz, Y., Matern, H., Thompson, B., Allegood, J. C., Warren, R. L., Ramirez, D. M. O., Hammer, R. E., Hamra, F. K., Matern, S. & Russell, D. W. Mutation of β-glucosidase 2 causes glycolipid storage disease and impaired male fertility. *J. Clin. Invest.* **116**, 2985–2994 (2006).
53. Boot, R. G., Verhoek, M., Donker-Koopman, W., Strijland, A., van Marle, J., Overkleeft, H. S., Wennekes, T. & Aerts, J. M. F. G. Identification of the Non-lysosomal Glucosylceramidase as β-Glucosidase 2. *J. Biol. Chem.* **282**, 1305–1312 (2007).
54. Schulze, H. & Sandhoff, K. Sphingolipids and lysosomal pathologies. *Biochim. Biophys. Acta - Mol. Cell Biol. Lipids* **1841**, 799–810 (2014).
55. de Duve, C., Pressman, B. C., Gianetto, R., Wattiaux, R. & Appelmans, F. Tissue fractionation studies. 6. Intracellular distribution patterns of enzymes in rat-liver tissue*. *Biochem. J.* **60**, 604–617 (1955).
56. Ballabio, A. The awesome lysosome. *EMBO Mol. Med.* **8**, 73–76 (2016).
57. Ballabio, A. & Bonifacino, J. S. Lysosomes as dynamic regulators of cell and organismal homeostasis. *Nat. Rev. Mol. Cell Biol.* **21**, 101–118 (2020).
58. Settembre, C., Fraldi, A., Medina, D. L. & Ballabio, A. Signals from the lysosome: A control centre for cellular clearance and energy metabolism. *Nat. Rev. Mol. Cell Biol.* **14**, 283–296 (2013).
59. Medina, D. L. & Ballabio, A. Lysosomal calcium regulates autophagy. *Autophagy* **11**, 970–971 (2015).
60. Todkar, K., Ilamathi, H. S. & Germain, M. Mitochondria and lysosomes: Discovering bonds. *Front. Cell Dev. Biol.* **5**, 1–7 (2017).
61. Parenti, G., Andria, G. & Ballabio, A. Lysosomal storage diseases: From pathophysiology to therapy. *Annu. Rev. Med.* **66**, 471–486 (2015).
62. El-Abassi, R., Singhal, D. & England, J. D. Fabry's disease. *J. Neurol. Sci.* **344**, 5–19 (2014).
63. Alaei, M. R., Tabrizi, A., Jafari, N. & Mozafari, H. Gaucher disease: New expanded classification emphasizing neurological features. *Iran. J. Child Neurol.* **13**, 7–24 (2019).
64. Futerman, A. H. & Platt, F. M. The metabolism of glucocerebrosides — From 1965 to the present. *Mol. Genet. Metab.* **120**, 22–26 (2016).
65. Sun, Y., Liou, B., Ran, H., Skelton, M. R., Williams, M. T., Vorhees, C. V., Kitatani, K., Hannun, Y. A., Witte, D. P., Xu, Y. H. & Grabowski, G. A. Neuronopathic Gaucher disease in the mouse: Viable combined selective saposin C deficiency and mutant glucocerebrosidase (V394L) mice with glucosylsphingosine and glucosylceramide accumulation and progressive neurological deficits. *Hum. Mol. Genet.* **19**, 1088–1097 (2010).
66. Sun, Y., Quinn, B., Witte, D. P. & Grabowski, G. A. Gaucher disease mouse models: Point mutations at the acid β-glucosidase locus combined with low-level

prosaposin expression lead to disease variants. *J. Lipid Res.* **46**, 2102–2113 (2005).
67. Schnabel, D., Schröder, M. & Sandhoff, K. Mutation in the sphingolipid activator protein 2 in a patient with a variant of Gaucher disease. *FEBS Lett.* **284**, 57–59 (1991).
68. Tayebi, N., Walker, J., Stubblefield, B., Orvisky, E., LaMarca, M. E., Wong, K., Rosenbaum, H., Schiffmann, R., Bembi, B. & Sidransky, E. Gaucher disease with parkinsonian manifestations: Does glucocerebrosidase deficiency contribute to a vulnerability to parkinsonism? *Mol. Genet. Metab.* **79**, 104–109 (2003).
69. Sidransky, E., Nalls, M. A., Aasly, J. O., Aharon-Peretz, J., Annesi, G., Barbosa, E. R., Bar-Shira, A., Berg, D., Bras, J., Brice, A., Chen, C.-M., Clark, L. N., Condroyer, C., De Marco, E. V., Dürr, A., Eblan, M. J., Fahn, S., Farrer, M. J., Fung, H.-C., Gan-Or, Z., Gasser, T., Gershoni-Baruch, R., Giladi, N., Griffith, A., Gurevich, T., Januario, C., Kropp, P., Lang, A. E., Lee-Chen, G.-J., Lesage, S., Marder, K., Mata, I. F., Mirelman, A., Mitsui, J., Mizuta, I., Nicoletti, G., Oliveira, C., Ottman, R., Orr-Urtreger, A., Pereira, L. V., Quattrone, A., Rogaeva, E., Rolfs, A., Rosenbaum, H., Rozenberg, R., Samii, A., Samaddar, T., Schulte, C., Sharma, M., Singleton, A., Spitz, M., Tan, E.-K., Tayebi, N., Toda, T., Troiano, A. R., Tsuji, S., Wittstock, M., Wolfsberg, T. G., Wu, Y.-R., Zabetian, C. P., Zhao, Y. & Ziegler, S. G. Multicenter Analysis of Glucocerebrosidase Mutations in Parkinson's Disease. *N. Engl. J. Med.* **361**, 1651–1661 (2009).
70. Sidransky, E. & Lopez, G. The link between the GBA gene and parkinsonism. *Lancet Neurol.* **11**, 986–998 (2012).
71. Westbroek, W., Gustafson, A. M. & Sidransky, E. Exploring the link between glucocerebrosidase mutations and parkinsonism. *Trends Mol. Med.* **17**, 485–493 (2011).
72. Meikle, P. J., Hopwood, J. J., Clague, A. E. & Carey, W. F. Prevalence of lysosomal storage disorders. *J. Am. Med. Assoc.* **281**, 249–254 (1999).
73. Cachon-Gonzalez, M. B., Zaccariotto, E. & Cox, T. M. Genetics and Therapies for GM2 Gangliosidosis. *Curr. Gene Ther.* 68–89 (2018) doi:10.2174/1566523218666180404162622.
74. Mahuran, D. J., Triggs-Raine, B. L., Feigenbaum, A. J. & Gravel, R. A. The molecular basis of Tay-Sachs disease: Mutation identification and diagnosis. *Clin. Biochem.* **23**, 409–415 (1990).
75. Hadfield, M. G., Mamunes, P. & David, R. B. The pathology of Sandhoff's disease. *J. Pathol.* **123**, 137–144 (1977).
76. Jeyakumar, M., Thomas, R., Elliot-Smith, E., Smith, D. A., Van der Spoel, A. C., D'Azzo, A., Perry, V. H., Butters, T. D., Dwek, R. A. & Platt, F. M. Central nervous system inflammation is a hallmark of pathogenesis in mouse models of GM1 and GM2 gangliosidosis. *Brain* **126**, 974–987 (2003).
77. Vanier, M. T. Niemann-Pick disease type C. *Orphanet J. Rare Dis.* **5**, 16 (2010).
78. Auer, I. A., Schmidt, M. L., Lee, V. M. Y., Curry, B., Suzuki, K., Shin, R. W., Pentchev, P. G., Carstea, E. D. & Trojanowski, J. Q. Paired helical filament tau (PHFtau) in Niemann-Pick type C disease is similar to PHFtau in Alzheimer's disease. *Acta Neuropathol.* **90**, 547–551 (1995).
79. Platt, F. M. Emptying the stores: lysosomal diseases and therapeutic strategies. *Nat. Rev. Drug Discov.* (2017) doi:10.1038/nrd.2017.214.
80. Garbade, S. F., Zielonka, M., Mechler, K., Kölker, S., Hoffmann, G. F., Staufner, C.,

Mengel, E. & Ries, M. FDA orphan drug designations for lysosomal storage disorders - A cross-sectional analysis. *PLoS One* **15**, 1–12 (2020).

81. Barton, N. W., Furbish, F. S., Murray, G. J., Garfield, M. & Brady, R. O. Therapeutic response to intravenous infusions of glucocerebrosidase in a patient with Gaucher disease. *Proc. Natl. Acad. Sci. U. S. A.* **87**, 1913–1916 (1990).
82. Grabowski, G. A., Barton, N. W., Pastores, G., Dambrosia, J. M., Banerjee, T. K., McKee, M. A., Parker, C., Schiffmann, R., Hill, S. C. & Brady, R. O. Enzyme therapy in type 1 Gaucher disease: Comparative efficacy of mannose- terminated glucocerebrosidase from natural and recombinant sources. *Ann. Intern. Med.* **122**, 33–39 (1995).
83. Brady, R. O. Enzyme replacement for lysosomal diseases. *Annu. Rev. Med.* **57**, 283–296 (2006).
84. Zimran, A., Belmatoug, N., Bembi, B., Deegan, P., Elstein, D., Fernandez-sasso, D., Giraldo, P., Goker-Alpan, O., Lau, H., Lukina, E., Panahloo, Z. & Schwartz, I. V. D. Demographics and patient characteristics of 1209 patients with Gaucher Disease: Descriptive analysis from the Gaucher Outcome Survey (GOS). *Am. J. Hematol.* 1–24 (2017) doi:10.1002/ajh.24957.
85. Smith, L., Rhead, W., Charrow, J., Shankar, S. P., Bavdekar, A., Longo, N., Mardach, R., Harmatz, P., Hangartner, T., Lee, H. M., Crombez, E. & Pastores, G. M. Long-term velaglucerase alfa treatment in children with Gaucher disease type 1 naïve to enzyme replacement therapy or previously treated with imiglucerase. *Mol. Genet. Metab.* **117**, 164–171 (2016).
86. Turkia, H. Ben, Gonzalez, D. E., Barton, N. W., Zimran, A., Kabra, M., Lukina, E. A., Giraldo, P., Kisinovsky, I., Bavdekar, A., Dridi, M. F. Ben, Gupta, N., Kishnani, P. S., Sureshkumar, E. K., Wang, N., Crombez, E., Bhirangi, K. & Mehta, A. Velaglucerase alfa enzyme replacement therapy compared with imiglucerase in patients with Gaucher disease. *Am. J. Hematol.* **88**, 179–184 (2013).
87. Bonam, S. R., Wang, F. & Muller, S. Lysosomes as a therapeutic target. *Nat. Rev. Drug Discov.* **18**, 923–948 (2019).
88. Van Hout, H. Den, Reuser, A. J. J., Vulto, A. G., Christa B Loonen, M., Cromme-Dijkhuis, A. & Van Der Ploeg, A. T. Recombinant human α-glucosidase from rabbit milk in Pompe patients. *Lancet* **356**, 397–398 (2000).
89. Schiffmann, R., Ries, M., Timmons, M., Flaherty, J. T. & Brady, R. O. Long-term therapy with agalsidase alfa for Fabry disease: Safety and effects on renal function in a home infusion setting. *Nephrol. Dial. Transplant.* **21**, 345–354 (2006).
90. Wraith, J. E., Tylki-Szymanska, A., Guffon, N., Lien, Y. H., Tsimaratos, M., Vellodi, A. & Germain, D. P. Safety and Efficacy of Enzyme Replacement Therapy with Agalsidase Beta: An International, Open-label Study in Pediatric Patients with Fabry Disease. *J. Pediatr.* **152**, 563-570.e1 (2008).
91. Kelly, J. M., Bradbury, A., Martin, D. R. & Byrne, M. E. Emerging therapies for neuropathic lysosomal storage disorders. *Prog. Neurobiol.* **152**, 166–180 (2017).
92. Schulz, A., Ajayi, T., Specchio, N., de Los Reyes, E., Gissen, P., Ballon, D., Dyke, J. P., Cahan, H., Slasor, P., Jacoby, D. & Kohlschütter, A. Study of Intraventricular Cerliponase Alfa for CLN2 Disease. *N. Engl. J. Med.* **378**, 1898–1907 (2018).
93. Wada, R., Tifft, C. J. & Proia, R. L. Microglial activation precedes acute neurodegeneration in Sandhoff disease and is suppressed by bone marrow transplantation. *Proc. Natl. Acad. Sci. U. S. A.* **97**, 10954–10959 (2000).

94. Jeyakumar, M., Norflus, F., Tiff, C. J., Cortina-Borja, M., Butters, T. D., Proia, R. L., Perry, V. H., Dwek, R. A. & Platt, F. M. Enhanced survival in Sandhoff disease mice receiving a combination of substrate deprivation therapy and bone marrow transplantation. *Blood* **97**, 327–329 (2001).
95. Cachón-González, M. B., Wang, S. Z., Lynch, A., Ziegler, R., Cheng, S. H. & Cox, T. M. Effective gene therapy in an authentic model of Tay-Sachs-related diseases. *Proc. Natl. Acad. Sci. U. S. A.* **103**, 10373–10378 (2006).
96. Chiricozzi, E., Niemir, N., Aureli, M., Magini, A., Loberto, N., Prinetti, A., Bassi, R., Polchi, A., Emiliani, C., Caillaud, C. & Sonnino, S. Chaperone Therapy for GM2 Gangliosidosis: Effects of Pyrimethamine on β-Hexosaminidase Activity in Sandhoff Fibroblasts. *Mol. Neurobiol.* **50**, 159–167 (2014).
97. Vu, M., Li, R., Baskfield, A., Lu, B., Farkhondeh, A., Gorshkov, K., Motabar, O., Beers, J., Chen, G., Zou, J., Espejo-Mojica, A. J., Rodríguez-López, A., Alméciga-Díaz, C. J., Barrera, L. A., Jiang, X., Ory, D. S., Marugan, J. J. & Zheng, W. Neural stem cells for disease modeling and evaluation of therapeutics for Tay-Sachs disease. *Orphanet J. Rare Dis.* **13**, 152 (2018).
98. Jeyakumar, M., Smith, D. A., Williams, I. M., Borja, M. C., Neville, D. C. A., Butters, T. D., Dwek, R. A. & Platt, F. M. NSAIDs increase survival in the Sandhoff disease mouse: Synergy with N-butyldeoxynojirimycin. *Ann. Neurol.* **56**, 642–649 (2004).
99. Marques, A. R. A. & Saftig, P. Lysosomal storage disorders – challenges, concepts and avenues for therapy: Beyond rare diseases. *J. Cell Sci.* **132**, (2019).
100. Neefjes, J. & van der Kant, R. Stuck in traffic: An emerging theme in diseases of the nervous system. *Trends Neurosci.* **37**, 66–76 (2014).
101. Fraldi, A., Klein, A. D., Medina, D. L. & Settembre, C. Brain Disorders Due to Lysosomal Dysfunction. *Annu. Rev. Neurosci.* **39**, 277–295 (2016).
102. Nixon, R. A. The role of autophagy in neurodegenerative disease. *Nat. Med.* **19**, 983–997 (2013).
103. Lie, P. P. Y. & Nixon, R. A. Lysosome trafficking and signaling in health and neurodegenerative diseases. *Neurobiol. Dis.* **122**, 94–105 (2019).
104. Boland, B. & Platt, F. M. Bridging the age spectrum of neurodegenerative storage diseases. *Best Pract. Res. Clin. Endocrinol. Metab.* **29**, 127–143 (2015).
105. Goker-Alpan, O., Giasson, B. I., Eblan, M. J., Nguyen, J., Hurtig, H. I., Lee, V. M.-Y., Trojanowski, J. Q. & Sidransky, E. Glucocerebrosidase mutations are an important risk factor for Lewy body disorders. *Neurology* **67**, 908–910 (2006).
106. Robak, L. A., Jansen, I. E., van Rooij, J., Uitterlinden, A. G., Kraaij, R., Jankovic, J., IPDGC, Heutink, P. & Shulman, J. M. Excessive burden of lysosomal storage disorder gene variants in Parkinson's disease. *Brain* 1–13 (2017) doi:10.1093/brain/awx285.
107. Aflaki, E., Westbroek, W. & Sidransky, E. The Complicated Relationship between Gaucher Disease and Parkinsonism: Insights from a Rare Disease. *Neuron* **93**, 737–746 (2017).
108. Spillantini, M. G., Schmidt, M. L., Lee, V. M.-Y., Trojanowski, J. Q., Jakes, R. & Goedert, M. α-Synuclein in Lewy bodies. *Nature* **388**, 839–840 (1997).
109. Lee, H. J., Khoshaghideh, F., Patel, S. & Lee, S. J. Clearance of α-Synuclein Oligomeric Intermediates via the Lysosomal Degradation Pathway. *J. Neurosci.* **24**, 1888–1896 (2004).
110. Freeman, D., Cedillos, R., Choyke, S., Lukic, Z., McGuire, K., Marvin, S., Burrage, A.

M., Sudholt, S., Rana, A., O'Connor, C., Wiethoff, C. M. & Campbell, E. M. Alpha-Synuclein Induces Lysosomal Rupture and Cathepsin Dependent Reactive Oxygen Species Following Endocytosis. *PLoS One* **8**, (2013).
111. Decressac, M., Mattsson, B., Weikop, P., Lundblad, M., Jakobsson, J. & Björklund, A. TFEB-mediated autophagy rescues midbrain dopamine neurons from α-synuclein toxicity. *Proc. Natl. Acad. Sci. U. S. A.* **110**, (2013).
112. Pitcairn, C., Wani, W. Y. & Mazzulli, J. R. Dysregulation of the autophagic-lysosomal pathway in Gaucher and Parkinson's disease. *Neurobiol. Dis.* 0–1 (2018) doi:10.1016/j.nbd.2018.03.008.
113. Lee, J. H., Yu, W. H., Kumar, A., Lee, S., Mohan, P. S., Peterhoff, C. M., Wolfe, D. M., Martinez-Vicente, M., Massey, A. C., Sovak, G., Uchiyama, Y., Westaway, D., Cuervo, A. M. & Nixon, R. A. Lysosomal proteolysis and autophagy require presenilin 1 and are disrupted by Alzheimer-related PS1 mutations. *Cell* **141**, 1146–1158 (2010).
114. Coen, K., Flannagan, R. S., Baron, S., Carraro-Lacroix, L. R., Wang, D., Vermeire, W., Michiels, C., Munck, S., Baert, V., Sugita, S., Wuytack, F., Hiesinger, P. R., Grinstein, S. & Annaert, W. Lysosomal calcium homeostasis defects, not proton pump defects, cause endo-lysosomal dysfunction in PSEN-deficient cells. *J. Cell Biol.* **198**, 23–35 (2012).
115. Lee, J. H., McBrayer, M. K., Wolfe, D. M., Haslett, L. J., Kumar, A., Sato, Y., Lie, P. P. Y., Mohan, P., Coffey, E. E., Kompella, U., Mitchell, C. H., Lloyd-Evans, E. & Nixon, R. A. Presenilin 1 Maintains Lysosomal Ca2+ Homeostasis via TRPML1 by Regulating vATPase-Mediated Lysosome Acidification. *Cell Rep.* **12**, 1430–1444 (2015).
116. Karran, E., Mercken, M. & Strooper, B. De. The amyloid cascade hypothesis for Alzheimer's disease: An appraisal for the development of therapeutics. *Nat. Rev. Drug Discov.* **10**, 698–712 (2011).
117. Jonsson, T., Atwal, J. K., Steinberg, S., Snaedal, J., Jonsson, P. V., Bjornsson, S., Stefansson, H., Sulem, P., Gudbjartsson, D., Maloney, J., Hoyte, K., Gustafson, A., Liu, Y., Lu, Y., Bhangale, T., Graham, R. R., Huttenlocher, J., Bjornsdottir, G., Andreassen, O. A., Jonsson, E. G., Palotie, A., Behrens, T. W., Magnusson, O. T., Kong, A., Thorsteinsdottir, U., Watts, R. J. & Stefansson, K. A mutation in APP protects against Alzheimer's disease and age-related cognitive decline. *Nature* **488**, 96 (2012).
118. Masters, C. L., Bateman, R., Blennow, K., Rowe, C. C., Sperling, R. A. & Cummings, J. L. Alzheimer's disease. *Nat. Rev. Dis. Prim.* **1**, 1–18 (2015).
119. Gowrishankar, S., Yuan, P., Wu, Y., Schrag, M., Paradise, S., Grutzendler, J., De Camilli, P. & Ferguson, S. M. Massive accumulation of luminal protease-deficient axonal lysosomes at Alzheimer's disease amyloid plaques. *Proc. Natl. Acad. Sci. U. S. A.* **112**, E3699–E3708 (2015).
120. Nixon, R. A. Amyloid precursor protein & endosomal-lysosomal dysfunction in Alzheimer's disease: Inseparable partners in a multifactorial disease. *FASEB J.* **31**, 2729–2743 (2017).
121. Rowland, L. P. How Amyotrophic Lateral Sclerosis Got Its Name. *Arch. Neurol.* **58**, 512–515 (2001).
122. Bäumer, D., Talbot, K. & Turner, M. R. Advances in motor neurone disease. *J. R. Soc. Med.* **107**, 14–21 (2014).
123. Hardiman, O., Al-Chalabi, A., Chio, A., Corr, E. M., Logroscino, G., Robberecht, W.,

Shaw, P. J., Simmons, Z. & Van Den Berg, L. H. Amyotrophic lateral sclerosis. *Nat. Rev. Dis. Prim.* **3**, (2017).
124. Logroscino, G., Traynor, B. J., Hardiman, O., Chió, A., Mitchell, D., Swingler, R. J., Millul, A., Benn, E. & Beghi, E. Incidence of amyotrophic lateral sclerosis in Europe. *J. Neurol. Neurosurg. Psychiatry* **81**, 385–390 (2010).
125. Hardiman, O., Chalabi, A. Al, Brayne, C., Beghi, E., van den Berg, L. H., Chio, A., Martin, S., Logroscino, G. & Rooney, J. The changing picture of amyotrophic lateral sclerosis: lessons from European registers. *J. Neurol. Neurosurg. Psychiatry* jnnp-2016-314495 (2017) doi:10.1136/jnnp-2016-314495.
126. Longinetti, E. & Fang, F. Epidemiology of amyotrophic lateral sclerosis: An update of recent literature. *Curr. Opin. Neurol.* **32**, 771–776 (2019).
127. Al-Chalabi, A., van den Berg, L. H. & Veldink, J. Gene discovery in amyotrophic lateral sclerosis: implications for clinical management. *Nat. Rev. Neurol.* **13**, 96–104 (2016).
128. Alonso, A., Logroscino, G. & Hernán, M. A. Smoking and the risk of amyotrophic lateral sclerosis: A systematic review and meta-analysis. *J. Neurol. Neurosurg. Psychiatry* **81**, 1249–1252 (2010).
129. Lacorte, E., Ferrigno, L., Leoncini, E., Corbo, M., Boccia, S. & Vanacore, N. Physical activity, and physical activity related to sports, leisure and occupational activity as risk factors for ALS: A systematic review. *Neurosci. Biobehav. Rev.* **66**, 61–79 (2016).
130. Sutedja, N. A., Veldink, J. H., Fischer, K., Kromhout, H., Heederik, D., Huisman, M. H. B., Wokke, J. H. J. & Van Den Berg, L. H. Exposure to chemicals and metals and risk of amyotrophic lateral sclerosis: A systematic review. *Amyotroph. Lateral Scler.* **10**, 302–309 (2009).
131. Malek, A. M., Barchowsky, A., Bowser, R., Heiman-Patterson, T., Lacomis, D., Rana, S., Ada Youk & Talbott, E. O. Exposure to hazardous air pollutants and the risk of amyotrophic lateral sclerosis. *Environ. Pollut.* **197**, 181–186 (2015).
132. Martin, S., Al Khleifat, A. & Al-Chalabi, A. What causes amyotrophic lateral sclerosis? *F1000Research* **6**, 371 (2017).
133. Foster, L. A. & Salajegheh, M. K. Motor Neuron Disease: Pathophysiology, Diagnosis, and Management. *Am. J. Med.* **132**, 32–37 (2019).
134. Murphy, J., Factor-Litvak, P., Goetz, R., Lomen-Hoerth, C., Nagy, P. L., Hupf, J., Singleton, J., Woolley, S., Andrews, H., Heitzman, D., Bedlack, R. S., Katz, J. S., Barohn, R. J., Sorenson, E. J., Oskarsson, B., Filho, J. A. M. F., Kasarskis, E. J., Mozaffar, T., Rollins, Y. D., Nations, S. P., Swenson, A. J., Koczon-Jaremko, B. A. & Mitsumoto, H. Cognitive-behavioral screening reveals prevalent impairment in a large multicenter ALS cohort. *Neurology* **86**, 813–820 (2016).
135. Neumann, M., Sampathu, D. M., Kwong, L. K., Truax, A. C., Micsenyi, M. C., Chou, T. T., Bruce, J., Schuck, T., Grossman, M., Clark, C. M., McCluskey, L. F., Miller, B. L., Masliah, E., Mackenzie, I. R., Feldman, H., Feiden, W., Kretzschmar, H. A., Trojanowski, J. Q. & Lee, V. M.-Y. Ubiquitinated TDP-43 in Frontotemporal Lobar Degeneration and Amyotrophic Lateral Sclerosis. *Science (80-.).* **314**, 130–133 (2006).
136. Burrell, J. R., Halliday, G. M., Kril, J. J., Ittner, L. M., Götz, J., Kiernan, M. C. & Hodges, J. R. The frontotemporal dementia-motor neuron disease continuum. *Lancet* **388**, 919–931 (2016).

137. Weishaupt, J. H., Hyman, T. & Dikic, I. Common Molecular Pathways in Amyotrophic Lateral Sclerosis and Frontotemporal Dementia. *Trends Mol. Med.* **22**, 769–783 (2016).
138. Masrori, P. & Van Damme, P. Amyotrophic lateral sclerosis: a clinical review. *Eur. J. Neurol.* **27**, 1918–1929 (2020).
139. Chia, R., Chiò, A. & Traynor, B. J. Novel genes associated with amyotrophic lateral sclerosis: diagnostic and clinical implications. *Lancet Neurol.* **17**, 94–102 (2018).
140. DeJesus-Hernandez, M., Mackenzie, I. R., Boeve, B. F., Boxer, A. L., Baker, M., Rutherford, N. J., Nicholson, A. M., Finch, N. C. A., Flynn, H., Adamson, J., Kouri, N., Wojtas, A., Sengdy, P., Hsiung, G. Y. R., Karydas, A., Seeley, W. W., Josephs, K. A., Coppola, G., Geschwind, D. H., Wszolek, Z. K., Feldman, H., Knopman, D. S., Petersen, R. C., Miller, B. L., Dickson, D. W., Boylan, K. B., Graff-Radford, N. R. & Rademakers, R. Expanded GGGGCC Hexanucleotide Repeat in Noncoding Region of C9ORF72 Causes Chromosome 9p-Linked FTD and ALS. *Neuron* **72**, 245–256 (2011).
141. Renton, A. E., Majounie, E., Waite, A., Simón-Sánchez, J., Rollinson, S., Gibbs, J. R., Schymick, J. C., Laaksovirta, H., van Swieten, J. C., Myllykangas, L., Kalimo, H., Paetau, A., Abramzon, Y., Remes, A. M., Kaganovich, A., Scholz, S. W., Duckworth, J., Ding, J., Harmer, D. W., Hernandez, D. G., Johnson, J. O., Mok, K., Ryten, M., Trabzuni, D., Guerreiro, R. J., Orrell, R. W., Neal, J., Murray, A., Pearson, J., Jansen, I. E., Sondervan, D., Seelaar, H., Blake, D., Young, K., Halliwell, N., Callister, J. B., Toulson, G., Richardson, A., Gerhard, A., Snowden, J., Mann, D., Neary, D., Nalls, M. A., Peuralinna, T., Jansson, L., Isoviita, V. M., Kaivorinne, A. L., Hölttä-Vuori, M., Ikonen, E., Sulkava, R., Benatar, M., Wuu, J., Chiò, A., Restagno, G., Borghero, G., Sabatelli, M., Heckerman, D., Rogaeva, E., Zinman, L., Rothstein, J. D., Sendtner, M., Drepper, C., Eichler, E. E., Alkan, C., Abdullaev, Z., Pack, S. D., Dutra, A., Pak, E., Hardy, J., Singleton, A., Williams, N. M., Heutink, P., Pickering-Brown, S., Morris, H. R., Tienari, P. J. & Traynor, B. J. A hexanucleotide repeat expansion in C9ORF72 is the cause of chromosome 9p21-linked ALS-FTD. *Neuron* **72**, 257–268 (2011).
142. Majounie, E., Renton, A. E., Mok, K., Dopper, E. G. P., Waite, A., Rollinson, S., Chiò, A., Restagno, G., Nicolaou, N., Simon-Sanchez, J., van Swieten, J. C., Abramzon, Y., Johnson, J. O., Sendtner, M., Pamphlett, R., Orrell, R. W., Mead, S., Sidle, K. C., Houlden, H., Rohrer, J. D., Morrison, K. E., Pall, H., Talbot, K., Ansorge, O., Hernandez, D. G., Arepalli, S., Sabatelli, M., Mora, G., Corbo, M., Giannini, F., Calvo, A., Englund, E., Borghero, G., Floris, G. L., Remes, A. M., Laaksovirta, H., McCluskey, L., Trojanowski, J. Q., Van Deerlin, V. M., Schellenberg, G. D., Nalls, M. A., Drory, V. E., Lu, C. S., Yeh, T. H., Ishiura, H., Takahashi, Y., Tsuji, S., Le Ber, I., Brice, A., Drepper, C., Williams, N., Kirby, J., Shaw, P., Hardy, J., Tienari, P. J., Heutink, P., Morris, H. R., Pickering-Brown, S., Traynor, B. J., Adamson, G., Bayer, A. J., Beck, J., Callister, J. B., Blake, D. J., Blumen, S. C., Collinge, J., Dunckley, T., Ealing, J., East, S., Elman, L., Gerhard, A., Guerreiro, R. J., Gwinn, K., Halliwell, N., Hamdalla, H. H., Hewitt, C., Ince, P., Jablonka, S., James, C., Kent, L., Knock, J. C., Lynch, T., Mahoney, C., Mann, D., Neal, J., Norris, D., O'Dowd, S., Richardson, A., Rossor, M., Rothstein, J., Scholz, S. W., Snowden, J., Stephan, D. A., Toulson, G., Turner, M. R., Warren, J. D., Young, K., Weng, Y. H., Kuo, H. C., Lai, S. C., Huang, C. L., Camuzat, A., Entraingues, L., Guillot-Noël, Verpillat, P., Clerget-Darpoux, F., Corcia, P., Couratier, P., Didic, M., Dubois, B., Duyckaerts, C., Guedj, E., Golfier, V., Habert, M. O., Hannequin, D., Lacomblez, L., Meininger, V., Salachas, F., Levy, R., Michel, B. F.,

Pasquier, F., Puel, M., Thomas-Anterion, C., Sellal, F., Vercelletto, M., Moglia, C., Cammarosano, S., Canosa, A., Gallo, S., Brunetti, M., Ossola, I., Marinou, K., Papetti, L., Pisano, F., Pinter, G. L., Conte, A., Luigetti, M., Zollino, M., Lattante, S., Marangi, G., la Bella, V., Spataro, R., Colletti, T., Battistini, S., Ricci, C., Caponnetto, C., Mancardi, G., Mandich, P., Salvi, F., Bartolomei, I., Mandrioli, J., Sola, P., Lunetta, C., Penco, S., Monsurrò, M. R., Tedeschi, G., Conforti, F. L., Gambardella, A., Quattrone, A., Volanti, P., Floris, G., Cannas, A., Piras, V., Marrosu, F., Marrosu, M. G., Murru, M. R., Pugliatti, M., Parish, L. D., Sotgiu, A., Solinas, G., Ulgheri, L., Ticca, A., Simone, I. & Logroscino, G. Frequency of the C9orf72 hexanucleotide repeat expansion in patients with amyotrophic lateral sclerosis and frontotemporal dementia: A cross-sectional study. *Lancet Neurol.* **11**, 323–330 (2012).

143. Agosta, F., Ferraro, P. M., Riva, N., Spinelli, E. G., Domi, T., Carrera, P., Copetti, M., Falzone, Y., Ferrari, M., Lunetta, C., Comi, G., Falini, A., Quattrini, A., Filippi, M., Jack, C. R., Josephs, K. A., Al-Sarraj, S., Boxer, A. L., MacIntosh, B. J., Rogaeva, E., Tang-Wai, D., Tartaglia, M. C., Laforce, R., Tagliavini, F., Tiraboschi, P., Redaelli, V., Prioni, S., Grisoli, M., Borroni, B., Padovani, A., Galimberti, D., Scarpini, E., Arighi, A., Fumagalli, G., Rowe, J. B., Coyle-Gilchrist, I., Graff, C., Fallstrom, M., Jelic, V., Stahlbom, A. K., Andersson, C., Thonberg, H., Lilius, L., Frisoni, G. B., Pievani, M., Bocchetta, M., Benussi, L., Ghidoni, R., Finger, E., Sorbi, S., Nacmias, B., Lombardi, G., Polito, C., Warren, J. D., Ourselin, S., Fox, N. C., Rossor, M. N., Rogaeva, E., Zinman, L., Rothstein, J. D., Sendtner, M., Drepper, C., Eichler, E. E., Alkan, C., Abdullaev, Z., Pack, S. D., Dutra, A., Pak, E., Hardy, J., Singleton, A., Williams, N. M., Heutink, P., Pickering-Brown, S., Morris, H. R., Tienari, P. J. & Traynor, B. J. Structural and functional brain signatures of C9orf72 in motor neuron disease. *Neurobiol. Aging* **45**, S173–S186 (2017).
144. Gitler, A. D. & Tsuiji, H. There has been an awakening: Emerging mechanisms of C9orf72 mutations in FTD/ALS. *Brain Res.* **1647**, 19–29 (2016).
145. Bowling, A. C., Schulz, J. B., Brown, R. H. & Beal, M. F. Superoxide Dismutase Activity, Oxidative Damage, and Mitochondrial Energy Metabolism in Familial and Sporadic Amyotrophic Lateral Sclerosis. *J. Neurochem.* **61**, 2322–2325 (1993).
146. Reaume, A. G., Elliott, J. L., Hoffman, E. K., Kowall, N. W., Ferrante, R. J., Siwek, D. R., Wilcox, H. M., Flood, D. G., Beal, M. F., Brown, R. H., Scott, R. W. & Snider, W. D. Motor neurons in Cu/Zn superoxide dismutase-deficient mice develop normally but exhibit enhanced cell death after axonal injury. *Nat. Genet.* **13**, 43–47 (1996).
147. Peters, O. M., Ghasemi, M. & Brown, R. H. Emerging mechanisms of molecular pathology in ALS. *J. Clin. Invest.* **125**, 1767–1779 (2015).
148. Rosen, D. R., Siddique, T., Patterson, D., Figlewicz, D. A., Sapp, P., Hentati, A., Donaldson, D., Goto, J., O'Regan, J. P., Deng, H.-X., Rahmani, Z., Krizus, A., McKenna-Yasek, D., Cayabyab, A., Gaston, S. M., Berger, R., Tanzi, R. E., Halperin, J. J., Herzfeldt, B., Van den Bergh, R., Hung, W.-Y., Bird, T., Deng, G., Mulder, D. W., Smyth, C., Laing, N. G., Soriano, E., Pericak–Vance, M. A., Haines, J., Rouleau, G. A., Gusella, J. S., Horvitz, H. R. & Brown, R. H. Mutations in Cu/Zn superoxide dismutase gene are associated with familial amyotrophic lateral sclerosis. *Nature* **362**, 59–62 (1993).
149. Huai, J. & Zhang, Z. Structural properties and interaction partners of familial ALS-associated SOD1 mutants. *Front. Neurol.* **10**, 1–5 (2019).
150. Tokuda, E., Takei, Y. I., Ohara, S., Fujiwara, N., Hozumi, I. & Furukawa, Y. Wild-type

Cu/Zn-superoxide dismutase is misfolded in cerebrospinal fluid of sporadic amyotrophic lateral sclerosis. *Mol. Neurodegener.* **14**, 1–21 (2019).

151. Gurney, M., Pu, H., Chiu, A., Dal Canto, M., Polchow, C., Alexander, D., Caliendo, J., Hentati, A., Kwon, Y., Deng, H.-X. & Et, A. Motor neuron degeneration in mice that express a human Cu,Zn superoxide dismutase mutation. *Science (80-.).* **264**, 1772–1775 (1994).
152. Tu, P. H., Raju, P., Robinson, K. A., Gurney, M. E., Trojanowski, J. Q. & Lee, V. M. Y. Transgenic mice carrying a human mutant superoxide dismutase transgene develop neuronal cytoskeletal pathology resembling human amyotrophic lateral sclerosis lesions. *Proc. Natl. Acad. Sci. U. S. A.* **93**, 3155–3160 (1996).
153. Deng, H., Gao, K. & Jankovic, J. The role of FUS gene variants in neurodegenerative diseases. *Nat. Rev. Neurol.* **10**, 337–348 (2014).
154. Mackenzie, I. R. A., Rademakers, R. & Neumann, M. TDP-43 and FUS in amyotrophic lateral sclerosis and frontotemporal dementia. *Lancet Neurol.* **9**, 995–1007 (2010).
155. Kwiatkowski, T. J., Bosco, D. A., LeClerc, A. L., Tamrazian, E., Vanderburg, C. R., Russ, C., Davis, A., Gilchrist, J., Kasarskis, E. J., Munsat, T., Valdmanis, P., Rouleau, G. A., Hosler, B. A., Cortelli, P., De Jong, P. J., Yoshinaga, Y., Haines, J. L., Pericak-Vance, M. A., Yan, J., Ticozzi, N., Siddique, T., McKenna-Yasek, D., Sapp, P. C., Horvitz, H. R., Landers, J. E. & Brown, R. H. Mutations in the FUS/TLS gene on chromosome 16 cause familial amyotrophic lateral sclerosis. *Science (80-.).* **323**, 1205–1208 (2009).
156. Vance, C., Rogelj, B., Hortobagyi, T., De Vos, K. J., Nishimura, A. L., Sreedharan, J., Hu, X., Smith, B., Ruddy, D., Wright, P., Ganesalingam, J., Williams, K. L., Tripathi, V., Al-Saraj, S., Al-Chalabi, A., Leigh, P. N., Blair, I. P., Nicholson, G., de Belleroche, J., Gallo, J.-M., Miller, C. C. & Shaw, C. E. Mutations in FUS, an RNA Processing Protein, Cause Familial Amyotrophic Lateral Sclerosis Type 6. *Science (80-.).* **323**, 1208–1211 (2009).
157. Van Langenhove, T., Van Der Zee, J., Sleegers, K., Engelborghs, S., Vandenberghe, R., Gijselinck, I., Van Den Broeck, M., Mattheijssens, M., Peeters, K., De Deyn, P. P., Cruts, M. & Van Broeckhoven, C. Genetic contribution of FUS to frontotemporal lobar degeneration. *Neurology* **74**, 366–371 (2010).
158. Nolan, M., Talbot, K. & Ansorge, O. Pathogenesis of FUS-associated ALS and FTD: insights from rodent models. *Acta Neuropathol. Commun.* **4**, 99 (2016).
159. Tan, A. Y., Riley, T. R., Coady, T., Bussemaker, H. J. & Manley, J. L. TLS/FUS (translocated in liposarcoma/fused in sarcoma) regulates target gene transcription via single-stranded DNA response elements. *Proc. Natl. Acad. Sci. U. S. A.* **109**, 6030–6035 (2012).
160. Lagier-Tourenne, C., Polymenidou, M., Hutt, K. R., Vu, A. Q., Baughn, M., Huelga, S. C., Clutario, K. M., Ling, S. C., Liang, T. Y., Mazur, C., Wancewicz, E., Kim, A. S., Watt, A., Freier, S., Hicks, G. G., Donohue, J. P., Shiue, L., Bennett, C. F., Ravits, J., Cleveland, D. W. & Yeo, G. W. Divergent roles of ALS-linked proteins FUS/TLS and TDP-43 intersect in processing long pre-mRNAs. *Nat. Neurosci.* **15**, 1488–1497 (2012).
161. Wang, W. Y., Pan, L., Su, S. C., Quinn, E. J., Sasaki, M., Jimenez, J. C., MacKenzie, I. R. A., Huang, E. J. & Tsai, L. H. Interaction of FUS and HDAC1 regulates DNA damage response and repair in neurons. *Nat. Neurosci.* **16**, 1383–1391 (2013).

162. Mastrocola, A. S., Kim, S. H., Trinh, A. T., Rodenkirch, L. A. & Tibbetts, R. S. The RNA-binding protein fused in sarcoma (FUS) functions downstream of poly(ADP-ribose) polymerase (PARP) in response to DNA damage. *J. Biol. Chem.* **288**, 24731–24741 (2013).
163. Bosco, D. A., Lemay, N., Ko, H. K., Zhou, H., Burke, C., Kwiatkowski, T. J., Sapp, P., Mckenna-Yasek, D., Brown, R. H. & Hayward, L. J. Mutant FUS proteins that cause amyotrophic lateral sclerosis incorporate into stress granules. *Hum. Mol. Genet.* **19**, 4160–4175 (2010).
164. Vance, C., Scotter, E. L., Nishimura, A. L., Troakes, C., Mitchell, J. C., Kathe, C., Urwin, H., Manser, C., Miller, C. C., Hortobágyi, T., Dragunow, M., Rogelj, B. & Shaw, C. E. ALS mutant FUS disrupts nuclear localization and sequesters wild-type FUS within cytoplasmic stress granules. *Hum. Mol. Genet.* **22**, 2676–2688 (2013).
165. Fuentealba, R. A., Udan, M., Bell, S., Wegorzewska, I., Shao, J., Diamond, M. I., Weihl, C. C. & Baloh, R. H. Interaction with polyglutamine aggregates reveals a Q/N-rich domain in TDP-43. *J. Biol. Chem.* **285**, 26304–26314 (2010).
166. Ayala, Y. M., De Conti, L., Avendaño-Vázquez, S. E., Dhir, A., Romano, M., D'Ambrogio, A., Tollervey, J., Ule, J., Baralle, M., Buratti, E. & Baralle, F. E. TDP-43 regulates its mRNA levels through a negative feedback loop. *EMBO J.* **30**, 277–288 (2011).
167. Buratti, E. & Baralle, F. E. Characterization and Functional Implications of the RNA Binding Properties of Nuclear Factor TDP-43, a Novel Splicing Regulator of CFTR Exon 9. *J. Biol. Chem.* **276**, 36337–36343 (2001).
168. Lagier-Tourenne, C., Polymenidou, M. & Cleveland, D. W. TDP-43 and FUS/TLS: Emerging roles in RNA processing and neurodegeneration. *Hum. Mol. Genet.* **19**, 46–64 (2010).
169. Buratti, E. & Baralle, F. E. TDP-43: Gumming up neurons through protein-protein and protein-RNA interactions. *Trends Biochem. Sci.* **37**, 237–247 (2012).
170. Lukavsky, P. J., Daujotyte, D., Tollervey, J. R., Ule, J., Stuani, C., Buratti, E., Baralle, F. E., Damberger, F. F. & Allain, F. H. T. Molecular basis of UG-rich RNA recognition by the human splicing factor TDP-43. *Nat. Struct. Mol. Biol.* **20**, 1443–1449 (2013).
171. Ratti, A. & Buratti, E. Physiological functions and pathobiology of TDP-43 and FUS/TLS proteins. *J. Neurochem.* **138**, 95–111 (2016).
172. Sreedharan, J., Blair, I. P., Tripathi, V. B., Hu, X., Vance, C., Rogelj, B., Ackerley, S., Durnall, J. C., Williams, K. L., Buratti, E., Baralle, F., de Belleroche, J., Mitchell, J. D., Leigh, P. N., Al-Chalabi, A., Miller, C. C., Nicholson, G. & Shaw, C. E. TDP-43 Mutations in Familial and Sporadic Amyotrophic Lateral Sclerosis. *Science (80-.).* **319**, 1668–1672 (2008).
173. Chen, H. J., Topp, S. D., Hui, H. S., Zacco, E., Katarya, M., McLoughlin, C., King, A., Smith, B. N., Troakes, C., Pastore, A. & Shaw, C. E. RRM adjacent TARDBP mutations disrupt RNA binding and enhance TDP-43 proteinopathy. *Brain* **142**, 3753–3770 (2019).
174. Arai, T., Hasegawa, M., Akiyama, H., Ikeda, K., Nonaka, T., Mori, H., Mann, D., Tsuchiya, K., Yoshida, M., Hashizume, Y. & Oda, T. TDP-43 is a component of ubiquitin-positive tau-negative inclusions in frontotemporal lobar degeneration and amyotrophic lateral sclerosis. *Biochem. Biophys. Res. Commun.* **351**, 602–611 (2006).
175. Feneberg, E., Gray, E., Ansorge, O., Talbot, K. & Turner, M. R. Towards a TDP-43-

Based Biomarker for ALS and FTLD. *Mol. Neurobiol.* 1–13 (2018) doi:10.1007/s12035-018-0947-6.

176. Lee, E. B., Lee, V. M. Y. & Trojanowski, J. Q. Gains or losses: molecular mechanisms of TDP43-mediated neurodegeneration. *Nat. Rev. Neurosci.* **13**, 38–50 (2012).
177. Ling, S. C., Polymenidou, M. & Cleveland, D. W. Converging mechanisms in als and FTD: Disrupted RNA and protein homeostasis. *Neuron* **79**, 416–438 (2013).
178. Brenner, D. & Weishaupt, J. H. Update on amyotrophic lateral sclerosis genetics. *Curr. Opin. Neurol.* **32**, 735–739 (2019).
179. Shahryari, A., Jazi, M. S., Mohammadi, S., Nikoo, H. R., Nazari, Z., Hosseini, E. S., Burtscher, I., Mowla, S. J. & Lickert, H. Development and clinical translation of approved gene therapy products for genetic disorders. *Front. Genet.* **10**, (2019).
180. Van Damme, P., Robberecht, W. & Van Den Bosch, L. Modelling amyotrophic lateral sclerosis: progress and possibilities. *Dis. Model. Mech.* **10**, 537–549 (2017).
181. Jaiswal, M. K. Riluzole and edaravone: A tale of two amyotrophic lateral sclerosis drugs. *Med. Res. Rev.* **39**, 733–748 (2019).
182. Bensimon, G., Lacomblez, L. & Meininger, V. A Controlled Trial of Riluzole in Amyotrophic Lateral Sclerosis. *N. Engl. J. Med.* **330**, 585–591 (1994).
183. Lacomblez, L., Bensimon, G., Leigh, P. N., Guillet, P. & Meininger, V. Dose-ranging study of riluzole in amyotrophic lateral sclerosis. *Lancet* **347**, 1425–1431 (1996).
184. Dharmadasa, T. & Kiernan, M. C. Riluzole, disease stage and survival in ALS. *Lancet Neurol.* **17**, 385–386 (2018).
185. Sala, G., Arosio, A., Conti, E., Beretta, S., Lunetta, C., Riva, N., Ferrarese, C. & Tremolizzo, L. Riluzole selective antioxidant effects in cell models expressing amyotrophic lateral sclerosis endophenotypes. *Clin. Psychopharmacol. Neurosci.* **17**, 438–442 (2019).
186. Fang, T., Al Khleifat, A., Meurgey, J. H., Jones, A., Leigh, P. N., Bensimon, G. & Al-Chalabi, A. Stage at which riluzole treatment prolongs survival in patients with amyotrophic lateral sclerosis: a retrospective analysis of data from a dose-ranging study. *Lancet Neurol.* **17**, 416–422 (2018).
187. Watanabe, K., Tanaka, M., Yuki, S., Hirai, M. & Yamamoto, Y. How is edaravone effective against acute ischemic stroke and amyotrophic lateral sclerosis? *J. Clin. Biochem. Nutr.* **62**, 20–38 (2018).
188. Otomo, E., Tohgi, H., Kogure, K., Hirai, S., Takakura, K., Terashi, A., Gotoh, F., Maruyama, S., Tazaki, Y., Shinohara, Y., Ito, E., Sawada, T., Yamaguchi, T., Kikuchi, H., Kobayashi, S., Fujishima, M. & Nakashima, M. Effect of a novel free radical scavenger, edaravone (MCI-186), on acute brain infarction: Randomized, placebo-controlled, double-blind study at multicenters. *Cerebrovasc. Dis.* **15**, 222–229 (2003).
189. Enomoto, M., Endo, A., Yatsushige, H., Fushimi, K. & Otomo, Y. Clinical effects of early edaravone use in acute ischemic stroke patients treated by endovascular reperfusion therapy. *Stroke* **50**, 652–658 (2019).
190. Lopez-Gonzalez, R., Lu, Y., Gendron, T. F., Karydas, A., Tran, H., Yang, D., Petrucelli, L., Miller, B. L., Almeida, S. & Gao, F. B. Poly(GR) in C9ORF72-Related ALS/FTD Compromises Mitochondrial Function and Increases Oxidative Stress and DNA Damage in iPSC-Derived Motor Neurons. *Neuron* **92**, 383–391 (2016).
191. Romano, N., Catalani, A., Lattante, S., Belardo, A., Proietti, S., Bertini, L., Silvestri, F., Catalani, E., Cervia, D., Zolla, L., Sabatelli, M., Welshhans, K. & Ceci, M. ALS skin

fibroblasts reveal oxidative stress and ERK1/2-mediated cytoplasmic localization of TDP-43. *Cell. Signal.* **70**, 109591 (2020).
192. Barber, S. C. & Shaw, P. J. Oxidative stress in ALS: Key role in motor neuron injury and therapeutic target. *Free Radic. Biol. Med.* **48**, 629–641 (2010).
193. Takei, K., Watanabe, K., Yuki, S., Akimoto, M., Sakata, T. & Palumbo, J. Edaravone and its clinical development for amyotrophic lateral sclerosis. *Amyotroph. Lateral Scler. Front. Degener.* **18**, 5–10 (2017).
194. Rothstein, J. D. Edaravone: A new drug approved for ALS. *Cell* **171**, 725 (2017).
195. Hardiman, O. & van den Berg, L. H. Edaravone: a new treatment for ALS on the horizon? *Lancet Neurol.* **16**, 490–491 (2017).
196. Abe, K., Aoki, M., Tsuji, S., Itoyama, Y., Sobue, G., Togo, M., Hamada, C., Tanaka, M., Akimoto, M., Nakamura, K., Takahashi, F., Kondo, K., Yoshino, H., Abe, K., Aoki, M., Tsuji, S., Itoyama, Y., Sobue, G., Togo, M., Hamada, C., Sasaki, H., Yabe, I., Doi, S., Warita, H., Imai, T., Ito, H., Fukuchi, M., Osumi, E., Wada, M., Nakano, I., Morita, M., Ogata, K., Maruki, Y., Ito, K., Kano, O., Yamazaki, M., Takahashi, Y., Ishiura, H., Ogino, M., Koike, R., Ishida, C., Uchiyama, T., Mizoguchi, K., Obi, T., Watanabe, H., Atsuta, N., Aiba, I., Taniguchi, A., Sawada, H., Hazama, T., Fujimura, H., Kusaka, H., Kunieda, T., Kikuchi, H., Matsuo, H., Ueyama, H., Uekawa, K., Tanaka, M., Akimoto, M., Ueda, M., Murakami, A., Sumii, R., Kudou, T., Nakamura, K., Morimoto, K., Yoneoka, T., Hirai, M., Sasaki, K., Terai, H., Natori, T., Matsui, H., Kotani, K., Yoshida, K., Iwasaki, T., Takahashi, F., Kondo, K. & Yoshino, H. Safety and efficacy of edaravone in well defined patients with amyotrophic lateral sclerosis: a randomised, double-blind, placebo-controlled trial. *Lancet Neurol.* **16**, 505–512 (2017).
197. Beghi, E., Chiò, A., Couratier, P., Esteban, J., Hardiman, O., Logroscino, G., Millul, A., Mitchell, D., Preux, P. M., Pupillo, E., Stevic, Z., Swingler, R., Traynor, B. J., Van Den Berg, L. H., Veldink, J. H. & Zoccolella, S. The epidemiology and treatment of ALS: Focus on the heterogeneity of the disease and critical appraisal of therapeutic trials. *Amyotroph. Lateral Scler.* **12**, 1–10 (2011).
198. Blokhuis, A. M., Groen, E. J. N., Koppers, M., Van Den Berg, L. H. & Pasterkamp, R. J. Protein aggregation in amyotrophic lateral sclerosis. *Acta Neuropathol.* **125**, 777–794 (2013).
199. Zheng-Hong, Q. *Autophagy: biology and diseases*. *Advances in Experimental Medicine and Biology* vol. 1206 (2019).
200. Darios, F. & Stevanin, G. Impairment of Lysosome Function and Autophagy in Rare Neurodegenerative Diseases. *J. Mol. Biol.* **432**, 2714–2734 (2020).
201. Rudnick, N. D., Griffey, C. J., Guarnieri, P., Gerbino, V., Wang, X., Piersaint, J. A., Tapia, J. C., Rich, M. M. & Maniatis, T. Distinct roles for motor neuron autophagy early and late in the SOD1G93A mouse model of ALS. *Proc. Natl. Acad. Sci. U. S. A.* **114**, E8294–E8303 (2017).
202. Morimoto, N., Nagai, M., Ohta, Y., Miyazaki, K., Kurata, T., Morimoto, M., Murakami, T., Takehisa, Y., Ikeda, Y., Kamiya, T. & Abe, K. Increased autophagy in transgenic mice with a G93A mutant SOD1 gene. *Brain Res.* **1167**, 112–117 (2007).
203. Bandyopadhyay, U., Nagy, M., Fenton, W. A. & Horwich, A. L. Absence of lipofuscin in motor neurons of SOD1-linked ALS mice. *Proc. Natl. Acad. Sci. U. S. A.* **111**, 11055–11060 (2014).
204. Chen, Y., Liu, H., Guan, Y., Wang, Q., Zhou, F., Jie, L., Ju, J., Pu, L., Du, H. & Wang, X.

The altered autophagy mediated by TFEB in animal and cell models of amyotrophic lateral sclerosis. *Am. J. Transl. Res.* **7**, 1574–1587 (2015).

205. Nassif, M., Valenzuela, V., Rojas-Rivera, D., Vidal, R., Matus, S., Castillo, K., Fuentealba, Y., Kroemer, G., Levine, B. & Hetz, C. Pathogenic role of BECN1/Beclin 1 in the development of amyotrophic lateral sclerosis. *Autophagy* **10**, 1256–1271 (2014).
206. Hsueh, K. W., Chiou, T. W., Chiang, S. F., Yamashita, T., Abe, K., Borlongan, C. V., Sanberg, P. R., Huang, A. H., Lin, S. Z. & Harn, H. J. Autophagic down-regulation in motor neurons remarkably prolongs the survival of ALS mice. *Neuropharmacology* **108**, 152–160 (2016).
207. Xie, Y., Zhou, B., Lin, M. Y., Wang, S., Foust, K. D. & Sheng, Z. H. Endolysosomal Deficits Augment Mitochondria Pathology in Spinal Motor Neurons of Asymptomatic fALS Mice. *Neuron* **87**, 355–371 (2015).
208. Xie, Y., Zhou, B., Lin, M. Y. & Sheng, Z. H. Progressive endolysosomal deficits impair autophagic clearance beginning at early asymptomatic stages in FALS mice. *Autophagy* **11**, 1934–1936 (2015).
209. Bilsland, L. G., Sahai, E., Kelly, G., Golding, M., Greensmith, L. & Schiavo, G. Deficits in axonal transport precede ALS symptoms in vivo. *Proc. Natl. Acad. Sci. U. S. A.* **107**, 20523–20528 (2010).
210. Henriques, A., Blasco, H., Fleury, M. C., Corcia, P., Echaniz-Laguna, A., Robelin, L., Rudolf, G., Lequeu, T., Bergaentzle, M., Gachet, C., Pradat, P. F., Marchioni, E., Andres, C. R., Tranchant, C., De Aguilar, J. L. G. & Loeffler, J. P. Blood cell palmitoleate-palmitate ratio is an independent prognostic factor for amyotrophic lateral sclerosis. *PLoS One* **10**, 1–14 (2015).
211. Dodge, J. C. Lipid Involvement in Neurodegenerative Diseases of the Motor System: Insights from Lysosomal Storage Diseases. *Front. Mol. Neurosci.* **10**, 1–14 (2017).
212. Tracey, T. J., Steyn, F. J., Wolvetang, E. J. & Ngo, S. T. Neuronal Lipid Metabolism: Multiple Pathways Driving Functional Outcomes in Health and Disease. *Front. Mol. Neurosci.* **11**, 10 (2018).
213. Tracey, T. J., Kirk, S. E., Steyn, F. J. & Ngo, S. T. The role of lipids in the central nervous system and their pathological implications in amyotrophic lateral sclerosis. *Semin. Cell Dev. Biol.* (2020) doi:10.1016/j.semcdb.2020.08.012.
214. Dodge, J. C., Treleaven, C. M., Pacheco, J., Cooper, S., Bao, C., Abraham, M., Cromwell, M., Sardi, S. P., Chuang, W.-L., Sidman, R. L., Cheng, S. H. & Shihabuddin, L. S. Glycosphingolipids are modulators of disease pathogenesis in amyotrophic lateral sclerosis. *Proc. Natl. Acad. Sci.* **1**, 201508767 (2015).
215. Henriques, A., Croixmarie, V., Priestman, D. A., Rosenbohm, A., Dirrig-Grosch, S., D'Ambra, E., Huebecker, M., Hussain, G., Boursier-Neyret, C., Echaniz-Laguna, A., Ludolph, A. C., Platt, F. M., Walther, B., Spedding, M., Loeffler, J. P. & De Aguilar, J. L. G. Amyotrophic lateral sclerosis and denervation alter sphingolipids and up-regulate glucosylceramide synthase. *Hum. Mol. Genet.* **24**, 7390–7405 (2015).
216. Henriques, A., Huebecker, M., Blasco, H., Keime, C., Andres, C. R., Corcia, P., Priestman, D. A., Platt, F. M., Spedding, M. & Loeffler, J.-P. Inhibition of β-Glucocerebrosidase Activity Preserves Motor Unit Integrity in a Mouse Model of Amyotrophic Lateral Sclerosis. *Sci. Rep.* **7**, 5235 (2017).
217. Henriques, A., Croixmarie, V., Bouscary, A., Mosbach, A., Keime, C., Boursier-

Neyret, C., Walter, B., Spedding, M. & Loeffler, J.-P. Sphingolipid Metabolism Is Dysregulated at Transcriptomic and Metabolic Levels in the Spinal Cord of an Animal Model of Amyotrophic Lateral Sclerosis. *Front. Mol. Neurosci.* **10**, 1–14 (2018).

218. Bouscary, A., Quessada, C., Mosbach, A., Callizot, N., Spedding, M., Loeffler-Philippe, J. & Henriques, A. Ambroxol Hydrochloride Improves Motor Functions and Extends Survival in a Mouse Model of Familial Amyotrophic Lateral Sclerosis. *Front. Pharmacol.* **10**, 1–9 (2019).
219. Petit, C. S., Lee, J. J., Boland, S., Swarup, S., Christiano, R., Lai, Z. W., Mejhert, N., Elliott, S. D., McFall, D., Haque, S., Huang, E. J., Bronson, R. T., Harper, J. W., Farese, R. V. & Walther, T. C. Inhibition of sphingolipid synthesis improves outcomes and survival in GARP mutant wobbler mice, a model of motor neuron degeneration. *Proc. Natl. Acad. Sci.* 1–10 (2020) doi:10.1073/PNAS.1913956117.
220. Blasco, H., Veyrat-Durebex, C., Bocca, C., Patin, F., Vourc'H, P., Kouassi Nzoughet, J., Lenaers, G., Andres, C. R., Simard, G., Corcia, P. & Reynier, P. Lipidomics Reveals Cerebrospinal-Fluid Signatures of ALS. *Sci. Rep.* **7**, 1–10 (2017).
221. Ohshima, T., Murray, G. J., Swaim, W. D., Longenecker, G., Quirk, J. M., Cardarelli, C. O., Sugimoto, Y., Pastan, I., Gottesman, M. M., Brady, R. O. & Kulkarni, A. B. α-Galactosidase A deficient mice: A model of fabry disease. *Proc. Natl. Acad. Sci. U. S. A.* **94**, 2540–2544 (1997).
222. Bowerman, M., Salsac, C., Coque, E., Eiselt, É., Deschaumes, R. G., Brodovitch, A., Burkly, L. C., Scamps, F. & Raoul, C. Tweak regulates astrogliosis, microgliosis and skeletal muscle atrophy in a mouse model of amyotrophic lateral sclerosis. *Hum. Mol. Genet.* **24**, 3440–3456 (2015).
223. Ripps, M. E., Huntley, G. W., Hof, P. R., Morrison, J. H. & Gordon, J. W. Transgenic mice expressing an altered murine superoxide dismutase gene provide an animal model of amyotrophic lateral sclerosis. *Proc. Natl. Acad. Sci. U. S. A.* **92**, 689–693 (1995).
224. Rouaux, C., Panteleeva, I., René, F., De Aguilar, J. L. G., Echaniz-Laguna, A., Dupuis, L., Menger, Y., Boutillier, A. L. & Loeffler, J. P. Sodium valproate exerts neuroprotective effects in vivo through CREB-binding protein-dependent mechanisms but does not improve survival in an amyotrophic lateral sclerosis mouse model. *J. Neurosci.* **27**, 5535–5545 (2007).
225. Halter, B., Gonzalez de Aguilar, J. L., Rene, F., Petri, S., Fricker, B., Echaniz-Laguna, A., Dupuis, L., Larmet, Y. & Loeffler, J. P. Oxidative stress in skeletal muscle stimulates early expression of Rad in a mouse model of amyotrophic lateral sclerosis. *Free Radic. Biol. Med.* **48**, 915–923 (2010).
226. Alexander, G. M., Erwin, K. L., Byers, N., Deitch, J. S., Augelli, B. J., Blankenhorn, E. P. & Heiman-Patterson, T. D. Effect of transgene copy number on survival in the G93A SOD1 transgenic mouse model of ALS. *Mol. Brain Res.* **130**, 7–15 (2004).
227. Gordon, D., Dafinca, R., Scaber, J., Alegre-Abarrategui, J., Farrimond, L., Scott, C., Biggs, D., Kent, L., Oliver, P. L., Davies, B., Ansorge, O., Wade-Martins, R. & Talbot, K. Single-copy expression of an amyotrophic lateral sclerosis-linked TDP-43 mutation (M337V) in BAC transgenic mice leads to altered stress granule dynamics and progressive motor dysfunction. *Neurobiol. Dis.* **121**, 148–162 (2018).
228. Mutihac, R., Alegre-Abarrategui, J., Gordon, D., Farrimond, L., Yamasaki-Mann, M., Talbot, K. & Wade-Martins, R. TARDBP pathogenic mutations increase cytoplasmic

translocation of TDP-43 and cause reduction of endoplasmic reticulum Ca2+signaling in motor neurons. *Neurobiol. Dis.* **75**, 64–77 (2015).
229. Chen, C. mun, Krohn, J., Bhattacharya, S. & Davies, B. A comparison of exogenous promoter activity at the ROSA26 locus using a PhiC31 integrase mediated cassette exchange approach in mouse es cells. *PLoS One* **6**, 6–13 (2011).
230. Sango, K., Yamanaka, S., Hoffmann, A., Okuda, Y., Grinberg, A., Westphal, H., McDonald, M. P., Crawley, J. N., Sandhoff, K., Suzuki, K. & Proia, R. L. Mouse models of Tay–Sachs and Sandhoff diseases differ in neurologic phenotype and ganglioside metabolism. *Nat. Genet.* **11**, 170–176 (1995).
231. Smith, P. K., Krohn, R. I., Hermanson, G. T., Mallia, A. K., Gartner, F. H., Provenzano, M. D., Fujimoto, E. K., Goeke, N. M., Olson, B. J. & Klenk, D. C. Measurement of protein using bicinchoninic acid. *Anal. Biochem.* **150**, 76–85 (1985).
232. Neville, D. C. A., Coquard, V., Priestman, D. A., Te Vruchte, D. J. M., Sillence, D. J., Dwek, R. A., Platt, F. M. & Butters, T. D. Analysis of fluorescently labeled glycosphingolipid-derived oligosaccharides following ceramide glycanase digestion and anthranilic acid labeling. *Anal. Biochem.* **331**, 275–282 (2004).
233. Abdul-Hammed, M., Breiden, B., Schwarzmann, G. & Sandhoff, K. Lipids regulate the hydrolysis of membrane bound glucosylceramide by lysosomal β-glucocerebrosidase GBA1. *J. Lipid Res.* **58**, jlr.M073510 (2017).
234. Oninla, V. O., Breiden, B., Babalola, J. O. & Sandhoff, K. Acid sphingomyelinase activity is regulated by membrane lipids and facilitates cholesterol transfer by NPC2. *J. Lipid Res.* **55**, 2606–2619 (2014).
235. MacDonald, R. C., MacDonald, R. I., Menco, B. P. M., Takeshita, K., Subbarao, N. K. & Hu, L. rong. Small-volume extrusion apparatus for preparation of large, unilamellar vesicles. *BBA - Biomembr.* **1061**, 297–303 (1991).
236. Huebecker, M., Moloney, E. B., Van Der Spoel, A. C., Priestman, D. A., Isacson, O., Hallett, P. J. & Platt, F. M. Reduced sphingolipid hydrolase activities, substrate accumulation and ganglioside decline in Parkinson's disease. *Mol. Neurodegener.* **14**, 1–21 (2019).
237. Ridley, C. M., Thur, K. E., Shanahan, J., Thillaiappan, N. B., Shen, A., Uhl, K., Walden, C. M., Rahim, A. A., Waddington, S. N., Platt, F. M. & Van Der Spoel, A. C. β-Glucosidase 2 (GBA2) activity and imino sugar pharmacology. *J. Biol. Chem.* **288**, 26052–26066 (2013).
238. Kirkegaard, T., Gray, J., Priestman, D. A., Wallom, K., Atkins, J., Olsen, O. D., Klein, A., Drndarski, S., Petersen, N. H. T., Ingemann, L., Smith, D. A., Morris, L., Bornæs, C., Jørgensen, S. H., Williams, I., Hinsby, A., Arenz, C., Begley, D., Jäättelä, M. & Platt, F. M. Heat shock protein–based therapy as a potential candidate for treating the sphingolipidoses. *Sci. Transl. Med.* **8**, (2016).
239. Jeyakumar, M., Smith, D., Eliott-Smith, E., Cortina-Borja, M., Reinkensmeier, G., Butters, T. D., Lemm, T., Sandhoff, K., Perry, V. H., Dwek, R. A. & Platt, F. M. An inducible mouse model of late onset Tay-Sachs disease. *Neurobiol. Dis.* **10**, 201–210 (2002).
240. Jeyakumar, M., Butters, T. D., Cortina-Borja, M., Hunnam, V., Proia, R. L., Perry, V. H., Dwek, R. a & Platt, F. M. Delayed symptom onset and increased life expectancy in Sandhoff disease mice treated with N-butyldeoxynojirimycin. *Proc. Natl. Acad. Sci. U. S. A.* **96**, 6388–93 (1999).
241. Futerman, A. H. & Pagano, R. E. Determination of the intracellular sites and

topology of glucosylceramide synthesis in rat liver. *Biochem. J.* **280**, 295–302 (1991).
242. Boer, D. E. C., van Smeden, J., Bouwstra, J. A. & Aerts, J. M. F. . Glucocerebrosidase: Functions in and Beyond the Lysosome. *J. Clin. Med.* **9**, 736 (2020).
243. Van Meer, G., Wolthoorn, J. & Degroote, S. The fate and function of glycosphingolipid glucosylceramide. *Philos. Trans. R. Soc. B Biol. Sci.* **358**, 869–873 (2003).
244. Vaccaro, A. M., Tatti, M., Ciaffoni, F., Salvioli, R., Barca, A. & Scerch, C. Effect of saposins A and C on the enzymatic hydrolysis of liposomal glucosylceramide. *J. Biol. Chem.* **272**, 16862–16867 (1997).
245. Alattia, J.-R., Shaw, J. E., Yip, C. M. & Privé, G. G. Molecular imaging of membrane interfaces reveals mode of beta-glucosidase activation by saposin C. *Proc. Natl. Acad. Sci. U. S. A.* **104**, 17394–9 (2007).
246. Tamargo, R. J., Velayati, A., Goldin, E. & Sidransky, E. The role of saposin C in Gaucher disease. *Mol. Genet. Metab.* **106**, 257–263 (2012).
247. Jennemann, R., Sandhoff, R., Wang, S., Kiss, E., Gretz, N., Zuliani, C., Martin-Villalba, A., Jäger, R., Schorle, H., Kenzelmann, M., Bonrouhi, M., Wiegandt, H. & Gröne, H.-J. Cell-specific deletion of glucosylceramide synthase in brain leads to severe neural defects after birth. *Proc. Natl. Acad. Sci. U. S. A.* **102**, 12459–64 (2005).
248. Platt, F. M., Reinkensmeier, G., Dwek, R. A. & Butters, T. D. Extensive glycosphingolipid depletion in the liver and lymphoid organs of mice treated with N-butyldeoxynojirimycin. *J. Biol. Chem.* **272**, 19365–19372 (1997).
249. Hallett, P. J., Huebecker, M., Brekk, O. R., Moloney, E. B., Rocha, E. M., Priestman, D. A., Platt, F. M. & Isacson, O. Glycosphingolipid levels and glucocerebrosidase activity are altered in normal aging of the mouse brain. *Neurobiol. Aging* **67**, 189–200 (2018).
250. Pozzilli, V., Giona, F., Ceccanti, M., Cambieri, C., Frasca, V., Onesti, E., Libonati, L., Di Bari, S., Fiorini, I., Cardarelli, L., Santopietro, M. & Inghilleri, M. A case of motor neuron involvement in Gaucher disease. *Mol. Genet. Metab. Reports* **21**, 100540 (2019).
251. Schmitt, F., Hussain, G., Dupuis, L., Loeffler, J.-P. & Henriques, A. A plural role for lipids in motor neuron diseases: energy, signaling and structure. *Front. Cell. Neurosci.* **8**, 25 (2014).
252. Alessenko, A. V. & Albi, E. Exploring Sphingolipid Implications in Neurodegeneration. *Front. Neurol.* **11**, 1–13 (2020).
253. Ito, M. & Yamagata, T. Purification and characterization of glycosphingolipid-specific endoglycosidases (endoglycoceramidases) from a mutant strain of Rhodococcus sp. Evidence for three molecular species of endoglycoceramidase with different specificities. *J. Biol. Chem.* **264**, 9510–9519 (1989).
254. Dvir, H., Harel, M., McCarthy, A. A., Toker, L., Silman, I., Futerman, A. H. & Sussman, J. L. X-ray structure of human acid-β-glucosidase, the defective enzyme in Gaucher disease. *EMBO Rep.* **4**, 704–709 (2003).
255. Anugraham, M., Everest-Dass, A. V., Jacob, F. & Packer, N. H. A platform for the structural characterization of glycans enzymatically released from glycosphingolipids extracted from tissue and cells. *Rapid Commun. Mass Spectrom.* **29**, 545–561 (2015).

256. Karlsson, H., Halim, A. & Teneberg, S. Differentiation of glycosphingolipid-derived glycan structural isomers by liquid chromatography/mass spectrometry. *Glycobiology* **20**, 1103–1116 (2010).
257. Palamiuc, L., Schlagowski, A., Ngo, S. T., Vernay, A., Dirrig-Grosch, S., Henriques, A., Boutillier, A., Zoll, J., Echaniz-Laguna, A., Loeffler, J. & René, F. A metabolic switch toward lipid use in glycolytic muscle is an early pathologic event in a mouse model of amyotrophic lateral sclerosis. *EMBO Mol. Med.* **7**, 526–546 (2015).
258. Desseille, C., Deforges, S., Biondi, O., Houdebine, L., D'amico, D., Lamazière, A., Caradeuc, C., Bertho, G., Bruneteau, G., Weill, L., Bastin, J., Djouadi, F., Salachas, F., Lopes, P., Chanoine, C., Massaad, C. & Charbonnier, F. Specific Physical Exercise Improves Energetic Metabolism in the Skeletal Muscle of Amyotrophic-Lateral-Sclerosis Mice. *Front. Mol. Neurosci.* **10**, 1–17 (2017).
259. Hegedus, J., Putman, C. T., Tyreman, N. & Gordon, T. Preferential motor unit loss in the SOD1 ^{G93A} transgenic mouse model of amyotrophic lateral sclerosis. *J. Physiol.* **586**, 3337–3351 (2008).
260. Vinsant, S., Mansfield, C., Jimenez-Moreno, R., Moore, V. D. G., Yoshikawa, M., Hampton, T. G., Prevette, D., Caress, J., Oppenheim, R. W. & Milligan, C. Characterization of early pathogenesis in the SOD1G93A mouse model of ALS: Part I, background and methods. *Brain Behav.* **3**, 335–350 (2013).
261. Vinsant, S., Mansfield, C., Jimenez-Moreno, R., Moore, V. D. G., Yoshikawa, M., Hampton, T. G., Prevette, D., Caress, J., Oppenheim, R. W. & Milligan, C. Characterization of early pathogenesis in the SOD1G93A mouse model of ALS: Part II, results and discussion. *Brain Behav.* **3**, 431–457 (2013).
262. Cohen, T. J., Hwang, A. W., Restrepo, C. R., Yuan, C. X., Trojanowski, J. Q. & Lee, V. M. Y. An acetylation switch controls TDP-43 function and aggregation propensity. *Nat. Commun.* **6**, (2015).
263. Cohen, T. J., Lee, V. M. Y. & Trojanowski, J. Q. TDP-43 functions and pathogenic mechanisms implicated in TDP-43 proteinopathies. *Trends Mol. Med.* **17**, 659–667 (2011).
264. Mackenzie, I. R. A., Bigio, E. H., Ince, P. G., Geser, F., Neumann, M., Cairns, N. J., Kwong, L. K., Forman, M. S., Ravits, J., Stewart, H., Eisen, A., McClusky, L., Kretzschmar, H. A., Monoranu, C. M., Highley, J. R., Kirby, J., Siddique, T., Shaw, P. J., Lee, V. M. Y. & Trojanowski, J. Q. Pathological TDP-43 distinguishes sporadic amyotrophic lateral sclerosis from amyotrophic lateral sclerosis with SOD1 mutations. *Ann. Neurol.* **61**, 427–434 (2007).
265. Robertson, J., Sanelli, T., Xiao, S., Yang, W., Horne, P., Hammond, R., Pioro, E. P. & Strong, M. J. Lack of TDP-43 abnormalities in mutant SOD1 transgenic mice shows disparity with ALS. *Neurosci. Lett.* **420**, 128–132 (2007).
266. Turner, B. J., Bäumer, D., Parkinson, N. J., Scaber, J., Ansorge, O. & Talbot, K. TDP-43 expression in mouse models of amyotrophic lateral sclerosis and spinal muscular atrophy. *BMC Neurosci.* **9**, 1–11 (2008).
267. Jeon, G. S., Shim, Y. M., Lee, D. Y., Kim, J. S., Kang, M. J., Ahn, S. H., Shin, J. Y., Geum, D., Hong, Y. H. & Sung, J. J. Pathological Modification of TDP-43 in Amyotrophic Lateral Sclerosis with SOD1 Mutations. *Mol. Neurobiol.* **56**, 2007–2021 (2019).
268. Kraemer, B. C., Schuck, T., Wheeler, J. M., Robinson, L. C., Trojanowski, J. Q., Lee, V. M. Y. & Schellenberg, G. D. Loss of Murine TDP-43 disrupts motor function and

plays an essential role in embryogenesis. *Acta Neuropathol.* **119**, 409–419 (2010).
269. Sephton, C. F., Good, S. K., Atkin, S., Dewey, C. M., Mayer, P., Herz, J. & Yu, G. TDP-43 is a developmentally regulated protein essential for early embryonic development. *J. Biol. Chem.* **285**, 6826–6834 (2010).
270. Wu, L. S., Cheng, W., Hou, S. C., Yan, Y. T., Jiang, S. T. & Shen, C. K. J. TDP-43, a neuro-pathosignature factor, is essential for early mouse embryogenesis. *Genesis* **48**, 56–62 (2010).
271. Nonaka, T., Kametani, F., Arai, T., Akiyama, H. & Hasegawa, M. Truncation and pathogenic mutations facilitate the formation of intracellular aggregates of TDP-43. *Hum. Mol. Genet.* **18**, 3353–3364 (2009).
272. Kabashi, E., Lin, L., Tradewell, M. L., Dion, P. A., Bercier, V., Bourgouin, P., Rochefort, D., Bel Hadj, S., Durham, H. D., Velde, C. Vande, Rouleau, G. A. & Drapeau, P. Gain and loss of function of ALS-related mutations of TARDBP (TDP-43) cause motor deficits in vivo. *Hum. Mol. Genet.* **19**, 671–683 (2009).
273. Igaz, L. M., Kwong, L. K., Chen-Plotkin, A., Winton, M. J., Unger, T. L., Xu, Y., Neumann, M., Trojanowski, J. Q. & Lee, V. M. Y. Expression of TDP-43 C-terminal fragments in vitro recapitulates pathological features of TDP-43 proteinopathies. *J. Biol. Chem.* **284**, 8516–8524 (2009).
274. Wegorzewska, I., Bell, S., Cairns, N. J., Miller, T. M. & Baloh, R. H. TDP-43 mutant transgenic mice develop features of ALS and frontotemporal lobar degeneration. *Proc. Natl. Acad. Sci. U. S. A.* **106**, 18809–18814 (2009).
275. Shan, X., Chiang, P. M., Price, D. L. & Wong, P. C. Altered distributions of Gemini of coiled bodies and mitochondria in motor neurons of TDP-43 transgenic mice. *Proc. Natl. Acad. Sci. U. S. A.* **107**, 16325–16330 (2010).
276. Stallings, N. R., Puttaparthi, K., Luther, C. M., Burns, D. K. & Elliott, J. L. Progressive motor weakness in transgenic mice expressing human TDP-43. *Neurobiol. Dis.* **40**, 404–414 (2010).
277. Tsai, K. J., Yang, C. H., Fang, Y. H., Cho, K. H., Chien, W. L., Wang, W. T., Wu, T. W., Lin, C. P., Fu, W. M. & Shen, C. K. J. Elevated expression of TDP-43 in the forebrain of mice is sufficient to cause neurological and pathological phenotypes mimicking FTLD-U. *J. Exp. Med.* **207**, 1661–1673 (2010).
278. Wils, H., Kleinberger, G., Janssens, J., Pereson, S., Joris, G., Cuijt, I., Smits, V., Ceuterick-De Groote, C., Van Broeckhoven, C. & Kumar-Singh, S. TDP-43 transgenic mice develop spastic paralysis and neuronal inclusions characteristic of ALS and frontotemporal lobar degeneration. *Proc. Natl. Acad. Sci. U. S. A.* **107**, 3858–3863 (2010).
279. Xu, Y. F., Gendron, T. F., Zhang, Y. J., Lin, W. L., D'Alton, S., Sheng, H., Casey, M. C., Tong, J., Knight, J., Yu, X., Rademakers, R., Boylan, K., Hutton, M., McGowan, E., Dickson, D. W., Lewis, J. & Petrucelli, L. Wild-type human TDP-43 expression causes TDP-43 phosphorylation, mitochondrial aggregation, motor deficits, and early mortality in transgenic mice. *J. Neurosci.* **30**, 10851–10859 (2010).
280. Xu, Y.-F., Zhang, Y.-J., Lin, W.-L., Cao, X., Stetler, C., Dickson, D. W., Lewis, J. & Petrucelli, L. Expression of mutant TDP-43 induces neuronal dysfunction in transgenic mice. *Mol. Neurodegener.* **6**, 73 (2011).
281. Schwenk, B. M., Hartmann, H., Serdaroglu, A., Schludi, M. H., Hornburg, D., Meissner, F., Orozco, D., Colombo, A., Tahirovic, S., Michaelsen, M., Schreiber, F., Haupt, S., Peitz, M., Brüstle, O., Küpper, C., Klopstock, T., Otto, M., Ludolph, A. C.,

Arzberger, T., Kuhn, P. & Edbauer, D. TDP-43 loss of function inhibits endosomal trafficking and alters trophic signaling in neurons. *EMBO J.* **35**, 2350–2370 (2016).
282. Sleigh, J. N., Tosolini, A. P., Gordon, D., Devoy, A., Fratta, P., Fisher, E. M. C., Talbot, K. & Schiavo, G. Mice Carrying ALS Mutant TDP-43, but Not Mutant FUS, Display In Vivo Defects in Axonal Transport of Signaling Endosomes. *Cell Rep.* **30**, 3655-3662.e2 (2020).
283. Xia, Q., Wang, H., Hao, Z., Fu, C., Hu, Q., Gao, F., Ren, H., Chen, D., Han, J., Ying, Z. & Wang, G. TDP-43 loss of function increases TFEB activity and blocks autophagosome–lysosome fusion. *EMBO J.* **35**, 121–142 (2016).
284. Ying, Z., Xia, Q., Hao, Z., Xu, D., Wang, M., Wang, H. & Wang, G. TARDBP/TDP-43 regulates autophagy in both MTORC1-dependent and MTORC1-independent manners. *Autophagy* **12**, 707–708 (2016).
285. Leibiger, C., Deisel, J., Aufschnaiter, A., Ambros, S., Tereshchenko, M., Verheijen, B. M., Büttner, S. & Braun, R. J. TDP-43 controls lysosomal pathways thereby determining its own clearance and cytotoxicity. *Hum. Mol. Genet.* **27**, 1593–1607 (2018).
286. Leibiger, C., Deisel, J., Aufschnaiter, A., Ambros, S., Tereshchenko, M., Verheijen, B. M., Buettner, S. & Braun, R. J. Endolysosomal pathway activity protects cells from neurotoxic TDP-43. *Microb. Cell* **5**, 212–214 (2018).
287. Tedeschi, Petrozziello & Secondo. Calcium Dyshomeostasis and Lysosomal Ca2+ Dysfunction in Amyotrophic Lateral Sclerosis. *Cells* **8**, 1216 (2019).
288. Burk, K. & Pasterkamp, R. J. Disrupted neuronal trafficking in amyotrophic lateral sclerosis. *Acta Neuropathol.* **137**, 859–877 (2019).
289. Dardis, A., Zampieri, S., Canterini, S., Newell, K. L., Stuani, C., Murrell, J. R., Ghetti, B., Fiorenza, M. T., Bembi, B. & Buratti, E. Altered localization and functionality of TAR DNA binding protein 43 (TDP-43) in niemann-pick disease type C. *Acta Neuropathol. Commun.* **4**, 1–13 (2016).
290. Beers, D. R. & Appel, S. H. Immune dysregulation in amyotrophic lateral sclerosis: mechanisms and emerging therapies. *Lancet Neurol.* **18**, 211–220 (2019).
291. Ito, H., Wate, R., Zhang, J., Ohnishi, S., Kaneko, S., Ito, H., Nakano, S. & Kusaka, H. Treatment with edaravone, initiated at symptom onset, slows motor decline and decreases SOD1 deposition in ALS mice. *Exp. Neurol.* **213**, 448–455 (2008).
292. Aoki, M., Warita, H., Mizuno, H., Suzuki, N., Yuki, S. & Itoyama, Y. Feasibility study for functional test battery of SOD transgenic rat (H46R) and evaluation of edaravone, a free radical scavenger. *Brain Res.* **1382**, 321–325 (2011).
293. Ikeda, K. & Iwasaki, Y. Edaravone, a free radical scavenger, delayed symptomatic and pathological progression of motor neuron disease in the wobbler mouse. *PLoS One* **10**, 1–11 (2015).
294. Ohta, Y., Nomura, E., Shang, J., Feng, T., Huang, Y., Liu, X., Shi, X., Nakano, Y., Hishikawa, N., Sato, K., Takemoto, M., Yamashita, T. & Abe, K. Enhanced oxidative stress and the treatment by edaravone in mice model of amyotrophic lateral sclerosis. *J. Neurosci. Res.* **97**, 607–619 (2019).
295. Mora, J. S. Edaravone for treatment of early-stage ALS. *Lancet Neurol.* **16**, 772 (2017).
296. Bozzo, F., Mirra, A. & Carrì, M. T. Oxidative stress and mitochondrial damage in the pathogenesis of ALS: New perspectives. *Neurosci. Lett.* **636**, 3–8 (2017).
297. Vandoorne, T., De Bock, K. & Van Den Bosch, L. Energy metabolism in ALS: an

underappreciated opportunity? *Acta Neuropathol.* **135**, 489–509 (2018).
298. Colombrita, C., Zennaro, E., Fallini, C., Weber, M., Sommacal, A., Buratti, E., Silani, V. & Ratti, A. TDP-43 is recruited to stress granules in conditions of oxidative insult. *J. Neurochem.* **111**, 1051–1061 (2009).
299. Li, Y. R., King, O. D., Shorter, J. & Gitler, A. D. Stress granules as crucibles of ALS pathogenesis. *J. Cell Biol.* **201**, 361–372 (2013).
300. Parker, S. J., Meyerowitz, J., James, J. L., Liddell, J. R., Crouch, P. J., Kanninen, K. M. & White, A. R. Endogenous TDP-43 localized to stress granules can subsequently form protein aggregates. *Neurochem. Int.* **60**, 415–424 (2012).
301. Chen, Y. & Cohen, T. J. Aggregation of the nucleic acid– binding protein TDP-43 occurs via distinct routes that are coordinated with stress granule formation. *J. Biol. Chem.* **294**, 3696–3706 (2019).
302. Fang, M. Y., Markmiller, S., Vu, A. Q., Javaherian, A., Dowdle, W. E., Jolivet, P., Bushway, P. J., Castello, N. A., Baral, A., Chan, M. Y., Linsley, J. W., Linsley, D., Mercola, M., Finkbeiner, S., Lecuyer, E., Lewcock, J. W. & Yeo, G. W. Small-Molecule Modulation of TDP-43 Recruitment to Stress Granules Prevents Persistent TDP-43 Accumulation in ALS/FTD. *Neuron* **103**, 802-819.e11 (2019).
303. Williamson, M. G., Finelli, M. J., Sleigh, J. N., Reddington, A., Gordon, D., Talbot, K., Davies, K. E. & Oliver, P. L. Neuronal over-expression of Oxr1 is protective against ALS-associated mutant TDP-43 mislocalisation in motor neurons and neuromuscular defects in vivo. *Hum. Mol. Genet.* **28**, 3584–3599 (2019).
304. Drory, V. E., Birnbaum, M., Peleg, L., Goldman, B. & Korczyn, A. D. Hexosaminidase a deficiency is an uncommon cause of a syndrome mimicking amyotrophic lateral sclerosis. *Muscle and Nerve* **28**, 109–112 (2003).
305. Khoueiry, M., Malek, E. & Salameh, J. S. Adult onset Sandhoff disease: a rare mimicker of amyotrophic lateral sclerosis. *Amyotroph. Lateral Scler. Front. Degener.* **21**, 144–146 (2020).
306. Kaya, E., Smith, D. A., Smith, C., Boland, B., Strupp, M. & Platt, F. M. Beneficial Effects of Acetyl-DL-Leucine (ADLL) in a Mouse Model of Sandhoff Disease. *J. Clin. Med.* **9**, 1050 (2020).
307. Lawson, C. & Martin, D. Animal models of GM2 gangliosidosis: utility and limitations. *Appl. Clin. Genet.* **Volume 9**, 111–120 (2016).
308. Phaneuf, D., Wakamatsu, N., Huang, J. Q., Borowski, A., Peterson, A. C., Fortunato, S. R., Ritter, G., Igdoura, S. A., Morales, C. R., Benoit, G., Akerman, B. R., Leclerc, D., Hanai, N., Marth, J. D., Trasler, J. M. & Gravel, R. A. Dramatically different phenotypes in mouse models of human Tay-Sachs and Sandhoff diseases. *Hum. Mol. Genet.* **5**, 1–14 (1996).
309. Liu, Y., Hoffmann, A., Grinberg, A., Westphal, H., Mcdonald, M. P., Miller, K. M., Crawley, J. N., Sandhoff, K., Suzuki, K. & Proia, R. L. Mouse model of GM2 activator deficiency manifests cerebellar pathology and motor impairment. *Med. Sci.* **94**, 8138–8143 (1997).
310. Torres, P. A., Zeng, B. J., Porter, B. F., Alroy, J., Horak, F., Horak, J. & Kolodny, E. H. Tay-Sachs disease in Jacob sheep. *Mol. Genet. Metab.* **101**, 357–363 (2010).
311. Seyrantepe, V., Demir, S. A., Timur, Z. K., Von Gerichten, J., Marsching, C., Erdemli, E., Oztas, E., Takahashi, K., Yamaguchi, K., Ates, N., Demir, B. D., Dalkara, T., Erich, K., Hopf, C., Sandhoff, R. & Miyagi, T. Murine Sialidase Neu3 facilitates GM2 degradation and bypass in mouse model of Tay-Sachs disease. *Exp. Neurol.* **299**,

26–41 (2018).
312. Pan, X., De Aragão, C. D. B. P., Velasco-Martin, J. P., Priestman, D. A., Wu, H. Y., Takahashi, K., Yamaguchi, K., Sturiale, L., Garozzo, D., Platt, F. M., Lamarche-Vane, N., Morales, C. R., Miyagi, T. & Pshezhetsky, A. V. Neuraminidases 3 and 4 regulate neuronal function by catabolizing brain gangliosides. *FASEB J.* **31**, 3467–3483 (2017).
313. Shiotsuki, H., Yoshimi, K., Shimo, Y., Funayama, M., Takamatsu, Y., Ikeda, K., Takahashi, R., Kitazawa, S. & Hattori, N. A rotarod test for evaluation of motor skill learning. *J. Neurosci. Methods* **189**, 180–185 (2010).
314. Amick, J., Roczniak-Ferguson, A. & Ferguson, S. M. C9orf72 binds SMCR8, localizes to lysosomes, and regulates mTORC1 signaling. *Mol. Biol. Cell* **27**, 3040–3051 (2016).
315. Amick, J. & Ferguson, S. M. C9orf72: At the intersection of lysosome cell biology and neurodegenerative disease. *Traffic* **18**, 267–276 (2017).
316. Shao, Q., Yang, M., Liang, C., Ma, L., Zhang, W., Jiang, Z., Luo, J., Lee, J. K., Liang, C. & Chen, J. F. C9orf72 and smcr8 mutant mice reveal MTORC1 activation due to impaired lysosomal degradation and exocytosis. *Autophagy* **16**, 1635–1650 (2020).
317. Picher-Martel, V., Valdmanis, P. N., Gould, P. V, Julien, J.-P. & Dupré, N. From animal models to human disease: a genetic approach for personalized medicine in ALS. *Acta Neuropathol. Commun.* **4**, 70 (2016).

Supplementary information

	Adjusted *p* value	Summary
Buffer 1		
Imiglucerase vs. New imiglucerase	0.9905	ns
Imiglucerase vs. Velaglucerase	0.0003	***
Imiglucerase vs. New velaglucerase	< 0.0001	****
Buffer 2		
Imiglucerase vs. New imiglucerase	0.8411	ns
Imiglucerase vs. Velaglucerase	0.3481	ns
Imiglucerase vs. New velaglucerase	< 0.0001	****
Buffer 3		
Imiglucerase vs. New imiglucerase	0.4688	ns
Imiglucerase vs. Velaglucerase	0.0056	**
Imiglucerase vs. New velaglucerase	< 0.0001	****

Table S.1. Adjusted *p* values from 2-way ANOVA with Dunnett's multiple comparisons analysis of the data from Figure 3.2.

	Adjusted *p* value	Summary
Buffer 1		
1.25 mg vs. 2.5 mg	0.1464	ns
vs. Buffer 2 (1.25 mg)	< 0.0001	****
vs. Buffer 3 (1.25 mg)	< 0.0001	****
vs. Buffer 4 (1.25 mg)	0.0010	**
vs. Buffer 2 (2.5 mg)	0.0001	***
vs. Buffer 3 (2.5 mg)	0.0008	***
vs. Buffer 4 (2.5 mg)	0.7171	ns
Buffer 2		
1.25 mg vs. 2.5 mg	0.1260	ns
vs. Buffer 3 (1.25 mg)	0.9988	ns
vs. Buffer 4 (1.25 mg)	< 0.0001	****
vs. Buffer 3 (2.5 mg)	0.9299	ns
vs. Buffer 4 (2.5 mg)	< 0.0001	****
Buffer 3		
1.25 mg vs. 2.5 mg	0.0047	**
vs. Buffer 4 (1.25 mg)	< 0.0001	****
vs. Buffer 4 (2.5 mg)	< 0.0001	****
Buffer 4		
1.25 mg vs. 2.5 mg	0.9730	ns

Table S.2. Adjusted *p* values from 2-way ANOVA with Tukey's multiple comparisons analysis of the data from Figure 3.3.

	Adjusted *p* value	Summary
5 % Enzyme		
Imiglucerase vs. Velaglucerase alfa	0.0035	ns
vs. 10 % Imiglucerase	< 0.0001	**
vs. 20 % Imiglucerase	< 0.0001	****
vs. 10 % Velaglucerase alfa	< 0.0001	ns
vs. 20 % Velaglucerase alfa	< 0.0001	****
10 % Enzyme		
Imiglucerase vs. Velaglucerase alfa	0.0032	**
vs. 20 % Imiglucerase	0.0020	****
vs. 20 % Velaglucerase alfa	0.9908	****
20 % Enzyme		
Imiglucerase vs. Velaglucerase alfa	0.9997	**

Table S.3. Adjusted *p* values from 2-way ANOVA with Tukey's multiple comparisons analysis of the data from Figure 3.4.

	Adjusted *p* value	Summary		Adjusted *p* value	Summary
10 % Imiglucerase			20 % Imiglucerase		
0.1 mg vs. 0.25 mg	0.1140	ns	0.1 mg vs. 0.25 mg	0.0060	**
0.1 mg vs. 0.5 mg	0.0003	***	0.1 mg vs. 0.5 mg	< 0.0001	****
0.1 mg vs. 0.625 mg	0.9999	ns	0.1 mg vs. 0.625 mg	0.0030	**
0.1 mg vs. 1.25 mg	0.1036	ns	0.1 mg vs. 1.25 mg	< 0.0001	****
0.1 mg vs. 2.5 mg	0.9995	ns	0.1 mg vs. 2.5 mg	< 0.0001	****
0.25 mg vs. 0.5 mg	0.5544	ns	0.25 mg vs. 0.5 mg	0.5519	ns
0.25 mg vs. 0.625 mg	0.0716	ns	0.25 mg vs. 0.625 mg	< 0.0001	****
0.25 mg vs. 1.25 mg	0.0002	***	0.25 mg vs. 1.25 mg	< 0.0001	****
0.25 mg vs. 2.5 mg	0.2308	ns	0.25 mg vs. 2.5 mg	< 0.0001	****
0.5 mg vs. 0.625 mg	0.0002	***	0.5 mg vs. 0.625 mg	< 0.0001	****
0.5 mg vs. 1.25 mg	< 0.0001	****	0.5 mg vs. 1.25 mg	< 0.0001	****
0.5 mg vs. 2.5 mg	0.0075	**	0.5 mg vs. 2.5 mg	< 0.0001	****
0.625 mg vs. 1.25 mg	0.1684	ns	0.625 mg vs. 1.25 mg	0.0008	***
0.625 mg vs. 2.5 mg	> 0.9999	ns	0.625 mg vs. 2.5 mg	< 0.0001	****
1. 25 mg vs. 2.5 mg	0.6253	ns	1. 25 mg vs. 2.5 mg	0.0135	*
40 % Imiglucerase			60 % Imiglucerase		
0.1 mg vs. 0.25 mg	< 0.0001	****	0.1 mg vs. 0.25 mg	< 0.0001	****
0.1 mg vs. 0.5 mg	< 0.0001	****	0.1 mg vs. 0.5 mg	< 0.0001	****
0.1 mg vs. 0.625 mg	0.9946	ns	0.1 mg vs. 0.625 mg	< 0.0001	****
0.1 mg vs. 1.25 mg	< 0.0001	****	0.1 mg vs. 1.25 mg	< 0.0001	****
0.1 mg vs. 2.5 mg	< 0.0001	****	0.1 mg vs. 2.5 mg	< 0.0001	****
0.25 mg vs. 0.5 mg	0.5564	ns	0.25 mg vs. 0.5 mg	0.4765	ns
0.25 mg vs. 0.625 mg	< 0.0001	****	0.25 mg vs. 0.625 mg	< 0.0001	****
0.25 mg vs. 1.25 mg	< 0.0001	****	0.25 mg vs. 1.25 mg	< 0.0001	****
0.25 mg vs. 2.5 mg	< 0.0001	****	0.25 mg vs. 2.5 mg	< 0.0001	****
0.5 mg vs. 0.625 mg	< 0.0001	****	0.5 mg vs. 0.625 mg	< 0.0001	****
0.5 mg vs. 1.25 mg	< 0.0001	****	0.5 mg vs. 1.25 mg	< 0.0001	****
0.5 mg vs. 2.5 mg	< 0.0001	****	0.5 mg vs. 2.5 mg	< 0.0001	****
0.625 mg vs. 1.25 mg	< 0.0001	****	0.625 mg vs. 1.25 mg	< 0.0001	****
0.625 mg vs. 2.5 mg	< 0.0001	****	0.625 mg vs. 2.5 mg	< 0.0001	****
1. 25 mg vs. 2.5 mg	0.0677	*	1. 25 mg vs. 2.5 mg	0.7069	ns

Table S.4. Adjusted *p* values from 2-way ANOVA with Tukey's multiple comparisons analysis of the data from Figure 3.7 (excluding data for 25 µL imiglucerase).